Observability and Decision Support for Supervision of Distributed Power System Control

Pertl, Michael

Publication date:
2018

Document Version
Publisher's PDF, also known as Version of record

Technical University of Denmark

Michael Pertl

Observability and Decision Support for Supervision of Distributed Power System Control

Dissertation, November 2017
Risø, Denmark

Center for Electric Power and Energy
Department of Electrical Engineering

DANMARKS TEKNISKE UNIVERSITET
Center for Electric Power and Energy (CEE)
DTU Electrical Engineering

Observability and Decision Support for Supervision of Distributed Power System Control

Observabilitet og beslutningsstøtte til overvågning af distribueret kontrol af elsystem

Dissertation, by Michael Pertl

Supervisors:
Senior Researcher Henrik W. Bindner, Technical University of Denmark
Associate Professor Mattia Marinelli, Technical University of Denmark
Assistant Professor Kai Heussen, Technical University of Denmark

DTU - Technical University of Denmark, Risø - November 2017

Observability and Decision Support for Supervision of Distributed Power System Control

This thesis was prepared by:
Michael Pertl

Supervisors:
Senior Researcher Henrik W. Bindner, Technical University of Denmark
Associate Professor Mattia Marinelli, Technical University of Denmark
Assistant Professor Kai Heussen, Technical University of Denmark

Dissertation Examination Committee:
Associate Professor Chresten Træholt (Chairman)
Department of Electrical Engineering, Technical University of Denmark, Denmark

Associate Professor Roberto Turri
Department of Industrial Engineering, University of Padova, Italy

Associate Professor Andrew Keane
Head of Energy Institute, University College Dublin, Ireland

Center for Electric Power and Energy (CEE)
DTU Electrical Engineering
Elektrovej, Building 325
DK-2800 Kgs. Lyngby
Denmark

Tel: (+45) 4525 3500
Fax: (+45) 4588 6111
E-mail: cee@elektro.dtu.dk

Release date: November 30, 2017

Edition: V 01

Class: Public

Field: Electrical Engineering

Remarks: The dissertation is presented to the Department of Electrical Engineering of the Technical University of Denmark in partial fulfillment of the requirements for the degree of Doctor of Philosophy.

ISBN: 000-00-00000-00-0

Anyone who has never made a mistake
has never tried anything new.

— Albert Einstein

To my parents

Preface

This thesis was prepared at the Department of Electrical Engineering of the Technical University of Denmark in partial fulfillment of the requirements for acquiring the degree of Doctor of Philosophy in Engineering. The Ph.D. project was funded by the EU FP7 project *ELECTRA* (grant: 609687) and the Danish Research Project *ELECTRA Top-up* (grant: 3594756936313).

This dissertation summarizes the work carried out by the author during his Ph.D. project. It started on 15th December 2014, and it was completed on 30th November 2017. During this period, he was hired by the Technical University of Denmark as a Ph.D. student at the Center for Electric Power and Energy (CEE).

The thesis is composed of 6 chapters and 5 attached scientific papers, 4 of which have been peer-reviewed and published, whereas the remaining one is currently under review.

Michael Pertl
November 30, 2017

Acknowledgements

The way to this thesis was characterized by a lot of hard work and long days in the office. Even Thomas Edison acknowledged that *"There is no substitute for hard work"*. But it was not only hard work which let me arrive at this point, there was a lot of support from people who I knew before starting the PhD and also from people who I have met during the PhD.

First of all I would like to thank my supervisory team Henrik W. Bindner, Mattia Marinelli and Kai Heussen for their consistent support and constructive feedback throughout the three years of my PhD studies. Each of them supported me in a different way which helped me to learn how to approach scientific problems from different perspectives and that there is not always a "right or wrong". They also taught me how to write scientific texts to properly communicate my results with the research community. On top of that, I am grateful to Mattia for giving me the chance (volunteering me ;)) to be his teaching assistant in the course *Integration of Wind Power in the Power System* which gave me the first teaching experiences. Going to "Big Mamma" for a pizza after the course has compensated us for the hard work (mainly carried out by Mattia).

I also have thank all my colleagues from famous "776" in Risø, because working there means not just working among colleagues but being part of the 776-family. If it was cooking dinner with colleagues after work or the legendary Christmas parties - all these traditions enlightened my working days and made working there a pleasure. Special thanks I have to dedicate to Michel, with whom I was not only sharing the office but he was also my PhD companion. We were studying, working and travelling together. It was my pleasure to have you as my colleague and friend.

During my PhD I also had the pleasure to do my external research stay with the GISMo (Grid Integration, Systems and Mobility) group at Stanford Linear Accelerator Laboratory (SLAC) in California. I enjoyed very much working with all the smart people there and I would like to thank them for hosting me and welcoming me so warmly. Especially I would like to thank Sila and Emre for making this possible in the first place.

My most important supporters, however, are my parents Evelin and Ernst. They have always showed understanding for my decisions and encouraged me to continue with my plans. Besides, I would like to thank my brother Felix for enlightening my days with his insights to the crazy physicist stuff he is doing at the University. Hopefully we will soon be able to realize our long-term plan to go to Jackson Hole for some shredding.

Last but not least, I would like to thank all my friends from Austria, Denmark and all over the world. Even though I am geographically separated from many of them, when we meet it feels like nothing has ever changed. That is one of the things I appreciate the most.

Michael

Risø, Denmark, 2017

Table of Contents

Abstract

Analyses of past disturbances and blackouts have shown that lack of situation awareness of control room operators led to wrong or suboptimal decisions. Two main issues are associated with lack of situation awareness. On the one hand, operators do not get the information needed to fully understand the current state of the grid. On the other hand, the information is not correctly interpreted. Along with the enhancement of existing tools, complementary monitoring methods must be developed for increased observability and situation awareness. To facilitate the decision process, tools that provide specific operational information, relevant to the current grid condition, need to be developed.

This dissertation covers three areas where specific challenges for improved observability and decision support in future control rooms are addressed: Classical large power system stability issues, innovative data-driven techniques for voltage estimation at the distribution level, and aggregation functions for geographically dispersed time-dependent distributed energy resources are investigated. In particular, this dissertation proposes a decision support tool for transient stability preventive control, a neural-network-based approach for real-time voltage estimation in active distribution grids, and a modeling approach to harness the flexibility of an aggregation of electric vehicles.

For improved monitoring and maintaining power system stability, a decision support tool for transient stability preventive control, based on time-domain simulations, is proposed. The approach employs a critical bus screening and a fast critical contingency screening prior to the assessment to reduce the computational burden. In addition, a fast-converging technique to determine the required dispatch for re-establishing a predefined stability margin is presented. The approach delivers a near optimal solution in terms of cost minimization due to its sequential nature and shows to be robust when applied to larger power systems.

The general problem of low distribution grid observability is addressed by proposing a data-driven approach for real-time voltage estimation in active distribution grids utilizing existing real-time and non-real-time measurements. The framework to establish such a neural real-time voltage estimator is described. Then, the capabilities and limitations of the approach under practical considerations are analyzed by means of field data. This includes a methodology to select the most relevant input variables and find a tradeoff solution between achievable performance and number of inputs and a sensitivity analysis of the performance and number of neurons. Moreover, the quantity of historical data which is needed to train an adequately functioning model is analyzed. In order to maintain the accuracy of the trained model, the impact of the retraining interval on the model performance is determined. Additionally, the sensitivity of the model to distributed generation is investigated.

The growth of electric vehicles results in additional demand for charging which will require large investments in power distribution, transmission, and generation. However, this demand is often

also flexible in time and can be actively managed to reduce the required investments and to enhance power system operation. Harnessing this flexibility requires forecasting and controlling electric vehicle charging at thousands of stations. A model to aggregate and forecast the flexible demand from tens to thousands of electric vehicle supply equipments is proposed. From an operational perspective, the aggregated EVs are represented as an equivalent time-variant storage model whose parameters can be easily aggregated and forecasted using autoregressive models. The forecastability of the uncontrolled demand and the storage parameters is evaluated using an extensive dataset from 1341 non-residential electric vehicle supply equipments located in Northern California. Two possible applications of the model are presented: peak reduction compared to uncontrolled charging, and an energy arbitrage scenario.

Overall, it is shown that a combination of classical and innovative approaches can contribute to improved situation awareness of control room operators. In addition, complementary decision support tools can further aid the control room operator in determining appropriate operational actions. However, observability and decision support tools must be integrated to allow optimal operational decisions that satisfy all constraints.

Resumé

Analyser af historiske driftsforstyrrelser og strømafbrydelser har vist at manglende overblik hos operatørerne i kontrolrummet har ført til uhensigtsmæssige eller direkte forkerte beslutninger. Der er to hovedproblemer forbundet med manglende overblik over situationen. I nogle tilfælde får operatøren ikke den nødvendige information for at forståhvilken tilstand el-nettet har. I andre tilfælde er informationen ikke rigtigt forstået af operatøren. I forbindelse med forbedringerne af de eksisterende værktøjer skal der udvikles metoder der giver øget adgang til den nødvendige information og forbedret overblik over situationen. For at sikre en optimal beslutningsproces skal der udvikles et system der giver den nødvendige operationelle information, given den aktuelle status påel-nettet.

Denne afhandling omfatter tre emner, hvor de specifikke udfordringer angående overblik og støtte til beslutningstagningen i fremtidens kontrolrum er adresseret: Klassiske stabilitetsproblemer i store el-systemer, innovative data-drevne teknikker til spændings estimering pådistributionsnettet og styrings funktioner til geografisk spredte tidsafhængige energiresurser, er undersøgt. I særdeleshed, foreslår denne afhandling et værktøj der støtter beslutningstagningen til præventiv styring af transient stabilitet, en neuralt-netværks baseret tilgang til realtids-spændingsestimering i aktive distributionsnet og en modelleringsmetode til udnyttelse af fleksibiliteten fra styringen af en gruppe elbiler.

For at opnåforbedret overvågning og opretholdelse af el-nettets stabilitet, er et præventivt beslutningsstøttende værktøj til opretholdelse af transient stabilitet, baseret påtidsdomæne simuleringer, foreslået. Metoden bruger en kritisk bus scanning og en hurtig kritisk scanning for uforudsete hændelser inden den laver vurderingen for at reducere den nødvendige mængde af regnekraft. Derudover bruger den en hurtigt konvergerende teknik til at vurdere om der er brug for at ændres påproduktionen for at genskabe den definerede stabilitetsmargin. Tilgangen giver en næsten optimal løsning når det kommer til at minimere prisen, pågrund af dens sekventielle natur og viser sig at være robust når testet påstore el-systemer.

Grundlæggende set er problemet med den lave observerbarhed i distributionsnettet, håndteret med den foreslåede data-drevne metode der i realtid estimerer spændingen i de aktive distributionsnet ved at bruge eksisterende real og ikke realtids målinger. Platformen der er brugt til at skabe denne neurale realtids estimeringsalgoritme er beskrevet. Derefter er mulighederne og begrænsningerne ved denne metode analyseret påbaggrund af ægte målinger. Dette inkluderer en metode til at vælge de mest relevante variabler, finde et kompromis mellem hvor god løsningen kan blive og antallet af inputs og en analyse af betydningen af antallet af neuroner for kvaliteten. Derudover er det analyseret hvor stor en mængde af historisk data der er nødvendig for at træne en model til et tilstrækkeligt funktionelt niveau. Med henblik påat opretholde præcisionen af modellen er det vurderet hvilken effekt det har hvor ofte man træner den. Det er ogsåundersøgt hvor sensitiv modellen er overfor distribueret elektricitetsproduktion.

Væksten i antallet af elbiler vil skabe et øget behov for opladning, hvilket vil kræve store investeringer i distributionsnettet, transmissionsnettet og af elektricitetsproduktionen. Tidspunktet for dette forbrug er dog ofte fleksibelt og kan styres aktivt for at reducere behovet for investeringer og for generelt at forbedre tilstanden af el-nettet. At udnytte denne fleksibilitet kræver omfattende prognoser og styring af elbilernes ladning ved tusindvis af ladestandere. Der er foreslået en model der kan styre og forudsige forbruget fra titusinder af elbilsladere. Fra et operationelt perspektiv kan gruppen af styrede elbiler repræsenteres med en tilsvarende tidsafhængig lagringsmodel hvis parametre nemt kan styres og forudsiges ved hjælp af adaptive modellering. Forudsigeligheden af det ukontrollerede forbrug og lagringsparametrene er evalueret ved hjælp af et vidtgående dataset fra 1341 kommercielle ladestandere i det nordlige Californien. Der er præsenteret to mulige anvendelser af modellen: reduktion af spidsforbruget sammenlignet med ukontrolleret ladning og et scenarie hvor der handles med energien.

Overordnet set, er det vist at en kombination af klassiske og innovative metoder kan bidrage til et bedre overblik over situationen for systemoperatørerne. Derudover kan assisterende beslutningshjælpemidler gøre det nemmere for operatørerne at tage en passende operationel beslutning. Der er dog nødvendigt både at have høj observerbarhed og beslutningshjælpemidler i en integreret løsning for at muliggøre optimale operationelle beslutninger der tilfredsstiller alle de fysiske begrænsninger.

Zusammenfassung

Analysen von vergangenen Störungen und Blackouts haben gezeigt, dass mangelndes Situationsbewusstsein in Leitwarten zu falschen oder suboptimalen Entscheidungen führen kann und mit zwei Hauptproblemen verbunden ist. Auf der einen Seite erhält das Leitwartenpersonal nicht die Informationen, die benötigt werden, um den aktuellen Zustand des Netzes vollständig zu beurteilen. Auf der anderen Seite wird die zur Verfügung stehende Information nicht richtig interpretiert. Neben der Verbesserung existierender Tools müssen auch neue Methoden zur Erhöhung der Beobachtbarkeit des Netzes und somit des Situationsbewusstseins entwickelt werden. Außerdem braucht es zusätzliche Tools, die spezifische operative Informationen auf Basis des derzeitigen Netzzustandes bereitstellen, um den Entscheidungen in der Leitwarte zu erleichtern.

Die vorliegende Dissertation deckt drei Bereiche ab, in denen spezifische Aspekte zur Erhöhung des Situationsbewusstseins und zur Unterstützung der Entscheidungsfindung im Betrieb unter Einfluss dezentraler Erzeugungsanlagen untersucht werden: Klassische Stabilitätsprobleme großer elektrischer Energiesysteme, datengestützte Methoden zur Spannungsbestimmung auf Verteilnetzebene und Techniken zur Zusammenfassung von geographisch verteilten, zeitabhängigen dezentralen Ressourcen. Im Speziellen wird ein Tool zur präventiven Gewährleistung transienter Stabilität, eine Methode basierend auf neuronalen Netzen zur Echtzeit-Spannungsbestimmung für Verteilnetze mit dezentraler Erzeugung, und ein Modellierungsansatz zur Nutzung der Flexibilität einer Flotte von Elektrofahrzeugen, vorgestellt.

Um die Stabilitätsgewährleistung von Netzen mit häufiger wechselnden Betriebspunkten zu verbessern wurde ein Tool zur raschen Analyse und Entscheidungsunterstützung zum Dispatch von Synchrongeneratoren, basierend auf Simulationen im Zeitbereich, entwickelt. Die Berechnungsintensität wird durch Nutzung eines Verfahrens zur Identifizierung kritische Eventualitäten reduziert. Darüber hinaus wird eine schnell konvergierende Methode zur Bestimmung des benötigten Generatordispatch zur Wiederherstellung eines vordefinierten Stabilitätslimits vorgestellt. Aufgrund der sequentiellen Natur des Ansatzes erreicht man eine Lösung nahe des Optimums hinsichtlich der Kostenminimierung. Die Simulationsergebnisse haben gezeigt, dass sich der Ansatz als robust für größere elektrische Übertragungsnetze erweist.

Zur Verbesserung der Beobachtbarkeit von Verteilnetzen mit dezentralen Erzeugungsanlagen wird ein datengestützter Ansatz zur Echtzeit-Spannungsbestimmung, basierend auf existierenden Echtzeit- und Nicht-Echtzeit-Messungen, vorgestellt. Die Rahmenbedingungen zur Erstellung eines hochgenauen neuronalen Echtzeit-Spannungsschätzers werden beschrieben. Die Möglichkeiten und Grenzen des Ansatzes unter praktischen Umständen werden anhand von Felddaten analysiert. Außerdem wird eine Methodik zur Auswahl der relevanten Eingangsvariablen und der bestmöglichen Performance für eine bestimmte Anzahl von Eingangsvariablen vorgestellt und die Empfindlichkeit der Performance in Abhängigkeit von der Anzahl der Neuronen wird analysiert. Ein weiterer wichtiger Punkt ist die Menge an historischen Daten, die benötigt wird um ein

Modell mit zweckentsprechender Performance zu trainieren. Um die Performance des Modells aufrechtzuerhalten, werden die Auswirkungen des Intervalls, indem das Modell neu trainiert wird, auf die Performance analysiert. Die Sensitivität der Performance des Spannungsschätzers wird auch im Hinblick auf Unterschiede mit hohem und niedrigem Anteil dezentraler Erzeugung analysiert.

Die steigende Anzahl von Elektrofahrzeugen erhöht den Bedarf an elektrischer Energie und erfordert große Investitionen in Energieverteilung, -übertragung und -erzeugung. Allerdings ist der Bedarf von elektrischer Energie oft auch zeitlich flexibel und kann aktiv dazu genutzt werden, um benötigte Investitionen zu reduzieren und einen Beitrag zum Betrieb des Stromnetzes zu leisten. Um diese Flexibilität nutzbar zu machen, erfordert es die Vorhersage und Steuerung des Bedarfs einer großen Anzahl von Elektrofahrzeugen. Ein Modell zur Zusammenfassung und Prognose des gesamten flexiblen Bedarfs von einigen wenigen bis Tausenden von Elektrofahrzeugen wird vorgestellt. Aus operativem Zweck werden die zusammengefassten Elektrofahrzeuge als eine äquivalente zeitveränderliche virtuelle Batterie dargestellt. Die Parameter der virtuellen Batterie können einfach berechnet und mit autoregressiven Modellen prognostiziert werden. Die Prognose des ungesteuerten Bedarfs und der Parameter der virtuellen Batterie wird anhand eines umfangreichen Datensatzes von 1341 kommerziellen Elektrofahrzeugladestationen in Kalifornien ausgewertet. Zwei mögliche Anwendungen des Modells wurden untersucht: Reduktion des Spitzenverbrauchs im Verglich zum ungesteuerten Laden und ein Arbitrage Szenario zur Kostenminimierung. Die Ergebnisse zeigen, dass das Model enormes technisches und wirtschaftliches Potenzial mit sich bringt.

Zusammenfassend kann man aus den drei untersuchten Bereichen ableiten, dass sowohl klassische und innovative Methoden das Situationsbewusstsein in Leitwarten verbessern können und deshalb eine Kombination aus beiden benötigt wird. Darüber hinaus kann das Leitwartenpersonal durch komplementäre Tools zur Unterstützung der Entscheidungsfindung leichter angemessene operative Entscheidungen treffen. Jedoch ist es wichtig, eine integrierte Lösung der verschiedenen Tools anzustreben, um optimale operative Entscheidungsfindung unter Berücksichtigung aller Limitierungen zu ermöglichen.

Acronyms

CAISO California Independent System Operator

CBS critical bus screening

CCT critical clearing time

COI center of inertia

CV Coefficient of Variation

DFIG doubly-fed induction generator

DPL DIgSILENT programming language

DSO distribution system operator

ELECTRA European liaison on electricity committed towards long-term research activity

EMS energy management system

ENTSO-E European network of transmission system operators for electricity

EVI Electric Vehicles Initiative

EVSE electric vehicle supply equipment

EV electric vehicle

FACTS flexible alternating current transmission systems

FCCS fast critical contingency screening

GPS global positioning system

HVDC high-voltage direct current

HVRT high voltage ride-through

ICT information and communication

IEA International Energy Association

IEA International Energy Agency

IEEE Institute of Electrical and Electronic Engineers

IM induction machine

LVRT low voltage ride-through

LV low voltage

MAE Mean Average Error

MAPE Mean Average Percentage Error

MPC model predictive control

MSE mean squared error

MT-HVDC multi-terminal HVDC

MV medium voltage

NN neural network

NRTVE neural real-time voltage estimator

OLTC on-load tap-changer

OPF optimal power flow

OPF optimal power flow

PMU phasor measurement unit

PV photovoltaics

PWM pulse-width modulation

RES renewable energy sources

RMSE Root Mean Squared Error

ROCOF rate of change of frequency

RTU remote terminal unit

SA situation awareness

SCADA supervisory control and data acquisition

SG synchronous generator

SOC state-of-charge

STATCOM Static synchronous compensator

SVC static var compensator

TCL thermostatically controlled load

TD time-domain

TSO transmission system operator

V2G vehicle-to-grid

VSC voltage source converter

WAMC wide-area monitoring and control

WAMPAC wide-area monitoring protection and control

WAMS wide-area monitoring system

WLS weighted-least-squares

Definitions

This section states and clarifies some definitions of functions, roles and responsibilities that are referred to in this thesis.

Control room: The control room is the center of power system operation where monitoring and control of the whole power system is coordinated. In the literature also the terms control center or control centre are used.

Control room operator or simply *operator:* The control room operator is the person that is responsible to monitor, supervise and control the power system in the control room.

Decision support tool: A decision support tool analyzes data from the power system aiming at delivering specific information and insights of a particular operational aspect to support the decision making process of the operator. The decision support tool possibly also suggests actions to address specific operational concerns.

Power system operation: Power system operation includes all manual and automated tasks that are performed to operate the power system safely, reliably and efficiently.

Supervisory control and data acquisition (SCADA): The SCADA system is the main component of the control room and comprises two main functions. It collects data from the power system and allows the operator to monitor, supervise and control the power system.

Energy management system (EMS): An EMS provides additional insights into the power system in terms of visualization, optimization and various other advanced analyses. An EMS can include a SCADA system directly or the EMS is coupled to a SCADA system that provides the data for the analyses.

Contingency, disturbance and fault: These terms are used interchangeably. They refer to a large change in the system state that is able to drive the system into instability. In the context of transient stability, a contingency may for example be a short-circuit, the loss of an important tie-line, or the loss of an important load.

CHAPTER 1

Introduction

1.1 On the justification of research on observability and decision support for power system control

Traditionally, electric power systems were operated with large stability margins. The liberalization of the European electricity market has increased the competition in the electricity market [1], and the transition to volatile renewable energy sources (RES) [2] have pushed the electric power system closer to its limits. The electrical distance between generation and consumption due to far-off RES increases long-distance flows on transmission grids, high penetration of photovoltaics (PV) in distribution grids may cause reverse power flows and potentially voltage limit violations whereas, on the demand side, uncontrolled electric vehicle (EV) charging strongly increases the consumption at certain times of the day and, thus, may lead to overloading of lines. Control room operators constantly monitor the transmission and distribution grid and dispatch generators to meet the demand at all times. Opposed to that, operators are under constant pressure to run the power system in the most economical way [3]. The control room operator has to perform complex technical tasks to reconcile the diverting interests while operating the power system with sufficient stability margins so that no credible contingency could trigger cascading outages or other instabilities.

Past disturbances and blackouts have shown several reasons for lack of situation awareness of the control room operators that led to wrong or suboptimal decisions. One of the main causes of the system disturbance in the continental European transmission grid on November 4, 2006 was lack of inter-transmission system operator (TSO) coordination [4]. Important information was communicated in the last moment which led to insufficient time for appropriate security analysis. One of the main reasons for the Italian blackout on September 28, 2003 was lack of sense of urgency regarding an overloaded line in the Swiss control area which could not be observed by the Italian TSO [5]. Insufficient countermeasures were taken and the line tripped which initiated the sequence of events that led to the blackout. On August 14, 2003, a large power blackout in the Midwest and Northeast United States (US) affected an estimated 50 million people [6]. Power was not restored for four days in some parts of the US. One of the main causes of the blackout was lack of situation awareness due to inadequate monitoring equipment to alert operators about important deviations in operating conditions and the need for appropriate corrective actions. A general lack of operations information and analysis tools which are needed for reliable grid operation was found. Two main problems related to lack of situation awareness of control room operators can be identified. On the one hand, operators do not get the information that is needed to fully understand the grid's current condition. On the other hand, the available information is not correctly understood [7].

Besides past major disturbances and blackouts, the increasing share of RES on transmission and distribution level requires additional monitoring and decision support tools for efficient large

scale integration. A survey, conducted by Alstom Grid Inc., among 33 operators of electric power systems in 18 countries about wind integration related challenges revealed that 94 % of the survey participants agree or strongly agree that adequate decision support tools to support control room operators are a necessity for integration of significant amounts of wind power [8]. In addition to wind power plants that are generally connected to the transmission system, large portions of small scale PV are connected to the distribution grid introducing further operational challenges in particular due to the low degree of observability of distribution grids. On the load side, EVs increase the demand in low voltage (LV) grids which may lead to issues in unobserved parts of the distribution grid if charging is not properly coordinated. Besides, smart integration of EVs opens new opportunities to positively contribute and improve power system operation.

In light of these current and future challenges and opportunities of electric power system operation, this thesis presents work that aims at increasing situation awareness of control room operators by introducing novel approaches for increased observability, and supporting the control room operator's decision making by introducing supplementary decision support tools.

1.2 Research objectives

This thesis selects particular aspects aimed at increasing the situation awareness of control room operators. To address future control room challenges, three representative cases covering classical large power system stability issues as well as innovative data-driven techniques for voltage estimation at the distribution level and aggregation functions for geographically dispersed time-dependent distributed energy resources are investigated. The first aspect concerns the traditional area of transient stability which basically exists since the first generator went online and it is mainly connected to the transmission grid. The second aspect addresses the general problem of low observability of distribution grids as this becomes more important with increasing share of active units on the generation and consumption side. The third aspect is related to the more recent development of utilizing the aggregated flexibility of EVs to enhance power system operation.

The research questions this thesis seeks to answer are divided into three categories relating to the above outlined research objectives: Transient stability, voltage estimation and aggregated EV flexibility as shown in Fig. 1.1.

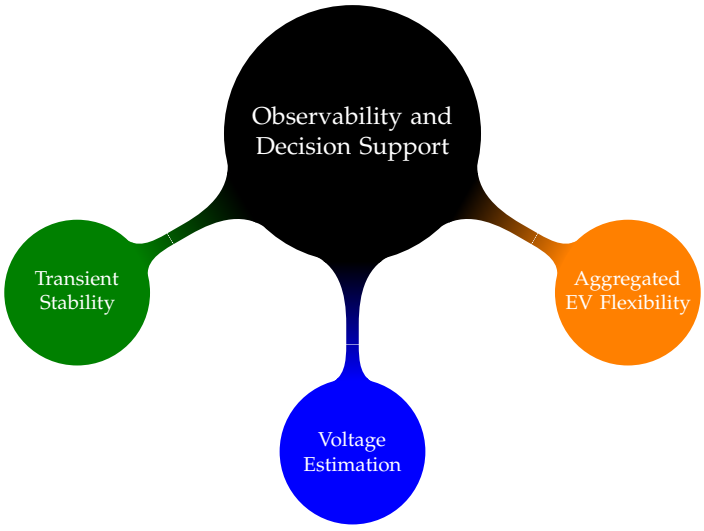

Figure 1.1: Structure of the Ph.D. project

1.2.1 Transient stability

[Q1] *What are the state-of-the-art techniques for transient stability preventive and emergency control and what are the deficiencies concerning the transition to a RES-based power system?*

The current transition to a RES-based power system changes the characteristics of the power system in various ways. Traditional transient stability schemes face new challenges and may not be longer appropriate under certain conditions. A literature review is needed to summarize the vast variety of transient stability improvement techniques for preventive and emergency control and reveal possible deficiencies.

[Q2] *How can transient stability be efficiently monitored and maintained in an online fashion?*

Transient stability assessment of multi-machine systems is usually time consuming due to time-domain (TD) simulations and an enormous number of possible contingencies. A tool that analyzes the transient stability margins of the current grid state in sufficient time is needed. The tool shall provide appropriate countermeasures if insufficient margins are detected.

1.2.2 Voltage estimation

[Q3] *How can currently available measurements be utilized to establish a data-driven neural network approach to increase the real-time voltage observability of active distribution grids?*

The large size of distribution grids prohibits high observability by means of measurement sensors due to cost restraints. A great proportion of available measurements is not available in real-time and can therefore not be efficiently utilized for grid operation. Past data of the available measurements can be used to establish data-driven models for real-time voltage estimation.

[Q4] *What are the capabilities and limitations of the neural network-based approach for real-time voltage estimation in active distribution grids?*

Before taking data-driven voltage estimation approaches to a real environment, the developed methods must be validated on field data to set the framework which defines the capabilities and limitations of the method.

1.2.3 Aggregated EV flexibility

[Q5] *How can the flexibility from tens to thousands of EVs be utilized to enhance power system operation?*

Flexible demand from EVs offers great potential for supporting and enhancing power system operation. Uncertainty in individual EV owner's behavior limits the forecastability of available flexibility so that an aggregated approach is envisioned to overcome this drawback. Models for aggregation and short-term forecast are needed.

1.3 Thesis outline and research contributions

The thesis is organized in six chapters: Introduction, four self-contained technical chapters and conclusion. The five scientific core publications **[Pub. A]** through **[Pub. E]** are attached to the thesis. The main results are published in these scientific papers which are referenced throughout this thesis as needed, but they may also be read independently of this thesis. In the following a short description of each chapter is given.

Chapter 2 defines the context for the work presented in this thesis. The necessity of observability and decision support tools for power system operation is outlined. The needed control room transformation and how observability and decision support tools fit in that context are described. A comprehensive summary of the state-of-the-art is presented and the current challenges of the observability and decision support tools are discussed.

Chapter 3 reviews the state-of-the-art techniques for transient stability preventive and emergency control. Techniques are categorized in conventional and renewable-based techniques. The techniques are qualitatively compared and future trends and research needs are identified. The chapter presents a decision support tool for transient stability preventive control that monitors the stability margins and suggests an appropriate economic dispatch for synchronous generators if needed. The tool builds on the experience of previous approaches and combines critical bus screening, transient stability assessment, visualization and decision support components to achieve online applicability. This chapter is based on **[Pub. A]** and **[Pub. B]**.

Chapter 4 presents a data-driven approach for voltage estimation in active distribution grids with high share of dispersed generation. A numerical implementation of the approach based on simulations analyzing several low/high load and renewable generation scenarios is presented. Furthermore, a validation on field data to determine the capabilities and limitations of the approach is presented. The validation is a necessary step for online application of the approach. This chapter is based on **[Pub. C]** and **[Pub. D]**.

Chapter 5 addresses the problem of forecasting the aggregate flexible demand from tens to thousands of EVs. An equivalent time-variant storage model to aggregate large populations of EVs and to harness their flexible demand is presented. The forecastability of the uncontrolled demand and the storage parameters is quantitatively evaluated using data from 1341 electric vehicle supply equipments (EVSEs) located in Northern California. Two possible applications demonstrate the technical capabilities and economical benefit that arises from the proposed model. This chapter is based on **[Pub. E]**.

Chapter 6 presents the conclusion of the thesis by elaborating on the outlined research questions and providing an outlook about identified future work.

1.4 List of publications

The relevant publications which are the core of this thesis are listed as follows:

[Pub. A] M. Pertl, T. Weckesser, M. Rezkalla, and M. Marinelli. Transient stability improvement: A review and comparison of conventional and renewable based techniques for preventive and emergency control. Springer Electrical Engineering, 2017.

[**Pub. B**] M. Pertl, T. Weckesser, M. Rezkalla, K. Heussen, and M. Marinelli. A decision support tool for transient stability preventive control. Electric Power Systems Research, vol. 147, pp. 88-96, 2017.

[**Pub. C**] M. Pertl, K. Heussen, O. Gehrke, and M. Rezkalla. Voltage estimation in active distribution grids using neural networks. IEEE Power and Energy Society General Meeting, 2016.

[**Pub. D**] M. Pertl, P. J. Douglass, K. Heussen, and K. Kok. Validation of a robust neural real-time voltage estimator for active distribution grids on field data. Electric Power Systems Research, vol. 154, pp. 182-192, 2018.

[**Pub. E**] M. Pertl, F. Carducci, M. Tabone, M. Marinelli, S. Kiliccote, and E. C. Kara. An equivalent time-variant storage model to harness EV flexibility: Forecast and aggregation. IEEE Transactions on Industrial Informatics, 2018, under review.

The following publications have also been prepared during the course of the Ph.D. study, but have been omitted from the thesis because they are not directly related to the primary objective, or they are partially covered by other presented papers.

[**Pub. F**] M. Pertl, M. Marinelli, and H. Bindner. Improved power quality monitoring through phasor measurement unit data interpretation. Universities Power Engineering Conference (UPEC), 2015

[**Pub. G**] M. Pertl, M. Rezkalla, and M. Marinelli. A novel grid-wide transient stability assessment and visualization method for increasing situation awareness of control room operators. IEEE Innovative Smart Grid Technologies Conference - Asia (ISGT-Asia), 2016

[**Pub. H**] M. Rezkalla, A. Zecchino, M. Pertl, and M. Marinelli. Grid frequency support by single-phase electric vehicles : fast primary control enhanced by a stabilizer algorithm. Universities Power Engineering Conference (UPEC), 2016

[**Pub. I**] M. Rezkalla, M. Marinelli, M. Pertl, and K. Heussen. Trade-off analysis of virtual inertia and fast primary frequency control during frequency transients in a converter dominated network. IEEE Innovative Smart Grid Technologies Conference - Asia (ISGT-Asia), 2016

[**Pub. J**] M. Marinelli, M. Pertl, M. Rezkalla, M. Kosmecki, S. Canavese, A. Obushevs, and A. Z. Morch. The Pan-European reference grid developed in ELECTRA for deriving innovative observability concepts in the web-of-cells framework. Universities Power Engineering Conference (UPEC), 2016

[**Pub. K**] A. Z. Morch, K. Visscher, S. H. Jakobsson, M. Marinelli, A. Obushevs, S. Uytterhoeven, A. M. Prostejovsky, M. Pertl, A. Nadar, and B. Dag. ELECTRA Deliverable 5.1: Increased observability: Adaptive assessment of future scenarios and mapping of observability needs. tech. report, The ELECTRA Consortium, 2015

[**Pub. L**] M. Marinelli, M. Pertl, M. Rezkalla, M. Kosmecki, B. Sobczak, R. Jankowski, A. Kubanek, A. Z. Morch, T. I. Reigstad, A. Obushevs, A. Gatti, S. Canavese, and M. Rossi. ELECTRA Deliverable 5.4: Increased observability: Functional description of the monitoring and observability detailed concepts for the Pan-European control schemes. tech. report, The ELECTRA Consortium, 2017

[Pub. M] M. Marinelli, K. Heussen, T. Strasser, R. Schwalbe, J. Merino-Fernandez, S. Riano, A. M. Prostejovsky, M. Pertl, M. Rezkalla, J. Croker, B. Evenblij, V. Catterson, and M. Chen. ELECTRA Deliverable 8.1: Future control room functionality: Demonstration of visualization techniques for the control room engineer in 2030. tech. report, The ELECTRA Consortium, 2017

CHAPTER 2

Observability and decision support for operation of electric power systems

This chapter first outlines the importance of observability and decision support tools for power system operation. The needed control room transformation, and how observability and decision support tools fit in that context, are described. A comprehensive summary of the state-of-the-art is presented and the current challenges of the observability and decision support tools are discussed. Moreover, this chapter reports on the lessons learned from the ELECTRA project in which a whole work package was dedicated to future control room functionalities.

2.1 Necessity of observability and decision support tools

Managing the power system is a complex task. The control room operator has to maintain the power system in secure state while operating it in the most economical way. The integration of large quantities of both, distributed generation based on RES, and other distributed resources such as storage systems and electric vehicles (EVs) increase the complexity of efficient power system operation even more [9, 10]. The active involvement of residential and industrial consumers for demand response introduces additional players with new resource types that allow more flexible solutions for power system operation [11–14]. The paradigm shift from centralized control of a few large-scale power plants to a high number of small distributed generation units that may be operated by different stakeholders with different interests adds an additional degree of complexity [15]. According to the International Energy Agency (IEA), one key technical challenge to successfully integrate high shares of variable renewable energy sources (RES)is to address these operational challenges [16].

In order to cope with the growing complexity of power system operation, the control room operator must be provided with adequate tools with respect to both, observability of the power system and decision support tools that analyze the grid data and deliver compact and precise information for specific operational aspects. Monitoring tools need to deliver information of various types that allow the control room operator to derive the current state of the power system under complex conditions. Monitoring must include conventional information such as bus voltages and line flows, and newly available data such as EV demand of a grid area. In addition, dedicated decision support tools need to be developed analyzing the already existing and newly available data to provide the control room operator with tailored information about specific operational aspects. Decision support tools aim at making power system operation more reliable, efficient and secure by increasing the control room operator's situation awareness (SA) and, therefore, reducing the space for human error [17].

One of the most widely used and formal definitions of situation awareness was introduced by Mica Endsley in 1988: "*Situation Awareness is the perception of the elements in the environment within a volume of time and space, the comprehension of their meaning, and the projection of their status in the near future.*" [18]. According to Endsley, situation awareness is comprised of three levels as shown in Fig. 2.1: (1) perception, (2) comprehension, and (3) projection.

At level 1 SA (perception), involves the sensory detection of relevant environmental cues, e.g. the operator needs to be able to see or hear relevant messages or alarms. At level 2 SA (comprehension), the operator understands the immediate effect of an event on the power system. At the highest level of SA, level 3, the operator is able to extrapolate into the near future to determine how the future states of the power system will be affected [19].

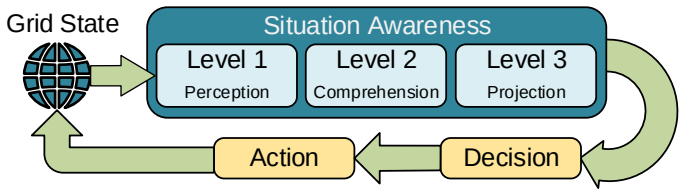

Figure 2.1: The three levels of situation awareness (adapted from [19])

A high level of SA is fundamental for effective decision-making. In order to maintain and increase the SA of operators to facilitate their decision process, dedicated observability and decision support tools that provide the suitable information are needed.

However, the massive amount of available information must be presented in an organized and integrated way to avoid overloading of the control room operator. The focus of this work is on particular aspects for increasing the observability and delivering decision support. It is not discussed how the developed tools should be integrated in an existing control room environment as this depends on many factors, such as generation portfolio, RES penetration and grid infrastructure.

2.2 Control room structure in the power system environment

Present control room functions were initially developed in the 1960s. In the past decades, the digitalization has led to dramatic development and improvement of analytical and control capabilities, and infrastructure built upon newly available information and communication techniques [20]. Computer-based tools in particular for visualization, state estimation and security assessment for power system operation were developed. However, present control rooms managed by transmission system operators (TSOs) and distribution system operators (DSOs) have to change and adapt to the new power system control paradigm with large quantities of small-scale distributed generation units, variable generation and demand, and a number of new participants. Future control rooms will play a critical role in the operation of complex, distributed power systems whereas the key characteristics of future control rooms will be as follows: human-centered, comprehensive, proactive, coordinated, and self-healing [21].

Human-centered: The massive amount of data that becomes available needs to be transformed into useful information for the operator. That means a shift from data-intensive to information-directed monitoring is needed because more data does not necessarily mean more information. As the perception and comprehension of information is different for every human being, the control room tools need to become more flexible and allow the operator to easily access customized information.

Comprehensive: The next-generation analysis functions shall provide a comprehensive overall picture of the operating boundaries. In this perspective, comprehensive means that a holistic overview which shows the "need-to-know" information about operating boundaries including thermal limits, stability margins and reserve capacity among other aspects needs to be provided to the operator.

Proactive: The analysis of current operating conditions needs to be extended to look-ahead simulations to determine issues that might arise in the near future and to apply preventive measures before issues occur. This means shifting from a reactive to a proactive operation. To achieve more economic and reliable operation, resources such as energy storages, e.g. from EVs, shall be included in the analysis.

Coordinated: Protection and control systems are traditionally designed to solve particular problems using (mostly) local measurements. In the future, protection and control systems shall include wide-area information and operation shall be coordinated among them. Additionally, the coordination between operators of adjacent power systems shall be extended as operating decisions also affect neighboring grids to a certain extend. Coordination could be improved by sharing information about operational changes that will take or took place close to tie-lines to the neighboring grid or changes in the protection equipment.

Self-healing: Control systems that can automatically handle complex situations where the time horizon for a response is too short for a human operator are needed. This could on the one hand, make the power system more resilient and may prevent widespread blackouts. On the other hand, a faster restoration after a blackout could be achieved by automated controls that support the process.

To clarify the role of observability and decision support tools, the structure of a control room and its components must be discussed. Depending on the implementation of a specific control room,

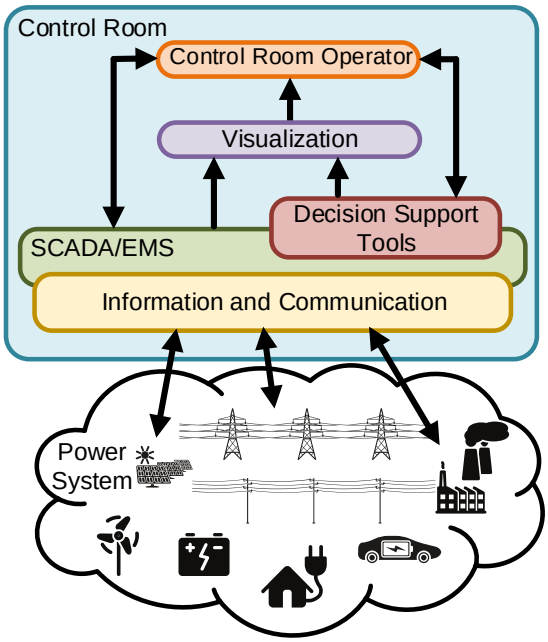

Figure 2.2: Control room structure in the power system environment

the integration of components can vary, thus, a high-level view of the most important components of a control room and their interactions are shown in Fig. 2.2. The control room comprises the visualization and decision support tools, the SCADA or energy management system (EMS), and an information and communication (ICT) system. The information and communication (ICT) layer gains more importance for two reasons. First, it is the enabler for implementation of future smart grid concepts and, second, future power system operation requires a higher level of coordination, e.g. more data exchange between neighboring TSOs [22, 23].

The control room operator monitors the power system conditions through visualization equipment. Visualizations show real-time information and also non-real-time information. Usually, a number of computer screens show an one-line overview of the power system showing basic information, such as bus voltages and line flows, with possibility of browsing to more detailed views.

The decision support tools are either directly integrated in the SCADA/EMS system or they are separated receiving data from the SCADA/EMS system [24]. The decision support tools provide data to be visualized whereas the operator can also directly interact with the decision support tools to get additional information or conduct specific analyses.

The SCADA/EMS is the central unit in the control room which provides the necessary infrastructure for communication of the power system components with the control room operator. Main functionalities of the SCADA system are data collection from power system equipment, processing of the data for visualization and providing the infrastructure for remote control of power system components [25].

The ICT layer is the interface between the SCADA/EMS and the components of the power system. It allows to remotely read data and to control the devices. In the smart grid context, the ICT infrastructure plays an important role because collecting data from a variety of sources, that are far apart and that deliver at different transfer rates, is a challenging task. Dedicated communication infrastructure is an integral part that is necessary to enable transition to a highly decentralized power system with many participants [26].

2.3 State-of-the-art observability and decision support tools

The process of monitoring the power system includes the examination of the current grid conditions. The basic system variables that are measured are as follows (adapted from [27]):

- Substation voltages
- Power flows on transmission/distribution lines
- Active and reactive power from generation units
- System load
- Interchange schedules
- Frequency
- Status of breakers and switches

In the ideal case, full observability is given by measuring all system variables. Clearly, this can not be achieved due to cost limitations. Therefore, control room operators rely on techniques that take in the available measurements and estimate the state of variables that are not measured. Integration of geographical information and phasor measurement units (PMUs) increase the observability by combining global positioning system (GPS) synchronized real-time measurements with locational information [28]. In addition, other advanced tools use the available data to analyze more sophisticated aspects, e.g. transient stability margins to provide the control room operator with deeper insights about the state of the power system. In addition to the visual and/or numerical information, these tools should also facilitate the decision-making process of control room operators by providing possible control actions to either optimize the existing state of the grid, or to take the necessary corrective actions to return the grid into a secure state.

In general, decision support tools either aim at preventive controls or at emergency controls. The distinction between these two types is of great importance as the associated decision support tools need to adhere completely different limitations and interests. It is the nature of preventive controls that issues are identified before they arise, hence, corrective actions can be taken to avoid the power system driving into the issue. This translates into versatility of preventive actions but faces the tradeoff between security and economics due to the fact that a preventive action is generally associated with additional operating costs. Therefore, design towards economic efficiency is of high priority for decision support tools for preventive controls. On the contrary, emergency controls are difficult to apply because the actual power system state needs to be analyzed and (predefined) actions need to be taken rapidly. This can be realized either with the operator in the loop or for faster emergencies by directly applying actions without the operator's intervention. That means, the design of decision support tools for emergency controls need to put emphasis on bringing back the system into a secure state leaving aside the associated costs.

In the following, a state-of-the-art overview of the currently used observability and decision support tools is presented.

2.3.1 State estimation

State estimation is a well covered field in the literature and an integral part of every control room. Figure 2.3 outlines the composition of the observeable part, unobservable part and the rest of the interconnected system. The motivation for state estimation is to solve an optimization problem using a set of available measurements and a network model to determine the most likely estimate of the power system state, i.e. the voltage magnitudes and angles at every bus, and the line flows. Usually, the state estimator is run every few minutes or on demand of the control room operator as the information is key for reliable operation of the power system. An early approach for state estimation was introduced by Fred Schweppe in 1970 [29–31]. Nowadays, most state estimation approaches are formulated as overdetermined system of nonlinear equations and solved by weighted-least-squares (WLS) problems [32–34]. Alternative state estimation approaches are based on the Kalman filter [35] and on the least absolute value technique [36].

State estimators are capable to filter measurement noise, handle measurement losses, identify bad data [37], and determine errors of the network model [38] given a sufficient measurement redundancy[1] and an observable[2] network. State estimation was traditionally only used in

[1] Defined as the ratio between the number of measurements and the number of state variables [39].

[2] A network is observable if all the state variables can be uniquely computed for a given set of measurements and network topology [40].

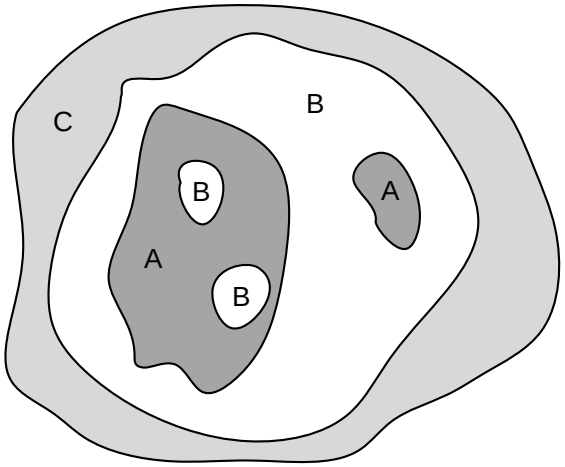

Figure 2.3: Characterization of observability of an interconnected network [47]. A: Observeable part of the system, B: Unobservable part of the system, C: Rest of the interconnected system

transmission networks. Due to the increased complexity of distribution grids, state estimation also gained attraction for distribution grids. The limited observability of distribution grids poses a barrier for the transition to future smart grids [41, 42]. Based on the assumption that, in the future, PMUs will be extensively deployed not only in transmission but also in distribution grids, numerous research papers focused on state estimation in active distribution grids utilizing PMU measurements [43–46].

2.3.2 Security assessment

Certainly, monitoring, analyzing and ensuring the security of the power system are key components of power system operation. Every control room hosts certain security assessment (decision support) tools depending on the specific needs of the operated grid. Security assessment can be divided in three levels [48]:

- Security monitoring: Checking if the operating conditions are satisfied.
- Security analysis: Checking if the system is able to withstand each specified disturbance. Obviously, not every possible disturbance can be taken into account, only disturbances with a reasonable probability to occur are considered.
- Security margin determination: Assessing the level of security for a given operating condition by defining the security margin. The aim is not only to maintain security but also adequate security margins.

The methods to assess the security of the power system can be classified in two categories, static and dynamic security assessment methods [49].

- Static security assessment: Steady-state analysis of post-contingency bus voltage and line power flow limits under the assumption that the transition from pre-contingency to post-contingency state has taken place without experiencing any instability phenomena.

- Dynamic security assessment: Analysis of the stability between the pre-contingency and post-contingency states to ensure that the system will be stable after an occurred contingency and that the caused transients will be damped, of small amplitude and with low impact on the system.

A securely operating system is one in which all operating criteria and constraints are satisfied in both, pre- an post-contingency conditions. This means, in terms of the control room environment, steady-state and transient aspects and all forms of stability have to be analyzed. This happens in two ways. First, offline tools are used to exhaustively determine security aspects in planning stage and near-future operation condition with load flow and time-domain (TD) calculations. Second, online tools provide the operator in real-time with exclusive information about the current system condition [49]. Both, offline and online tools are needed, however, the latter one gained more traction for the operation of power systems recently, because the development of information and communication technology, advanced measurement devices (e.g. PMUs) and dedicated efficient algorithms have contributed to reduce computation time and, therefore, enable application in (close to) real-time.

Contingency analysis

Contingency analysis is regarded as a static security assessment and is an important tool in every control room. When speaking about contingency it is usually referred to electrical faults of any type (e.g. three-phase fault), breaker faults/failure, transformer fault/failure or generator tripping. However, the definition of contingency depends on the specific grid operator. Steady-state contingency analysis includes the assessment of the operating conditions after any credible contingency by conducting load flow studies. It is also referred to as what-if analysis because it is analyzed what happens when a specific contingency occurs. The analyzed conditions include voltage limits, thermal limits of the lines and generator operating points. If unacceptable conditions after any contingency are identified, the control room operator needs to develop an action plan to drive the system into a state where the conditions after the contingency are acceptable [27]. This kind of assessment is usually referred to as N-1 criterion, where the power system is operated in such a way, so that it can withstand the outage of one major component. To improve this static approach, other aspects were incorporated in the assessment. A large-scale non-linear optimization model which considers the post-contingency steady-state security distance was proposed in [50]. The method shows to be able to identify the stable operating points that are close to the limits, thus, increasing operational efficiency by allowing less conservative results. An approach that incorporates dynamic line rating of transmission lines into N-1 security assessment was proposed in [51]. The authors showed that this approach can reduce REScurtailment and costs of dispatch but at the expense of higher computation time. Therefore, only selected transmission lines shall be considered to keep the computation time reasonably low. Hydro-Quebec has a lot of experience with contingency analysis. In steady-state, the contingency assessment is run in real-time to ensure thermal and voltage limits are not violated. Their analysis even considers extreme contingencies, such as loss of all lines in a corridor, and environmental contingencies, such as geomagnetic storms [52].

Stability assessment

In contrast to the static contingency assessment, it is important to analyze the dynamic behavior of the power system for different stability aspects. The critical question is: Can the power system survive all credible contingencies without becoming unstable? All relevant stability aspects are summarized in Fig. 2.4. Power system stability is divided in rotor angle stability, frequency stability and voltage stability. Frequency and voltage stability is also divided into short and long-term phenomena whereas rotor angle stability is a short term phenomenon. For each of the domains specific assessment tools were developed for offline analysis, but recent developments also focused on real-time stability assessment using PMU measurements [53]. As these stability phenomena do not only appear in a distinct way but as a combination of two or more stability phenomena, tools that consider several aspects were developed.

The Cigré working group C4.601 published an extensive review of the state-of-the-art dynamic security assessment techniques and tools [49]. Table 2.1 shows a selected list of tools that are either installed or under development worldwide. As the report is from 2007, the status of the tools/projects under development is updated with up-to-date information and a reference is provided by the author in 2017. Considering Table 2.1, it can be seen that transient and voltage stability assessment is well covered whereas small signal and frequency stability assessment is not. Another observation is that most of the tools are model-based and are not based on actual measurements. The European research and development plan for the European grid towards 2020 also points out the need for increased situation awareness by developing tools for real-time assessment of stability margins using measurement-based techniques [55].

The shortcoming of online tools for stability assessment was tackled by several projects in the last years. Two projects that have developed significant advances towards online stability assessment are mentioned here. First, the SOSPO (Secure Operation of Sustainable Power Systems) project focused on development of methods for real-time stability assessment, and intelligent wide-area prosumption control [53, 56]. The developed methods in the project are based on PMU measurements. The project resulted in numerous publications disseminating the novel approaches across the whole stability domain. For the whole set of publications, the reader is referred to the project website [57]. Second, the PEGASE (Pan European Grid Advanced Simulation and State Estimation) project developed two TD simulation prototypes of the European transmission grid to make it possible to analyze stability aspects on a Pan European scale, e.g. inter-area

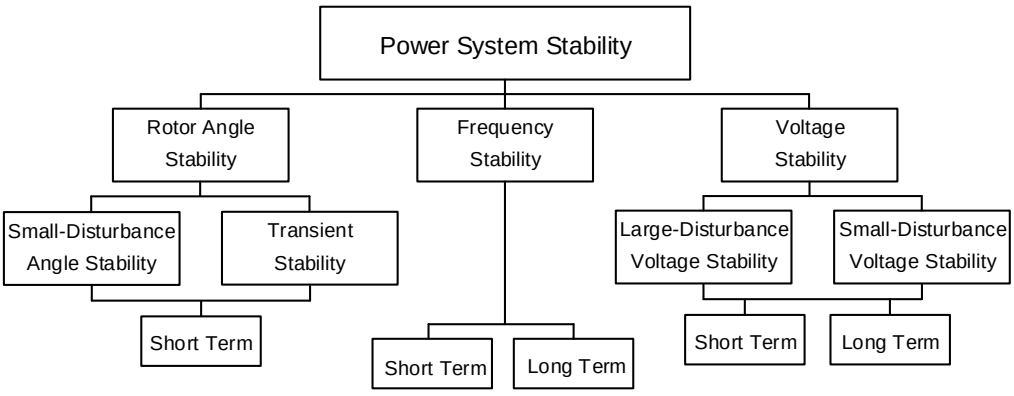

Figure 2.4: Classification of power system stability [54].

Table 2.1: State-of-the-art dynamic security assessment installations [49]. TSA: Transient stability assessment, VSA: Voltage Stability Assessment, SSSA: Small Signal Stability Assessment, FSA: Frequency Stability Assessment, MB: Measurement based, I/S: in service, O/S: tested but out-of-service, U/D: under development, N/U: no up-to-date information

Country	Location/Company/Proj.	Scope				Status
		TSA	VSA	SSSA	FSA	
Australia	NEMMCO	x		x (MB)	x	I/S
Bosnia	NOS	x	x			I/S
Brazil	ONS	x	x	x	x	I/S
Canada	BCTC	x	x			(U/D) I/S [59]
Canada	Hydro-Quebec	x	x			I/S
China	Beijing Elect. Power Corp.	x				I/S
China	CEPRI	x				I/S
China	Guangxi Elect. Power Co.	x		x	x	I/S
Finland	Fingrid		x	x (MB)		I/S
Greece	Hellenic Power System		x			I/S
Ireland	ESB	x	x			I/S
Italy & Greece	Omases Project	x	x			O/S
Japan	TEPCO	x	x			I/S
Malaysia	Tenaga Nasional Berhad	x	x			I/S
New Zealand	Transpower	x	x		x	I/S
Panama	ETESA	x	x			I/S
Romania	Transelectrica	x	x			I/S
Russia	Unif. Elect. Power System	x	x			I/S
Saudi Arabia	SEC	x	x			(U/D) I/S [60]
South Africa	ESKOM	x	x			(U/D) N/U
USA	PJM	x	x	x		I/S
USA	Southern Company	x				I/S
USA	Northern States Power	x				I/S
USA	MidWest ISO		x			I/S
USA	Entergy		x			I/S
USA	ERCOT	x	x			I/S
USA	FirstEnergy		x			(U/D) no N/U
USA	BPA		x			I/S
USA	PG&E		x			(U/D) I/S [61]
USA	Southern Cal Edison		x			(U/D) I/S [62]

oscillations [58]. To achieve a high performance in the TD simulations, novel algorithms and parallelization techniques were developed.

Wide-area monitoring and control

The deployment of geographically distributed and synchronized PMUs in power systems and dedicated ICT [64] has enabled the development of advanced wide-area monitoring systems (WAMSs) and wide-area monitoring and control (WAMC), or also WAMPAC. Figure 2.5 shows the general architecture of a WAMPAC system. GPS synchronized PMUs send measurements through a communication network to utility's and/or system operator's data concentrators or directly to the SCADA/EMS or specific applications. The data server provides the data in the needed format to the wide-area monitoring, and real-time protection and control tools. The data is also stored in an archive to allow post-disturbance or event analysis.

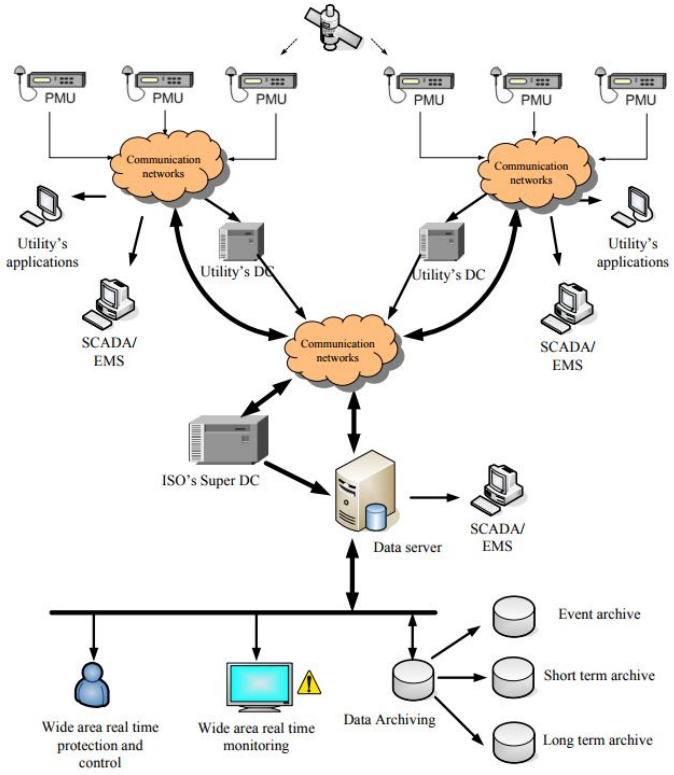

Figure 2.5: General architecture of a WAMPAC system. ISO: Independent system operator, DC: Data concentrator [63].

The motivation to deploy such a system is that transmission system conditions over large areas are monitored and instabilities and other issues are identified and resolved on a larger scale rather than locally [65]. In addition, WAMPAC allows for benchmarking and validation of power system models and design of adaptive protection systems [66]. wide-area monitoring has a long history at Hydro-Quebec, but with the PMU deployment new advanced methods were realized, e.g. real-time detection of geomagnetic storms that initiate preventive actions that are put in place by the control room operators, and oscillation monitoring [67]. Experiences in Norway showed that WAMS is suitable to monitor power oscillations and improve small signal stability by proper tuning of power system stabilizers (PSS) and use of area wide measurements as input signal [68].

2.3.3 Forecast of RES generation

The importance of forecasting wind and photovoltaics (PV) generation for power system operation and planning is acknowledged in several reports from different stakeholders [69–72]. The importance is even increasing with higher penetrations of RES. Wind and PV are the two main RES with uncontrollable varying output over time that are being installed. The power output fluctuations from wind and PV cover all time scales, i.e. daily, hourly and minutely. The variation of other RES, such as hydropower, biomass and geothermal is more apparent on longer timescales, i.e. yearly and seasonal. Figure 2.6 shows an example of variability and uncertainty of wind and PV generation over a two-day period, however, both resources entail the two characteristics.

As generation must meet demand at every time instance, this creates challenges for keeping the balance between generation and demand. These variations on the generation side are generally

compensated by ramping up/down conventional power plants that are constrained by their min./max. ramping rate and min. generation limits. Control schemes that allow control of active and reactive power setpoints of wind power plants partially smoothen the impact of the variability [73]. However, the uncertain forecast of RES generation creates a mismatch between actual generation and demand. To reduce the uncertainty and understand the impact of uncertainty on power system operation, numerous research articles have focused on investigation of these aspects.

Wind power forecasting can be categorized in two groups. The first group involves analysis of historical data, e.g. time series data of historical wind power production. The second group uses predicted values from a numerical weather prediction model as an input. Nowadays, traditional physical and statistical models get complemented with new data-driven approaches, e.g. neural networks. Additionally, there are hybrid methods that can involve aspects of different approaches [74]. For a comprehensive overview of forecasting models the reader is referred to [74]. A detailed review of probabilistic forecasting methods for wind power generation is presented in [75], describing forecasting methods classified into three categories regarding uncertainty representation, i.e. (non-) parametric probabilistic forecasts, risk index forecasts, and space-time scenario forecasts.

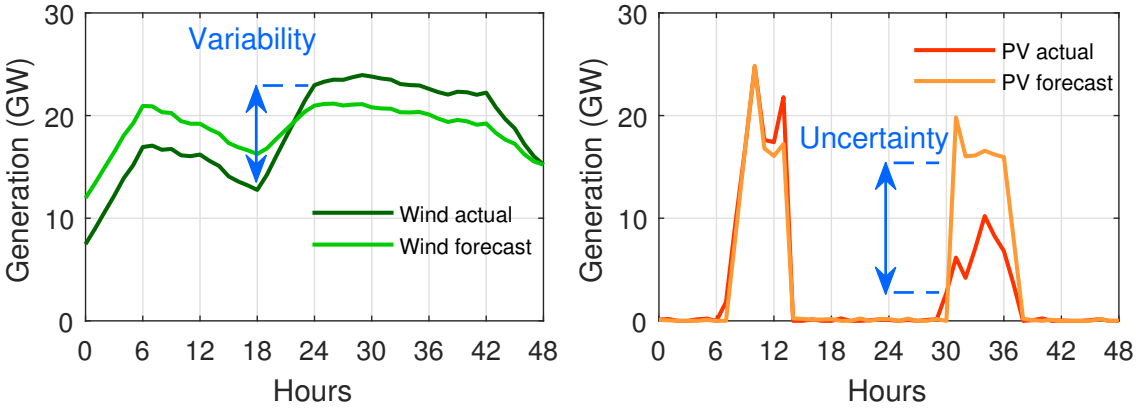

Figure 2.6: Variability and uncertainty of wind and PV generation over a two-day period (adapted from [76]).

2.4 Current challenges for observability and decision support tools

Conventional state estimators are usually run every few tens of seconds or even minutes due to computational limitations and communication delays. State estimators highly dependent on topology information and accurate line parameters to be able to produce accurate results. Proposed state estimation approaches that are based on PMU measurements rely on the assumption that future power systems will be equipped with numerous PMUs. In particular, high coverage of PMUs in distribution grids is inhibited by cost constraints due to the large size of distribution grids. Moreover, the infrastructure to manage these large data streams efficiently needs to be extended to allow for real-time application. However, historical data from existing or newly installed measurement sensors that are not available in real-time, such as smart meters or PMUs, can be used to establish data-driven models that benefit from both, historical non-real-time and actual real-time measurements. For example, historical data could be used to train neural networks for specific

applications and available real-time data is then input to the established model delivering results in real-time. The high degree of flexibility to combine different data sources makes data-driven approaches attractive for complex problems and development of online applications.

Security assessment methods in current control rooms are mostly based on offline analysis. The large number of possible contingencies and the computationally heavy TD simulations for the assessment pose a serious challenge. The accuracy of the security assessment strongly relies on accurate power system models, inaccurate models would lead either to too conservative results causing inefficient and expensive operation, or to results that lead to too small stability margins that might end up in instabilities or even blackouts. Well established steady-state models must be complemented with accurate dynamic models that represent the system characteristics after a fault to allow assessment for preventive control, i.e. changing the system's operating conditions before a contingency to ensure that the system can withstand it [17]. In that perspective, the steady-state and dynamic security assessments shall be carried out in real-time or at least close to real-time to provide the operator with a comprehensive view of operating boundaries and leave enough time to react on identified issues [77]. To allow real-time application, contingency screening to filter the most critical contingencies and efficient fast converging TD simulations are needed. In addition, the simulation-based approaches shall be complemented with measurement-based approaches to confirm and validate the results of the model-based analysis avoiding incorrect decisions [21]. Most protection schemes are based on local information that might not be sufficient to depict the state of the system appropriately. Real-time information shall be incorporated to build adaptable protection schemes with parameters that dynamically adjust to current grid conditions. This protection schemes could benefit from WAMS that include PMUs and smart meters.

Forecasting RES generation from utility-scale wind and PV power plants is an important asset for operators. Improved forecasts lead to increased value of RES because related challenges regarding cost and operation can be alleviated. It is expected that the forecasting will also expand to small-scale distributed wind and PV generation as the penetration becomes higher [78]. Other distributed resources are less mature regarding forecastability. With increasing deployment of EVs, an analysis of charging behavior and development of methods to forecast the demand are needed. From grid operator's perspective, the EVs shall be aggregated to form a single resource that can be used to support and enhance power system operation [79]. To represent EVs that are connected to the grid as a single asset, a model that allows aggregation over an arbitrary number EVs needs to be developed. The model shall be general so that it can be used for planning and operation.

An important note regarding the implementation of new tools into existing control rooms needs to be made here. Developing new tools, integrating them into the system and presenting the control room operator a visualization of the specific assessment is certainly not enough. The integration needs to be done in a holistic way not to overload the control room operator with too much unnecessary information [68]. Important information shall be highlighted and simple alarm functions shall warn the operator if issues are identified and decision support tools shall suggest possible solutions to resolve them.

2.5 Lessons learned from the ELECTRA project

ELECTRA is an EU FP7 project that investigated innovative approaches for real-time operation to accommodate the coordinated control of distributed resources accross all voltage levels including requirements and concepts for increased observability. Functionalities and requirements for future

control rooms in terms of observability and decision support were developed based on the results obtained in the related work packages. A condensed form of the lessons learned from the work related to increased observability and decision support is presented in the following while for the full results including an extensive discussion, the interested reader is referred to the public deliverables shown in Table 2.2 (available at electrairp.eu).

Table 2.2: ELECTRA deliverables concerned with increased observability and decision support

Deliverable	Work Package	Title
D5.1 [80]	Increased Observability	Adaptive Assessment of Future Scenarios and Mapping of Observability Needs
D5.2 [81]		Functional description of the monitoring and observability detailed concepts for the Distributed Local Control Schemes
D5.4 [82]		Functional description of the monitoring and observability detailed concepts for the Pan-European Control Schemes
D8.1 [83]	Future Control Room Functionality	Demonstration of visualization techniques for the control room engineer in 2030
D8.2 [84]		Demonstration of decision support for real time operation

A survey among six DSOs from four different countries consolidates the view on a changing role of control room operators in the future. The increased automation of distribution grids will essentially lead to more interaction of the operator with decision support systems which suggest operational actions to be taken. The surveyed DSOs also agree that monitoring and control concepts need to be taken even to the lowest voltage levels focusing on power quality and load flow management.

The survey participants foresee that DSOs will get additional responsibilities, e.g. in terms of maintaining active power balance in their area using regulation of distributed generation and demand response mechanisms. Generally speaking, local issues should be solved more locally. In ELECTRA, a new tuningless load frequency control scheme that actively engages distributed resources was proposed in [85]. These new controllers and activities require also new tools for decision support of the operator in an environment with an enormous amount of available data and tremendous complexity. However, the most important overall requirement is that all new types of activities and decision support systems, which interpret the data, contribute to guarantee the continuity and quality of service.

Great potential for improving the observability in control rooms is seen in the data from smart meters which can benefit state estimation, localization of faults, network reconfigurations after a fault, minimization of losses and voltage control. However, the most relevant observability needs were found to be state estimation and availability of reserves.

An increased need for sharing of grid information with neighbouring operators was determined. In particular operational information about actions that influence also the neighbouring grids should be shared. Additionally, information about the general state of the grid in terms of normal, alert or emergency operation could be shared to improve inter-area observability. In ELECTRA, the Pan-European reference grid was developed to derive novel observability concepts of large interconnected grids [86]. Concerning the area-wide observability of synchronously interconnected AC grids, monitoring of inertia was determined crucial to allow the shift to a converter-dominated

future grid. Low-inertia grids have significant faster frequency dynamics that need to be tackled by provision of synthetic inertia from converter-based units. ELECTRA introduced inertia control as a new control level to take place before primary frequency control to limit the rate of change of frequency (ROCOF). Therefore, in ELECTRA, the performance of synthetic inertia was compared to fast frequency containment control [87, 88] and how the grid frequency can be supported by EVs equipped with a synthetic virtual inertia controller [89].

Another important factor that was highlighted is that control room operators should be notified and presented the necessary information to understand the situation only when an issue is detected and its intervention is needed. If the system is operating in a normal state without any issues, the operator should have access to in-depth information at various levels. Future control rooms should shift to a modular architecture which allows integration of various new applications and visualization modules, and also replacement of existing modules. In addition, each operator should be able to customize its modules.

Geographical location of distributed resources was identified to become more important in order to allow to solve local problems efficiently. For example voltage control is a local problem and, therefore, it is important to have accurate locational information of the resources to make more optimal decisions.

Enhanced forecasting of numerous electric and non-electric variables was found extremely important to ensure the secure and efficient power system operation in the future. More frequently updated load and generation forecasts are necessary for the operator to foresee possible critical situations which allows proactive activation of preventive actions. Real-time weather and forecasting information possibly represented in geographic displays would further enhance observability. Another important aspect is the forecast of available flexibility. This is a challenging task as the flexibility is time-dependent and affected by specific resource characteristics. On top of that, a number of small resources should be aggregated to achieve a workable resource capacity.

In summary, due to the fact that observability decreases as the voltage level decreases, monitoring and control concepts are/should be taken down even to the lowest voltage level. This, in turn, produces tremendous amounts of newly available data which must be interpreted by decision support tools which present the operator prioritized actions for specific operational aspects. The overarching goal is to develop an integrated solution for all existing and new observability/decision support tools to enable seamless co-operation of them.

2.6 Summary

This chapter described the necessity of observability and decision support tools for managing the growing complexity of power system operation. Situation awareness is identified as one key requirement for secure and efficient grid operation. The most commonly used model of situation awareness that comprises the three levels perception, comprehension and projection into the future is described. In this context it is discussed how the current control room structure needs to transform to be able to manage the operation of the complex and distributed power system we are transitioning to. The transition to a smart future control room strongly relies on new observability and decision support tools that are either directly integrated into the SCADA/EMS or are added supplementary. Observability and decision support tools play a crucial role in ensuring secure and reliable power system operation by increasing situation awareness and supporting the control room operator's decision-making process by reducing the space for human error.

The chapter gives a comprehensive state-of-the-art overview of currently available tools related to state estimation, security assessment and forecasting of RES generation. A large portion of the observability and decision support tools are deployed as offline tools which is owed to several technical limitations, such as computationally heavy TD simulations, delays in communication equipment, and missing or delayed measurements. Moreover, model-based analyses must be combined or supplemented with measurement-based analyses to verify the results and identify issues, e.g. errors in the model. New methods need to bring observability and decision support (closer) to real-time to shift from reactive to proactive grid operation. These new methods can benefit from newly available real-time and non real-time measurements. However, the information that is presented to the control room operator must be based on a "need-to-know" basis, which means that actual crucial information needs to be highlighted and get the deserved attention from the operator. The integration of new tools into the control room environment must be done in a holistic way because more data does not necessarily mean more information. The findings in the ELECTRA project support the approach of an integrated solution for existing and new observability and decision support tools to allow seamless co-operation of them. In future control rooms, operators must be given more flexibility in getting customized information from the available tools when requested.

CHAPTER 3

Transient stability improvement techniques and decision support for preventive control

This chapter focuses on the research questions **[Q1]** and **[Q2]** which are outlined in the research objectives in Section 1.2 and are repeated below. First, the background of transient stability preventive and emergency approaches is described. Then, a review of techniques for transient stability improvement for both, preventive and emergency control, is presented. Foreseen future trends and specific deficiencies for the transition to RES-based power systems are pointed out. Following that, a decision support tool for transient stability preventive control is described. The tool analyzes the current grid state and suggests the control room operator a re-dispatch of generators if the transient stability margins are insufficient. This chapter includes content and results of **[Pub. A]** and **[Pub. B]** which are attached to the thesis.

[Q1] *What are the state-of-the-art techniques for transient stability preventive and emergency control and what are the deficiencies concerning the transition to a RES-based power system?*

[Q2] *How can transient stability be efficiently monitored and maintained in an online fashion?*

3.1 Background on transient stability preventive and emergency control for power system operation

3.1.1 Transient stability mechanisms

As pointed out in Chapter 1, maintaining and ensuring the transient stability of a power system is one of the key operational objectives to prevent severe disturbances and blackouts. Transient stability is the ability of a power system to maintain in synchronism after being subject to a large disturbance, e.g. three-phase fault or tripping of a large generator [54]. Transient stability belongs to the category of short term rotor angle stability, since this type of instability generally occurs within very few seconds after the disturbance inception. Transient stability is the fastest developing stability phenomena among the stability phenomenons mentioned in Fig. 2.4 [90]. Large disturbances will not only affect the rotor angle displacement of synchronous generators, but also other system variables, such as voltage magnitudes and frequency. Transient stability and short term voltage stability are closely linked and, thus, they often occur simultaneously. A large rotor angle displacement leads to a large voltage angle displacement that causes a progressive drop in bus voltages at intermediate points in the network close to the electrical center [54, 91, 92].

Due to the fact that transient stability is such a complex process, which is affected by many variables, a large number of improvement techniques can be found in the literature. According to [91], the techniques of transient stability improvement are aiming to achieve one or more of the following effects:

I) Reduction of the impact of the disturbance or the fault severity.

- Example: The impact of the disturbance can be reduced by using high speed breakers which results in reduced fault clearing time.

II) Increase of the synchronization forces to support the restoration of steady-state operation after a disturbance.

- Example: Synchronization forces can be increased by voltage support at a long transmission line using flexible alternating current transmission systems (FACTS) devices.

III) Reduction of the acceleration or deceleration power through control of the prime mover to meet the equilibrium of mechanical and electrical power.

- Example: Fast valving of thermal units can rapidly reduce the mechanical power supplied to the turbine during the disturbance in order to follow the reduced electrical power.

IV) Applying artificial load to SG to reduce accelerating power by increasing electrical power.

- Example: Activation of a braking resistor which increases the electrical load and, thus, allows to evacuate more electrical power from the generator.

3.1.2 States of power system operation

During power system operation, transient stability is controlled in two distinct ways. First, preventive controls are deployed to prepare the power system for future uncertain (but credible) disturbances which may occur. Second, emergency controls are applied to save the power system after a disturbance has occurred. Noteworthy, in the literature also approaches that combine preventive and emergency actions to systematically assess various tradeoffs between sufficiently moderate emergency control and economically acceptable preventive control are found [93]. The control room operator may select a suitable solution from the provided tradeoff solutions.

Both, transient stability preventive and emergency controls are needed for secure operation. Fig. 3.1 shows the different security states of power system operation. The security states are divided into three vertical levels that are called secure, insecure and asecure [90].

Secure state: The operation is secure when the system is in normal state, i.e. all operational limits, such as voltage limits are respected and security assessment confirms all stability margins are sufficient. At the same time, the power system economy is maximized. The security assessment is concerned with the analysis of whether a system is capable to withstand all credible contingencies. If that is not the case, the operational state is considered insecure, i.e. transition from normal to alert state. In extreme scenarios, a direct transition from normal to emergency state is possible.

Insecure state: In alert state, the power system is in normal operation without violating any physical constraints. However, the security assessment detected insufficient stability margins of

one or more stability aspects, e.g. transient stability margins. That means, the power system would not be able to withstand certain credible contingencies which may result in cascading outages or a widespread blackout. As seen in Fig. 3.1, the grey framed preventive state includes normal and alert state. The difference between these two states is, that in alert state preventive actions need to be taken to steer the system back into a secure operating region, i.e. normal state, whereas in normal state, preventive actions could be taken to increase the stability margins. Increasing the stability margins usually also increases the costs and, thus, a tradeoff between security and economy must be made in both, alert and normal state.

The restorative state is only reached after the system has passed alert and emergency state that led to a partial or total blackout. The restoration plan includes re-synchronization and load pickup among a variety of other aspects. This aspect is not discussed in further detail here as it is not in the focus of this thesis. The reader is referred to [94] which is a compendium compiled from 40 IEEE transaction and conference papers that covers a broad spectrum of power system restoration techniques.

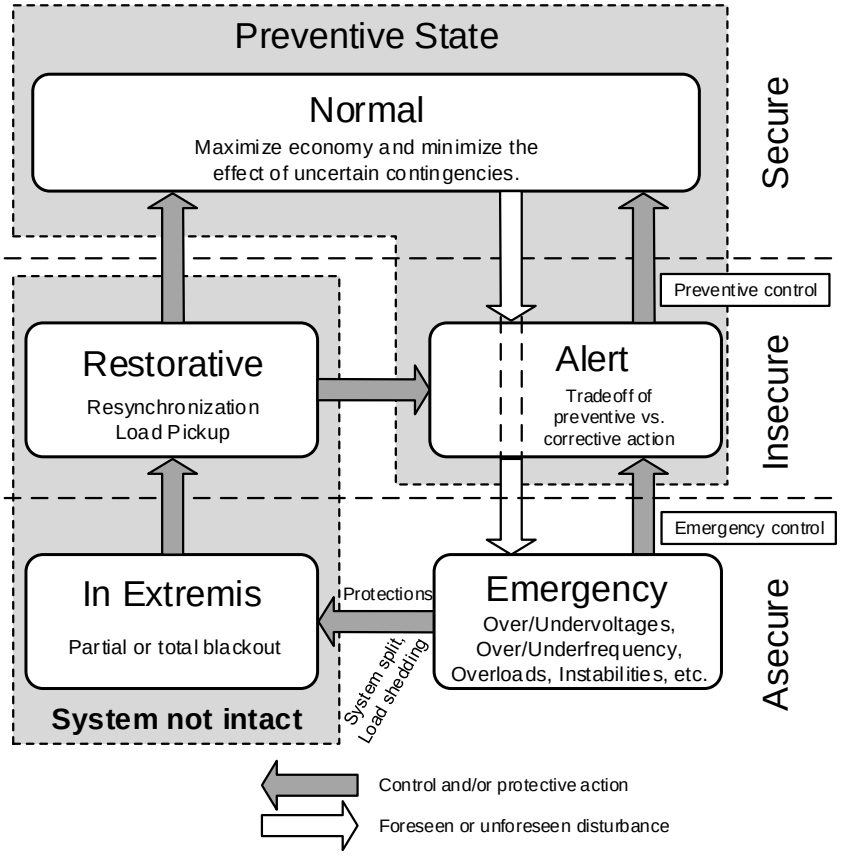

Figure 3.1: Security states of power system operation (adapted from [95]).

Asecure state: The asecure state comprises the emergency and in extremis state. In case of an extreme disturbance or insufficient deployment of preventive actions, the system moves to emergency state. In this state, voltages, frequency, thermal limits and/or other system variables exceed their normal operating limits. Immediate emergency actions have to be taken to bring back the critical variables and, thus, the system to alert and then to normal state.

Emergency controls are broadly classified into two groups: closed-loop and open loop controls [90, 96]. Closed-loop emergency controls analyze on basis of real-time data, if a contingency, that has actually occurred, will drive the system into an instability. If that is the case, the emergency control triggers appropriate control actions to avoid the instability, and observes the system evolution to make additional readjustments, if needed. The complete closed-loop cycle includes: a) predictive assessment of the instability, b) design of corresponding control action, c) decision making and triggering. For an effective emergency control, these tasks must be completed within a few cycles as transient stability is the fastest evolving instability. Therefore, even though closed-loop emergency control is appealing, in practical application it might be too slow for effective deployment, e.g. due to communication delays.

An interesting alternative is open-loop emergency control which automatically triggers pre-defined control actions just after contingency inception. The severity of the anticipated contingencies are identified on the basis of simulations and the appropriate (protection) devices are armed. Basically, these schemes are designed with a trial and error approach, using time-domain (TD) simulations [97–99]. Today, transient stability emergency control relies mostly on open-loop schemes [93].

3.2 Review and qualitative comparison of improvement techniques

This section presents a condensed version of the state-of-the-art transient stability improvement techniques for preventive and emergency control. Here, the focus is laid on techniques that are interesting from an operational perspective. For a detailed description of each technique, the reader is referred to [Pub. A]. Within preventive and emergency transient stability control, the techniques are categorized into conventional and renewable-based techniques. Conventional techniques are well established and have been widely employed in the past. Renewable techniques investigate how generators based on renewable energy sources (RES) can contribute to improve transient stability.

The techniques are compared qualitatively in the tables 3.1 and 3.2. Specific notes, an expected future outlook of each technique and the related references are given. Moreover, future research needs are pointed out.

3.2.1 Preventive improvement techniques - conventional

SG re-dispatch

Re-dispatch of synchronous generators (SGs) is one of the most effective and widely used preventive actions to ensure sufficient transient stability margins. The generators are re-dispatched in order to reduce the active power setpoint of critical generators while distributing the power to non-critical generators. The reduced active power setpoint moves the generators further away from the stability limit. As mentioned before, preventive actions are generally associated to increased operational costs. In order to operate efficiently, an optimal power flow (OPF) calculation is carried out to determine the dispatch. The transient stability constraints are usually derived in two ways. Either, transient stability constraints are derived from a TD sensitivity analysis, or the whole set of power flow equations is directly included in the OPF formulation [100–102].

The authors of [100] propose a 4^{th}-order Taylor expansion to speed up solving the OPF calculations including transient stability constraints. A linearization of transient stability contraints outside the

OPF calculation is proposed in [101]. This methods aims at reducing the complexity of the OPF formulation, thus, speeding up the calculation.

A decision support tool for transient stability preventive control is proposed in [Pub. B]. To reduce the computational burden of the TD simulations for the stability assessment, a pre-assessment contingency filtering is employed and a fast re-dispatch estimation is proposed. The approach is discussed in detail in Section 3.3.

Load shedding

Load shedding is most commonly associated with frequency regulation, i.e. under frequency load shedding as a last measure to prevent a power system from collapse due to a generation deficit. However, load shedding can also be used to reduce the loading of generators by reducing the demand. The reduced active power setpoint of the generator implies a reduction of the rotor angle and thus an increased stability margin.

A risk-based coordination of generation rescheduling and load shedding to improve transient stability is proposed in [103]. The authors first try to re-establish sufficient transient stability margins by generation rescheduling and if this cannot resolve the issue, load shedding is added to ensure that the system is within the defined security boundaries.

3.2.2 Preventive improvement techniques - RES-based

Temporarily increased voltage setpoint

Converter-based RES with reactive power capability, such as doubly-fed induction generators (DFIGs), full-scale converter-based wind power plants and PVs could operate at a higher voltage setpoint for a limited time span. This, however, is strictly constrained by the voltage limits of the particular grid as specified in the grid codes. The increased voltage setpoint improves the flow of synchronizing power. In [104], an approach to improve transient stability by increasing the voltage setpoint of DFIGs from 1 to 1.05 pu in pre-fault conditions is shown.

3.2.3 Emergency improvement techniques - conventional

Controlled system separation

Coordinated separation of a heavily disturbed system into two or more subsystems is a possibility to save (parts of) a system that is under risk of collapsing as a whole, i.e. prevent a generator or a group of generators from loss of synchronism. The aim of the system separation is to keep as much as possible of the power system operating and to minimize the disruption of consumers. Splitting the power system in real-time is a complex process. Therefore, different triggers to initiate the separation process and to determine the location for the separation are proposed.

The authors of [105] propose to predict the voltage phase difference 200 ms ahead based on online voltage waveform measurements. The system separation is triggered if the predicted voltage phase difference exceeds a certain threshold.

An approach to determine the optimal point of separation by analyzing the voltage fluctuations in the system is proposed by the authors of [106]. The highest voltage fluctuation determines the point of separation, hence, it is called the out-of-step center. According to this methodology, the separation interface, where the system is to be split, is derived.

In order to avoid tripping of out-of-step relays at undesired locations, blocking schemes by using blinders in the impedance plane for relays is proposed in [107].

In [108], the authors propose an approach to derive an a priori indicator based on the extended equal area criterion to determine whether the islanded power systems remain transiently stable after the network has been split or not.

The authors of [109] propose an islanding scheme that minimizes the power imbalance of the systems to be split by power flow tracing in order to minimize the power disruption.

An islanding scheme that uses a non-iterative spectral clustering approach is proposed by the authors of [110]. This allows to directly determine an islanding solution with minimal power flow disruption for any given number of islands.

High speed circuit breaker, single-pole operation, auto re-closing

During severe faults, generators are accelerating and picking up kinetic energy due to to the mismatch of mechanical and electrical power. The picked up kinetic energy is directly proportional to the fault duration, hence, it is desired to clear faults as fast as possible, i.e. the shorter the fault duration the smaller the severity of the disturbance [91, 111]. The tripping times of state-of-the-art high-speed circuit breakers are around 2 cycles for high voltage and one cycle for low- and medium voltage circuit breakers [112–114]. Fast overcurrent sensors and dedicated communication equipment are required to achieve this fast clearing times.

Circuit breakers with independent-pole operation where every phase can be operated separately can contribute to further transient stability improvement. Single-phase to ground faults can be cleared by switching off only the faulty phase instead of all three phases. That allows synchronizing power to flow on the remaining two phases. Moreover, the failure of one pole of the circuit breaker will not affect the operation of the other two poles [115]. Careful considerations regarding asymmetrical operation of generators due to flow of negative-sequence currents during the fault period must be made when using single-pole operation

Re-establishing pre-fault conditions by auto re-closing of the breaker can contribute to further improve the transient stability, i.e. re-establishing the transmission reactance and, thus, increase transmission capacity in post-fault conditions [91, 116, 117]. One main challenge is to find the optimal re-closing time because it has a major impact on the stability and research has been carried out on determining the optimal time for re-closure of the circuit breaker [118, 119]. As several power system properties, such as inertia, topology, and fault location influence the optimal re-closure time, no general rule for the optimal timing can be defined.

HVDC transmission link control

Due to long distances between generation and load centers, e.g. offshore wind power plants, high-voltage direct current (HVDC) systems are becoming increasingly important. HVDC systems that are based on voltage source converters (VSCs) using pulse-width modulation (PWM) are characterized by fast response time ($30 - 50$ ms) and precise control [120]. The high controllability can be utilized to support the AC system by fast and independent control of active and reactive power. Reactive power is usually controlled in constant voltage or droop mode. If the converters have low voltage ride-through (LVRT) capability, they can enhance the transient stability behavior

by reactive power provision during the fault. If the active power of the DC-link is controlled in constant power mode during the disturbance, no support is provided to the AC system.

The authors of [121] propose a model predictive control (MPC) based on online measurements that are collected through a wide-area monitoring system (WAMS). A sequence of control actions that maximize a transient stability index over a short time horizon is calculated in every discrete time instant. The used transient stability index combines acceleration power, coherency and energy. The control setting of the HVDC-link in steady-state conditions is the first action that was computed.

Three control techniques that add supplementary signals to the constant power control of converters are proposed by the authors of [122, 123]. The DC power flow control signal P_{DC} is comprised of the DC power flow setpoint P_{DC_0} and the supplementary signal for transient conditions DC_{suppl} as shown in (3.1).

$$P_{DC} = P_{DC_0} + P_{DC_{suppl}} \tag{3.1}$$

In the following paragraphs the three controllers are explained in more detail. The index R and I correspond to rectifier and inverter, respectively. K_P and K_D are the respective proportional and differential gains of the PD controllers.

i) The aim of the first controller is to provide synchronization power between the area where the SGs are rotating faster and the area where the SGs are slower. The respective rotor speeds ω_R and ω_I of the SGs that are located closest to the inverter and rectifier buses of the HVDC link.

$$P_{DC_{suppl}} = K_P(\omega_R - \omega_I) + K_D \cdot \frac{d}{dt}(\omega_R - \omega_I) \tag{3.2}$$

ii) The aim of the second controller is to minimize the voltage angel displacement between generators at either side of the HVDC link by controlling the DC power flow. The voltage angle displacement provides a good image of the mechanical rotor displacement and, therefore, the controller's input are the voltage angles φ_{V_R} and φ_{V_I} at both ends of the HVDC link.

$$P_{DC_{suppl}} = K_P(\varphi_{V_R} - \varphi_{V_I}) + K_D \cdot \frac{d}{dt}(\varphi_{V_R} - \varphi_{V_I}) \tag{3.3}$$

iii) The third controller modulates the DC power flow based on the inter-area power flow on AC tie-lines as shown in (3.4) where P_{TL_k} is the sum of all tie-line flows and k the number of tie-lines. This control strategy supposes well-defined control areas which are interconnected by HVDC links.

$$P_{DC_{suppl}} = K_P \cdot \sum_k P_{TL_k} + K_D \cdot \frac{d}{dt} \sum_k P_{TL_k} \tag{3.4}$$

These control concepts are only applicable to point-to-point HVDC transmission links. Control concepts for multi-terminal HVDC (MT-HVDC) systems are more sophisticated because more aspects have to be considered.

Three DC power flow control concepts for MT-HVDC based on local and global frequency measurements are proposed in [124]. Local measurements are used to compare the frequency to the nominal value and control the active power flow according to (3.2). Weighting factors are added to

the control signal to maintain the required active power balance of the MT-HVDC system. The global frequency measurements are used to inject a fixed supplementary active power considering the speed of the center of inertia (COI).

The authors of [125] propose a time-optimal control strategy to enhance transient stability by coordinated control of MT-HVDC system's power injections based on Lyapunov's theory.

3.2.4 Emergency improvement techniques - RES-based

Low voltage ride-through

Generally, LVRT capability of RES (and conventional units) improves the transient stability. The disconnection of a large portion of distributed generation during a disturbance would stress the power system even more. Hence, it is desired that RES units remain connected during faults within specified limits. The limits are defined in many network codes where generation units must comply with certain LVRT capabilities, e.g. reactive power provision during the disturbance. Conventional and renewable generation units in the five synchronous areas in Europe must meet the regulations of the network codes issued by ENTSO-E [126, 127]. However, in some countries national grid codes even specify particular requirements for wind and PV generation.

The Danish network code requires wind and photovoltaics (PV) power plants with an power output above 1.5 MW to stay connected for a certain time during disturbances of voltage and frequency [128, 129]. Generation units with a rated current up to 16 Amperes do not have any LVRT requirements [130].

Fig. 3.2 shows the requirements for wind and PV power plants in Denmark. The requirements for PVs are slightly more demanding than the requirements for wind power plants as they have to be able to withstand voltage drops down to 10 % of the voltage at the point of connection whereas wind power plants only down to 20 %. Germany and other European countries have similar requirements for wind and PV generation units [131, 132].

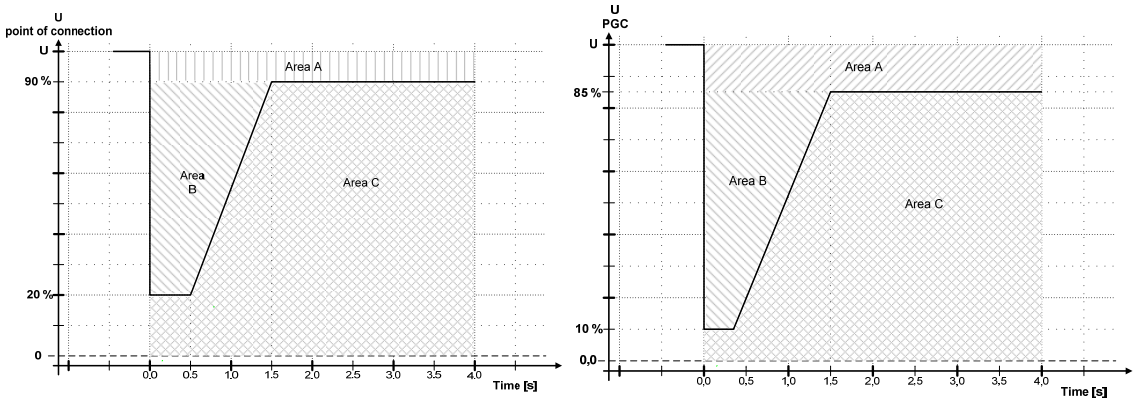

(a) Wind power plants > 1.5 MW

(b) PV power plants > 1.5 MW

Figure 3.2: Energinet's requirements for tolerance of voltage drops for (a) wind power plants and (b) PVs with a power output greater than 1.5 MW. **Area A:** The power plant must stay connected to the network and uphold normal production. **Area B:** The power plant must stay connected to the network provide maximum voltage support. **Area C:** Disconnecting the power plant is allowed. [128, 129]

Converter-based RES

Wind power plants of Type 1 and two with directly grid-connected induction machines (IMs) are not able to control the reactive power at their terminals, instead reactive power is consumed from the grid. During transient conditions, the reactive power consumption even increases. Due to that shortcoming, a large number of publications for transient stability improvement of IMs-based wind power plants using FACTS devices [133–141] are found in the literature. The main aim of the improvement approaches is to provide reactive power support. SVCs and STATCOMs are particularly suitable to provide reactive power support during transient conditions due to their good controllability and responsiveness.

Due to the drawbacks of Type 1 and 2 wind power plants, the trend moves towards configurations which allow reactive power control, i.e. Type 3 and 4 which are based on doubly-fed induction generators (DFIGs) and fully-rated converters, respectively. Recent analysis shows that there is a trend towards full converter configurations, whereas DFIGs which currently make the largest share of the market, are losing ground [142].

Besides wind power, solar PV generation is another promising RES which is connected to the grid through a converter. The authors of [143] investigate the impact of large-scale and distributed PV on the stability of the Ontario, Canadadian system. The analysis shows that the large-scale centralized PV system does not improve the transient stability whereas a trend for improvement is identified for increasing penetration of decentralized PV generation. A detailed review of power system challenges with large-scale integration of PV is presented in [144].

Virtual Inertia

With the increasing share of converter-based RES, the provision of virtual inertia to compensate the decreasing amount of inertia from SGs has gained more importance. Usually, virtual inertia is referred to frequency stability to limit the rate of change of frequency (ROCOF) and prolong the time for response of the controls. However, virtual inertia has also a substantial impact on transient stability, although, the installation of virtual inertia devices does not affect the inertia of SGs, but it may reroute some active power flows in the system and, thus, affect the critical clearing time (CCT), i.e. the stability margin, in certain situations. Since no research articles about the effect of virtual inertia on the transient stability of power systems can be found in the literature, it is not clear whether or not, virtual inertia has an exclusively positive impact on the overall transient stability of the power system. Therefore, this topic provides opportunities for further research.

Research articles in the literature propose virtual inertia provision using units which have stored additional energy, either in rotational or chemical form. Wind turbines of Type 3 and 4, and battery storages equipped with an 'inertia' control algorithm are suitable for virtual inertia provision.

In [145–147], the authors suggest an implementation of virtual inertia control of DFIG wind turbines using a derivative controller which uses the frequency as an input signal to modify the active power setpoint of the machine according to the ROCOF.

In [148, 149], the authors propose virtual inertia provision by adding a supplementary derivative control signal to the grid-side converter of Type 4 (type D) wind turbines. The supplementary control signal changes the active power setpoint of the grid-side converter by adding an active power contribution which depends on the deviation of the system frequency.

A general overview about virtual inertia of wind power plants was recently published in [150].

The authors of [151–154] propose virtual inertia provision based on PV power plants. The DC capacitor is utilized as an energy source to provide temporary additional power during virtual inertia provision.

A novel innovative approach to provide virtual inertia by using electric vehicles (EVs) is proposed in [87] and experimentally validated in [88]. The analysis was carried out considering the technical constraints imposed by IEC 61851 which specifies the general requirements for EV charging systems. Virtual inertia is provided by implementation of a droop control which modulates the current of the battery system depending on the ROCOF.

3.2.5 Discussion of the techniques and future challenges

The strengths and weaknesses of the transient stability preventive and emergency improvement techniques are highlighted by means of the qualitative comparison in Table 3.1 and 3.2, respectively. Here, no quantitative comparison of the techniques is presented because it highly depends on the selected network and the analyzed use cases. The following aspects are evaluated: Installation need of an additional physical device, investment costs and effectiveness in terms of overall system impact. Moreover, the most important considerations of each technique are highlighted and an expected future trend is indicated.

Generally, there are more conventional than renewable techniques for transient stability improvement, and there are many more emergency than preventive techniques. Due to the transition to renewable-based generation where a growing number of conventional units are being phased-out, new techniques to preserve transient stability utilizing new generation units must be developed for preventive and emergency controls.

Preventive techniques have to be enhanced to allow online transient stability monitoring including assessment of counteractions, if insufficient stability margins are identified. These preventive techniques have to be extended by non-disruptive approaches of stability improvement based on both, conventional and RES units. Techniques that need low investments and have low operational costs are preferred. Therefore, future research shall focus on developing new non-disruptive methods, which include RES units in existing preventive control strategies. Re-dispatch procedures could include RES units to relieve SGs if they are operated close to their stability limits. Conventional techniques that are constrained by grid limitations must be carefully considered at the grid planning stage to minimize subsequent investment costs, while preserving stability and a high reliability of electricity supply.

Conventional emergency techniques, such as fast excitation systems, generator tripping, high-speed circuit breakers including single-pole operation and auto re-closing, and controlled system operation will remain an important part of transient stability improvement. The need for shunt and series compensation devices will decrease as the increase of converter-based units poses opportunities for distributed voltage control for stability enhancement. The importance of dedicated control of HVDC links to support the AC system will increase with the increasing installation of HVDC links as they do not support the AC system when operated in constant power mode.

The literature provides a wide variety of techniques for transient stability emergency control. LVRT is already part of most grid codes as it is highly important to preserve stability whereas the (less

Table 3.1: Qualitative comparison of **preventive** improvement techniques (adapted from [Pub. A]).

	Conventional					Renewable
	Re-Dispatch	Load Shedding	Reduction of System Reactances	Upgrade of System Voltage	Variable Series Compensation	Increased Voltage Setpoint
Additional Device	No	No	Yes	No	Yes	No
Investment Costs	Low	Low	High	High	Medium/High	Low
Operational Costs	Medium	High	Low	Low	Low	Low
Effectiveness	High	Medium	Medium	High	Low/Medium	Medium
Notes	Additional costs due to dispatch to more expensive generators.	Last option due to customer interruption.	High investment costs are associated with new lines.	Limited by power system's voltage constraints.	Device design sets limitations for application. Resonance effects to be considered.	Limited by device capability and system's voltage constraints.
Future Trend	Inclusion of renewable generation in re-dispatch procedure.	Other techniques that do not disrupt customers are preferred. Generation located in distribution grids may be shed at the same time.	Distance between generation and load centers is increasing due to far off RES, e.g. off-shore wind parks.	To be considered when designing new grids. Not applicable for existing grids.	Careful cost-benefit evaluation before installation is needed.	Only to be used temporarily in situations with low stability margins.
References	[100–102], [Pub. B]	[103]	[91]	[91]	[155, 156]	[104]

Table 3.2: Qualitative comparison of **emergency** improvement techniques (adapted from [Pub. A]).

	Conventional									Renewable		
	Fast Excitation System	Braking Resistor	Fast Valving	Generator Tripping	Variable Shunt Compensation	Variable Series Compensation	Combined Series and Parallel Compensation	Controlled System Separation	High Speed Circuit Breaker; Single Pole Operation; Auto Re-Closing	Fault Current Limiter	HVDC Control	LVRT	Converter-based RES	Virtual Inertia
Additional Device	No	Yes	No	No	Yes	Yes	Yes	No	Yes	Yes	No	No	No	Yes
Investment Costs	Low/Medium	Medium/High	Low/Medium	Low	Medium/High	Medium/High	Medium/High	Low	Medium/High	Medium/High	Low	Low	Medium	Medium/High
Operational Costs	Low	Low	Low	Medium	Low	Low	Low	High	Low	Low	Low	Low	Low	Low/Medium
Effectiveness	Medium/High	High	High	High	Medium	Medium	Medium	High	High	Medium	Medium/High	Medium	Medium/High	Medium
Notes	Ineffective for nearby faults. Effective for far faults.	Careful cost-benefit evaluation necessary. Stress on shaft and other adverse effects may arise.	Can be applied to thermal units only. Showed to be effective when combined with braking resistor. Governor upgrade might be needed.	Stress on shaft due to overspeed and sudden load change.	Increases the synchronization power by voltage support at selected nodes.	Control of the effective line reactance during and post fault for improved stability.	Full controllability of series injected voltage in magnitude and angle but expensive equipment.	System separation so that least consumers are disrupted. Difficult dynamic process to determine the location to separate the system.	High speed breakers effectively reduce severity of disturbance. Single-pole operation might be critical due to asymmetrical operation. Difficulties in determining the optimal auto re-closing time.	Superconducting FCLs are sensitive to temperature, current and magnetic field variations whereas bridge-type FCLs include active elements to be controlled.	HVDC links operated in constant power mode do not support AC grid's oscillation damping. Reactive power support at terminals and dedicated active power controls enhance transient stability.	LVRT generally positive as disconnection of large amount of RES stresses power system even more.	Main aim of converter-based RES and STATCOMs is to provide fast responding reactive power support.	Virtual inertia gains more attention with respect to frequency stability, however, virtual inertia also influences the transient stability.
Future Trend	Will stay part of future transient stability improvement, but fewer units may be online because of the substitution due to RES.	Decreased use is foreseen due to transition to RES. Other techniques for RES-based generation to be used and/or developed.	Due to the limited applicability and transition to RES, decreased use is foreseen in the future.	Will still be one of the options for severe grid disturbances to prevent pole-slipping causing even more severe grid disturbances.	Less need for additional shunt devices as newly integrated converter-based RES could provide voltage support.	The foreseen increased number of HVDC connections will allow to control active power flow (and so voltage angle) to certain extend. Less need for serial compensation.	Decreased use of these rather expensive devices due to other emerging possibilities involving converter-based RES units.	Will still be part of grid defense strategy for severe disturbances to save the overall system from large blackouts.	Dedicated communication equipment is foreseen to improve speed and reliability of high speed breakers. Research on effects of asymmetrical single-pole operation and auto re-closing of breakers on RES-based generation is needed.	Fault currents in future power systems might decrease due to current-limited devices, such as converters. Might result also in lower need for fault current limiters.	Higher need for dedicated HVDC control with increasing number of HVDC lines. AC system needs to be supported in terms of voltage support and oscillation damping.	LVRT capabilities will be crucial in future systems with highly decentralized generation to avoid auto-disconnection of large portions of generation.	Trend towards WPP designs with reactive power capability (DFIG & fully-rated converter WPPs) decrease need for frequency control will also affect the transient behavior.	The relation of transient stability and virtual inertia must be investigated as the implementation of virtual inertia for supplementary STATCOM.
References	[115, 157, 158]	[159–161]	[162–164]	[165–168]	[169]	[170–180]	[181–184]	[105–110]	[111–119]	[185–192, 192–195]	[120–125]	[126–132, 196–198]	[133–144]	[87, 88, 145–154]

frequent) opposite case of high voltage ride-through (HVRT) is not always thoroughly defined in the grid codes. Temporary high voltages, e.g. caused by sudden load drops, could cause a large portion of RES units to disconnect. A discussion about HVRT and an evaluation of the need to include it into grid codes should be started. Virtual inertia is currently a hot topic with applications to frequency control, but the impact of virtual inertia on the transient stability behavior has not been sufficiently investigated. That aspect is certainly important to preserve stability and definitely needs attention to enable the transition to future low inertia systems.

The qualitative comparison showed that a mix of conventional and RES-based techniques will be needed in a future power system based on diverse and distributed RES. Conventional techniques need to be further developed and new techniques for RES-based generators need to be investigated.

3.3 A decision support tool for transient stability preventive control

As pointed out in Chapter 2, the power system operation must shift from a reactive to a more proactive operation. That means, preparing the power system for disturbances that might occur in the near future by changing the operating conditions in a way that the power system can withstand the disturbances. In addition to that, and as pointed out in Section 3.2, non-disruptive preventive control approaches need to be further developed.

The main scientific advances of the proposed approach are twofold. First, a novel fast converging technique to determine the needed dispatch for re-establishing a predefined stability level is introduced. Second, the proposed approach combines transient stability assessment, determination of preventive dispatch and analysis of critical contingencies to enable online application.

3.3.1 Description of the approach

The proposed online decision support tool for transient stability preventive control builds up on existing tools, which are improved and extended. The input is the current grid state and the developed tool analyzes the grid's capability to withstand three-phase faults for a user-specified duration (desired limit, minimum CCT, further called CCT_{lim}) at the most severe locations (buses) of the grid. A TD approach considering the full dynamics of the grid is used to assess the transient stability on a grid-wide basis and, if CCTs below the desired limit are identified, a re-dispatch of the SGs is suggested to the control room operator to re-establish the desired stability margins. As TD simulations are computationally heavy and the tool is intended to support control room operators in taking their decisions, a critical bus screening (CBS) is carried out prior to the assessment. To get a tradeoff solution between the economic aspect and stability margin, which is crucial for preventive measures, consecutive OPFs are carried out to minimize the generation costs while respecting the technical constraints. The derived re-dispatch presents the best tradeoff solution between costs and stability. Here, the minimum desired CCT (CCT_{lim}) is assumed to be 200 ms which is a reasonable limit as it can be assumed that the protection equipment will detect and clear the fault by opening the breakers within this time span [199]. The needed re-dispatch for re-establishing the desired CCT and the associated costs are presented to the control room operator who has to make the final decision whether to apply the proposed re-dispatch or not. The operator may also introduce additional constraints, e.g. the unavailability of generators to take over the dispatched power and re-run the procedure, taking into account the additional constraints. The flow chart of the proposed transient stability preventive control approach is shown in Fig. 3.3. The flow chart is comprised of the elements which are needed to establish the transient stability preventive control and visualizes how they interact. In the following each element is described comprehensively.

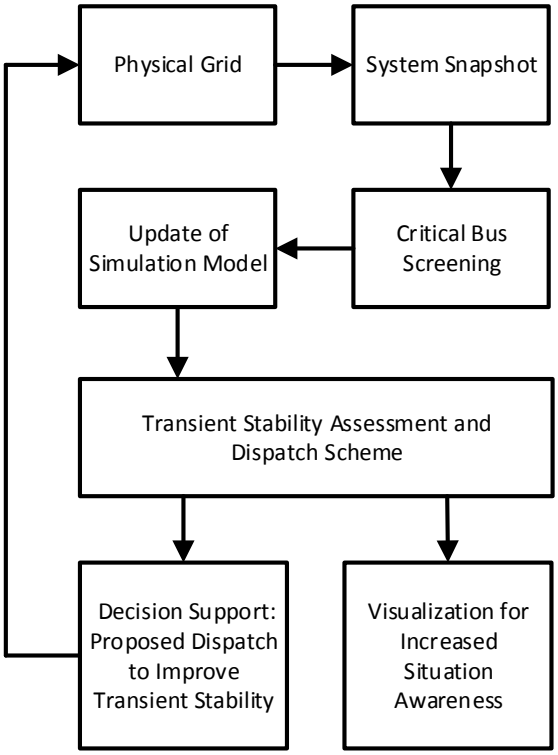

Figure 3.3: Flow chart of the transient stability preventive control approach [Pub. B].

Physical grid

This block represents the real physical grid, for which the transient stability control is applied. The control room operator makes the decision whether or not the suggested re-dispatch is applied to the physical grid. This is represented by the feedback from the decision support to the physical grid block.

System snapshot

The current system snapshot is needed to provide updated information to the TD simulation model. Three possible variants to obtain a system snapshot are envisioned.

The first variant extracts the data from the existing SCADA system or EMS. The extracted data includes: breaker status, generation output, activation of capacitor banks, RES generation, line flows and further relevant data. This is currently possible, but snapshots are provided with a low refresh rate.

The second variant directly uses phasor measurement units (PMUs) to obtain a system snapshot, hence, full observability of the power system by PMUs is assumed. In this case, snapshots would be available in real-time, but it is expensive to have PMUs deployed everywhere in the grid.

The third variant is a combination of the two previous variants using both supervisory control and data acquisition (SCADA) and PMU data to obtain the needed information [200]. This variant is a good option if more frequent snapshots than in variant one are required.

Critical bus screening (CBS)

The CBS is carried out prior to the update of the simulation model. The CBS aims at determining the most critical fault locations within the system based on the current system snapshot. Here, the focus is on assessing bus bar faults. Therefore, in the following the term critical buses is used, instead of the more generic term critical fault location. Potentially critical buses with regard to three-phase faults are identified by analyzing the pre-disturbance conditions. The CBS identifies the potentially critical buses solely by means of the pre-disturbance conditions without the need for TD simulations. This significantly reduces the needed computational time for further assessment as only the set of potentially critical buses is considered in the further procedures.

The approach of the CBS is based on the work presented in [201–203]. The buses which are regarded as most critical are identified heuristically. The buses are scanned for three criteria indicating their criticality. Only buses which satisfy all three criteria are regarded as critical and qualify for the analysis in the TD simulation. Table 3.3 summarizes the three criteria of the CBS including the thresholds that are suggested by the authors of [201–203].

Table 3.3: Summary of the Critical Bus Screening Criteria [Pub. B].

Criterion	Formulation	Suggested Threshold
1	$V_{bus} \geq V_{min}$ $ln \geq ln_{min}$	highest voltage level $ln_{min} = 2$
2	$n_{min} \leq \frac{P_{in}}{P_{SG}} \leq n_{max}$	$n_{min} = \{0.5 - 0.75\}$ $n_{max} = \{1.2 - 1.5\}$
3	$P_{out} \geq P_{out,\,min}$	$P_{out,\,min} \approx 0.01 \cdot P_{SG_{tot}}$

The three criteria are only briefly described here. For a detailed description of the three criteria, the interested reader is referred to [Pub. B].

- *Criterion 1 - Bus Properties:* This criterion consists of two sub-criteria. The voltage level of the bus V_{bus} has to be above the specified threshold V_{min} and the bus must be connected to at least one other bus by at least two in-service transmission lines ($ln \geq 2$).

- *Criterion 2 - Bus Injected Active Power vs. Generator Active Power:* The active power P_{in}, which is injected in the bus, is compared to the active power P_{SG}, produced by synchronous generators in the vicinity of this bus. The vicinity of the bus is defined as one or two buses away from the generator bus. The lower and upper thresholds for the injected active power are defined as follows:

  - The injected active power of the bus must be greater than the specified threshold n_{min} and is suggested to be between $50 - 75$ % of the active power produced by the SGs in the vicinity of the bus. This lower threshold makes sure that locally produced active power flows to the bus.
  - The injected active power of the bus must be lower than the specified threshold n_{max} and is suggested to be between $120 - 150$ % of the active power produced by the SGs in the vicinity of the bus. This upper threshold ensures that long distance flows are excluded.

- *Criterion 3 - Bus Leaving Active Power:* The amount of active power P_{out} which is leaving the bus on transmission lines (power flows on transformers are not considered) must be greater than the specified threshold $P_{out,\,min}$ and is suggested to be approximately 1 % of the total active power $P_{SG_{tot}}$ produced by the SGs of the system. This puts into perspective the active power that leaves the bus with the total generated active power of the considered power system.

Update of simulation model

The real power system that is represented as a simulation model has to be updated with the data from the current system snapshot. The data includes generator schedule, breaker status, dispatch of capacitor banks and RES generation. After the simulation model is updated, it is ready to be used in the TD simulation. In addition to the update of the simulation model, the results of the CBS are stored in a list which contains the identified potentially critical buses. Only these buses are further considered.

Transient stability assessment and dispatch scheme

The potentially critical buses are analyzed in the transient stability assessment and dispatch scheme which is the core of the approach. The assessment utilizes a hybrid approach using an estimation of the necessary re-dispatch combined with TD simulations. Fig. 3.4 shows the flow chart of the dispatch procedure. The goal of the proposed procedure is to determine the dispatch volume that is needed to achieve the desired CCT and return the system in a safe state. At the same time, all technical constraints must be respected and costs minimized.

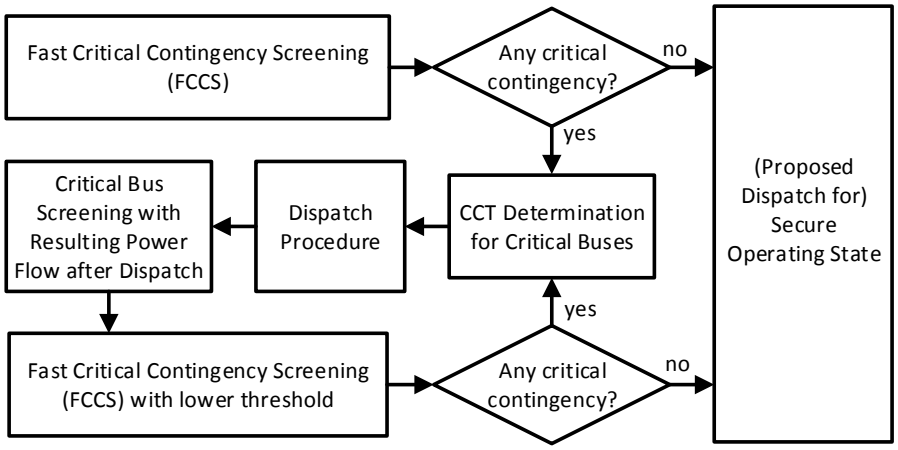

Figure 3.4: Flow Chart of the Transient Stability Assessment and Dispatch Scheme [Pub. B].

Fast critical contingency screening (FCCS): The potentially critical buses, identified by the CBS, are subject to a fast critical contingency screening (FCCS) which ultimately identifies if a certain bus is critical or not. The FCCS carries out TD simulations and delivers yes/no decisions whether the system can withstand three-phase faults for the duration of the desired limit CCT_{lim} at the potentially critical buses without any generator(s) losing synchronism. This separates the critical from the non-critical buses by indicating whether the CCT for a three-phase fault at these buses is above or below the specified limit. However, no margins or CCTs are calculated in this step. This step solely aims at separating critical from non-critical buses.

Decision: The FCCS evaluated whether buses are critical or not. If no critical buses are identified, i.e. none of the applied three-phase faults caused a loss of synchronism, the assessment ends and the system is in a secure operating state with respect to transient stability. If the FCCS identified critical buses where SGs are losing synchronism, the procedure continues with the determined set of critical buses.

CCT determination: For the set of critical buses, CCTs are determined up to an accuracy of three decimals and the associated SGs which lose synchronism are noted. These SGs are regarded as the critical generators and their active power has to be re-dispatched, i.e. reduced by a certain amount. The CCT is numerically determined within DIgSILENT PowerFactory environment using a DPL-script [204]. Consecutive bolted three-phase faults are applied on each line close to the bus bar and removed by opening the breakers of the line after varying durations until the lowest CCT is found. At the end of the procedure, all CCTs that are lower than CCT_{lim} and its associated critical SGs are determined.

Dispatch procedure: The dispatch procedure starts with the SG which is associated with the bus with the lowest CCT and continues consecutively with the CCTs in ascending order. Starting the procedure from the lowest CCT and continuing in ascending order has two main reasons. On the one hand, this prevents a too large re-dispatch, due to the fact that the CCTs at adjacent buses can be close to each other whereas, generally, the bus that is closer to the SG has a lower CCT. On the other hand, the number of required iterations to reach the optimal dispatch is reduced because the re-dispatch of one SG usually also affects the stability margins of adjacent SGs. If the newly calculated setpoint for the generator is not compatible with the current setpoint, e.g. the time window given for ramping the generator is too short, a new OPF, considering this new constraint, is calculated.

The dispatch procedure consists of four steps that are briefly described in the following. For a detailed description, the interested reader is referred to [Pub. B].

- *Step 1:* Note the initial power setpoint of the SG with the lowest CCT. The two variables of the initial condition are called P_{init} and CCT_{init}, respectively.
- *Step 2:* To get the first estimation, it is proposed to use the linear approximation shown in (3.5) to (3.7), where η represents the ratio between initial and desired minimum CCT and m the dispatch estimation factor, which is used to calculate the estimated power setpoint P_{est} from the initial setpoint P_{init}.

  The idea behind the linear approximation of the active power using the CCT ratio originates from the almost linear relationship between the two variables. However, the relationship is not exactly known unless several power-CCT pairs are determined, which poses a computational burden and, thus, the approximation is proposed. The proposed relationship of m and η is determined heuristically, i.e. by simulation of numerous scenarios with different grid configurations, however, the relationship may need to be adjusted for different grids.

$$\eta = \frac{CCT_{init}}{CCT_{lim}} \tag{3.5}$$

$$m = \begin{cases} 0.5 \cdot \eta + 0.5 \; for \; \eta \geq 0.7 \\ 0.6429 \cdot \eta + 0.4 \; for \; \eta < 0.7 \end{cases} \tag{3.6}$$

$$P_{est} = m \cdot P_{init} \tag{3.7}$$

- *Step 3:* The estimated power setpoint P_{est} is used as the new power setpoint of the SG. The difference of power between the initial and the new setpoint is distributed to other SGs using an OPF calculation minimizing the costs of generation considering all technical constraints. The active power setpoints of other critical SGs are locked, i.e. they cannot increase their active power setpoint. The OPF calculation determines the new setpoints.

- *Step 4:* With the mentioned PowerFactory script, the CCT for the new load flow condition is calculated and is in the following referred to as CCT_{est}. Since the power setpoint is estimated, the respective CCT will (most likely) not match CCT_{lim} but be close to it. Therefore, a linear inter- or extrapolation between the initial and actual setpoint is carried out to obtain the next active power setpoint P'_{est} (see Fig. 3.5). CCT'_{est} for the new setpoint P'_{est} is determined and the procedure is terminated if CCT'_{est} lies between ± 5 ms of CCT_{lim}. This ± 5 ms accuracy band is suggested in order to avoid too many iterations.

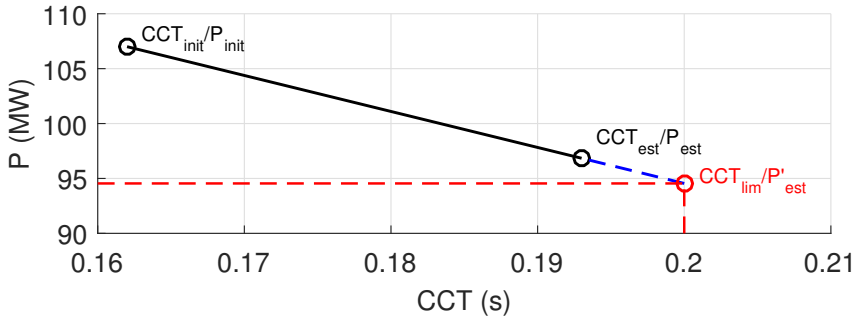

Figure 3.5: Extrapolation of initial and estimated condition to obtain the next power setpoint P'_{est}, for which CCT'_{est} is determined. (Values of the plot are irrelevant, but they are shown for clarity [Pub. B])

CBS with resulting power flow after re-dispatch: Once the re-dispatch of all critical SGs is determined, another CBS is carried out to identify the critical buses of the new load flow condition. That step serves as preparation for the final FCCS.

FCCS with lower threshold: Another FCCS is needed to verify if the re-dispatch has re-established the desired transient stability margins in the whole system. Since the dispatch procedure introduces an accuracy range of ± 5 ms of the desired CCT (see step 4 of the dispatch procedure) to avoid too many iterations, the final FCCS is executed with the lower limit of the accuracy range, i.e. $CCT_{lim} - 5$ ms. If the FCCS identifies CCTs below that limit, the procedure starts again from the CCT determination.

Secure operating state: The operational state of the system is considered secure in terms of transient stability if no further violations are identified. The procedure is completed and the results are presented to the control room operator.

Visualization and decision support for the control room operator

The results of the transient stability assessment and the suggested re-dispatch are presented in comprehensive but condensed form to the control room operator as shown in Fig. 3.7. The visualization comprises a graphical representation of the CCTs of the buses of the initial condition and after the suggested re-dispatch. To give the operator more details, a table presents numerical

information about the CCTs and power setpoint of the critical SGs. As the preventive re-dispatch involves additional costs, the associated costs of the re-dispatch are stated. The control room operator can interact with the decision support tool to make specific changes if the suggested re-dispatch does not meet the requirements, e.g. blocking the setpoint of a generator for the re-dispatch due to unavailability. Then, the tool restarts the procedure considering the additional demands of the operator and provides a new re-dispatch suggestion.

The amount of information presented to the control room operator is kept low in order not to overload it and to facilitate fast comprehension of the current condition. However, it is important that this information shall only be shown if insufficient margins are detected and an action needs to be taken by the operator. If sufficient margins are given, the operator's attention does not need to be drawn to this information, hence, attention can be paid to other operational tasks. In case of insufficient margins, warning signals could be generated signalizing different levels of severity, e.g. depending on the size of the critical unit. Moreover, the control room operator should have the possibility to get access to in-depth information, e.g. reactive power setpoints.

3.3.2 Case study: New England system

The New England test system with 39 buses and 10 SGs, shown in Fig. 3.6, is used to show the capabilities of the approach. The New England system represents a medium-sized grid and it is used to show that the approach is robust when taking into account a larger grid with numerous components and complex dynamic behavior. The approach is also applied to a nine-bus system to highlight the steps of the procedure while keeping the complexity low. For that, the reader is referred to [Pub. B].

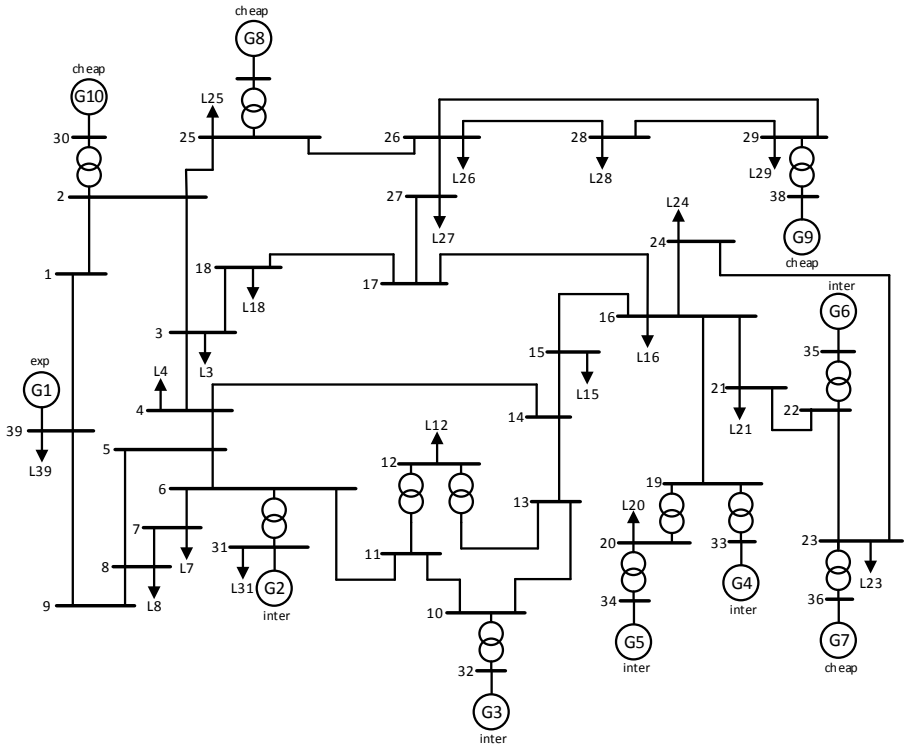

Figure 3.6: New England System with indication of associated cost functions: cheap (cheap), intermediate (inter) and expensive (exp) [Pub. B].

A few minor changes are introduced to the system described in [205]. The nominal frequency is set to 50 Hz and all generators are operated in PV-mode with voltage setpoints of 1.02 pu. G_1 serves as slack generator. The initial operating point is determined by an OPF calculation, minimizing the generation costs. Standard linear cost functions that can be found in [Pub. B] are used. Loads are modelled as voltage and frequency dependent (P = const. current, Q = const. impedance, f_p = 1.5, f_q = -1) [86]. The voltage dependence is defined according to the ZIP definition, the frequency dependence is linear and the parameters are set according to the common practice for stability studies [206].

In the following all elements of the transient stability approach are shown.

CBS: The thresholds of the CBS and the potentially critical buses are shown in Table 3.4. Thirteen out of 39 buses are identified to be potentially critical. That means, the computational effort is significantly reduced because only one third of the buses has to be considered in the further assessment.

FCCS: The FCCS identified the buses 21, 22, 23 and 29 as critical. That means a further reduction to only four actually critical buses.

Table 3.4: Thresholds and results of CBS and FCCS [Pub. B]

Criterion	**Threshold**
1	$V_{min} = 345\,kV$, $ln_{min} = 2$
2	$0.6 \leq \frac{P_{in}}{P_{Gen}} \leq 1.4$
3	$P_{out,\,min} = 62\,MW$
Potentially Critical Buses According to CBS	
2, 5, 10, 11, 13, 16, 21, 22, 23, 25, 26, 29, 39	
Buses, Identified as Critical by FCCS	
21, 22, 23, 29	

CCT determination: The CCTs of the four critical buses are determined. The CCTs are equal to 0.181 s, 0.137 s, 0.153 s and 0.158 s for bus 21 (G_6), 22 (G_6), 23 (G_7) and 29 (G_9), respectively. The associated critical generators are given in brackets. As expected, all CCTs are below the specified limit and considered critically low.

Dispatch of G_6:

- *Step 1:* The dispatch starts with the lowest CCT, which is 0.137 s at bus 22, caused by G_6. The initial active power setpoint and the associated CCT are noted.
- *Step 2:* The estimated dispatch is calculated by using the formulas (3.5)-(3.7) and results in $P_{est}^{(G_6)} = 423.47$ MW.
- *Step 3:* The estimated power setpoint for G_6 is fixed in the OPF calculation. The setpoints of G_7 and G_9 are also fixed as they are critical, i.e. their maximum active power setpoint is limited to the initial one.

- *Step 4:* The CCT for the new load flow condition is determined and it is equal to $CCT_{est}^{(Bus\ 22)} = 0.173$ s. The linear extrapolation between the initial and new conditions, according to Fig. 3.5, results in $P'\ (Bus\ 22)_{est} = 363.14$ MW and $CCT'^{(Bus\ 22)}_{est} = 0.199$ s. The dispatch of G_6 is terminated as $CCT'^{(Bus\ 22)}_{est}$ lies between $CCT_{lim} \pm 5$ ms.

Dispatch of G_7 and G_9: After the dispatch of G_6, the same procedure is carried out for G_7 and G_9. Table 3.5 shows the variables during the dispatch procedure.

Table 3.5: Variables during the dispatch procedure of each generator [Pub. B]

	G_6		G_7		G_9	
	P_g (MW)	CCT (s)	P_g (MW)	CCT (s)	P_g (MW)	CCT (s)
initial	503.90	0.137	594.98	0.155	620	0.158
est	423.47	0.173	528.04	0.2	554.90	0.207
est'	363.14	0.199	-	-	564.19	0.199

Discussion of the case study

Table 3.5 shows the active power setpoints and its resulting CCTs throughout the re-dispatch procedure. The procedure for all three SGs converges within one iteration. The estimated setpoint for G_7 is already correctly approximated and the linearization between initial and new condition is not necessary. That indicates that the linear estimation of the re-dispatch setpoint by means of the initial condition works well. The CCTs and active power dispatch of the initial condition and after the dispatch procedure are summarized in Fig. 3.7. All CCTs meet the specified limit after the successful re-dispatch. The CCTs at bus 23 and 29 are exactly at the limit, whereas bus 22 is even more elevated than it was actually determined. Due to the close proximity of G_7 to G_6, the re-dispatch of G_7 also affected the CCT at bus 22. That shows the influence of the generators in close proximity and, hence, only a near optimal solution is found which is one of the drawbacks of the sequential approach.

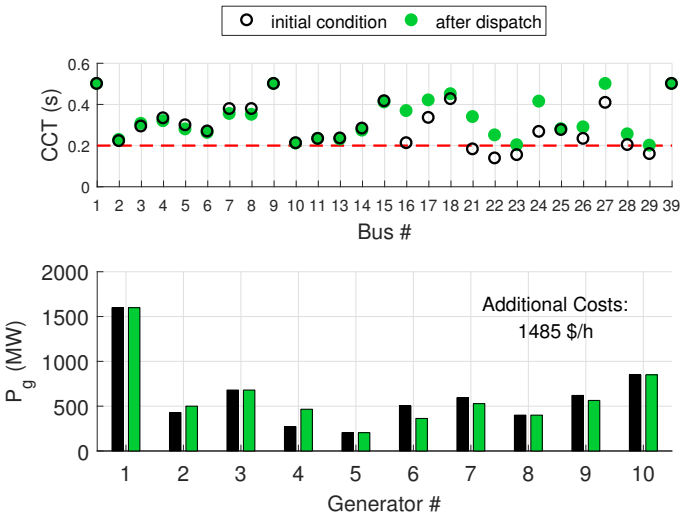

Additional costs of dispatch: 1485 $/h					
	critical CCTs (s)				
Bus	21	22	23	29	
initial	0.181	0.137	0.153	0.158	
after	0.338	0.249	0.201	0.199	
	Pg (MW)				
Gen.	2	4	6	7	9
initial	427.8	272	503.9	595	620
after	500	465.9	363.1	528	564.2
delta	+72.2	+193.9	-140.8	-67	-55.8

Figure 3.7: CCTs and active power setpoints for initial condition and after successful dispatch [Pub. B]

3.3.3 Evaluation of the execution time of the assessment

For online application of the tool it is of crucial importance that the results of the assessment are delivered within a reasonable time, irrespectively of the size and complexity of the power system. Therefore, the execution time for three systems of different size are evaluated. The execution time for the nine-bus [207], New England and for the IEEE 118-bus test system [208] is analyzed.

Table 3.6 shows the results of the execution time assessment. To make the results comparable between the different sized power systems, the execution times are expressed as execution time per critical bus fault location, i.e. the total execution time of the different process steps is divided by the number of assessed buses for which it is carried out. The CBS is only shown for the New England system and is equal to 0.103 s. For the two other buses it was not implemented, but it can be expected to be in the same order of magnitude as the calculation complexity of this step is fairly low. The determining factors of the overall execution time are the CCT and FCCS calculations which have the highest execution time per bus. However, the CCT determination strongly increases with the system size and is therefore seen as the most critical part of the assessment time. The overall execution time is not presented as it does not provide insightful information because it highly depends on the state of the system, i.e. the number of buses, for which the FCCS is carried out and the CCT has to be determined. The execution time of the OPF is also relatively small compared to the other process steps because the optimization only considers the costs. Noteworthy, the execution time of the OPF will increase with increased complexity of the problem, e.g. inclusion of additional objectives. Hence, careful considerations regarding execution time need to be made when increasing the complexity of the OPF by including additional objectives and constraints. As expected, the observed execution times increase with increased grid size.

Table 3.6: Results of the execution time evaluation

System	# of SGs	CBS (s)	FCCS/Bus (s)	CCT/Bus (s)	OPF (s)
9-Bus	3	-	0.3	1.13	0.2
39-Bus	10	0.103	0.85	2.59	0.4
118-Bus	54	-	1.08	6.95	0.75

However, the presented execution times have not been optimized and have been achieved on a standard laptop (quad-core i7 4600, 8 GB RAM) with PowerFactory V 15.2 and Matlab 2016b software. One should bear in mind that the execution time will be reasonably lower with more powerful units that are used in control rooms. In addition, the implementation of the assessment has a significant impact on the execution time, e.g. the authors of [209] claim that they can assess the CCT of 39.000 buses within minutes. Therefore, it is expected that an efficient implementation of the presented approach, paired with more powerful hardware, will result in acceptable execution times suitable for online application. In accordance with [210], an execution time within 15 min is seen as a reasonable time horizon for online application.

3.4 Summary

This chapter presented a review of the state-of-the-art transient stability improvement techniques and a decision support tool for transient stability preventive control. The background of transient stability preventive and emergency control and its relation to the power system operation states is

presented. The different transient stability mechanisms are described first, and a comprehensive overview of the state-of-the-art improvement techniques for both preventive and emergency control aiming at these stability mechanisms is presented. The review of the state-of-the-art transient stability techniques revealed deficiencies related to the transition to a RES-based power system.

Preventive techniques need to be extended by non-disruptive approaches based on both, conventional and RES-based units. Preventive approaches need to be enhanced to allow online monitoring of transient stability including assessment of possible counteractions if insufficient stability margins are identified. Moreover, future research shall focus on novel preventive approaches that include RES generation units in existing preventive control strategies.

Existing conventional emergency techniques, such as fast excitation systems, generator tripping, high-speed breakers including single-pole operation and auto re-closing, and controlled system separation will remain an important part of future transient stability schemes. The increase of converter-based units poses opportunities for distributed voltage control aiming at stability enhancement. The increasing number of HVDC links increases the importance of dedicated controls to support the AC system during disturbances as HVDC links operated in constant power mode do not support the AC system.

The presented decision support tool is based on TD simulations and takes into account the full power system dynamics. The tool reduces the computational time of the assessment by employing a CBS and FCCS to determine the potential and actual critical buses with respect to three-phase faults. The dispatch procedure uses a novel fast converging technique to determine the needed re-dispatch by approximating the generator setpoint on basis of the initial condition. The case study on the New England system showed that a significant reduction of critical buses, that need to be analyzed, is achieved by employing the CBS and FCCS. The approximation of the needed re-dispatch showed to be well functioning and, thereby, reducing the number of iterations to find the exact re-dispatch. The evaluation of the execution time of the assessment shows that the CCT determination is the most time-consuming step of the procedure and, additionally, the execution time of this step increases with the system size. However, one should note that the execution time was achieved on a standard laptop (quad-core i7 4600, 8 GB RAM) with PowerFactory V 15.2 and Matlab 2016b software. The execution time will be reasonably lower with more powerful units used in control rooms and an efficient implementation allowing the online application for control room operator decision support.

CHAPTER 4

Voltage estimation in active distribution grids

This chapter focuses on the research questions **[Q3]** and **[Q4]** which are outlined in the research objectives in Section 1.2 and are repeated below. First, the general background of voltage estimation in active distribution grids including a literature review is presented. Then, a numerical implementation of a neural network (NN)-based voltage estimation approach for active distribution grids is presented. The voltage estimation approach is tested by means of simulation data from an active low voltage (LV) benchmark grid modelled in DIgSILENT PowerFactory. Following that, the voltage estimation approach is systematically validated by means of field data from two feeders of a real active LV distribution grid. The validation determines the capabilities and limitations of the method. This chapter includes content and results of **[Pub. C]** and **[Pub. D]** which are attached to the thesis.

[Q3] *How can currently available measurements be utilized to establish a data-driven neural network approach to increase the real-time voltage observability of active distribution grids?*

[Q4] *What are the capabilities and limitations of the neural network-based approach for real-time voltage estimation in active distribution grids?*

4.1 Background on voltage estimation for active distribution grids

As pointed out in Chapter 2, it is crucial to increase the observability of distribution grids to enable high penetration of renewable energy sources (RES). A large portion of RES is being connected at the distribution level, e.g. photovoltaics (PV) on residential rooftops [211]. Distribution feeders are transitioning to host both, energy consumers and producers, hence, the power flow of distribution grids changes significantly in the presence of dispersed generation units [212]. Under certain circumstances, even reverse power flows can occur, e.g. when low demand and high PV generation coincide [213, 214]. In addition to that, voltage becomes more volatile due to the fluctuating power output of renewable generation and the charging of single-phase electric vehicles at the lowest voltage level [215, 216].

To prevent voltage variations beyond the acceptable limits, different control techniques are applied to regulate the voltage in power systems, e.g. tap-changing transformers. A requirement for voltage control is the knowledge of the system state, i.e. the voltage magnitude. That means, data from a sufficient number of measurement points in the system must be available in real-time. In general, the observability of today's distribution systems is still low due to their large size. Increasing the observability usually translates into a need for additional measurement sensors, e.g. smart meters. However, achieving full observability of distribution grids is prohibited by major

cost limitations and, therefore, innovative cost-efficient methods must be used to complement existing physical measurements. Data driven methods benefit from the availability of offline measurements from different sources and offer a cost-efficient alternative to the installation of additional real-time measurements.

Previous research has focused on the application and adaptation of conventional state estimation methods for distribution grids which are widely used and well understood for transmission grids. In order to make state estimation applicable in distribution grids, approaches aim either at adapting the used algorithm [217–219] or study how to optimally place measurement sensors [220, 221] to reduce the absolute number of needed devices. However conventional state estimation approaches, such as [222, 223], suffer from the assumption that the network topology and accurate line parameters are given. The accuracy strongly depends on accurate line parameters and actual topology, and seriously degrades in presence of inaccurate parameters [47, 224]. To overcome these drawbacks of conventional state estimation, the authors of [225–227] propose to generate pseudo measurements for the state estimator using (artificial) NNs to improve the accuracy of the calculation.

NNs belong to the family of statistical learning methods which are capable of approximating or estimating the relationship between any number of given inputs and outputs, also called targets. This powerful asset opens the approach for a wide variety of applications where non-trivial or non-analytical relationships between a number of parameters exist, and a solution with conventional methods becomes too complex and unhandy. Due to that versatility, NN-based approaches are appealing for application in power systems. In contrast to their conventional counterparts, NN approaches do not need to model the electric network as admittance matrix, hence, there is no dependency on accurate line parameters. However, similar to conventional state estimation, topology changes have to be detected and accounted for, i.e. the model needs to be retrained when topology changes. Another advantage is that after establishing the model, no iterative process is needed in the calculation. This high flexibility paired with higher speed, accuracy and efficiency compared to conventional approaches makes NN approaches interesting for complex problems and development of online applications [228]. In the following, a brief state-of-the-art overview of NN-based approaches for voltage estimation is presented.

The authors of [229] propose a NN-based bottom-up monitoring approach for distribution grids. In the approach, the monitoring problem is split-up into sub-problems for each voltage level. First, local estimators are trained to estimate the voltage at specific nodes at the lowest voltage level using voltage and current measurements at the medium-voltage/low-voltage transformer. The estimation results from these buses are communicated to the upper-level estimator and, thereby, creating an overall picture of the distribution system. The authors show that a monitoring approach with NNs can be implemented cost-efficiently and with low computational effort.

In [230, 231], the authors investigate the impact of phasor measurement units (PMUs) measurements on the accuracy of NN-based estimation of voltage magnitude and angle. They conclude that the NN-based estimator including input data from PMUs achieves similar results as a classic state estimation algorithm.

The authors of [232] propose a NN with two hidden layers and entropy-based selection of input variables. They concluded that the selection of appropriate input variables is of crucial importance.

The authors of [233] employ a NN voltage estimator to calculate the voltage profile along a feeder. The estimated voltage profile is send to a master controller by remote terminal units (RTUs) aiming at enhanced operation of an on-load tap-changer (OLTC) transformer for voltage regulation.

In Section 4.3, a NN approach for voltage estimation in active distribution grids with high RES penetration is proposed. The approach utilizes data from already existing measurement sensors in today's distribution grids, e.g. substation measurements and smart meter data.

In the above presented works and throughout the literature, NN-based voltage estimation approaches are tested and validated by means of simulation models alone. Generally, a large number of different load flow scenarios are simulated and the results of the simulations are divided into training and test set. In order to move towards implementation in real environment, Section 4.4 presents the validation of a robust neural real-time voltage estimator on field data.

4.2 Description of the NN voltage estimation approach

The motivation for this voltage estimation approach is to use currently existing measurements in distribution grids to establish a NN model for real-time voltage estimation. The voltage at particular LV buses, where measurements are not available in real-time, but historical data is available, is to be estimated. This is for example true for smart meter measurements which are not available in real-time, but they are available as historical data. In particular, the phase-neutral voltage magnitudes (U_a, U_b, U_c) at a downstream bus of a distribution feeder are to be estimated based on available measurements from the substation. Voltage angles are not part of the solution because they are typically small in LV grids while the magnitude is from paramount interest [234]. In order to illustrate the motivation for this approach, a general sketch of an active LV distribution grid which includes distributed generation among loads is shown in Fig. 4.1. The substation and the downstream measurement are highlighted in red and blue, respectively.

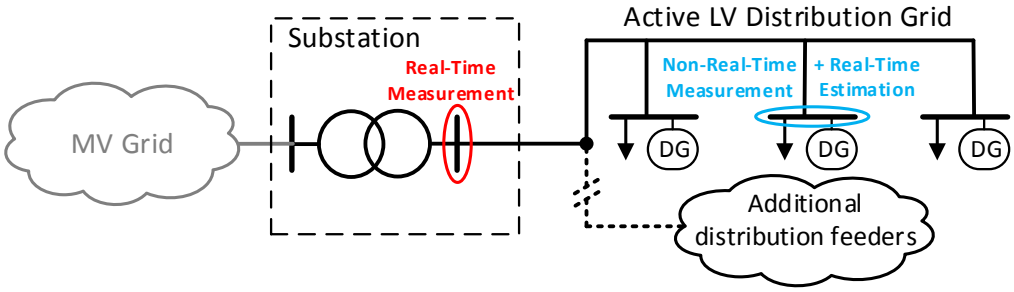

Figure 4.1: Sketch of an active low voltage distribution grid indicating the substation and downstream measurements [Pub. D]

Two different phases of the voltage estimator are distinguished as shown in Fig. 4.2. The available input and output variables are indicated, whereas the colors of the input and output arrows are aligned with the colors in Fig. 4.1.

- *Training phase:* The estimator is established in the training process by use of an suitable training algorithm. The choice of training algorithm depends on the problem type and complexity of the NN. Here, the well known Levenberg-Marquardt algorithm is used to train the NNs because it is usually the fastest training method for function approximation up

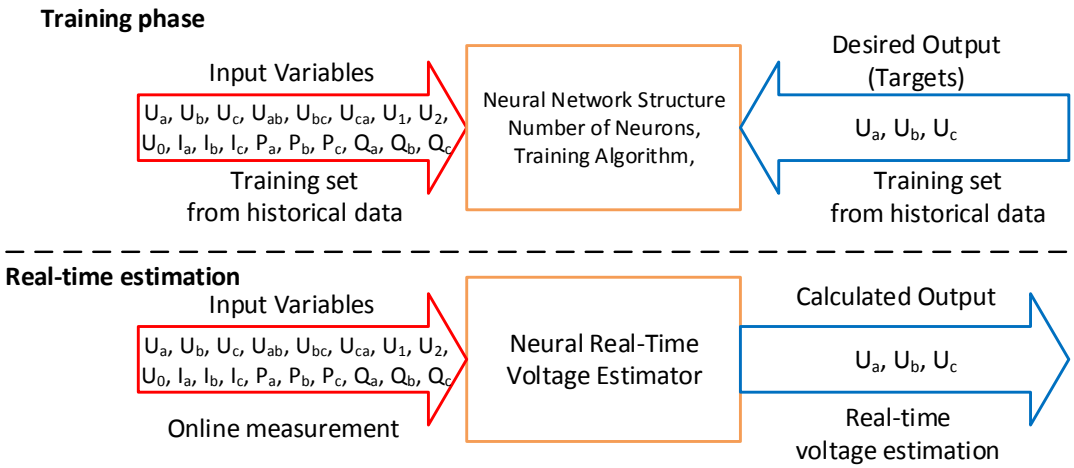

Figure 4.2: Training phase and real-time estimation phase [Pub. D]

to a few hundred weights and biases, it is very accurate and it shows superior convergence behavior over other algorithms [235, 236]. For more details about the training algorithm, the reader is referred to [Pub. D]. Prior to the training, the architecture and number of neurons in the hidden layer have to be defined.

- *Real-time estimation:* After the training process, the voltage estimator can be used for real-time voltage estimation at the specific bus, i.e. substation measurements are fed into the estimator and the voltages of the downstream bus are calculated in the order of milliseconds on a standard laptop due to the direct calculation without further iterations. It is crucial for real-time applications that the computation time is deterministic, since it has to be accounted for the worst case.

The training of the voltage estimator is carried out in Matlab. The training parameters and its corresponding values are shown in Table 4.1. The training parameters are set up such that the algorithm stops when either the maximum number of consecutive failed validations is reached, the performance gradient falls below the minimum threshold or the maximum number of training

Table 4.1: Training parameters of the Levenberg-Marquardt algorithm [Pub. D]

Parameter abbreviation	Value	Explanation
$epochs$	2500	max. epochs to train
$goal$	0	performance goal (MSE)
min_grad	10^{-7}	minimum improvement from one epoch to the next
val_fail	10	maximum consecutive validation fails
μ_{init}	10^{-3}	initial mu
μ_{dec}	0.1	mu decrease factor
μ_{inc}	10	mu increase factor
μ_{max}	10^{10}	maximum mu

epochs is reached. The stopping criteria of validation fails means that the model performance on the validation data set does not improve for the defined number of consecutive iterations in the training process. The term performance refers to the mean squared error (MSE) between the model output and the real measured values. The maximum number of epochs and failed validations are increased above the default values in Matlab's NN implementation, while the other parameters are suggested default values. The number of training epochs must be reasonably high in order not to stop training prematurely. Usually, the number of maximum failed validations is the stopping condition that is met first. This highly speeds up the training and, moreover, prevents overfitting. Validation checks are carried out on the validation data set at the end of each epoch during the training process.

It is important to emphasize that the proposed voltage estimator is exclusively established for normal operating conditions. Distribution network operation includes faults, topology changes and outages. For estimation under these conditions, a separate model would need to be trained for abnormal conditions as the characteristics of the disturbed grid are different than in normal operation. Certainly, the characteristics of the grid change with changing topology and separate models need to be trained for each topology. In this work, topology changes are not considered.

In the following, the advantages of the proposed approach are highlighted:

i) Use of available real-time and/or non-real-time measurements grants high flexibility to the model.

ii) No need to establish additional real-time measurements.

iii) The model is established offline with low computational effort, i.e. less than one minute on a standard laptop.

iv) Non-iterative calculation of the estimated voltages once model is established.

v) Suitable for real-time monitoring since the method is computationally light.

vi) No need for admittance matrix and accurate line parameters.

vii) No information about active and reactive power injections within the network is needed.

4.3 Implementation of the neural voltage estimator by means of simulated distribution grid data

This section presents the numerical implementation of the NN-based voltage estimator for active distribution grids with high penetration of RES. The approach is tested by means of simulated data from the LV distribution grid with high share of small-scale RES generation shown in Fig. 4.4.

4.3.1 Architecture of the neural voltage estimator

The voltage estimator is comprised of a two layer cascade-forward NN as shown in Fig. 4.3. The model includes an hidden and an output layer. The size of each element is determined by the number of inputs, outputs and used neurons. The number of neurons was determined empirically, trials with networks of between 6 and 18 neurons yielded an optimal number of 14 as the best tradeoff between accuracy and overfitting. The red bar represents the input vector with R rows

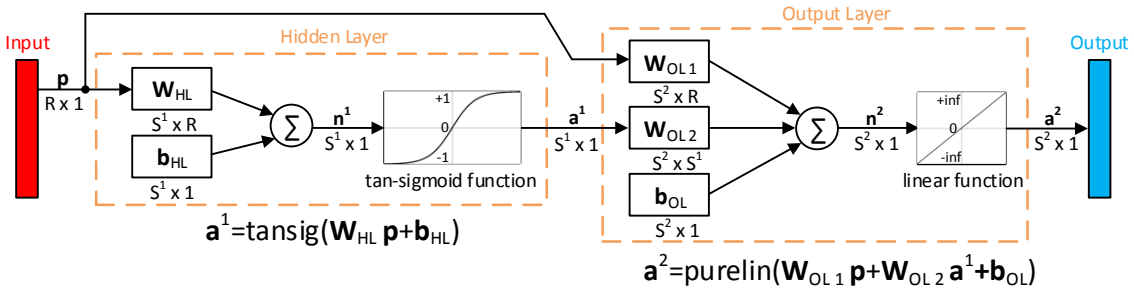

Figure 4.3: Two layer cascade-forward NN architecture. Bold capital letters in the figure represent matrices while bold lower case letters represent vectors. The size of each element is given underneath. (adapted from [Pub. C])

where R is determined by the number of input variables. The weight matrices are given as capital **W** with the respective indices HL and OL for hidden layer and output layer. The size of the weight matrices is determined by the number of neurons ($S^1 = 14$) and input variables ($R = 10$) for the hidden layer and by the number of output variables ($S^2 = 6$) for the output layer. The bias vectors are given with the parameter **b** indexed in the same way as the weights. The number of rows for the two bias vectors is determined by the number of neurons and output variables, respectively. The transfer functions of the hidden and output layer are a tangent sigmoid and a linear transfer function as indicated underneath the respective layers. Generally, this transfer functions are working well for function approximation problems including input variables that contain positive and negative values.

4.3.2 Active distribution grid simulation model

Historical data has to be collected before the training of the voltage estimator. Here, the data for the analysis is generated by simulation of a distribution grid in the PowerFactory DIgSILENT

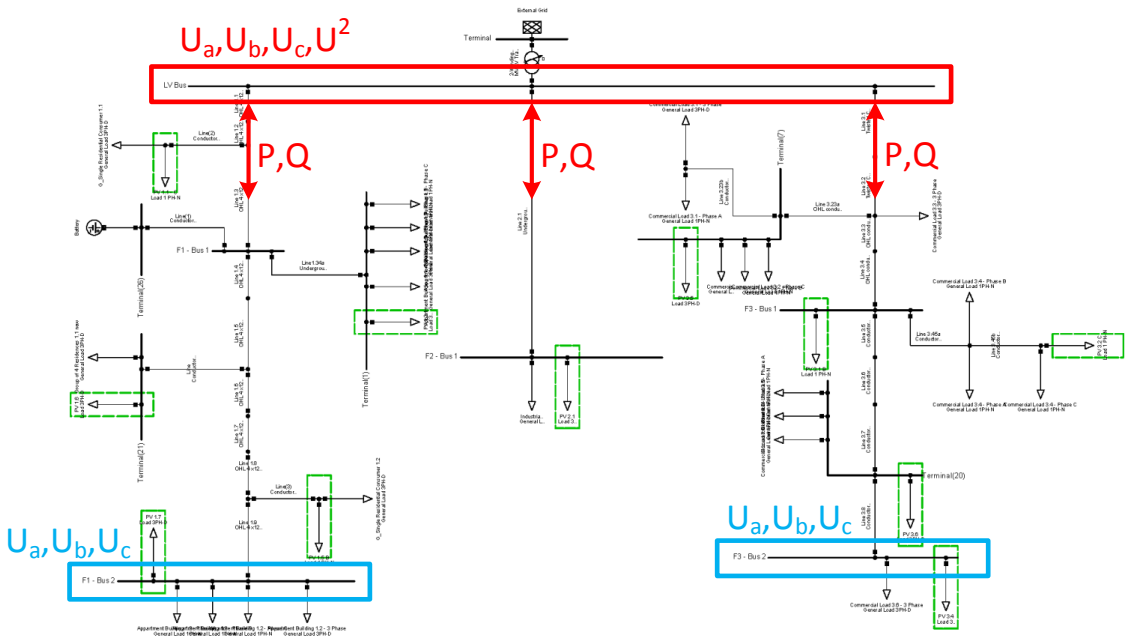

Figure 4.4: Active LV distribution grid model in PowerFactory (adapted from [Pub. C])

simulation environment shown in Fig. 4.4. The distribution grid is based on a LV benchmark microgrid proposed in [237]. The benchmark grid includes three radial feeders which are connected to a common LV bus. The common LV bus is connected to an external grid via a MV/LV transformer. More distributed generation is added to the proposed grid in order to produce a particularly challenging distribution grid for the analysis. Distributed generation units represent single- and three-phase PV generation systems and are highlighted in green as shown in Fig. 4.4. The three feeders represent different consumption patterns that are associated with residential, commercial and industrial loads according to [237]. The LV bus highlighted in red is defined as the reference bus where the input parameters for the voltage estimation model are taken from. The two LV buses highlighted in blue define the buses for which the voltage is estimated.

4.3.3 Simulation scenarios for training data collection

Five different scenarios are simulated using the distribution grid model in Fig. 4.4 to generate the data for training the voltage estimator. The granularity of the training data is 1 s, i.e. 24 h = 86400 data points. The scenarios differ in terms of load and PV penetration level, and all scenarios are summarized in Table 4.2. All simulations are carried out as time-domain (TD) simulations over a period of 24 h. That means, each scenario represents one day with different load and PV injection. The scenarios are derived from a single base case which defines a certain load and PV injection and which is referred to as the 100 % case. The load PV injection level varies from 0 to 200 % of the base case. The first four scenarios describe four different load/PV scenarios while scenario five is a pure load scenario without any embedded PV generation. The feeders are enumerated from left to right.

Table 4.2: Simulation scenarios for training data collection [Pub. C].

Scenarios	Feeder 1		Feeder 2		Feeder 3	
	Load (%)	PV (%)	Load (%)	PV (%)	Load (%)	PV (%)
1	0	100	100	100	0	100
2	0	100	100	100	200	100
3	200	100	100	100	0	100
4	200	100	100	100	200	100
5	100	0	100	0	100	0

4.3.4 Results of test cases

The voltage estimator is tested on a representative scenario with high PV injection. The setup of the load and PV generation is shown in Table 4.3. The load on all feeders is set to the base case, i.e. 100 %. The PV generation on all feeders is increased to 130 - 170 % with regard to the base case. The interested reader is referred to [Pub. C] for an additional test scenario.

The input parameters that are fed into the estimator over a 24 h period are shown in Fig. 4.5. The voltage profile at the common bus is quite flat despite the fact that the load is at 100 %. That is mainly due to the high level of PV generation in all three feeders which, in addition, changes the load flow condition within all feeders significantly. The active power flow of feeder 1 and 2 has a negative sign which means that active power is flowing in reverse direction between 09:00

Table 4.3: Load and PV setup for the test scenario (adapted from [Pub. C])

Test scenario	Feeder 1		Feeder 2		Feeder 3	
	Load (%)	PV (%)	Load (%)	PV (%)	Load (%)	PV (%)
1	100	130	100	150	100	170

and roughly 18:00. Feeder 3 is consuming active power throughout the day. In contrast, reactive power is supplied to all three feeders at all times because there are no units downstream the feeder that inject reactive power. The negative sequence voltage increases with increasing PV generation which is due to the fact that a large share of PV units are connected single-phase.

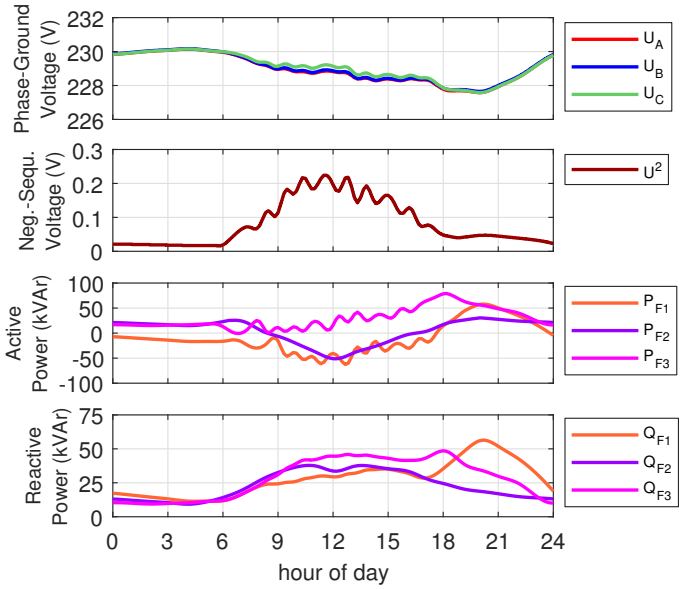

Figure 4.5: Input variables supplied to the estimator over the 24 h period (adapted from [Pub. C])

The comparison between the estimated and actual phase-ground voltages at the two downstream buses on Feeder 1 and 3 is shown in Fig. 4.6. The two upper plots show the results for the downstream bus of Feeder 1 including the absolute error of the estimation and the two lower plots for the downstream bus of Feeder 3. The estimated and actual voltages are shown as dashed and solid lines, respectively. The difference between the estimated and actual values are small and can hardly be noticed but the plots of the absolute error reveal that there is a difference between the real and actual voltages. It can be seen that the absolute error reaches its maximum at around midday, coinciding with the PV generation peak. Before and after this period the error is smaller. As the voltage estimator has been established with five scenarios which differ primarily in terms of load distribution, this is expected. The voltage estimator had not been trained with a high PV penetration scenario, therefore its ability to estimate the voltages under high PV production is limited. However, when analyzing the results in Fig. 4.6, it can be seen that the absolute error is still small compared to the nominal voltage as its max deviation is less than 1.5 V for the downstream bus at Feeder 3 despite the presence of complex load and generation patterns within the feeders.

The results indicate that NNs are suitable for accurate voltage estimation in active distribution grids

with high distributed generation using data from currently available real-time and non-real-time measurements. As seen in the results, the error of the estimation increases when the PV generation reaches the highest level at around midday due to the fact that no such scenario was considered in the training process of the NN. This could be improved when such scenarios are considered in the training process. However, the estimator was exclusively trained on simulated data and, therefore, the method needs to be validated on data from a real distribution grid in order to allow application in practice. The following section presents a systematic validation of the approach on field data from a real distribution grid with PV generation.

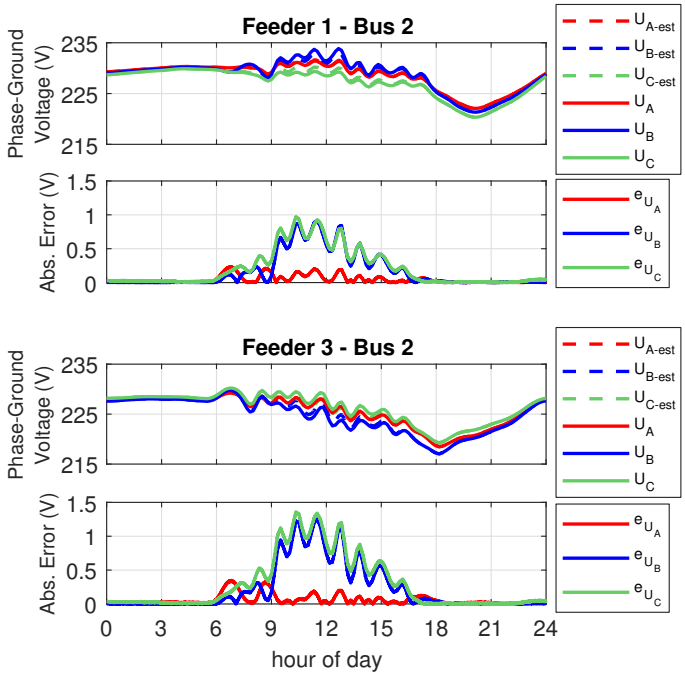

Figure 4.6: Estimated voltage compared with actual voltage of the buses including the absolute errors of the estimation. Top plots (adapted from [Pub. C])

4.4 Validation of a neural real-time voltage estimator on field data

This section presents a systematic validation of the voltage estimator on field data by setting the framework for a neural real-time voltage estimator (NRTVE) which is a necessary step towards implementation in a real control room environment. As in the section before, the phase-neutral voltage magnitudes (U_a, U_b, U_c) at downstream buses of two LV distribution feeders are estimated based on available measurements from the substation as outlined by the sketch of the active LV distribution grid in Fig. 4.1. The validation of the NRTVE includes the following:

I Methodology to select the most relevant input variables and find the best achievable performance for a particular number of inputs.

II Sensitivity analysis of the performance to the number of neurons.

III Analysis of the quantity of historical data that is needed to train an adequately functioning model.

IV Determination of the impact of the retraining interval on the performance of the model.

V Sensitivity analysis of the model performance to the level of PV generation.

4.4.1 Available data for the analysis

This section describes the data that is available for the validation. All measurements are taken in a LV distribution grid. Seven power quality meters, which comply with measurement class A defined in IEC 61000-4-30 [238], are placed in two different feeders. Both feeders include loads and rooftop PV generation. Two meters are placed at the substation and five downstream the feeder. Considering Fig. 4.1, two meters are located at the red measurement point and five at the blue one, respectively. The distribution feeders are located in a residential area of Copenhagen region. For reasons of confidentiality, the exact specifications of the feeder including the exact topology cannot be disclosed.

The measurements were taken over a period of approximately 1.5 years starting from 01.10.2014 until 14.05.2016. The resolution is a mixture of 1-min and 10-min measurements, i.e. in some periods a measurement is averaged over 10 minutes and in other periods averaged over one minute. The measurement data is filtered to extract synchronized measurements from the substation and downstream feeder measurements with the same time stamp. Five possible combinations of substation and downstream meters are included in the data. Table 4.4 summarizes the dataset size, measurement period and indication of PV generation. All datasets include the available measurements shown in Table 4.5.

Table 4.4: Available meter combinations including set size, measurement period and indication of PV generation on the feeder. $S = substation\ meter$, $D = downstream\ meter$ [Pub. D]

Meter combination	$S_1 - D_1$	$S_1 - D_2$	$S_1 - D_3$	$S_2 - D_4$	$S_2 - D_5$
Data points	274,739	274,515	213,660	83,985	84,693
Period	01.10.2014-14.05.2016	01.10.2014-14.05.2016	30.11.2015-14.05.2016	01.10.2014-14.05.2016	01.10.2014-14.05.2016
PV on feeder	yes	yes	yes	yes	yes

Table 4.5: Measured variables [Pub. D]

Variable	Explanation
U_a, U_b, U_c	phase-to-neutral voltages (V)
U_{ab}, U_{bc}, U_{ca}	phase-to-phase voltages (V)
U_1, U_2, U_0	positive-, negative- and zero-sequence voltage (V)
I_a, I_b, I_c	currents (A)
P_a, P_b, P_c	active powers (W)
Q_a, Q_b, Q_c	reactive powers (VAr)

4.4.2 Architecture of the neural real-time voltage estimator

Fig. 4.7 shows the architecture of the NRTVE which is slightly different than the architecture shown in Section 4.3.1. The complexity of the estimator is reduced by removing the direct feed-forward term of the input to the output layer, i.e. all input variables are passed through the hidden layer and then through the output layer. This adjustment of the architecture is done because, generally, a standard feed-forward NN with one hidden layer is sufficient for most fitting problems as

elaborated in [236]. However, if the performance of the model is not sufficient, additional hidden layers can be added.

Inputs and outputs are scaled to values between ± 1 since the hyperbolic tangent-sigmoid function in the hidden layer operates between ± 1. Large inputs would mainly generate values in the saturated area of the sigmoid function and in order to exploit the full flexibility of the transfer function it is advised to scale the inputs to values in the linear region.

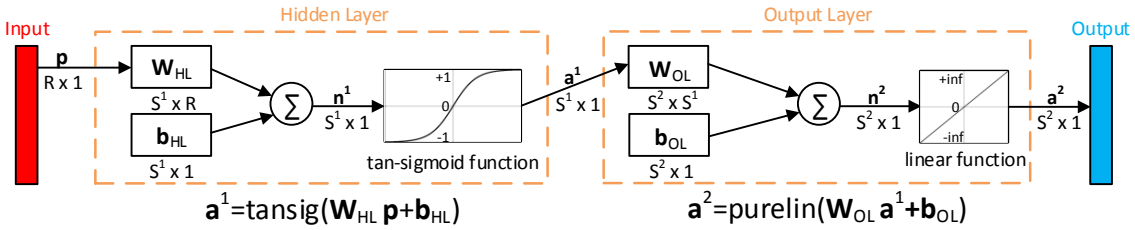

Figure 4.7: Architecture of the feed-forward neural network. Bold capital letters represent matrices and bold lower case letters vectors. The size of each element is given underneath. $\mathbf{W_{HL}}/\mathbf{W_{OL}}$ = weight matrices, $\mathbf{b_{HL}}/\mathbf{b_{OL}}$ = bias vectors, S^1 = # neurons, R = # input variables, S^2 = # output variables [Pub. D].

4.4.3 Selection of input variables

The selection of appropriate input variables strongly affects the performance of the trained NN. A tradeoff between the number of selected inputs and the model performance must be found. Input variables with negligible or low impact on the output variables should be excluded to reduce the complexity of the model. Once input variables are excluded, the performance of the NN will get worse because even input variables with low impact contain a certain amount of useful information which is lost when the variable is excluded. To identify the most relevant input variables, linear and non-linear relationships between the input and output variables must be identified. There is no general algorithm to optimally select the input variables, but the most commonly used relevance measure is the Pearson correlation [239], i.e. the input variables are ranked according to their linear correlation with the output variables as shown in 4.1 where X and Y are the two variables and k is the number of data points of each variable. In addition to the correlation of input and output variables, there is generally also correlation among input variables. The correlation among input variables provides redundant information to the model which is not considered in the linear ranking approach. Hence, it is not suitable to find a tradeoff between selected input variables and performance.

$$R_{(X,Y)} = \frac{\sum_{i=1}^{k}(x_i - \overline{x})(y_i - \overline{y})}{\sqrt{\sum_{i=1}^{k}(x_i - \overline{x})^2 \sum_{i=1}^{k}(y_i - \overline{y})^2}} \tag{4.1}$$

The ranking approach is elaborated by use of a dataset which contains measurements of the meter combination S_1 - D_1 from 01.10 - 01.11.2014, corresponding to 3124 data points for training and 670 for validation and testing each. In order to produce comparable results, the same data sets are used for training, validation and testing throughout the whole input selection process. The number of neurons in the hidden layer is set to 10 and is not changed during the input selection process. The exact number of neurons is not of great importance in this case as long as the model is

not underdetermined. In the following, a ranking approach that considers both, the correlation between input and output variables and among input variables is proposed.

Two important preceding considerations for the ranking approach are made:

- In the following, when referring to the correlation of an input variable to the output, the average correlation of the input variable to all three output variables is meant. This is done because the correlation between any input variable and the three output variables is virtually the same.
- The input variables are grouped into six categories according to the presented variables in Table 4.5 where each row presents one category: 1) phase-neutral voltages {U_{ph}}, 2) phase-to-phase voltages {U_{pp}}, 3) voltage's sequence-components {$U_{0,1,2}$}, 4) currents {I}, 5) active powers {P}, 6) reactive powers {Q}. The categories are chosen from an electrotechnical perspective so that input variables represent a mix of node and branch parameters. For more detailed information about the correlations, the interested reader is referred to [Pub. D].

Note: Here, the variables are grouped into categories during the input selection process, but the method is also applicable to individual variables.

In order to rank the input variables, the variable importance VI_C for a particular input category is introduced. The calculation of VI_C is shown in (4.2) and it consists of two terms. The first term $R_{I,O}$ describes the average correlation of the particular input category C, which includes several variables X, with the output Y. Ind_C denotes the indices of the variables within a category, n_C the number of variables in the category and m the total number of variables. Note that it is the absolute value of the correlation which is averaged. Values close to 1 indicate the strongest correlation. The second term $R_{I,I}$ describes the average correlation between the particular input category and the other input variables. This value does not necessarily need to be close to zero, but it has to be optimized if the model complexity is to be reduced while maintaining acceptable performance.

To express the impact of redundancy, an additional parameter $\beta \geq 0$ is introduced. If $\beta = 0$, the variable importance equals the correlation between inputs and outputs, ignoring the correlations among input categories. The greater the value of β, the more importance is given to reducing the redundancy of input variables. The variation of β depends on the purpose of the NN for which the input variables shall be selected. If the model complexity does not matter, β can be chosen to be zero. If the selection process aims at sorting out as many input variables as possible while keeping satisfying performance, β must be increased. To find a tradeoff between model complexity and performance, β must be varied between zero and a value where the product of β and $R_{I,I}$ is in the same order of magnitude of $R_{I,O}$.

$$VI_C = R_{I,O} - \beta \cdot R_{I,I} \tag{4.2}$$

with

$$R_{I,O} = \frac{1}{n_C} \sum_{\substack{i=1 \\ i \in Ind_C}}^{n_C} |R_{(X_i,Y)}| \quad and \quad R_{I,I} = \frac{1}{n_C} \sum_{\substack{i=1 \\ i \in Ind_C}}^{n_C} \frac{1}{m - n_C} \sum_{\substack{j=1 \\ j \notin Ind_C}}^{m} |R_{(X_i,X_j)}| \tag{4.3}$$

To show the capabilities of the proposed selection method, a backward elimination approach is used to sort out the least important variable categories step-by-step. Initially, all variables are

selected and one after another category with the lowest ranking gets eliminated. The computation of the approach is heavier compared to other approaches because a NN has to be trained for all available input variables and with varying β-values. This computation only needs to be done once, offline. The advantage of the backward elimination approach is that it shows the maximum achievable performance when all input variables are used and how the performance declines when some of the input variables are sorted out. However, it is a 'greedy' algorithm because it eliminates the least relevant variables according to the ranking index one by one while the global optimum might be found only by trying all possible combinations. As this is computationally infeasible, a greedy approach is used instead.

To achieve different input variable combinations, the elimination process needs to be repeated with different β-values. Here, beta is varied between 0 and 3 in 0.2 increments. The range of the variation originates from the fact that the largest correlation among input categories is about one third of the input-output correlation.

Fig. 4.8 shows the results of the elimination process. Estimations with varying input variable combinations achieve different performances. The blue lines show the results for variations of beta, whereas the black line shows the best achievable performance for a given number of input variables. The plot shows that the performance declines slightly when the first two categories are sorted out while the performance starts to decline more between 12 and 6 variables, and it drops significantly when one category is left only. The blue lines show that a variation of beta is necessary to find a tradeoff solution because the results change significantly with the variation of beta and no one value of beta gave the smallest error for all number of input variables. This confirms that the variation of beta is needed. For additional information about the variable selection process, the interested reader is referred to [Pub. D].

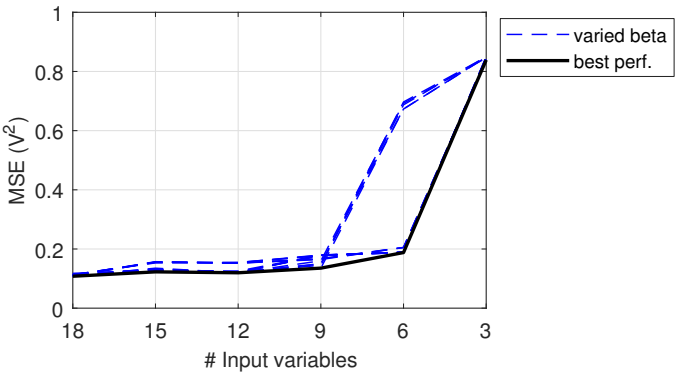

Figure 4.8: The blue lines represent the performance throughout the input elimination process with β varied between 0 - 3, whereas the black line shows the best performance achieved for a certain number of input variables (adapted from [Pub. D]).

4.4.4 Sensitivity of performance to number of neurons

The sensitivity analysis is carried out with the same dataset as the input selection analysis. The input variable combination with the best performance for the specific number of input variables according to the black solid line in Fig. 4.8 is used for the sensitivity analysis. Fig. 4.9 shows the performance of the voltage estimator with the varying neurons in the hidden layer for the different number of input variables. Clearly, the performance stabilizes for each number of input variables

before 10 neurons are reached. Thus, the choice to use 10 neurons during the input variable selection process is reasonable. Another observation is that the model performance is not sensitive to the number of neurons in the hidden layer as long as the model is not underdetermined.

For the further studies, twelve input variables are used. The four categories U_{ph}, U_{pp}, P and I are chosen. The reactive powers and sequence components are sorted out when achieving best performance with 12 input variables. As shown in Fig. 4.8, satisfying performance is maintained when these two categories are eliminated and only the remaining 12 input variables are used.

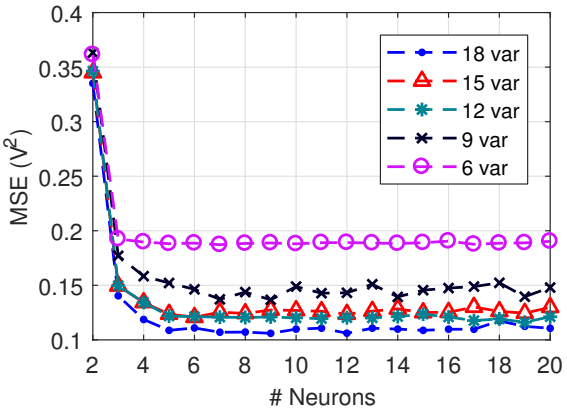

Figure 4.9: Performance of the estimator with the determined input selections for different number of neurons (adapted from [Pub. D]).

4.4.5 Data quantity and retraining analysis

Two fundamental questions before establishing a neural voltage estimator are how much historical data should be used to train the model and when should it be retrained? This section analyses the relationship between the performance of the neural voltage estimator and the historical data quantity that is used to train them and how often they have to be retrained to be suitable for real-time application. The two questions can be summarized as follows:

i How much historical data is needed to create a model with a satisfying performance for real-time application?

ii When does the model have to be retrained in order to maintain satisfying performance for real-time application?

Note: Satisfying performance is achieved when the accuracy of the estimation is comparable to the measurement uncertainties of meters, such as meters of class A and B, defined in IEC 61000-4-30, which shall not exceed ± 0.1 *and* $\pm 0.5\,\%$ *of the declared input voltage, respectively.*

The analysis for both is carried out for four meter combinations in order to derive meaningful information about the needed data quantity and retrain intervals. The data of each meter combination includes one full year of measurements to also capture seasonal effects.

Data quantity analysis

The data quantity analysis is carried out stepwise. Here, a condensed version of the procedure is presented. For a more detailed description, the interested reader is referred to [Pub. D].

1 Set starting point t_0 which is in this case 01.01.2015 00:00 at the beginning of the dataset.

2 Train a NN with data from the past 3 days. The historical data is randomly split into 85 % for training and 15 % for validation.

3 Evaluate the performance of the trained estimator on the test set denoted which consists of the 7 days following t_0.

4 Repeat step 2 and 3, increasing the amount of data that is used for training and validation by 3 days in each step until the maximum considered amount of 90 days is reached.

5 Once step 4 is completed, i.e. the performance of the NN with training set size from 3 to 90 days is evaluated, t_0 is shifted forward in time by 5 days and steps 2-4 are repeated.

6 The procedure finishes when the end of the year (end of the dataset) is reached.

The results of the data quantity analysis of the four different meter combinations are averaged per month as shown in Fig. 4.10. The behavior shows to be similar for all meter combinations, but the order of magnitude of the estimation error is different for each meter combination as the y-axes have different scaling. In this case, the y-axes scaling is not that important because the graph should highlight the trend of the performance versus the data quantity. However, the magnitude gives insight on the achievable performance for each meter combination, i.e. the estimation accuracy for the bus where the downstream meter is located.

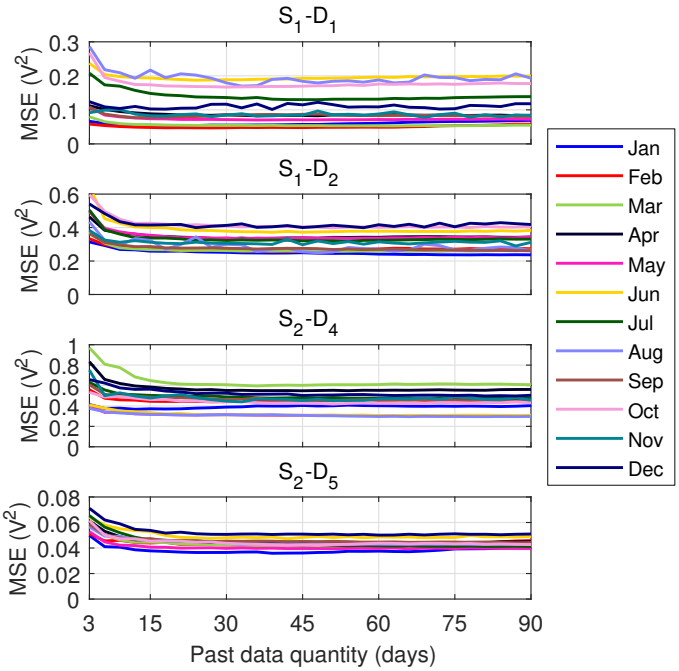

Figure 4.10: Results of the data quantity analysis for four different meter combinations (adapted from [Pub. D]).

As seen from the four subplots, the general statement for machine learning that more data will provide better performance is not valid in this case. The performance stabilizes at about 30 days of historical training data and there is even a slight tendency that performance starts to decline afterwards. The analysis is carried out as close as possible to real world conditions by taking the test set data from the "future", which would be the same when applied in practice. A possible explanation for the stabilization of performance could be that the data which is too far in the past does not reflect the current grid situation and, therefore, the more recent data is sufficient to establish a suitable model.

Retrain analysis

According to the findings in the data quantity analysis, about 30 days of historical data with a granularity of 1 min to 10 min average is sufficient to train a well performing estimator. Therefore, 30 days of historical data is used in the training process of the further analysis.

The retrain analysis is carried out stepwise. Here, a condensed version of the procedure is presented. For a more detailed description, the interested reader is referred to [Pub. D].

1 Set starting point t_0 which is again 01.01.2015 00:00 at the beginning of the dataset.

2 Train a NN with data from the past 30 days. The data is randomly split into 85 % for training and 15 % for validation.

3 The error of the estimation from the model is calculated for the test set which set size depends on the retrain interval, e.g. it is 7 days when the model is retrained every 7 days.

4 Shift t_0 forward in time by the amount of days which are defined by the retrain interval and repeat steps 2 and 3.

5 Once the errors are calculated for the whole year, the performance of the estimator is evaluated over the whole period, i.e. the confidence interval of the expected estimation error is calculated by fitting a normal distribution.

6 Repeat step 1 to 5 with different retrain intervals.

The results of the retraining analysis for the four meter combinations with varying retraining intervals are shown in Fig. 4.11. The plot shows the 3-σ confidence interval which includes 99.73 % of the expected errors of the estimation over the retraining interval on logarithmic scale. The mean of the estimation error is fairly close to zero for all meter combinations whereas the width of the 3-σ confidence interval is different. The best performance is achieved at the meter combination $S_2 - D_5$ which shows the narrowest confidence interval. The confidence interval for the meter combinations $S_1 - D_1$ and $S_1 - D_2$ first slightly increases, but significantly drops when the retrain interval is greater than 40 days, which means that the performance of the estimator drastically declines. However, the performance for the meter combinations $S_2 - D_4$ and $S_2 - D_5$ is more stable and declines less. From that, it can be concluded that the retrain interval depends on the properties of the feeder, e.g. amount of PV generation, but the estimation errors can be kept at an reasonably low level with adequate choice of the retrain interval, e.g. every 20 days. The training procedure only takes a few seconds on a standard computer with Intel i7 processor with 8 GB RAM and a training/validation set of 30 days with time resolution of about 1 minute averaged measurements. Therefore, there is no foreseen limitation regarding duration of the retraining procedure.

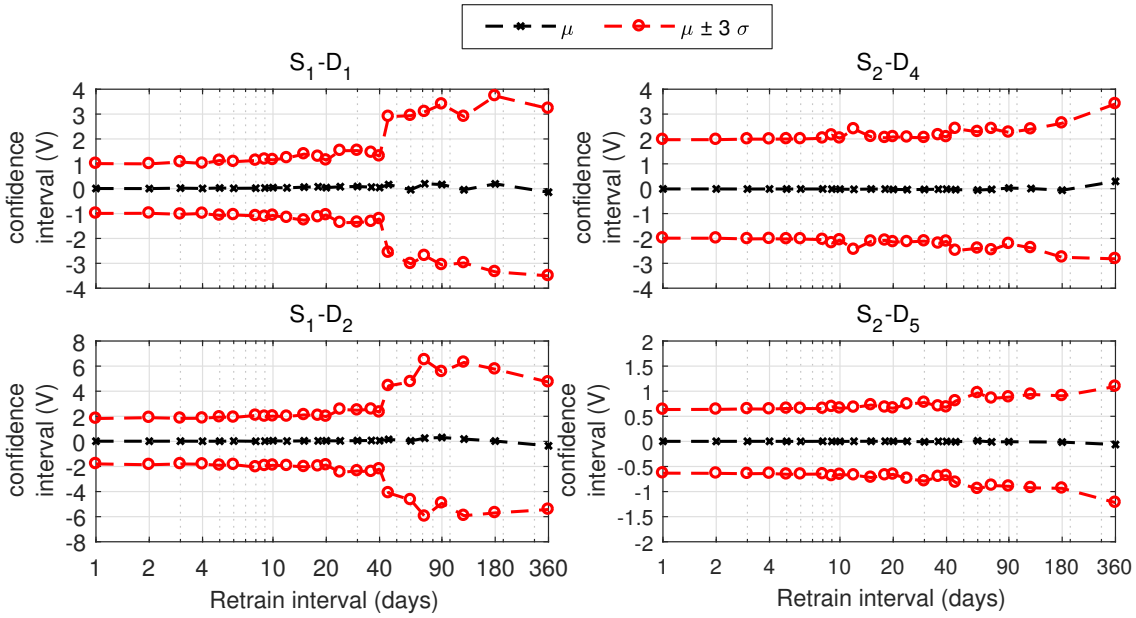

Figure 4.11: Mean error μ with 3-σ confidence interval of the voltage estimations for all meter combinations (adapted from [Pub. D].)

Sensitivity of estimation performance to level of PV generation

In order to assess the model performance during high PV in-feed, the estimation error of the meter combinations $S_1 - D_1$ and $S_1 - D_2$ for the full month of June in 2015 is plotted versus the active power flow at the substation meter S_1 as shown in Fig. 4.12. These meter combinations are chosen because this feeder contains more PV generation. The retrain interval is chosen to be 1 day.

Positive active power means 'normal' power flow direction into the feeder and negative means

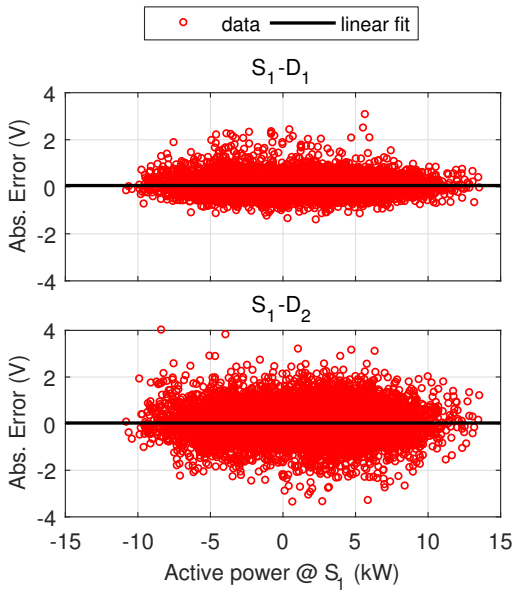

Figure 4.12: Active power flow at substation versus estimation error of the meter combinations $S_1 - D_1$ and $S_1 - D_2$ for the full month of June 2015 (adapted from [Pub. D]).

reverse power flow due to excess of PV generation over consumption. The peak power flows into the feeder and reverse from the feeder are approximately 14 kW and 11 kW, respectively. That means, a broad range of power flow conditions is covered in the data of the evaluation period. As seen in Fig. 4.12, no significant differences of the estimation performance over varying load flow conditions can be identified. The solid black line shows the linear fit of the estimation errors which confirms that the performance during high PV in-feed is comparable to 'normal' conditions as the linear fit is close to zero with zero slope. Essentially, this confirms that the neural voltage estimation approach is suitable for high accuracy voltage estimation under presence of distributed generation.

4.5 Summary

This chapter described the general background of voltage estimation in active distribution grids. Then, a neural voltage estimator for real-time estimation utilizing currently existing measurements is proposed. First, the estimator is trained and tested on simulated data from an active LV distribution grid with high share of dispersed renewable generation. The obtained results suggested that the neural voltage estimation approach is suitable to provide accurate voltage estimations under challenging load flow conditions with high share of distributed generation. The deviations of the estimation from the actual voltage showed to be lower than 1.5 V. These encouraging results achieved on simulated data require a validation on field data.

The validation of the approach was carried out on field data from a real Danish LV distribution grid with PV generation. A methodology to select the most relevant input variables for the estimator based on both the linear correlation of input and output variables and the linear correlation among input variables was proposed. A backward elimination process was used to sort out the least relevant input variables and to find the input variable combination with the best performance for each number of input variables. However, this is a 'greedy' algorithm because it eliminates the least relevant variables one by one while the global optimum might be found only by trying all possible input variable combinations. The validation also showed that the number of neurons in the hidden layer is not of great importance as long as the model is not underdetermined because the validation checks during the training procedure prevent overfitting. However, it is suggested not to use an unnecessary large number of neurons to keep the model complexity as low as possible. The data quantity analysis showed that about 30 days of historical data, given a granularity of 1 min average, is enough to establish an accurate estimator whereas the performance of the estimator varies for different feeders due to their different characteristics. The retrain analysis showed that the performance of the estimator declines with longer retrain intervals. The width of the 3-σ confidence interval, which includes 99.73 % of the calculated estimations, is different for each meter combination, but at maximum $3\sigma \approx \pm$ 2 V for the lowest retrain intervals. That means, the error of the estimation for retrain intervals under 20 days is approximately 0.87 % of the nominal phase-neutral voltage (230 V). That is still acceptable considering the measurement uncertainty of 0.5 % for class B meters defined in IEC 61000-4-30. Additionally, the estimator was found not to be sensitive to high PV in-feed and reverse power flows. The errors during periods of high load, and periods of high PV generation do not show noticeable differences.

CHAPTER 5

Harnessing the aggregate flexibility of electric vehicles

This chapter focuses on the research question **[Q5]** which is outlined in the research objectives in Section 1.2 and are repeated below. First, the background and motivation for smart electric vehicle (EV) integration, in particular with respect to flexibility offered by a large number of EVs, are discussed. Then, an equivalent time-variant storage model to harness the aggregate flexibility from tens to thousands of EVs is presented. The forecastability of the uncontrolled demand and the equivalent storage model is analyzed. Eventually, two envisioned applications show the technical possibilities and economical benefits that emerge from the developed model. This chapter includes content and results of **[Pub. E]** which is attached to the thesis.

[Q5] *How can the flexibility from tens to thousands of EVs be utilized to enhance power system operation?*

5.1 Background and motivation for smart electric vehicle integration

According to the International Energy Agency (IEA), 1.26 million electric cars were on the road worldwide by the end of 2015. The global Clean Energy Ministerial's Electric Vehicles Initiative (EVI) 20 by 20 target calls for 20 million EVs by 2020 globally. The Paris declaration on Electro-Mobility and Climate Change and Call to Action sets a global goal of 100 million electric cars and 400 million electric 2- and 3-wheelers by 2030 [240]. The market needs to grow substantially to increase the current EV population towards these ambitious targets.

The rapid growth of EVs poses a challenge and an opportunity for electric power systems. On the one hand, the demand for vehicle charging will require large investments in power distribution, transmission, and generation. On the other hand, this demand is often also flexible in time, and can be actively managed to reduce the required investments, and to enhance the integration of renewable assets. Harnessing this flexibility requires forecasting and controlling of the charging from tens to thousands of EVs for the benefit of distribution and transmission systems [87, 241].

Coordinated control of various EVs is usually referred to as either smart charging where power flows only into the battery, or vehicle-to-grid (V2G), where the power is allowed to flow in both directions, i.e. into and from the battery. Two control strategies that fit either of these approaches are identified in [242]: A) Direct centralized control where an aggregator[1] clusters and controls a large number of EVs [243, 244]. B) Indirect and fully decentralized control where the control authority stays with the EV owner [245]. Here, it is focused on the challenge of aggregating large populations of EVs to allow centralized control approaches. However, the particular control strategies for individual EVs is not discussed as this is beyond the scope.

[1] Aggregators can be a third party organization or the owners of the electric vehicle supply equipments (EVSEs).

There are several reasons why an aggregation of multiple EVs connected to electric vehicle supply equipments (EVSEs) is necessary and even beneficial. For aggregators that want to participate in a market, a minimum resource capacity is generally required. For instance, the European EPEX spot market [246], the Nordic Nord Pool spot market [247] and the demand response programs of the California Independent System Operator (CAISO) [248] require a minimum capacity of 100 kW.

Moreover, studies show that the economical benefit increases by aggregating larger numbers of EVs [249, 250]. Naturally, the larger the population of EVSEs, the more flexibility in terms of deferrable load is available [251, 252].

The effect of aggregation on the EV charging pattern is highlighted in Fig. 5.1. The plot shows the uncontrolled charging of EVs at different aggregation levels over the course of one week. For low aggregations, the charging pattern is volatile and unpredictable whereas for large aggregations the pattern becomes more regular and predictable. This observation suggests that the charging demand becomes more forecastable with increasing aggregation. As the EVSEs are located at commercial facilities, weekdays show a significantly higher demand than weekends. In order to harness the flexibility that is offered by aggregating multiple EVs, a model is proposed in the following section.

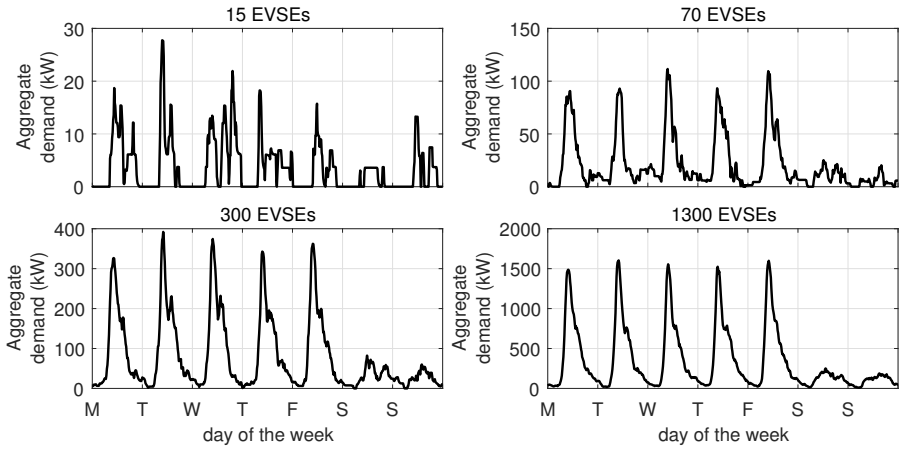

Figure 5.1: Weekly demand at different aggregations (adapted from [Pub. E]).

5.2 Equivalent time-variant storage model to harness the aggregate flexibility of electric vehicles

This section presents an equivalent time-variant storage model to harness the aggregate flexibility from tens to thousands of EVs. The virtual storage model can be controlled to fulfill specific objectives and serve as a demand-side flexibility asset. An aggregator could use it to directly participate in the wholesale market and minimize the operational costs [242, 253]. DSOs could use the flexibility to resolve local issues, or in the future, provide ancillary services to the TSOs [9, 254–257]. The equivalent storage model could also be used for short-term planning purposes, e.g. day-ahead scheduling of demand, in order to avoid abnormal conditions when the grid is operated close to its technical limits [258].

The presented model is evaluated using data from 1341 EVSEs located in Northern California. The data was provided by ChargePoint, the owner of the EVSEs. The EVSEs are spread throughout

75 zip code regions in Northern California with 451,999 charging sessions covering the full year of 2013. For each charging session, i.e. from plug-in to departure of an EV, following data is reported:

- Plug-in and departure time stamps
- Average and peak power every 15 min
- Charged energy every 15 min
- Charging port type
- Zip code
- Non-residential building category

A detailed description of the data is provided in [Pub. E] where also the data preprocessing is explained.

5.2.1 Proposed storage model

The proposed approach is inspired by a model for thermostatically controlled loads (TCLs) proposed in [259]. Similarly, the equivalent storage model can be described by a number of parameters that are related to physical quantities as shown in Fig. 5.2. The main advantage of the proposed model is that all parameters can be evaluated per EVSE and easily aggregated by summation over an arbitrary number of EVSEs. Seven time-dependent parameters comprise the model whereas t is the time step of the storage model and Δt (= 15 min) is the discretization step. The parameters are described in the following:

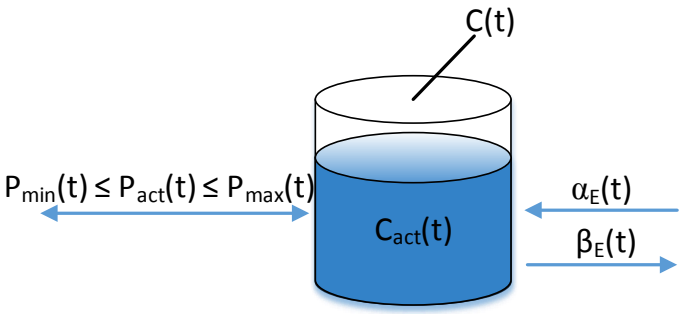

Figure 5.2: Proposed equivalent time-variant storage model [Pub. E].

Capacity boosting rate $\alpha_{\mathbf{E}}(\mathbf{t})$ (kWh)

Represents the amount of energy capacity added to the equivalent storage at time t. It is proportional to the amount of capacity connecting to the system at time t. The added capacity is equal to the amount of energy that will be charged in the sessions, it is not the actual total capacity of EV batteries that are connecting. The total EV battery would include any residual energy left in the batteries when they plug in and also any uncharged capacity that remains when they depart. Due to that, the capacity represents a conservative estimation of the total capacity of the system.

Equation (5.1) shows how α_E is aggregated for an arbitrary number of EVSEs denoted n_{EVSEs} whereas E_i represents the amount of energy to be charged during the charging session of EV i.

Equation (5.2) defines $\delta_{a,i}$, which is a Kronecker impulse function centered at the arrival time of the i-th EV. It assumes the value 1 during the interval where the EV arrives and is 0 elsewhere.

$$\alpha_E(t) = \sum_{i=1}^{n_{EVSEs}} E_i \cdot \delta_{a,i}(t) \tag{5.1}$$

$$\delta_{a,i}(t) = \begin{cases} 1 \text{ at arrival time of EV i} \\ 0 \text{ otherwise} \end{cases} \tag{5.2}$$

Energy dissipation rate $\beta_{\mathbf{E}}(\mathbf{t})$ (kWh)

Represents the amount of energy and capacity leaving from the system when a car is unplugged. Here, E_i represents the amount of energy that has been charged during the session whereas $\delta_{d,i}$ is again the Kronecker impulse function centered at the EV departure time. Note that the removed capacity is of equal magnitude as the added capacity when plugging in, but with opposite sign.

$$\beta_E(t) = \sum_{i=1}^{n_{EVSEs}} -E_i \cdot \delta_{d,i}(t) \tag{5.3}$$

$$\delta_{d,i}(t) = \begin{cases} 1 \text{ at departure time of EV i} \\ 0 \text{ otherwise} \end{cases} \tag{5.4}$$

Total capacity $\mathbf{C}(\mathbf{t})$ (kWh)

Represents the total capacity of the system at time t and is equal to the sum of capacity at the previous time step and the added and removed capacity from plugging and unplugging EVs, respectively.

$$C(t) = C(t-1) + \alpha_E(t) + \beta_E(t) \tag{5.5}$$

Actual energy content $\mathbf{C_{act}}(\mathbf{t})$ (kWh)

The state variable representing the actual energy content of the equivalent storage. $P_{act}(t)$ denotes the actual charging/discharging rate of all connected EVs at time t. Reminder: the discretization step size Δt is 15 minutes.

$$C_{act}(t) = C_{act}(t-1) + P_{act}(t) \cdot \Delta t + \beta_E(t) \tag{5.6}$$

Actual charging/discharging rate $\mathbf{P_{act}}(\mathbf{t})$ (kW)

Represents the actual charging/discharging rate of the plugged EVs at time t. Positive sign means charging while negative sign means discharging.

Minimum/maximum charging rates $\mathbf{P_{min}(t)}$/$\mathbf{P_{max}(t)}$ (kW)

Represents the minimum/maximum charging rate of all plugged EVs at time t. The physical charging/discharging limitations of individual EVSEs are represented by P_i^+ and P_i^-, respectively. For V2G capability, P_i^- can be set to a negative value.

$$P_{min}(t) = P_{min}(t-1) + \sum_{i=1}^{n_{EVSEs}} P_i^- \cdot \delta_{a,i}(t) + \sum_{i=1}^{n_{EVSEs}} -P_i^- \cdot \delta_{d,i}(t) \tag{5.7}$$

$$P_{max}(t) = P_{max}(t-1) + \sum_{i=1}^{n_{EVSEs}} P_i^+ \cdot \delta_{a,i}(t) + \sum_{i=1}^{n_{EVSEs}} -P_i^+ \cdot \delta_{d,i}(t) \tag{5.8}$$

State-of-charge $\mathbf{SOC(t)}$ (%)

Is defined according to the general convention as the actual energy content of the equivalent storage $C_{act}(t)$ divided by the total capacity $C(t)$. If the total capacity is zero, the SOC is defined to be zero.

$$SOC(t) = \begin{cases} \frac{C_{act}(t)}{C(t)} \cdot 100\ \% \text{ for } C(t) \neq 0 \\ 0 \text{ else} \end{cases} \tag{5.9}$$

Important note regarding V2G: Additional considerations around the assumption that there is no residual energy left in the battery when the EV is connected shall be made when V2G is available. In a V2G scenario with unknown residual energy storage capacity, only the energy that has been charged into the battery can be used for V2G operation. Additionally, a constraint for the minimum SOC at the end of charging session needs to be defined. This means that the optimum may be found only if the residual energy storage capacity is known when an EV connects. Here, V2G is not included in the scenarios, but, the proposed storage model does allow for inclusion of V2G capability.

5.2.2 Uncontrolled demand and storage parameters: aggregation and forecast

From a grid operator's perspective it is already interesting to forecast the uncontrolled demand of EV charging in the near future (e.g. day-ahead) for improved short-term planning. In case the EVs can be controlled, the grid operator is interested in the forecast of the parameters of the proposed equivalent storage model in order to utilize the available flexibility in short-term operation's planning[2]. In particular, the forecastability of the four parameters P_{act} representing the uncontrolled demand, and P_{max}, C and α_E representing the storage parameters, is analyzed. Depending on the application of the storage model, different parameters need to be forecasted. Here, the storage model is used as a flexibility asset for short-term planning and it is shown in Section 5.2.3 that only this set of parameters is needed to run the optimization. However, the unforecasted parameters P_{min} and β_E have similar properties as their counter equivalents P_{max} and α_E, hence, the forecast performance is assumed to be in the same order of magnitude.

Uncertainties in these forecasts cause the operator to procure more expensive generation to manage unexpected changes in demand, hence, these uncertainties and their relation to the aggregation of EVs need to be analyzed.

[2]This assumes an active market participation of future distribution system operators (DSOs) where flexibility is contracted by the DSO on behalf of the transmission system operator (TSO) [257].

Aggregation metric

First, a metric that allows the comparison of different aggregation levels has to be defined, because aggregating over the number of EVSEs does not provide a suitable metric for comparison due to varying energy demand at different EVSEs. Comparing EVSEs with different energy demand levels would not deliver insightful results.

Therefore, it is proposed to aggregate EVSEs by the average daily energy demand over the past two weeks before the forecasting period, as shown in (5.10), where $\overline{E}_i^{14\,d}$ denotes the 14-day-average energy demand at EVSE i. Thus, a certain aggregation level can be achieved by the combination of different numbers of EVSEs depending on how frequently the EVSEs have been used. The aggregation can be achieved by a small number of EVSEs with many charging sessions or by a larger number of EVSEs with a lower charging frequency.

$$E_{agg} = \sum_{i=1}^{n_{EVSEs}} \overline{E}_i^{14\,d} \tag{5.10}$$

Fig. 5.3 shows the relation between the aggregation metric and the actual number of EVSEs to highlight that a specific aggregation can be achieved by a different number of EVSEs. However, the trend shows a linear relation between the actual number of EVSEs and the aggregation metric.

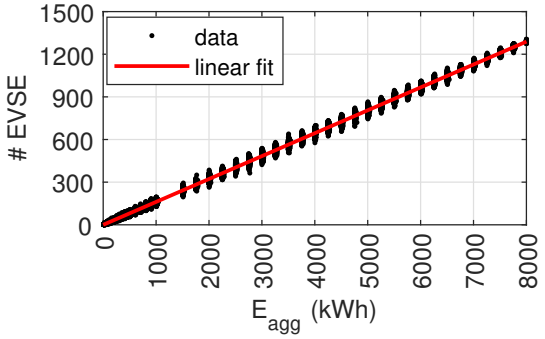

Figure 5.3: EVSEs versus aggregation and linear fit.

Autoregressive forecast model

Autoregressive integrated moving average (ARIMA) models are used for short-term forecasting. An ARIMA model is fit for each forecasted parameter, i.e. P_{act}, P_{max}, C and α_E and aggregation level in the analysis. The Box-Jenkins methodology analyzing the autocorrelation function (ACF) and partial autocorrelation function (PACF) of the input series is used to identify the model parameters [260]. The procedure resulted in the use of seasonal autoregressive models (AR) without moving average (MA) terms for all parameters. For a detailed description of the autoregressive models the interested reader is referred to [Pub. E].

Metric to measure the forecast performance

The literature provides a number of metrics to quantify the forecast performance. In particular in the forecasting literature, the Mean Average Error (MAE), Root Mean Squared Error (RMSE), Mean Average Percentage Error (MAPE) and Coefficient of Variation (CV) are used whereas the two most commonly used metrics are the CV and MAPE [261].

Here, the CV is used to quantify the forecast performance because it allows to compare time series at different scales [261], which are the different aggregation levels in this case. The CV is defined as the ratio of the RMSE and the mean of the signal as shown in (5.11) where y denotes the signal and $\hat{y}$ its forecast. T denotes the length of the signals, i.e. the number of data points. Due to the fact that the mean of the signal is used in the denominator, the CV still provides reasonable results even if the forecasted signal has some data points close to zero.

$$CV(y,\hat{y}) = \frac{\sqrt{\frac{1}{T}\sum_{t=1}^{T}(\hat{y}(t)-y(t))^2}}{\frac{1}{T}\sum_{t=1}^{T} y(t)} \tag{5.11}$$

Forecast analysis

To analyze how the aggregation affects the performance of the forecast, 1000 random combinations of EVSEs for each aggregation level for seven consecutive days are generated. Then, for each day and aggregation level, the parameters are forecasted for the following day, i.e. 96 values each representing a 15-min-interval, and the performance of each day-ahead forecast is evaluated by means of the CV. Forecasting for an entire week should capture effects that may occur on weekdays or on weekends only.

Fig. 5.4 shows the results for the forecast of the uncontrolled demand. To put the results into perspective, the three upper subplots show the results for a low, medium and high aggregation including the achieved performance of the forecast in form of the CV. The black line shows the actual demand whereas the red one shows the forecasted demand. The plots show qualitatively and quantitatively that the accuracy of the forecast improves with higher aggregations. This is indicated by the CVs where it decreases from 70 % for the low, to 46 % and 21 % for the medium and high aggregation, respectively.

The results for the entire aggregation spectrum, including 1000 random EVSE combinations for 7 consecutive days, are shown in the lower subplot of Fig. 5.4. This plot reveals that the forecast

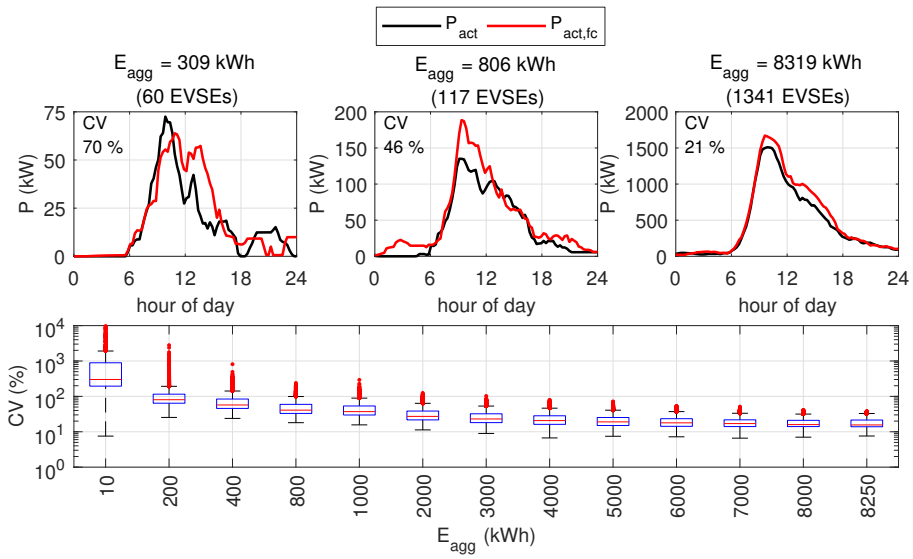

Figure 5.4: Time-domain plot of forecast for three different aggregation levels and variation of forecast errors versus aggregation level [Pub. E].

uncertainty considerably decreases with higher aggregation levels. The median of the forecast performance approaches about 16 % whereas the 25th and 75th percentiles lie at 14 % and 21 %, respectively.

Recapping the qualitative assessment of Fig. 5.1 where higher aggregations showed to be more regular and predictable, the presented results in Fig. 5.4 definitely confirm this hypothesis. Indeed, the uncontrolled demand at higher aggregation levels is forecastable with lower uncertainty. Moreover, employing more advanced forecasting algorithms is expected to further improve the performance. One should note that the forecasts in this study are done using basic AR models because implementation of advanced forecasting algorithms is beyond the scope of the work.

Similar to the analysis of the uncontrolled demand, 1000 random EVSE combinations for each aggregation for 7 consecutive days are generated with the storage parameters. Then, the parameters are forecasted for the next 24 h and the performance of the forecast is evaluated by means of the CV.

Fig. 5.5 shows the results for the forecast analysis of the storage parameters C, α_E and P_{max}. The results are similar to the ones obtained for the uncontrolled demand. With larger aggregations, the forecast uncertainty for all storage parameters decreases significantly. The achieved performance for day-ahead forecasts for all storage parameters lies at around 10 % for the highest aggregation in this case.

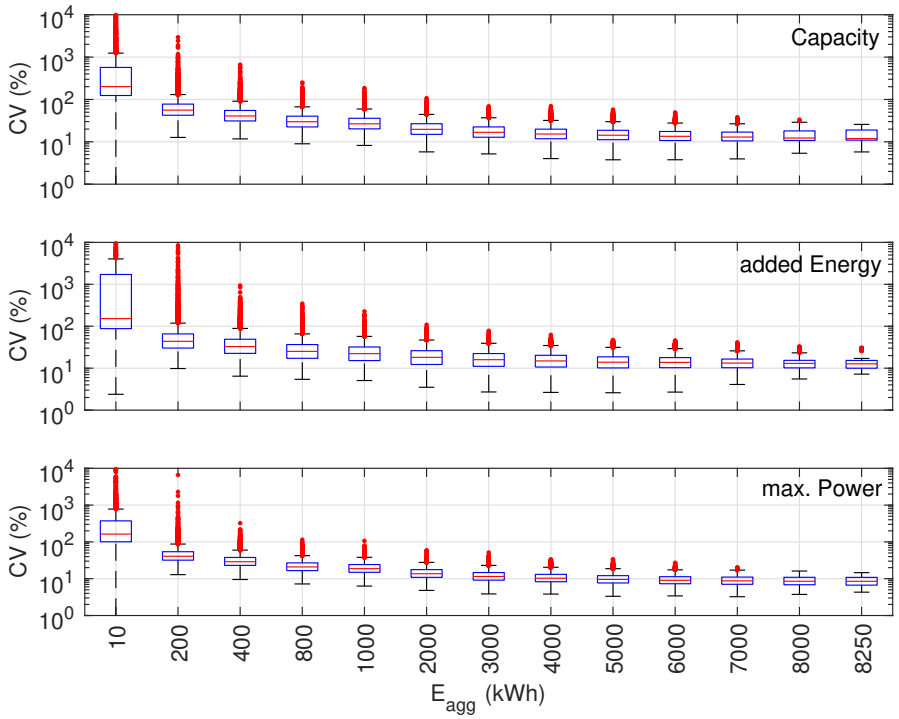

Figure 5.5: Variation of forecast accuracy versus aggregation level [Pub. E].

5.2.3 Application of the storage model

This section presents two possible applications of the storage model which are described in the following:

Application I Peak reduction of EV charging with respect to the uncontrolled charging case. The maximum possible reduction of the peak power consumption relative to the maximum peak power of the uncontrolled charging is analyzed. The power schedule is arranged such that costs are minimized over the day-ahead price whereas the maximum allowed charging power is stepwise reduced until no feasible solution is found anymore. The lowest maximum charging power where a feasible solution is found marks the maximum peak reduction.

Application II Energy arbitrage scenario where energy is purchased in the day-ahead market and the power schedule is arranged, such that costs are minimized over the day-ahead price. An additional cost evaluated on the real-time price is added for deviating from the optimum due to the imperfect forecast of storage parameters.

For both presented applications, the storage parameters C, P_{max} and α_E are forecasted for the next day, i.e. for the next 24 h in 15 min intervals which is equal to 96 data points. The EVs do not have V2G capability and therefore P_{min} is equal to zero. The parameter β_E is not forecasted as it is not needed.

The optimized charging schedules for the 15 min intervals (equal to 96 intervals per day) for both applications is calculated by using the linear optimization problem described in (5.12). The total costs are minimized by optimally scheduling the demand given the day-ahead price $p_{DA}(t)$ and the forecasted and original storage parameters, respectively. The first constraint describes the physical power limits within which charging is possible. The second constraint describes the initial energy state of the storage. In this case it is set to 50 % of the total capacity. This value is arbitrary and can be chosen as preferred. The third constraint tracks the energy state of the storage model and ensures that the energy content is between zero and the total capacity for every 15 min interval Δt. The initial energy content of the storage is C_0 whereas $\sum_{i=1}^{t} -P_{act}(i) \cdot \Delta t$ is the cumulative sum of the charged energy, and $\sum_{i=1}^{t} \alpha_E(i)$ is the cumulative sum of the added energy. The fourth constraint ensures that the state-of-charge (SOC) of the storage model at the end of the day (t_{96}) is again 50 % as defined also for the beginning of the day. That means that the storage model is in the same state at the beginning and at the end of the day. The forecasted parameters are checked for certain conditions to guarantee a feasible solution in the optimization: a) P_{max} must be greater than zero at all times, b) cumulative sum of α_E must be greater or equal than the cumulative sum of the positive changes of C. Moreover, boundary conditions are defined, such that the storage capacity, the maximum power and the SOC at t_1 and t_{96} are equal, respectively.

$$
\begin{aligned}
&\min_{P} \textstyle\sum_{t=1}^{96} P(t) \cdot p_{DA}(t) \\
&\text{subject to} \\
&0 \leq P(t) \leq P_{max}(t) \\
&C_0 = \tfrac{C(t_1)}{2} \\
&0 \leq C_0 + \textstyle\sum_{i=1}^{t}(-P(i) \cdot \Delta t + \alpha_E(i)) \leq C(t) \\
&C_0 + \textstyle\sum_{t=1}^{96}[-P(t) \cdot \Delta t + \alpha_E(t)] = \tfrac{C(t_{96})}{2}
\end{aligned}
\tag{5.12}
$$

Application I

The first application is peak reduction of EV charging where the peak power of uncontrolled charging serves as a reference. As shown in Fig. 5.1, uncontrolled charging produces significant

peaks at around midday (commercial EVSEs) which could lead to congestion at DSO level. Therefore, it would be beneficial to reduce the peak and shift some of the demand in time. In order to do so, the parameters of the storage model are forecasted and the power schedule for the next day is arranged so that the costs are minimized over the day-ahead price. The maximum allowed charging limit is stepwise reduced until the minimum, where all constraints are fulfilled, is found. This minimum corresponds to the maximum charging power reduction with respect to the uncontrolled peak consumption. This is done for 1000 random EVSE combinations for each aggregation level.

To visualize the procedure, the upper plot of Fig. 5.6 shows an example of peak reduction for a 24 h period. The two dotted lines show the maximum demand of uncontrolled charging (black) and controlled charging with reduced peak (orange). The uncontrolled charging demand P_{uc} is shown in black, the maximum charging limit P_{max} is shown in red, and the optimal charging schedule P_{opt} within this boundaries is shown in green. This example illustrates a possible peak reduction of 50 % with respect to the maximum of P_{uc} which always serves as the reference. In the next iteration, the upper limit of P_{max} is reduced by 1 % and the schedule recalculated. If a feasible solution is found, P_{max} is reduced again by 1 %. This procedure continues until the problem becomes infeasible. The lowest upper limit of P_{max}, where a feasible solution is found, marks the maximum possible peak reduction.

The lower plot in Fig. 5.6 shows the maximum possible peak reductions over the aggregation. The results of all random EVSE combinations (1000 combinations per aggregation) are shown in orange, whereas the median for each aggregation level is shown in red. At small aggregations, there are no or only small reductions possible whereas at higher aggregations the peak can be reduced to around 45 % of the uncontrolled peak. Significant reductions are already possible at aggregations around 1000 kWh, but also the variations within the different EVSE combinations are larger. This application shows the practical usefulness of the proposed storage model. However, this example does not consider forecast errors which considerably decrease with increasing aggregation. Thus,

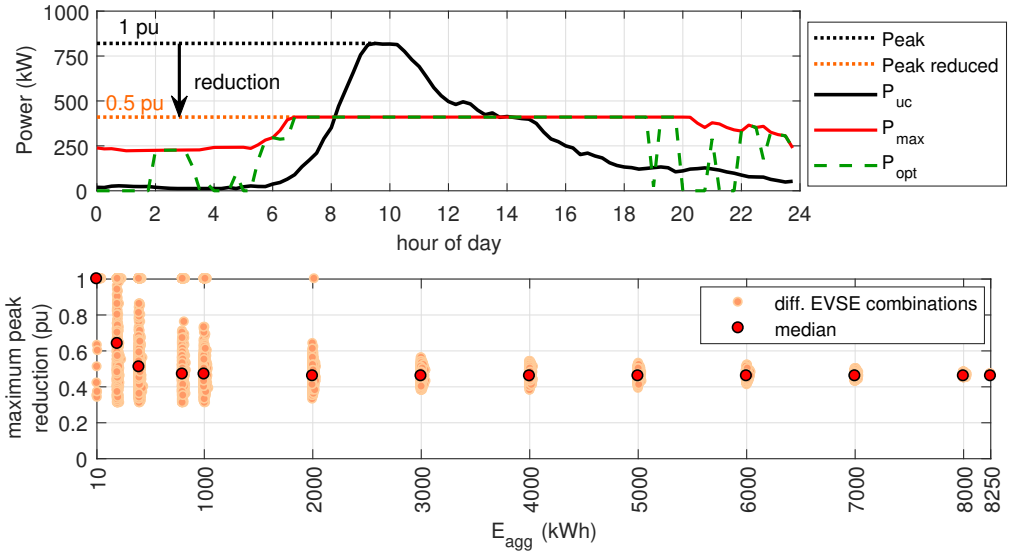

Figure 5.6: Upper plot: example of peak reduction. Lower plot: maximum possible peak reduction over aggregation with respect to maximum demand of uncontrolled charging.

the forecast uncertainty must be considered when analyzing a specific application of the storage model as it will significantly affect the results. The presented application intends to show the technical possibilities of the storage model, hence, the forecast uncertainty is not considered. However, the second application incorporates also the forecast uncertainty in the analysis.

Application II

The second application is an energy arbitrage scenario where energy to charge the EVs is purchased in the day-ahead market. The benefit of aggregation by reducing the uncertainty of the forecast is analyzed. Additional costs are imposed due to imperfect forecast of the storage parameters. To show the advantage of the proposed storage model for this application, a comparison with the current practice is made. Therefore, three scenarios are considered given a day-ahead price p_{DA} and a real-time price p_{RT}. The day-ahead price is from the CAISO day-ahead market from June 01, 2017 and the real-time price is chosen to be 1.5 times the day-ahead price. The three scenarios are described in the following:

1) **uncontrolled charging $\mathbf{P}_{uc}$** (current practice): the costs are determined by multiplying the uncontrolled demand with the real-time price as shown in (5.13),
2) **controlled charging with forecasted storage parameters $\mathbf{P}_{fc}$** (application of storage model): the power schedule is arranged, such that costs are minimized over the day-ahead price. An additional cost evaluated on the real-time price is added for deviating from the optimum due to imperfect forecast of storage parameters as shown in (5.14),
3) **controlled charging with perfect forecast $\mathbf{P}_{opt}$** (benchmark case): the optimal case describes the minimal costs for the given market context due to a perfect forecast of all involved parameters and is calculated according to (5.15).

Only the optimal cost in (5.15) is calculated by solving the optimization problem shown in (5.12). The cost of uncontrolled charging can be directly calculated by multiplying the demand with the real-time price and the cost of the forecasted scenario is evaluated after the optimization.

$$cost_{uc} = \sum_{t=1}^{96} P_{uc}(t) \cdot p_{RT}(t) \tag{5.13}$$

$$cost_{fc} = \sum_{t=1}^{96} P_{fc}(t) \cdot p_{DA} + |P_{fc}(t) - P_{opt}(t)| \cdot p_{RT}(t) \tag{5.14}$$

$$cost_{opt} = \sum_{t=1}^{96} P_{opt}(t) \cdot p_{DA}(t) \tag{5.15}$$

Similar as before, 1000 random EVSE combinations for each aggregation level are generated. Then the storage parameters are forecasted, the optimization is run, and the total costs for each scenario are evaluated according to (5.13) - (5.15).

Fig. 5.7 shows the costs over the aggregation level. The upper plot shows the total costs for all random EVSE combinations and each scenario in light color whereas the median is shown in dark color. Naturally, the total costs of charging are increasing with increasing aggregation level because more energy is requested. To get an insight on how well the optimization with forecasted parameters performs, a comparison to the optimal case with perfect information is carried out. Here, the costs of the uncontrolled/forecasted scenarios are normalized over the optimum, i.e.

$(cost_{\{uc,fc\}} - cost_{opt})/cost_{opt}$. The lower plot shows the additional costs that are added to the optimum in percent of the total optimal costs. The plot shows that at higher aggregations the additional costs due to imperfect forecasts decreases. The median cost of uncontrolled charging stabilizes at an aggregation of about 1000 kWh, but is more than double of the minimal costs. In the forecast scenario, the costs are only about 50 % higher as in the optimal scenario at the highest aggregation.

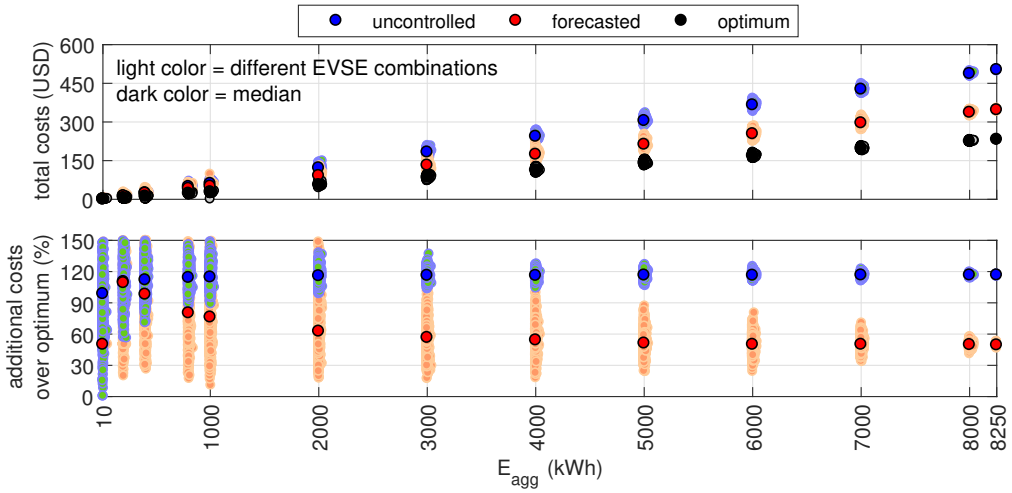

Figure 5.7: Total costs and additional costs of the uncontrolled and forecasted scenario over the optimal scenario for different aggregation levels [Pub. E].

5.3 Summary

This chapter described the background and motivation for smart EV integration. In particular, the large-scale integration of EVs not only poses a challenge for future power systems, but also an opportunity if the charging is actively managed. In order to allow the active management of large populations of EVs, an equivalent storage model for aggregation aiming at centralized control approaches is proposed. The storage model is described by a number of parameters that are related to physical quantities and allows to aggregate an arbitrary number of EVs, i.e. there is no limitation about the aggregation size. As the model aims at enhancing power system operation, the relation between forecastability of the model parameters and aggregation level is investigated on a day-ahead horizon. The analysis shows that the forecast uncertainty significantly reduces for higher aggregations, which applies for both uncontrolled charging and the storage model parameters. This confirms that forecasts are more accurate for larger populations of EVs and, therefore, it is beneficial to aggregate over a larger number of EVs.

Two possible applications of the storage model are presented to show the technical possibilities and economical benefits that emerge from the proposed model. The first application shows how much the peak of uncontrolled charging can be reduced by using the storage model at different aggregation levels. The analysis showed that the peak can be reduced to around 45 % of the uncontrolled charging for larger aggregations. Smaller aggregations present a higher variability for the possible peak reduction. Expressed in terms of flexibility, higher aggregations provide higher flexibility. The second application shows an energy arbitrage case where energy is purchased in the day-ahead market based on an optimized charging schedule on forecasted storage parameters.

The forecast uncertainty is considered by adding additional costs for deviating from the optimal charging power which is determined by perfect forecasts. The costs are put into perspective by comparison of uncontrolled charging, optimized charging schedule using forecasted storage parameters and the optimal charging case. The results show that an economical benefit arises by using the storage model to optimize the charging schedule despite imperfect forecasts. However, the aggregation size plays again a key role as higher aggregations have more accurate forecasts leading to higher economical benefits.

The two presented applications clearly showed the technical and economical potential offered by the proposed equivalent storage model, but the application of the model is by far not limited to these. At higher aggregations, even reserve provision is possible due to the high flexibility in shiftable energy, e.g. manual reserve that is activated for a specified time by the control center as it is the case in Denmark. That means that deployment of the model could significantly enhance power system operation in different ways. Naturally, some aspects need to be addressed when taking the developed models to real power system environment. For example how the charging schedule is disaggregated from aggregated level to individual EVs. This is considered future work, as the setup of these control techniques will also depend on the type of information which will be available in real-time.

CHAPTER 6

Conclusion and future work

This dissertation focused on selected aspects aimed at increasing the situation awareness of control room operators by developing innovative monitoring and decision support tools. The presented work covers classical power system issues such as transient stability, innovative data-driven approaches for voltage estimation, and aggregation functions for harnessing time-dependent flexibility from geographically distributed EVs. Around this three major areas, five research questions for the PhD project have been outlined in Section 1.2. In the following they are concluded.

[Q1] *What are the state-of-the-art techniques for transient stability preventive and emergency control and what are the deficiencies concerning the transition to a RES-based power system?*

The state-of-the-art review revealed that there are more conventional than renewable-based transient stability techniques by now. A large number of improvement techniques are for emergency control whereas fewer are available for preventive control. Two conclusions can be drawn from this.

First, fewer units are being available for transient stability control due to phasing-out of conventional units in favor of renewable-based units. Therefore, transient stability improvement techniques including RES-based units must be developed.

Second, existing preventive techniques must be enhanced and new techniques including RES-based units must be developed. From an operational perspective it is preferred to operate and maintain a secure state through preventive controls rather than moving into emergency state relying on successful functioning of emergency controls risking a blackout.

Due to the fact that HVDC links do not support the AC system when operated in constant power mode, dedicated control of HVDC links to support the AC system will become more important.

Another important aspect related to grid code requirements is high voltage ride-through (HVRT). Whereas low voltage ride-through (LVRT) is part of most grid codes, HVRT is not always thoroughly defined. Temporary overvoltages could cause large portions of RES units to disconnect putting additional strain on synchronous generators. Therefore, a discussion about HVRT and an evaluation of the need to include it into grid codes must be started.

Virtual inertia has also been identified as a topic of interest for transient stability emergency control. Currently it is only discussed with respect to frequency stability, but the impact on the transient stability has not been sufficiently investigated. Therefore, large-scale deployment of virtual inertia will require an investigation of effects on other stability aspects.

[Q2] *How can transient stability be efficiently monitored and maintained in an online fashion?*

As pointed out in the previous research question, existing preventive techniques must be enhanced and future control rooms must shift to a more proactive operation. Therefore, a

decision support tool for transient stability preventive control considering the full system dynamics is proposed. The tool analyzes the CCT of critical buses and suggests the control room operator a re-dispatch of generators if the pre-defined stability margins are insufficient. To allow online application of the tool, a fast converging technique to determine the needed re-dispatch for multi-machine systems by first approximating the needed dispatch using the virtually linear relationship between the CCT and active power setpoint of the generator is proposed. In addition, the computational burden is reduced significantly by employing a critical bus screening (CBS) and a fast critical contingency screening (FCCS) to identify and analyze exclusively the critical buses. As the proposed re-dispatch approach is of sequential nature, only a near-optimal solution is found. This is an important aspect as the preventive re-dispatch imposes additional generation costs. The optimality of the solution has not been compared to approaches that yield the optimal solution as this was beyond the scope of the work, but it is acknowledged as future work. However, it was shown that the proposed re-dispatch approach finds the needed re-dispatch within 2 iterations and delivers a solution where all critical clearing times (CCTs) satisfy the pre-defined limit. The execution time evaluation of the approach showed that the most time-consuming step of the procedure is the CCT determination, but it is foreseen that efficient implementation paired with more powerful processing units in a control room will decrease the total execution time of the procedure significantly.

[Q3] *How can currently available measurements be utilized to establish a data-driven neural network approach to increase the real-time voltage observability of active distribution grids?*

This dissertation presents a novel NN-based approach for real-time voltage estimation at particular LV buses where measurements are not available in real-time, but historical data is available. A specific case are smart meter measurements which are not available in real-time, but they are available as historical data. On the other hand, data from the substation is available in real-time. These two data sources can be used to establish a real-time voltage estimator for the LV buses whose measurements are not available in real-time.

In the training phase, the estimator is established using the available historic data to train a cascade-forward neural network with one hidden layer which is suitable for fitting problems like this. In the real-time estimation phase, the data stream from the substation is fed in the estimator and the phase-neutral voltages at the downstream buses are estimated.

In this work only electrical measurement data was used to establish the voltage estimator. The approach can be extended to include additional non-electric data that is available, e.g. solar radiation measurements. Incorporating these kind of data might allow further improvement of the estimation accuracy. However, further investigation must be carried out on how non-electric measurements affect the performance of the estimator.

[Q4] *What are the capabilities and limitations of the neural network-based approach for real-time voltage estimation in active distribution grids?*

The approach was first tested on simulated data where encouraging results testified a high suitability for voltage estimation under complex load flow scenarios caused by distributed generation. The maximum absolute errors of the estimation on the simulated data were below 1.5 V at a nominal phase-neutral voltage of 230 V.

To take the approach closer to application in real environment it is validated on field data from a real distribution grid with PV generation. The validation on field data has revealed deeper insights of the capabilities and limitations of the approach.

In the first step, a ranking approach for choosing appropriate input variables of the estimators has been proposed. Based on the correlation between input and output variables and among input variables, the best performance for a certain number of input variables was determined. The results showed that the performance declines with lower number of input variables, but for each number of input variables there exists an combination of variables for which the performance of the estimator is best. However, the proposed algorithm is a greedy algorithm that eliminates the least relevant variables one by one while the global optimum might be found only by trying all possible combinations. The assessment also showed that the number of neurons in the hidden layer is not of great importance as long as the model is not underdetermined. Overfitting is prevented by validation checks after each iteration in the training process, i.e. training stops if the model fails to improve the performance on the validation data set for 10 consecutive iterations.

Another important aspect is the data quantity used for the training of the model. The analysis showed that about 30 days of historical data with a resolution of 1 - 10 min is enough to establish an accurate estimator. However, the achieved performance varies for different feeders as they have different characteristics.

The estimator must be retrained in recurring intervals in order to maintain an acceptable estimation performance. The analysis showed that the 3-σ confidence interval of the estimation error is around $\pm$2 V for retrain intervals below 20 days. That means, the error of the estimation for retrain intervals under 20 days is approximately 0.87 % of the nominal phase-neutral voltage (230 V). That is comparable to the measurement uncertainty of 0.5 % of class B meters defined in IEC 61000-4-30.

Additionally, the estimator was found not to be sensitive to high PV in-feed and reverse power flows. The errors during periods of high load, and periods of high PV generation do not show any noticeable differences.

[Q5] *How can the flexibility from tens to thousands of EVs be utilized to enhance power system operation?*

In order to harness the aggregate flexibility of EVs, an equivalent time-variant storage model aimed at centralized control approaches is proposed in this dissertation. The storage model is described by a number of parameters that are related to physical quantities and allows to aggregate an arbitrary number of EVs, i.e. there is no limitation on the aggregation size.

The forecastability assessment for both the uncontrolled charging and the equivalent storage parameters showed that the forecast uncertainty significantly reduces with larger aggregations. The median of the CV of the forecasts is about 16 % and 10 % for the uncontrolled charging and the storage parameters at the highest investigated aggregation level, respectively. As the forecasts were made using basic autoregressive models it is expected that the forecasting performance would further improve when more advanced forecasting algorithms are used. However, in general, it is beneficial to aggregate over a larger number of EVs because the forecasts become more certain.

The two presented applications showed that the proposed model introduces great technical possibilities and economical benefits. It was shown that the peak demand of uncontrolled

charging can be reduced to 45 % by using the storage model at higher aggregations. Lower aggregations showed a higher variability of the possible peak reduction, i.e. sometimes the peak can be reduced only to 80 % and sometimes even down to about 40 %. Expressed in terms of flexibility, higher aggregations provide higher flexibility. The energy arbitrage scenario showed that the proposed model also offers economic benefits with uncertain forecasts. The costs of charging compared to the optimal case with perfect forecast can be reduced from more than double for uncontrolled charging to only about 50 % more when using the storage model. However, the aggregation size plays a key role as higher aggregations have more certain forecasts, thus, higher economic benefit. Of course, the presented numbers depend on the given market context and application of the model and will be different in other contexts.

6.1 Future work

The presented work in this dissertation has also uncovered some questions that have not been answered and are subject to future work. They are elaborated in the following:

- The proposed transient stability approach is of sequential nature which delivers a near-optimal solution. It was not investigated how much this near-optimal solution differs from the optimal one. This would be interesting because the re-dispatch solution is directly linked to additional costs which is of crucial importance for preventive control.
- An evaluation of the execution time of the transient stability preventive control tool must be made in real control room environment. This includes more efficient implementation and use of more powerful processing units and would help to understand more the limitations of the approach regarding the total execution time.
- In the proposed voltage estimation approach exclusively electric variables have been used to establish the estimator. Due to the flexibility of the approach also non-electric variables could be used as input for the estimator, e.g. solar radiation measurements. The incorporation of such non-electric variables may improve the estimation performance, therefore, a detailed analysis of the impact of non-electric variables on the performance is needed.
- Regarding data cleaning and treatment for the proposed voltage estimator it is necessary to analyze how bad and missing data would affect the performance of the estimator in real-time estimation mode. Corrupted measurements cannot be prevented in real environment and therefore it is of crucial importance to understand the reliability/performance of the approach under these circumstances.
- The voltage estimator has been established for steady-state conditions only. However, it is in the nature of power systems that also abnormal and transient conditions occur during operation. Thus, it has to be investigated how the proposed approach can be extended to these conditions.
- An important aspect regarding the control of charging of aggregated EVs must be analyzed. Namely, how the aggregated charging signal will be disaggregated to charging signals for individual EVs. This has not been discussed in this dissertation but is crucial for real implementation. However, the set up of these control algorithms will also depend on which type of information will be available in real-time.

Bibliography

[1] Mehmet Baha Karan and Hasan Kazdagli. The development of energy markets in europe. In *Financial Aspects in Energy*, chapter 2, pages 11–32. Springer, 2011.

[2] European Commission. Energy roadmap 2050. Technical report, European Commission, Luxembourg, 2012.

[3] Daniel Kirschen and Goran Strbac. Why investments do not prevent blackouts. *The Electricity Journal*, 17(2):29–36, 2004.

[4] UCTE Investigation Committee. Final report - system disturbance on 4 November 2006. Technical report, UCTE, 2007.

[5] UCTE Investigation Committee. Final report of the investigation committee on the 28 September 2003 blackout in Italy. Technical report, UCTE, 2004.

[6] U.S.-Canada Power System Outage Task Force. Final report on the August 14, 2003 blackout in the United States and Canada: causes and recommendations. Technical report, U.S. Department of Energy and Canadian Ministry of Natural Resources, 2004.

[7] Mica Endsley. Situation Awareness in the Bulk Power System. In *Human Performance Conference*, Atlanta, 2012.

[8] Lawrence E. Jones. Strategies and Decision Support Systems for Integrating Variable Energy Resources in Control Centers for Reliable Grid Operations. Technical report, Alstom Grid Inc., Washington, DC, 2011.

[9] Wencong Su, Habiballah Rahimi-Eichi, Wente Zeng, and Mo-yuen Chow. A Survey on the Electrification of Transportation in a Smart Grid Environment. *IEEE Transactions on Industrial Informatics*, 8(1):1–10, 2012.

[10] Fabian Kennel, Daniel Görges, and Steven Liu. Energy Management for Smart Grids With Electric Vehicles Based on Hierarchical MPC. *IEEE Transactions on Industrial Informatics*, 9(3):1528–1537, 2013.

[11] Peter Palensky and Dietmar Dietrich. Demand side management: Demand response, intelligent energy systems, and smart loads. *IEEE Transactions on Industrial Informatics*, 7(3):381–388, 2011.

[12] V. Cagri Gungor, Dilan Sahin, Taskin Kocak, Salih Ergut, Concettina Buccella, Carlo Cecati, and Gerhard P. Hancke. A Survey on smart grid potential applications and communication requirements. *IEEE Transactions on Industrial Informatics*, 9(1):28–42, 2013.

[13] Ricardo Augusto Souza Fernandes, Ivan Nunes Da Silva, and Mario Oleskovicz. Load profile identification interface for consumer online monitoring purposes in smart grids. *IEEE Transactions on Industrial Informatics*, 9(3):1507–1517, 2013.

[14] Amir Safdarian, Mahmud Fotuhi-Firuzabad, and Matti Lehtonen. A distributed algorithm for managing residential demand response in smart grids. *IEEE Transactions on Industrial Informatics*, 10(4):2385–2393, 2014.

[15] Fabien Roques and Charles Verhaeghe. Options for the future of power system regional coordination. Technical report, Report for ENTSO-E, 2016.

[16] International Energy Agency (IEA). Status of Power System Transformation. System integration and local grids. Technical report, International Energy Agency (IEA), 2017.

[17] Felix F. Wu, Khorsrow Moslehi, and Anjan Bose. Power System Control Centers: Past, Present, and Future. *Proceedings of the IEEE*, 93(11):1890–1908, 2005.

[18] Mica R. Endsley. Situation awareness global assessment technique (SAGAT). In *IEEE National Aerospace and Electronics Conference*, pages 789–795, Dayton, 1988.

[19] Mica R. Endsley and Erik S. Connors. Situation Awareness: State of the Art. In *Power and Energy Society General Meeting - Conversion and Delivery of Electrical Energy in the 21st Century*, pages 1–4, Pittsburgh, 2008.

[20] Ya Jing Gao, Bo Ming Zhang, and Wen Chuan Wu. Functional requirements of next generation control center applications. In *International Conference on Advanced Power System Automation and Protection (APAP)*, pages 396–401, Beijing, 2011.

[21] Pei Zhang, Fangxing Li, and Navin Bhatt. Next-Generation Monitoring, Analysis, and Control for the Future Smart Control Center. *IEEE Transactions on Smart Grids*, 1(2):186–192, 2010.

[22] Vidya Vankayala, Ebrahim Vaahedi, Douglas Cave, and Martin Huang. Opening up for interoperability. *IEEE Power and Energy Magazine*, pages 61–69, 2008.

[23] Mini S. Thomas and John D. McDonald. Power System SCADA and Smart Grids. *IEEE power & energy magazine*, 2016.

[24] Dariush Shirmohammadi, W.H.E. H Edwin Liu, K.C. Ken C Lau, and H.W. Wayne Hong. Distribution automation system with real-time analysis tools. *IEEE Computer Applications in Power*, 9(2):31–35, 1996.

[25] Rajib Baran Roy. Application of SCADA for Controlling Electrical Power System Network. *UITS Journal*, 1(2):85–97, 2003.

[26] U.S. Department of Energy. Measurements, Communications, and Controls. Technical report, U.S. Department of Energy, 2015.

[27] Ebrahim Vaahedi. *Practical Power System Operation*. John Wiley & Sons, Inc., 2014.

[28] Thomas J. Overbye, Esa Rantanen, Sakis Meliopoulos, and George Cokkinides. Effective Power System Control Center Visualization. Technical report, Power Systems Engineering Research Center, 2008.

[29] Fred C. Schweppe and J. Wildes. Power System Static-State Estimation, Part I: Exact Model. *IEEE Transactions on Power Apparatus and Systems*, PAS-89(1):120–125, 1970.

[30] F.C. Schweppe and D.B. Rom. Power System Static-State Estimation, Part II: Approximate Model. *IEEE Transactions on Power Apparatus and Systems*, PAS-89(1):125–130, 1970.

[31] Fred Schweppe. Power System Static-State Estimation, Part III: Implementation. *IEEE Transactions on Power Apparatus and Systems*, PAS-89(1):130–135, 1970.

[32] Shan Zhong and Ali Abur. Auto tuning of measurement weights in WLS state estimation. *IEEE Transactions on Power Systems*, 19(4):2006–2013, 2004.

[33] Jeong-Won Kang and Dae-Hyun Choi. Distributed multi-area WLS state estimation integrating measurements weight update. *IET Generation, Transmission & Distribution*, 11(10):2552–2561, 2017.

[34] Catalina Gómez-Quiles, Antonio De La Villa Jaén, and Antonio Gómez-Expósito. A factorized approach to WLS state estimation. *IEEE Transactions on Power Systems*, 26(3):1724–1732, 2011.

[35] R. E. Kalman. A New Approach to Linear Filtering and Prediction Problems. *Journal of Basic Engineering*, 82:35–45, 1960.

[36] Terry E. Dielman. Least absolute value regression: recent contributions. *Journal of Statistical Computation and Simulation*, 75(4):263–286, 2005.

[37] A. Monticelli and A. Garcia. Reliable Bad Data Processing for Real-Time State Estimation. *IEEE Power Engineering Review*, PER-3(5):31–32, 1983.

[38] Jun Zhu and Ali Abur. Identification of network parameter errors. *IEEE Transactions on Power Systems*, 21(2):586–592, 2006.

[39] Lorenzo Zanni. *Power-System State Estimation based on PMUs : Static and Dynamic Approaches - from Theory to Real Implementation*. Dissertation, Ecole Polytechnique Federale de Lausanne (EPFL), 2017.

[40] A. Monticelli and Felix F. Wu. Network observability: Identification of observable islands and measurement placement. *IEEE Transactions on Power Apparatus and Systems*, PAS-104(5):1035–1041, 1985.

[41] S. Lefebvre, J. Prevost, and L. Lenoir. Distribution state estimation: A necessary requirement for the smart grid. In *IEEE Power and Energy Society General Meeting*, National Harbor, 2014.

[42] Anggoro Primadianto and Chan-Nan Lu. A Literature Review on Distribution System State Estimation. *IEEE Transactions on Power Systems*, 32(5):3875–3883, 2017.

[43] Lorenzo Zanni, Jean Yves Le Boudec, Rachid Cherkaoui, and Mario Paolone. A Prediction-Error Covariance Estimator for Adaptive Kalman Filtering in Step-Varying Processes: Application to Power-System State Estimation. *IEEE Transactions on Control Systems Technology*, 25(5):1683–1697, 2016.

[44] Styliani Sarri, Lorenzo Zanni, Miroslav Popovic, Jean Yves Le Boudec, and Mario Paolone. Performance Assessment of Linear State Estimators Using Synchrophasor Measurements. *IEEE Transactions on Instrumentation and Measurement*, 65(3):535–548, 2016.

[45] Marco Pignati, Lorenzo Zanni, Paolo Romano, Rachid Cherkaoui, and Mario Paolone. Fault Detection and Faulted Line Identification in Active Distribution Networks Using Synchrophasors-Based Real-Time State Estimation. *IEEE Transactions on Power Delivery*, 32(1):381–392, 2017.

[46] Andreas Martin Kettner and Mario Paolone. Sequential Discrete Kalman Filter for Real-Time State Estimation in Power Distribution Systems: Theory and Implementation. *IEEE Transactions on Instrumentation and Measurement*, 66(9):2358–2370, 2017.

[47] A. Monticelli. Electric power system state estimation. *Proceedings of the IEEE*, 88(2):262–282, 2000.

[48] A. A. Fouad. Dynamic Security Assessment Practices in North America. *IEEE Transactions on Power Systems*, 3(3):1310–1321, 1988.

[49] CIGRE Working Group C4.601. Review of on-line dynamic security assessment tools and techniques. Technical Report June, CIGRE, 2007.

[50] Sijie Chen, Qixin Chen, Qing Xia, Haiwang Zhong, and Chongqing Kang. N-1 security assessment approach based on the steady-state security distance. *IET Generation, Transmission & Distribution*, 9(15):2419–2426, 2015.

[51] Michael Tschampion, Matthias A. Bucher, Andreas Ulbig, and Göran Andersson. N-1 security assessment incorporating the flexibility offered by dynamic line rating. In *19th Power Systems Computation Conference (PSCC)*, Genoa, 2016.

[52] J. A. Huang, L. Loud, G. Vanier, B. Lambert, and S. Guillon. Experiences and challenges in contingency analysis at Hydro-Quebec. In *IEEE Power and Energy Society General Meeting*, San Diego, 2012.

[53] Hugo Morais, Pieter Vancraeyveld, Allan Pedersen, Morten Lind, Hjörtur Johannsson, and Jacob Østergaard. SOSPO - SP: Secure Operation of Sustainable Power Systems Simulation Platform for Real - Time System State Evaluation and Control. *IEEE Transactions on Industrial Informatics*, 10(4):2318–2329, 2014.

[54] Prabha Kundur, John Paserba, Venkat Ajjarapu, Göran Anderson, Anjan Bose, Claudio Canizares, Nikos Hatziargyriou, David Hill, Alex Stankovic, Carson Taylor, Thierry Van Vutsem, and Vijay Vittal. Definition and Classification of Power System Stability. *IEEE Transactions on Power Systems*, 21(3):1387–1401, 2004.

[55] ENTSO-E. Research and Development Plan: European Grid Towards 2020 Challenges and Beyond. Technical Report March, ENTSO-E, 2010.

[56] Guangya Yang, Hjörtur Jóhannsson, Morten Lind, Rodrigo Garcia-Valle, Mogens Blanke, Arne Hejde Nielsen, and Jacob Østergaard. Addressing the Security of a Future Sustainable Power System: The Danish SOSPO Project. In *IET International Conference on Advances in Power System Control, Operation and Management (APSCOM)*, Hong Kong, 2012.

[57] SOSPO Project, www.sospo.dk, 2016.

[58] PEGASE Project, www.fp7-pegase.com, 2012.

[59] Devinder Ghangass. Voltage stability operating limits and procedures for using the real time voltage stability application (RTVSA). Technical report, BC Hydro, 2015.

[60] Bander A. Allaf and Amin A. Elkhatib. Power system dynamics during disturbances. In *IEEE GCC Conference and Exhibition*, Kuwait City, 2009.

[61] PG&E Synchrophasor Project Team. Alstom and PG&E to advance Synchrophasor Grid Monitoring into Proactive Grid Stability Management, 2014.

[62] Robert Yinger. Irvine Smart Grid Demonstration, a Regional Smart Grid Demonstration Project. Technical report, U.S. Department of Energy (DoE), 2016.

[63] Deyu Cai. *Wide area monitoring, protection and control in the future Great Britain power system*. Dissertation, University of Manchester, 2012.

[64] Kun Zhu, Moustafa Chenine, and Lars Nordström. ICT Architecture Impact on Wide Area Monitoring and Control Systems' Reliability. *IEEE Transactions on Power Delivery*, 26(4):2801–2808, 2011.

[65] Marek Zima, Mats Larsson, Petr Korba, Christian Rehtanz, and Göran Andersson. Design Aspects for Wide-Area Monitoring and Control Systems. *Proceedings of the IEEE*, 93(5):980–996, 2005.

[66] Vladimir Terzija, Gustavo Valverde, Devu Cai, Pawel Regulski, Vahid Madani, John Fitch, Srdjan Skok, Miroslav M. Begovic, and Arun Phadke. Wide-area monitoring, protection, and control of future electric power networks. *Proceedings of the IEEE*, 99(1):80–93, 2011.

[67] I. Kamwa, J. Beland, G. Trudel, R. Grondin, C. Lafond, and D. McNabb. Wide-area monitoring and control at Hydro-Quebec: past, present and future. In *IEEE Power & Energy Society General Meeting*, Montreal, 2006.

[68] A. B. Leirbukt, J. O. Gjerde, P. Korba, K. Uhlen, L. K. Vormedal, and L. Warland. Wide Area Monitoring experiences in Norway. In *IEEE PES Power Systems Conference and Exposition*, pages 353–360, Atlanta, 2006.

[69] ENTSO-E. Impact of Increased Amounts of Renewable Energy on Nordic Power System Operation. Technical report, ENTSO-E, Brussels, 2010.

[70] Thomas Nikolakakis and Debabrata Chatopadhyay. Integrating Variable Renewable Energy into Power System Operations. Technical report, Live Wire, Washington, DC, 2015.

[71] K. Ogimoto. Power System Operation and Augmentation Planning with PV Integration. Technical report, University of Tokyo, Tokyo, 2014.

[72] Wilhelm Winter. European Wind Integration Study (EWIS) - Towards A Successful Integration of Large Scale Wind Power into European Electricity Grids. Technical report, ENTSO-E, Brussels, 2010.

[73] Ricardo Bessa, Carlos Moreira, Bernardo Silva, and Manuel Matos. Handling renewable energy variability and uncertainty in power systems operation. *Wiley Interdisciplinary Reviews: Energy and Environment*, 3:156–178, 2014.

[74] Aoife M. Foley, Paul G. Leahy, Antonino Marvuglia, and Eamon J. McKeogh. Current methods and advances in forecasting of wind power generation. *Renewable Energy*, 37:1–8, 2012.

[75] Yao Zhang, Jianxue Wang, and Xifan Wang. Review on probabilistic forecasting of wind power generation. *Renewable and Sustainable Energy Reviews*, 32:255–270, 2014.

[76] E Ela, V Diakov, E Ibanez, and M Heaney. Impacts of Variability and Uncertainty in Solar Photovoltaic Generation at Multiple Timescales. Technical report, National Renewable Energy Laboratory (NREL), Denver, 2013.

[77] Fangxing Li, Pei Zhang, and Navin Bhatt. Next Generation Monitoring and Control Functions for Future Control Centers. *Engineer*, 1(2):186–192, 2010.

[78] Michael Milligan, Bethany Frew, Ella Zhou, Douglas J. Arent, Michael Milligan, Bethany Frew, and Ella Zhou. Advancing System Flexibility for High Penetration Renewable Integration. Technical report, National Renewable Energy Laboratory (NREL), Denver, 2015.

[79] Ruud Kempener, Paul Komor, and Anderson Hoke. Smart Grids and Renewables - A Guide for Effective Deployment. Technical report, International Renewable Energy Agency (IRENA), 2013.

[80] Andrei Z. Morch, Klaas Visscher, Sigurd Hofsmo Jakobsson, Mattia Marinelli, Artjoms Obushevs, Stijn Uytterhoeven, Alexander M. Prostejovsky, Michael Pertl, Abdullah Nadar, Bülent Dag, and Irina Oleinikova. ELECTRA Deliverable 5.1: Increased Observability: Adaptive Assessment of Future Scenarios and Mapping of Observability Needs. Technical report, The ELECTRA Consortium, 2015.

[81] Klaas Visscher, Andrei Z. Morch, Sigurd Hofsmo Jakobsson, Håkon Marthinsen, Evangelos Rikos, Julia Merino Fernandez, Emilio Rodriguez, Berend Evenblij, Thomas Strasser, Roman Schwalbe, Eric Nens, and Martin Legry. ELECTRA Deliverable 5.2: Increased Observability: Functional description of the monitoring and observability detailed concepts for the Distributed Local Control Schemes. Technical report, The ELECTRA Consortium, 2015.

[82] Mattia Marinelli, Michael Pertl, Michel Rezkalla, Michal Kosmecki, Bogdan Sobczak, Robert Jankowski, Arkadiusz Kubanek, Andrei Z. Morch, Tor Inge Reigstad, Artjoms Obushevs, Antonio Gatti, Silvia Canavese, and Marco Rossi. ELECTRA Deliverable 5.4: Increased Observability: Functional description of the monitoring and observability detailed concepts for the Pan-European Control Schemes. Technical report, The ELECTRA Consortium, 2017.

[83] Mattia Marinelli, Kai Heussen, Thomas Strasser, Roman Schwalbe, Julia Merino Fernandez, Sandra Riano, Alexander M. Prostejovsky, Michael Pertl, Michel Rezkalla, Julian Croker, Berend Evenblij, Victoria Catterson, and Minjiang Chen. ELECTRA Deliverable 8.1: Future Control Room Functionality: Demonstration of visualization techniques for the control room engineer in 2030. Technical report, The ELECTRA Consortium, 2017.

[84] Victoria Catterson, Stephen McArthur, Minjiang Chen, Michael Pertl, Tor Inge Reigstad, Roberto Ciavarella, Marialaura Di Somma, Sandra Riano, and Roberto Zuelli. ELECTRA Deliverable 8.2: Future Control Room Functionality: Demonstration of decision support for real time operation. Technical report, The ELECTRA Consortium, 2017.

[85] Alexander M. Prostejovsky, Mattia Marinelli, Michel Rezkalla, Mazheruddin Syed, and Efren Guillo Sansano. Tuningless Load Frequency Control Through Active Engagement of Distributed Resources. *IEEE Transactions on Power Systems*, pages 1–10, 2017.

[86] Mattia Marinelli, Michael Pertl, Michel Rezkalla, Michal Kosmecki, Silvia Canavese, Artjoms Obushevs, and Andrei Morch. The Pan-European Reference Grid Developed in the ELECTRA Project for Deriving Innovative Observability Concepts in the Web-of-Cells Framework. In *51th International UniversitiesPower Engineering Conference (UPEC)*, pages 1–6, Coimbra, 2016.

[87] Michel Rezkalla, Antonio Zecchino, Michael Pertl, and Mattia Marinelli. Grid Frequency Support by Single-Phase Electric Vehicles Employing an Innovative Virtual Inertia Controller. In *International Universities Power Engineering Conference (UPEC)*, pages 1–6, Coimbra, 2016.

[88] Michel Rezkalla, Antonio Zecchino, Sergejus Martinenas, Alexander M. Prostejovsky, and Mattia Marinelli. Comparison between synthetic inertia and fast frequency containment control based on single phase EVs in a microgrid. *Applied Energy*, in press, 2017.

[89] M. Rezkalla, M. Marinelli, M. Pertl, and K. Heussen. Trade-off analysis of virtual inertia and fast primary frequency control during frequency transients in a converter dominated network. In *IEEE Innovative Smart Grid Technologies - Asia (ISGT-Asia)*, pages 890–895, Melbourne, 2016.

[90] Mania Pavella, Damien Ernst, and Daniel Ruiz-Vega. Transient Stability of Power Systems A Unified Approach to Assessment and Control. *Kluwer Academic Publishers*, pages 1–254, 2000.

[91] Prabha Kundur. *Power system stability and control*. McGraw Hill, 1994.

[92] Tilman Weckesser, Hjörtur Johannsson, Jacob Østergaard, and Thierry Van Cutsem. Derivation and application of sensitivities to assess transient voltage sags caused by rotor swings. *International Journal of Electrical Power and Energy Systems*, 72:75–82, 2015.

[93] Daniel Ruiz-Vega and Mania Pavella. A Comprehensive Approach to Transient Stability Control: Part II-Open Loop Emergency Control. *IEEE Transactions on Power Systems*, 18(4):1454–1460, 2003.

[94] Power System Dynamic Performance Committee, Power System Stability Controls Subcommittee, and Restoration Dynamics Task Force. Power System Restoration Dynamics (Issues, Techniques, Planning, Training & Special Considerations). Technical report, IEEE, 2014.

[95] Lester H. Fink and Kjell Carlsen. Operating under stress and strain. *IEEE Spectrum*, 15(3):48–53, 1978.

[96] L Wehenkel. Emergency Control and Its Strategies. In *Power Systems Computation Conference (PSCC)*, Trondheim, 1999.

[97] Masakazu Koaizawa, Kazuya Omaata, Masato Nakane, and Yutaka Kokaai. Actual operating experience of on-line transient stability control systems (tsc systems). In *Power and Energy Society Winter Meeting*, Singapore, 2000.

[98] Yong Jie Fang and Yusheng Xue. An on-line pre-decision based transient stability control system for the Ertan power system. In *International Conference on Power System Technology (PowerCon)*, pages 287–292, Perth, 2000.

[99] L. R. Clarke, M. E. Bradley, and A. O. Ekwue. Development of a general intertrip monitoring system for the NGC network. *Control Engineering Practice*, 9(7):785–789, 2001.

[100] A. Alam and E. B. Makram. Transient Stability Constrained Optimal Power Flow. In *IEEE Power & Energy Society General Meeting*, pages 1–6, Montreal, 2006.

[101] T.T. Nguyen, V.L. Nguyen, and A. Karimishad. Transient stability-constrained optimal power flow for online dispatch and nodal price evaluation in power systems with flexible AC transmission system devices. *IET Generation, Transmission & Distribution*, 5(3):332, 2011.

[102] Edgardo D. Castronuovo, Pablo Ledesma, and Ignacio A. Calle. Advanced application of transient stability constrained-optimal power flow to a transmission system including an HVDC-LCC link. *IET Generation, Transmission & Distribution*, 9(13):1765–1772, 2015.

[103] Zhen Wang, Xiaozhe Song, Huanhai Xin, Deqiang Gan, and Kit Po Wong. Risk-Based Coordination of Generation Rescheduling and Load Shedding for Transient Stability Enhancement. *IEEE Transactions on Power Systems*, 28(4):4674–4682, 2013.

[104] Michael Pertl, Michel Rezkalla, and Mattia Marinelli. A Novel Grid-Wide Transient Stability Assessment and Visualization Method for Increasing Situation Awareness of Control Room Operators. In *IEEE PES Innovative Smart Grid Technologies Conference Asia (ISGT)*, pages 1–6, Melbourne, 2016.

[105] Y. Ohura, M. Suzuki, K. Yanagihashi, M. Yamaura, K. Omata, T. Nakamura, and H. Watanabe. A Predictive Out-Of-Step Protection System Based On Observation Of The Phase Difference Between Substations. *IEEE Transactions on Power Delivery*, 5(4):1695–1704, 1990.

[106] Chao Wang, Peng Gao, Taoxi Zhu, and Wei Shao. New method of searching for the out-of-step separation interface based on reactive power. In *IEEE PES Transmission and Distribution Conference and Exposition*, pages 1–5, Chicago, 2008.

[107] M. M. Adibi, R. J. Kafka, Sandeep Maram, and Lamine M. Mili. On Power System Controlled Separation. *IEEE Transactions on Power Systems*, 21(4):1894–1902, 2006.

[108] Patrick McNabb and Janusz Bialek. A priori transient stability indicator of islanded power systems using Extended Equal Area Criterion. In *IEEE Power and Energy Society General Meeting*, page 7, San Diego, 2012.

[109] Zhenzhi Lin, Seán Noms, Hongbo Shao, and Janusz Bialek. Transient stability assessment of controlled islanding based on power flow tracing. In *Power Systems Computation Conference (PSCC)*, page 7, Wroclaw, 2014.

[110] Jairo Quirós-Tortós, Rubén Sánchez-García, Jacek Brodzki, Janusz Bialek, and Vladimir Terzija. Constrained spectral clustering-based methodology for intentional controlled islanding of large-scale power systems. *IET Generation, Transmission & Distribution*, 9(1):31–42, 2015.

[111] R. O. Berglund, W. A. Mittelstadt, M. L. Shelton, P. Barkan, C. G. Dewey, and K. M. Skreiner. One-Cycle Fault Interruption at 500 kV: System Benefits and Breaker Design. *IEEE Transactions on Power Apparatus and Systems*, 93(5):1240–1251, 1974.

[112] Schneider Electric. Circuit Breaker Characteristic Trip Curves and Coordination. Technical report, Schneider Electric, Cedar Rapids, 2001.

[113] Siemens. High-Voltage Circuit Breakers. Technical report, Siemens, 2012.

[114] ABB. Power Circuit Breaker 245 kV, up to 63 kA. Technical report, ABB, 2009.

[115] Charles J. Mozina. Power System Instability - What Relay Engineers Need to Know. In *64th Annual Conference for Protective Relay Engineers*, pages 103–112, College Station, 2011.

[116] Hassan Khorashadi-Zadeh and Zuyi Li. Transmission Line Single Phase Auto Re-Closing Scheme Based on Wavelet Transform and Adatptive Fuzzy Neuro Inference System. In *39th North American Power Symposium (NAPS)*, pages 43–48, Las Cruces, 2007.

[117] H. Takani, Y. Sonobe, T. Kagami, F. Kawano, P. Beaumont, G.P. Baber, and G.T. Main. The Application and Advantages of Multi-Phase Autoreclosing. In *10th IET International Conference on Developments in Power System Protection (DPSP)*, pages 1–5, Manchester, 2010.

[118] P. Li, B. H. Zhang, Z. G. Hao, Y. F. Rao, Y. T. Wang, Z. Q. Bo, and A. Klimek. Optimizing the Re-closing Time to Improve the Transmission Capacity of Power System. In *43rd International Universities Power Engineering Conference (UPEC)*, pages 1–5, Padova, 2008.

[119] P. Li, B. H. Zhang, Z. G. Hao, Z. Q. Bo, A. Klimek, Y. F. Rao, and Y. T. Wang. The study on optimizing re-closing time to improve the transmission capacity. In *IEEE/PES Power Systems Conference and Exposition (PSCE)*, pages 1–6, Seattle, 2009.

[120] Dragan Jovcic and Khaled Ahmed. *High-Voltage Direct-Current Transmission*. John Wiley & Sons, Ltd, Aberdeen, 2015.

[121] Y. Phulpin, J. Hazra, and D. Ernst. Model predictive control of HVDC power flow to improve transient stability in power systems. In *IEEE International Conference on Smart Grid Communications (SmartGridComm)*, pages 593–598, Brussels, 2011.

[122] J. Hazra, Y. Phulpin, and D. Ernst. HVDC Control Strategies to Improve Transient Stability in Interconnected Power Systems. In *IEEE PowerTech*, pages 1–6, Bucharest, 2009.

[123] R. Eriksson, V. Knazkins, and L. Söder. On the assessment of the impact of a conventional HVDC on a test power system. In *iREP Symposium- Bulk Power System Dynamics and Control - VII, Revitalizing Operational Reliability*, pages 1–5, Charleston, 2007.

[124] Javier Renedo, Aurelio Garcia-Cerrada, and Luis Rouco. Active Power Control Strategies for Transient Stability Enhancement of AC/DC Grids With VSC-HVDC Multi-Terminal Systems. *IEEE Transactions on Power Systems*, PP(99):1–10, 2016.

[125] Robert Eriksson. Coordinated control of multiterminal DC grid power injections for improved rotor-angle stability based on Lyapunov theory. *IEEE Transactions on Power Delivery*, 29(4):1789–1797, 2014.

[126] ENTSO-E. ENTSO-E Network Code for Requirements for Grid Connection Applicable to all Generators. Technical Report June, ENTSO-E, 2012.

[127] ENTSO-E. Draft - Network Code on Requirements for Grid Connection Applicable to all Generators. Technical report, ENTSO-E, Brussels, 2015.

[128] Energinet. Technical Regulation 3.2.5 For Wind Power Plants With A Power Ouput Greater Than 11 kW. Technical report, Energinet (TSO Denmark), 2010.

[129] Energinet. Technical regulation 3.2.2 for PV power plants with a power output above 11 kW. Technical report, Energinet (TSO Denmark), 2015.

[130] Energinet. Technical Regulation 3.2.1. for electricity generation facilities with a rated current of 16 A per phase or lower. Technical report, Energinet (TSO Denmark), 2011.

[131] Verband der Netzbetreiber - VDN. TransmissionCode 2007 - Network and System Rules of the German Transmission System Operators. Technical Report August, Verband der Netzbetreiber - VDN - e.V. beim VDEW, 2007.

[132] Fichtner. Grid Codes for Wind Power Integration in Spain and Germany: Use of Incentive Payments to Encourage Grid-Friendly Wind Power Plants. Technical report, FICHTNER, 2010.

[133] Marta Molinas, S. Vazquez, T. Takaku, J. M. Carrasco, R. Shimada, and T. Undeland. Improvement of Transient Stability Margin in Power Systems with Integrated Wind Generation Using a STATCOM : An Experimental Verification. In *International Conference on Future Power Systems*, pages 1–6, Amsterdam, 2005.

[134] A. Arulampalam, M. Barnes, N. Jenkins, and J. B. Ekanayake. Power quality and stability improvement of a wind farm using STATCOM supported with hybrid battery energy storage. *IEE Proceedings - Generation, Transmission and Distribution*, 153(6):701–710, 2006.

[135] Marta Molinas, Jon Are Suul, and Tore Undeland. Wind farms with increased transient stability margin provided by a STATCOM. In *Power Electronics and Motion Control Conference (IPEMC)*, pages 1–7, Shanghai, 2006.

[136] Guizhen Tian, Shengtie Wang, and G Liu. Power quality and transient stability improvement of wind farm with fixed-speed induction generators using a STATCOM. In *International Conference on Power System Technology (POWERCON)*, pages 1–6, Hangzhou, 2010.

[137] Hua Zhou, Hongfen Wei, Xiaoyan Qiu, Jian Xu, Xiwen Wei, and Song Wang. Improvement of Transient Voltage Stability of the Wind Farm using SVC and TCSC. In *Asia-Pacific Power and Energy Engineering Conference (APPEEC)*, pages 1–4, Wuhan, 2011.

[138] Hossein Hosseini and Mohsen Kalantar. Transient Stability Enhancement of Power System Including Wind Farms Using Improved ECS. In *3rd IEEE International Symposium on Power Electronics for Distributed Generation Systems (PEDG)*, pages 782–787, 2012.

[139] Mohamad Amiri and Mina Sheikholeslami. Transient Stability Improvement of Grid Connected Wind Generator using SVC and STATCOM. In *International conference on Innovative Engineering Technologies (ICIET)*, pages 136–140, Bangkok, 2014.

[140] P. Sravanthi, K. Radha Rani, J. Amarnath, and S. Kamakshaiah. Critical Clearing Time and Transient Stability Analysis of SCIG based Wind Farm with STATCOM. In *International Conference on Smart Electric Grid (ISEG)*, pages 1–8, Guntur, 2014.

[141] M.G. Hemeida, H. Rezk, and M.M. Hamada. A comprehensive comparison of STATCOM versus SVC-based fuzzy controller for stability improvement of wind farm connected to multi-machine power system. *Electrical Engineering*, 2017.

[142] Javier Serrano-Gonzalez and Roberto Lacal-Arantegui. Technological evolution of onshore wind turbines - a market-based analysis. *Wind Energy*, 19:2171–2187, 2016.

[143] Behnam Tamimi, Claudio Canizares, and Kankar Bhattacharya. System stability impact of large-scale and distributed solar photovoltaic generation: The case of Ontario, Canada. *IEEE Transactions on Sustainable Energy*, 4(3):680–688, 2013.

[144] Rakibuzzaman Shah, N. Mithulananthan, R. C. Bansal, and V. K. Ramachandaramurthy. A review of key power system stability challenges for large-scale PV integration. *Renewable and Sustainable Energy Reviews*, 41:1423–1436, 2015.

[145] Mattia Marinelli, Stefano Massucco, Andrea Mansoldo, and Mark Norton. Analysis of Inertial Response and Primary Power-Frequency Control Provision by Doubly Fed Induction Generator Wind Turbines in a Small Power System. In *17th Power Systems Computation Conference (PSCC)*, pages 1–7, Stockholm, 2011.

[146] Moghammadreza Fakhari Moghaddam Arani and Ehab F. El-Saadany. Implementing virtual inertia in DFIG-based wind power generation. *IEEE Transactions on Power Systems*, 28(2):1373–1384, 2013.

[147] Elyas Rakhshani, Daniel Remon, Antoni Mir Cantarellas, and Pedro Rodriguez. Analysis of derivative control based virtual inertia in multi-area high-voltage direct current interconnected power systems. *IET Generation, Transmission & Distribution*, 10(6):1458–1469, 2016.

[148] Yi Wang, Jianhui Meng, Xiangyu Zhang, and Lie Xu. Control of PMSG-Based Wind Turbines for System Inertial Response and Power Oscillation Damping. *IEEE Transactions on Sustainable Energy*, 6(2):565–574, 2015.

[149] Li Xu, Gang Wang, Lijun Fu, You Wu, and Qiaoming Shi. General average model of D-PMSG and its application with virtual inertia control. In *IEEE International Conference on Mechatronics and Automation (ICMA)*, pages 802–807, Beijing, 2015.

[150] X. Wang and W. Du. Virtual Inertia Control of Grid-Connected Wind Farms. In *International Conference on Renewable Power Generation (RPG)*, pages 1–6, Beijing, 2016.

[151] Won-sang Im, Cheng Wang, Wenxin Liu, Liming Liu, and Jang-Mok Kim. Distributed Virtual Inertia based Control of Multiple Photovoltaic Systems in Autonomous Microgrid. *IEEE/CAA Journal of Automatica Sinica*, pages 1–9, 2016.

[152] Eberhard Waffenschmidt. Virtual inertia grid control with LED lamp driver. In *International Energy and Sustainability Conference (IESC)*, pages 1–6, Cologne, 2016.

[153] Eberhard Waffenschmidt and Ron S. Y. Hui. Virtual inertia with PV inverters using DC-link capacitors. In *18th European Conference on Power Electronics and Applications (EPE'16 ECCE Europe)*, pages 1–10, Karlsruhe, 2016.

[154] Xiaoyu Wang, Meng Yue, and Eduard Muljadi. PV generation enhancement with a virtual inertia emulator to provide inertial response to the grid. In *IEEE Energy Conversion Congress and Exposition (ECCE)*, pages 17–23, Pittsburgh, 2014.

[155] R. Grünbaum and J. Pernot. Thyristor-Controlled Series Compensation: A State Of The Art Approach For Optimization Of Transmission Over Power Links. Technical report, ABB, 2001.

[156] Kalyan K Sen. SSSC - Static Synchronous Series Compensator: Theory, Modeling, and Applications. *IEEE Transactions on Power Delivery*, 13(1):241–246, 1998.

[157] J. M. Ramirez, F. V. Arroyave, and R. E. Correa Gutierrez. Transient stability improvement by nonlinear controllers based on tracking. *International Journal of Electrical Power and Energy Systems*, 33(2):315–321, 2011.

[158] M. A. Mahmud, H. R. Pota, M. Aldeen, and M. J. Hossain. Partial Feedback Linearizing Excitation Controller for Multimachine Power Systems to Improve Transient Stability. *IEEE Transactions on Power Systems*, 29(2):561–571, 2014.

[159] Riya Saluja, Sagnika Ghosh, and Mohd Hasan Ali. Transient Stability Enhancement of Multi-Machine Power System by Novel Braking Resistor Models. In *IEEE Southeastcon*, pages 1–6, Jacksonville,FL, 2013.

[160] Riya Saluja and M.H. Ali. Novel Braking Resistor Models for Transient Stability Enhancement in Power Grid System. In *IEEE PES Innovative Smart Grid Technologies Conference (ISGT)*, pages 1–6, Washington, DC, 2013.

[161] Mohd Hasan Ali, Toshiaki Murata, and Junji Tamura. Augmentation of Transient Stability by Fuzzy- Logic Controlled Braking Resistor in Multi-Machine Power System. In *IEEE Power Tech*, pages 1–7, St. Petersburg, 2005.

[162] R.H. Park. Fast Turbine Valving. *IEEE Transactions on Power Apparatus and Systems*, 92(3):1065–1073, 1973.

[163] Ramnarayan Patel, T.S. Bhatti, and D.P. Kothari. Improvement of Power System Transient Stability Using Fast Valving: A Review. *Electric Power Components and Systems*, 29(10):927–938, 2001.

[164] R. Patel, T. S. Bhatti, and D. P. Kothari. Improvement of power system transient stability by coordinated operation of fast valving and braking resistor. *IEE Proceedings - Generation, Transmission and Distribution*, 150(3):311–316, 2003.

[165] Y. Ohura, K. Matsuzawa, H. Ohtsuka, N. Nagai, T. Gouda, H. Oshida, S. Takeda, and S. Nishida. Development of a Generator Tripping System for Transient Stability Augmentation Based on The Energy Function Method. *IEEE Transactions on Power Delivery*, 1(3):68–77, 1986.

[166] ME Baydokhty, M Eidiani, H ZEYNAL, H TORKAMANI, and H MORTAZAVI. Efficient Generator Tripping Approach with Minimum Generation Curtailment based on Fuzzy System Rotor Angle Prediction. *PRZEGLĄD ELEKTROTECHNICZNY (Electrical Review)*, 88(9):266–271, 2012.

[167] George G. Karady and Jun Gu. A Hybrid Method for Generator Tripping. *IEEE Transactions on Power Systems*, 17(4):1102–1107, 2002.

[168] G. G. Karady and Mansour A. Kattamesh. Improving Transient Stability Using Generator Tripping Based on Tracking Rotor-Angle. In *IEEE Power Engineering Society Winter Meeting*, pages 1113–1118, 2002.

[169] M. O'Brien and G. Ledwich. Static reactive-power compensator controls for improved system stability. *IEE Proceedings C Generation, Transmission and Distribution*, 134(1):38–42, 1987.

[170] X. Zhou and J. Liang. Overview of control schemes for TCSC to enhance the stability of power systems. *IEE Proceedings - Generation, Transmission and Distribution*, 146(2):125–130, 1999.

[171] S. R. Wagh, A. K. Kamath, and N. M. Singh. A Nonlinear TCSC Controller based on Control Lyapunov Function and Receding Horizon Strategy For Power System Transient Stability Improvement. *2009 Ieee International Conference on Control and Automation, Vols 1-3*, pages 813–818, 2009.

[172] Nguyen Tuan Anh, Dirk Van Hertem, and Johan Driesen. Effectiveness of TCSC Controllers Using Remote Input Signals for Transient Stability Enhancement. In *IEEE PowerTech*, pages 1–8, Trondheim, 2011.

[173] Lei Zhang, Aimin Zhang, and Junfeng Jing. I&I Stabilization Based Novel Nonlinear Adaptive TCSC Control Algorithm for Improving Transient Stability. In *The 26th Chinese Control and Decision Conference (2014 CCDC)*, pages 1610–1615, Changsha, 2014.

[174] X.-Z. Dai, D. He, L. L. Fan, N.-H. Li, and H. Chen. Improved ANN αth-order inverse TCSC controller for enhancing power system transient stability. *IEE Proceedings - Generation, Transmission and Distribution*, 146(6):550–556, 1999.

[175] S. Sankara Prasad. Transient Stability Enhancement of Multi-machine Power System using Fuzzy Controlled TCSC. *Journal of Electrical and Electronics Engineering (IOSR-JEEE)*, 1(6):1–7, 2012.

[176] Prechanon Kumkratug. Improving Power System Transient Stability with Static Synchronous Series Compensator. *American Journal of Applied Sciences*, 8(1):77–81, 2011.

[177] Majid Poshtan, Brij N. Singh, and Parviz Rastgoufard. A Nonlinear Control Method for SSSC to Improve Power System Stability. In *International Conference on Power Electronic, Drives and Energy Systems (PEDES)*, pages 1–7, 2006.

[178] V.K. Chandrakar and A.G. Kothari. MFFN based Static Synchronous Series Compensator (SSSC) for Transient Stability Improvement. In *International Conference on Intelligent Systems Applications to Power Systems (ISAP)*, pages 5–8, Niigata, 2007.

[179] Sidhartha Panda and N. P. Padhy. A PSO-based SSSC Controller for Improvement of Transient Stability Performance. *International Journal of Electrical, Computer, Energetic, Electronic and Communication Engineering*, 1(9):1295–1302, 2007.

[180] V.K. Chandrakar and A.G. Kothari. Fuzzy Logic based Static Synchronous Series Compensator(SSSC) for Transient Stability Improvemen. In *IEEE International Conference on Electric Utility Deregulation, Restructuring and Power Technologies (DRPT)*, pages 240–245, Hong Kong, 2004.

[181] E. Gholipour and S. Saadate. Improving of Transient Stability of Power Systems Using UPFC. *IEEE Transactions on Power Delivery*, 20(2):1677–1682, 2005.

[182] Chia Chi Chu and Hung Chi Tsai. Application of Lyapunov-Based Adaptive Neural Network UPFC Damping Controllers For Transient Stability Enhancement. In *IEEE Power and Energy Society General Meeting - Conversion and Delivery of Electrical Energy in the 21st Century*, pages 1–6, Pittsburgh, 2008.

[183] Sukumar Mishra. Neural-Network-Based Adaptive UPFC for Improving Transient Stability Performance of Power System. *IEEE Transactions on Neural Networks*, 17(2):461–470, 2006.

[184] A Gupta and P.R. Sharma. Static and Transient Stability Enhancement of Power System by Optimally Placing UPFC (Unified Power Flow Controller). In *Third International Conference on Advanced Computing & Communication Technologies*, pages 121–125, 2013.

[185] Y. Goto, K. Yukita, H. Yamada, K. Ichiyanagi, and T. Matsumura. A Study on Power System Transient Stability due to Introduction of Superconducting Fault Current Limiters. In *International Conference on Power System Technology*, pages 275–280, Perth, 2000.

[186] G. Y. Yokomizu, K. Yukita, K. Mizuno, K. Ichiyanagi, Y. Yokomizu, and T. Matsumura. Experimental Studies on Power System Transient Stability due to Introduction of Superconducting Fault Current Limiters. In *IEEE Power Engineering Society Winter Meeting*, pages 1129–1134, Singapore, 2000.

[187] M. Tsuda, Y. Mitani, K. Tsuji, and K. Kakihana. Application of Resistor Based Superconducting Fault Current Limiter to Enhancement of Power Svstern Transient Stabilitv. *IEEE Transactions on Applied Superconductivity*, 11(1):2122–2125, 2001.

[188] M Yagami, S Shibata, T Murata, and J Tamura. Improvement of Power System Transient Stability by Superconducting Fault Current Limiter. In *IEEE/PES Transmission and Distribution Conference and Exhibition*, pages 359–364, Yokohama, 2002.

[189] Y. Shirai, K. Furushiba, Y. Shouno, M. Shiotsu, and T. Nitta. Improvement of Power System Stability by Use of Superconducting Fault Current Limiter With ZnO Device and Resistor in Parallel. *IEEE Transactions on Applied Superconductivity*, 18(2):680–683, 2008.

[190] Abdulla Emhemed, Ryan M. Tumilty, Nand Singh, Graeme M. Burt, and James R. McDonald. Analysis of Transient Stability Enhancement of LV-Connected Induction Microgenerators by Using Resistive-Type Fault Current Limiters. *IEEE Transactions on Power Systems*, 25(2):885–893, 2010.

[191] Mehrdad Tarafdar Hagh, Seyed Behzad Naderi, and Mehdi Jafari. Application of Non-superconducting Fault Current Limiter to Improve Transient Stability. In *International Conference on Power and Energy (PECon)*, pages 646–650, Kuala Lumpur, 2010.

[192] M. Tarafdar Hagh, M. Jafari, and S. B. Naderi. Transient Stability Improvement Using Non-superconducting Fault Current Limiter. In *1st Power Electronic & Drive Systems & Technologies Conference (PEDSTC)*, pages 367–370, Tehran, 2010.

[193] Mohammad Ashraf, Hossain Sadi, and M. H. Ali. Transient Stability Enhancement of Multi-Machine Power System By Parallel Resonance Type Fault Current Limiter. In *North American Power Symposium (NAPS)*, pages 1–6, Charlotte, 2015.

[194] M. Kamal Hossain and M. Hasan Ali. Transient Stability Augmentation of PV/DFIG/SG-Based Hybrid Power System by Nonlinear Control-Based Variable Resistive FCL. *IEEE Transactions on Sustainable Energy*, 6(4):1638–1649, 2015.

[195] Technology Watch. Superconducting Fault Current Limiters. Technical report, EPRI, Palo Alto, 2009.

[196] Lasantha Meegahapola and Damian Flynn. Impact on Transient and Frequency Stability for a Power System at Very High Wind Penetration. In *IEEE Power and Energy Society General Meeting*, pages 1–8, Minneapolis, 2010.

[197] Lasantha Gunaruwan Meegahapola, Tim Littler, and Damian Flynn. Decoupled-DFIG fault ride-through strategy for enhanced stability performance during grid faults. *IEEE Transactions on Sustainable Energy*, 1(3):152–162, 2010.

[198] Shuhui Dong, Heming Li, and Yi Wang. Low Voltage Ride Through Capability Enhancement of PMSG-Based Wind Turbine. In *International Conference on Sustainable Power Generation and Supply (SUPERGEN)*, pages 1–5, Hangzhou, 2012.

[199] J. L. Pardo, J. C. Elmore, and V. G. Duong. 500 kV IPT Breaker Failure Protection: An Application of Dual Timer Scheme for Short Critical Clearing Time. In *65th Annual Conference for Protective Relay Engineers*, pages 120–128, College Station, 2012.

[200] Mevludin Glavic and Thierry Van Cutsem. Reconstructing and tracking network state from a limited number of synchrophasor measurements. *IEEE Transactions on Power Systems*, 28(2):1921–1929, 2013.

[201] V Kolluri, S Mandal, M Y Vaiman, M M Vaiman, S Lee, and P Hirsch. Fast Fault Screening Approach to Assessing Transient Stability in Entergy's Power System. In *IEEE Power Engineering Society General Meeting*, pages 1–6, Tampa, 2007.

[202] S Lee, L Min, and M Vaiman. Fast Fault Screening for Real-Time Transient Stability Assessment. Technical report, Electric Power Research Institute (EPRI) and V&R Energy System Research Inc., 2010.

[203] M Y Vaiman, M M Vaiman, and A Gaikwad. Fast Fault Screening Methodology for Transient Stability Analysis of Bulk Power Systems. In *IEEE Power and Energy Society General Meeting*, pages 1–5, Vancouver, 2013.

[204] DIgSILENT PowerFactory. Use of DPL to determine the critical clearing time of a fault, 2016.

[205] DIgSILENT PowerFactory. Description of the 39 Bus New England System. Technical report, DIgSILENT GmbH, Gomaringen, 2015.

[206] Kai Sun. Power System Operations & Planning - Load Modeling, 2015.

[207] P M Anderson and A A Fouad. *Power System Control and Stability*. Iowa State University Press, Ames, 1 edition, 1977.

[208] Panayiotis Demetriou, Markos Asprou, Jairo Quiros-Tortos, and Elias Kyriakides. IEEE 118-bus modified test system, 2016.

[209] Sharma Kolluri, Mei Li, Adrian Lazo, Peng Yu, Michael Vaiman, and Marianna Vaiman. Automated Critical Clearing Time Calculation for Analyzing Faults at Entergy. In *IEEE/PES Transmission and Distribution Conference and Exposition (T&D)*, pages 1–5, Dallas, 2016.

[210] A Bihain, D Cirio, M Fiorina, R Lopez, D Lucarella, S Massucco, Daniel Ruiz-Vega, C Vournas, Thierry Van Cutsem, and L Wehenkel. Omases : A Dynamic Security Assessment Tool for the New Market Environment. In *IEEE PowerTech*, pages 1–8, Bologna, 2003.

[211] KEMA Consulting. Integration of Renewable Energy in Europe. Technical report, Imperial Collaege London, 2014.

[212] T. J. Hammons. Integrating renewable energy sources into European grids. *International Journal of Electrical Power and Energy Systems*, 30(8):462–475, 2008.

[213] Estefania Caamano, Jim Thornycroft, Hugo De Moor, and Sjef Cobben. State-of-the-Art on Dispersed PV Power Generation: Publications review on the impacts of PV Distributed Generation and Electricity networks (Technical Report). Technical report, PV upscale, 2007.

[214] E. Caamaño-Martín, H. Laukamp, M. Jantsch, T. Erge, J. Thornycroft, H. De Moor, S. Cobben, D. Suna, and B. Gaiddon. Interaction between photovoltaic distributed generation and electricity networks. *Progress in Photovoltaics: Research and Applications*, 16(7):629–643, 2008.

[215] Katarina Knezovic, Mattia Marinelli, Rene Juul Moller, Peter Bach Andersen, Chresten Træholt, and Fabrizio Sossan. Analysis of voltage support by electric vehicles and photovoltaic in a real Danish low voltage network. In *Universities Power Engineering Conference (UPEC)*, page 6, Cluj-Napoca, 2014.

[216] Katarina Knezović and Mattia Marinelli. Phase-wise enhanced voltage support from electric vehicles in a Danish low-voltage distribution grid. *Electric Power Systems Research*, 140:274–283, 2016.

[217] Iñigo Cobelo, Ahmed Shafiu, Nick Jenkins, and Goran Strbac. State estimation of networks with distributed generation. *European Transactions on Electrical Power*, 17(1):21–36, 2007.

[218] Marco Pignati, Miroslav Popovic, Sergio Barreto, Rachid Cherkaoui, German Dario Flores, Jean-yves Le Boudec, Mario Paolone, Paolo Romano, Styliani Sarri, Teklemariam Tesfay, Dan-cristian Tomozei, and Lorenzo Zanni. Real-Time State Estimation of the EPFL-Campus Medium-Voltage Grid by Using PMUs. In *6th IEEE PES International Conference and Exhibition on Innovative Smart Grid Technologies*, 2015.

[219] Jianzhong Wu, Yan He, and Nick Jenkins. A robust state estimator for medium voltage distribution networks. *IEEE Transactions on Power Systems*, 28(2):1008–1016, 2013.

[220] A. Shafiu, N. Jenkins, and G. Strbac. Measurement location for state estimation of distribution networks with generation. *IEE Proceedings on Generation, Transmission and Distribution*, 152(2):240, 2005.

[221] A Abdel-Majeed, S Tenbohlen, D Schöllhorn, and M Braun. Meter placement for low voltage system state estimation with distributed generation. In *22nd International Conference and Exhibition onElectricity Distribution (CIRED)*, 2013.

[222] S. Sarri, M. Paolone, R. Cherkaoui, A. Borghetti, F. Napolitano, and C. A. Nucci. State estimation of Active Distribution Networks: Comparison between WLS and iterated kalman-filter algorithm integrating PMUs. In *IEEE PES Innovative Smart Grid Technologies Conference Europe*, pages 1–8, Berlin, 2012.

[223] Aleksandar Ranković, Branko M. Maksimović, and Andrija T. Sarić. A three-phase state estimation in active distribution networks. *International Journal of Electrical Power & Energy Systems*, 54:154–162, 2014.

[224] Felix F. Wu. Power system state estimation: a survey. *International Journal of Electrical Power & Energy Systems*, 12(2):80–87, 1990.

[225] Andrea Bernieri, Giovanni Betta, Consolatina Liguori, and Arturo Losi. Neural networks and pseudo-measurements for real-time monitoring of distribution systems. *IEEE Transactions on Instrumentation and Measurement*, 45(2):645–650, 1996.

[226] T. Nakagawa, Y. Hayashi, and S. Iwamoto. Neural network application to state estimation computation. In *Proceedings of the First International Forum on Applications*, pages 188–192, 1991.

[227] Ahmad Abdel-Majeed, Christoph Kattmann, Stefan Tenbohlen, and Roland Saur. Usage of Artificial Neural Networks for pseudo measurement modeling in low voltage distribution systems. *2014 IEEE PES General Meeting | Conference & Exposition*, pages 1–5, 2014.

[228] Lokman H. Hassan, M. Moghavvemi, Haider a.F. Almurib, and Otto Steinmayer. Current state of neural networks applications in power system monitoring and control. *International Journal of Electrical Power & Energy Systems*, 51:134–144, 2013.

[229] M Ferdowsi and A Lowen. New monitoring approach for distribution systems. In *IEEE International Conference on Instrumentation and Measurement Technology*, pages 1506–1511, Montevideo, 2014.

[230] Ovidiu Ivanov and Mihai Gavrilas. State Estimation with Neural Networks and PMU Voltage Measurements. In *International Conference and Exposition on Electrical and Power Engineering (EPE)*, pages 983–988, Iasi, 2014.

[231] Ovidiu Ivanov, Mihai Gavrilas, and Bogdan Neagu. Intelligent monitoring and control in transmission and distribution networks. In *International Conference on Optimization of Electrical and Electronic Equipment (OPTIM)*, pages 185–191, Bran, 2014.

[232] Yuan-Yih Hsu and Chien-Chun Yang. Fast voltage estimation using an artificial neural network. *Electric Power Systems Research*, 27:1–9, 1993.

[233] R. Kamali, R. Sharifi, H. Radmanesh, and S.H. Fathi. Online voltage estimation for distribution networks in presence of distributed generation. *Indian Journal of Science and Technology*, 9(18):1–5, 2016.

[234] M. Paolone, A. Borghetti, and C. A. Nucci. A synchrophasor estimation algorithm for the monitoring of active distribution networks in steady state and transient conditions. In *17th Power Systems Computation Conference (PSCC)*, pages 1–8, Stockholm, 2011.

[235] Martin T. Hagan and Mohammad B. Menhaj. Training Feedforward Networks with the Marquardt Algorithm. *IEEE Transactions on Neural Networks*, 5(6):989–993, 1994.

[236] M T Hagan, H B Demuth, M H Beale, and Orlando De Jesús. *Neural Network Design*. PWS Publishing Co. Boston, MA, 2nd edition, 1996.

[237] Stavros Papathanassiou, Nikos Hatziargyriou, and Kai Strunz. A benchmark low voltage microgrid network. In *CIGRE Symposium"Power systems with dispersed generation: technologies, impacts on developement, operation and performances"*, Athens, Greece, 2005.

[238] IEC. IEC Standard 61000-4-30: Testing and measurement techniques -power quality measurement methods, 2016.

[239] Robert May, Graeme Dandy, and Holger Maier. Review of Input Variable Selection Methods for Artificial Neural Networks. In *Methodological Advances and Biomedical Applications*, pages 19–44. InTech, 2011.

[240] International Energy Agency. Global EV Outlook 2016 - Beyond one million electric cars. Technical report, International Energy Agency, Paris, 2016.

[241] Katarina Knezović, Mattia Marinelli, Paul Codani, and Yannick Perez. Distribution grid services and flexibility provision by electric vehicles: A review of options. In *Universities Power Engineering Conference (UPEC)*, page 6, Stoke-on-Trent, 2015.

[242] Matthias D. Galus, Marina Gonzalez Vaya, Thilo Krause, and Göran Andersson. The role of electric vehicles in smart grids. *Wiley Interdisciplinary Reviews: Energy and Environment*, 2:384–400, 2013.

[243] Christophe Guille and George Gross. A conceptual framework for the vehicle-to-grid (V2G) implementation. *Energy Policy*, 37(11):4379–4390, 2009.

[244] Casey Quinn, Daniel Zimmerle, and Thomas H. Bradley. The effect of communication architecture on the availability, reliability, and economics of plug-in hybrid electric vehicle-to-grid ancillary services. *Journal of Power Sources*, 195(5):1500–1509, 2010.

[245] Duncan S. Callaway and Ian A. Hiskens. Achieving Controllability of Electric Loads. *Proceedings of the IEEE*, 99(1):184–199, 2011.

[246] EPEX SPOT SE. Trading on EPEX Spot, 2016.

[247] Nord Pool Spot AS. Trading Appendix 3: Product Specifications - Physical Markets, 2011.

[248] Jill Powers. Implementation Overview for PDR, 2014.

[249] Alec Brooks and Tom Gage. Integration of Electric Drive Vehicles with the Electric Power Grid - a New Value Stream. In *18th International Electric Vehicle Symposium and Exhibition*, pages 20–24, Berlin, 2001.

[250] Wencong Su and Mo-yuen Chow. Performance Evaluation of an EDA-Based Large-Scale Plug-In Hybrid Electric Vehicle. *IEEE Transactions on Smart Grids*, 3(1):308–315, 2012.

[251] Zhongjing Ma, Duncan Callaway, and Ian Hiskens. Decentralized Charging Control for Large Populations of Plug-in Electric Vehicles: Application of the Nash Certainty Equivalence Principle. In *IEEE Conference on Control Applications (CCA)*, pages 191–195, Yokohama, 2010.

[252] Francesca Parise, Marcello Colombino, Sergio Grammatico, and John Lygeros. Mean field constrained charging policy for large populations of Plug-in Electric Vehicles. In *IEEE Conference on Decision and Control*, pages 5101–5106, Los Angeles, 2014.

[253] Ahmed Yousuf Saber and Ganesh Kumar Venayagamoorthy. Plug-in vehicles and renewable energy sources for cost and emission reductions. *IEEE Transactions on Industrial Electronics*, 58(4):1229–1238, 2011.

[254] ENTSO-E, CEDEC, GEODE, EURELECTRIC, and EDSO for Smart Grids. TSO-DSO Data Management Report. Technical report, TSO - DSO data management Project Team, Brussels, 2015.

[255] Marina González Vayá, Luis Baringo, Thilo Krause, Göran Andersson, Pedro Almeida, Frederik Geth, and Stéphane Rapoport. EV Aggregation Models for Different Charging Scenarios. In *23rd International Conference on Electricity Distribution (CIRED)*, page 5, Lyon, 2015.

[256] Helena Gerard, Enrique Rivero, and Daan Six. Basic Schemes for TSO-DSO coordination and ancillary services provision. Technical report, VITO, 2016.

[257] Antonio Zecchino, Katarina Knezovic, and Mattia Marinelli. Identification of Conflicts between Transmission and Distribution System Operators when Acquiring Ancillary Services from Electric Vehicles. In *IEEE PES Innovative Smart Grid Technologies Conference (ISGT)*, pages 1–6, Torino, 2017.

[258] J. A. Pecas Lopes, F. J. Soares, and P. M. Rocha Almeida. Integration of electric vehicles in the electric power system: A conceptual framework for integrating electric vehicles into electric power systems is given; impacts and benefits arising from their use are discussed. *Proceedings of the IEEE*, 99(1):168–183, 2011.

[259] He Hao, Borhan M. Sanandaji, Kameshwar Poolla, and Tyrone L. Vincent. Aggregate flexibility of thermostatically controlled loads. *IEEE Transactions on Power Systems*, 30(1):189–198, 2015.

[260] George E. P. Box, Gwilym M. Jenkins, and Gregory C. Reinsel. *Time Series Analysis - Forecasting and Control*, volume 39. John Wiley & Sons, Inc., New Jersey, 4 edition, 2008.

[261] Rob J. Hyndman. Measuring forecast accuracy, 2014.

Collection of relevant publications

[**Pub. A**] M. Pertl, T. Weckesser, M. Rezkalla, and M. Marinelli. Transient stability improvement: A review and comparison of conventional and renewable based techniques for preventive and emergency control. Springer Electrical Engineering, 2017.

[**Pub. B**] M. Pertl, T. Weckesser, M. Rezkalla, K. Heussen, and M. Marinelli. A decision support tool for transient stability preventive control. Electric Power Systems Research, vol. 147, pp. 88-96, 2017.

[**Pub. C**] M. Pertl, K. Heussen, O. Gehrke, and M. Rezkalla. Voltage estimation in active distribution grids using neural networks. IEEE Power and Energy Society General Meeting, 2016.

[**Pub. D**] M. Pertl, P. J. Douglass, K. Heussen, and K. Kok. Validation of a robust neural real-time voltage estimator for active distribution grids on field data. Electric Power Systems Research, vol. 154, pp. 182-192, 2018.

[**Pub. E**] M. Pertl, F. Carducci, M. Tabone, M. Marinelli, S. Kiliccote, and E. C. Kara. An equivalent time-variant storage model to harness EV flexibility: Forecast and aggregation. IEEE Transactions on Industrial Informatics, 2018, under review.

[Pub. A] Transient stability improvement: a review and comparison of conventional and renewable based techniques for preventive and emergency control

Noname manuscript No.
(will be inserted by the editor)

Transient Stability Improvement: A Review and Comparison of Conventional and Renewable based Techniques for Preventive and Emergency Control

Michael Pertl* · **Tilman Weckesser** · **Michel Rezkalla** · **Mattia Marinelli**

Received: date / Accepted: date

Abstract This paper aims at reviewing and summarizing the vast variety of techniques to improve transient stability of power systems. A qualitative comparison of the techniques is presented and the future outlook is discussed. The techniques are categorized into conventional and renewable-based techniques. Conventional techniques are well established and have been employed in the past. Renewable techniques investigate how generators based on renewable energy sources (RES) can contribute to improving stability. Moreover, it is distinguished between techniques applying preventive and emergency controls. For preventive control, re-dispatch of generators and series compensation are extensively used in practice, whereas for emergency control, a great share of the techniques aim at voltage support during fault conditions. Regarding preventive control using RES-based generation, one approach which temporarily increases the voltage setpoint of the units in order to increase the synchronizing power, is reported. Regarding renewable energy source based emergency control, low voltage ride-through (LVRT) capability including voltage support is a well established method. Nevertheless, it is also highlighted that high voltage ride-through (HVRT) capability plays a critical role. The findings show that distributed generation must be included in existing control schemes for preventive control, and new improvement techniques taking full advantage of them need to be developed.

Keywords Transient Stability Improvement · Power System Stability · Preventive Control · Emergency Control · Renewable Energy Sources

This work is supported by the EU FP7 project ELECTRA (grant: 609687; electrairp.eu) and the Danish Research Project ELECTRA Top-up (grant: 3594756936313).

* corresponding author

M. Pertl, M. Rezkalla, M. Marinelli
Technical University of Denmark
Department of Electrical Engineering
Frederiksborgvej 399
4000 Roskilde, Denmark
Tel.: +45 93511248 (Michael Pertl)
E-mail: {mpertl,mirez,matm}@elektro.dtu.dk

T. Weckesser
University of Liège, Belgium
Department of Electrical Engineering and Computer Science
Quartier Polytech 1
10, Allée de la dcouverte
4000 Liège, Belgium
E-mail: j.weckesser@ulg.ac.be

1 Introduction

The generation of electric power is currently shifting from large centralized to small distributed generation units [1]. The continuing integration of renewable energy sources (RES) also changes the characteristics of the power systems due to their different behavior compared to conventional synchronous generators (SG) [2]. Therefore, great effort in research is put into investigating different aspects on how RES, such as wind and photovoltaics (PV), are affecting the stability of power systems. A particularly important property of power systems is their transient rotor angle stability, which is the ability of the generators to remain in synchronism after a large disturbance [3]. Synchronism means that all SGs in a power system are running at the same speed. On the contrary, converter-based generation units are not rotating machines and thus do not have a rotor angle but they are synchronized to the connected grid through a phase-locked loop (PLL) [4–6]. Such a disturbance can lead to widespread outages due

to unintended and/or uncoordinated tripping of protection devices. Here, large disturbance does not necessarily need to refer to a fault, since an instability can also be triggered by tripping of a heavily loaded line or generator [7].

Anticipating a future scenario with high share of converter-based generation, the approaches to maintain or re-establish transient stability have to change since converters have other properties and capabilities than conventional SGs [8]. Converter-based generation units do not inherently provide inertia to the grid, unless they are equipped with an explicit control to do so. Moreover, a great share of wind power plants include asynchronous generators which do provide inertia to the system, but their contribution is small compared to SGs [9]. That means, the dynamic behavior of the whole power system continuously changes in course of time, depending on the actual energy mix of synchronous and converter-based generation, which may compromise transient stability in certain situations and, thus, the reliability [10]. Therefore it is important to develop new techniques for transient stability preventive and emergency control, also taking into account asynchronous and converter-based generation units to guarantee the reliability of future power systems [11].

This paper intends to summarize the state-of-the-art for transient stability improvement. A categorization in conventional and RES-based techniques is carried out. Within these two categories it is further distinguished between preventive and emergency control. Finally, the techniques are qualitatively compared and a future outlook is presented. The paper is organized as follows. In section 2, the basics of transient stability assessment and improvement are revisited. Conventional improvement techniques are described in section 3. Improvement techniques using RES are described in section 4. The qualitative aspects of the techniques are discussed in section 5. The conclusion and future outlook are given in section 6 where the most important improvement techniques are summarized and future research needs are highlighted.

2 Basics of Transient Stability Assessment and Improvement

2.1 Nomenclature

$P_{e,pre}$ (W) - Active power transfer capability before the fault.
$P_{e,f}$ (W) - Active power transfer capability during the fault.
$P_{e,post}$ (W) - Active power transfer capability after the fault.
P_m (W) - Mechanical power supplied to the turbine.
P_a (W) - Acceleration/deceleration power defined as difference between mechanical and electrical power.
J (kgm^2) - Moment of inertia.
δ_0 (rad) - Steady-state rotor angle before the fault.
δ_1 (rad) - Steady-state rotor angle after the fault.
δ_c (rad) - Critical rotor angle which defines stability limit during fault.
δ_m (rad) - Maximum permissible rotor angle perturbation after fault clearance.
A_1, A_2 - Acceleration and deceleration areas.

2.2 Transient Stability Mechanism

In order to understand the different effects of the improvement techniques, the basics of transient stability assessment are briefly summarized by means of the well-known equal area criterion (EAC) [12,13].

The EAC determines the transient stability limit according to the acceleration and deceleration area A_1 and A_2, respectively. The corresponding $P-\delta$ diagram is shown in Fig. 1. The physical relation between the mechanical and electrical quantities is given by the equation of motion shown in (1). Generators are accelerating or decelerating once there is a mismatch between mechanical power supplied to the turbine and electrical power delivered to the grid.

$$P_a = P_m - P_e = J\omega_0 \frac{d^2\delta}{dt^2} \tag{1}$$

The stability limit is derived by calculating the maximum clearing angle and, based on that, the critical clearing time (CCT) which describes the time that the generator takes to advance from the initial rotor angle to the critical rotor angle. Hence, the greater the CCT, the more severe disturbances the generator (system) can withstand.

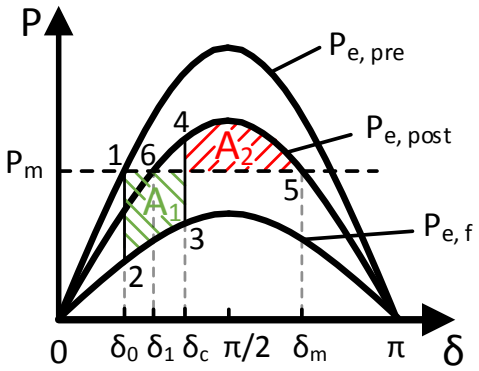

Fig. 1: P-δ curve

2.3 Improvement Mechanisms

Several variables affect the transient stability. Thus, a wide variety of techniques for improvement of power system stability can be found in the literature. All discussed transient stability improvement techniques can be referred to one of the following effects.

On the one hand, improving transient stability can be achieved by reducing the fault severity, e.g. faster fault clearance, or, on the other hand, by increasing the CCT. According to [13], the techniques of transient stability improvement are aiming to achieve one or more of the following effects:

a) Reduction of the impact of the disturbance or the fault severity.
b) Increase of the synchronization forces to support the restoration of steady-state operation after a disturbance.
c) Reduction of the acceleration or deceleration power through control of the prime mover to meet the equilibrium of mechanical and electrical power.
d) Applying artificial load to SG to reduce accelerating power by increasing electrical power.

Effects related to a) can be achieved by faster fault clearing times through high speed breakers and, thus, reduces the fault severity by decreasing the clearing angle. An increase of the synchronization forces mentioned in b) can be realized by the use of Flexible Alternating Current Transmission Systems (FACTS) by e.g. voltage support at a long transmission line. techniques related to c) and d) refer to the re-establishment of the equilibrium between the mechanical and electrical power, thus, reducing the acceleration/deceleration power on the shaft of the synchronous machine.

3 Conventional Techniques

In this section conventional techniques for transient stability improvement are discussed. A technique is considered conventional when no RES are involved. conventional techniques make up the greatest part in the literature since they includes techniques with SGs, FACTS and any other approaches that do not involve RES-based units.

3.1 Preventive Transient Stability Control

3.1.1 SG Re-Dispatch

One of the most effective preventive actions to increase the transient stability margin is to re-dispatch generators in order to reduce their active power setpoint. That means, generators are operated further away from the stability limit. Considering Fig. 1, the acceleration area decreases and the deceleration area increases. Due to cost efficiency, the dispatch of generators is usually determined by the use of optimal power flow (OPF) calculations where either transient stability constraints are derived from a time-domain sensitivity analysis, or the whole set of power flow equations is directly included in the OPF formulation [14–17]. In [14], a 4^{th}-order Taylor expansion is used to speed up solving of OPF calculations including transient stability constraints. The authors of [15] propose to derive linearized transient stability constraints outside the OPF calculation to not further complicate the OPF formulation. In [17], time-domain simulations are combined with pre-assessment contingency filtering and a fast re-dispatch estimation to reduce the computational burden of the stability assessment.

3.1.2 Load Shedding

When referring to load shedding most commonly it will be associated with frequency regulation such as under frequency load shedding to prevent a power system from collapse due to generation deficit. However, load shedding can also be used to improve transient stability of power systems, e.g. reduce the loading of generators by reducing the demand. That can be again boiled down to the power-angle relationship in Fig. 1, i.e. the reduced active power set point of the generator implies a reduction of the rotor angle and thus an increased stability margin. The authors of [18] have proposed a risk-based coordination of generation rescheduling and load shedding to improve transient stability. If the generation rescheduling cannot resolve the issue, load shedding is added to ensure that the system is within the defined security boundaries.

3.1.3 Reduction of System Reactances

Transmission networks are mainly determined by their inductive series reactances which have distinct impact on the transient stability. The power transfer capacity scales inversely proportional with the transmission reactance. The transfer capability in pre-fault conditions can be increased by reducing the series reactances of the network. A reduction of the system reactances can be achieved by adding parallel transmission lines and/or use of transformers with low leakage reactances [13]. Since this two techniques for reducing the system reactances are rather expensive, other techniques as fixed or variable series compensation based on FACTS are used (refer to sections 3.1.5 and 3.2.6).

3.1.4 Upgrade of System Voltage

The transfer capacity increases proportionally to the square of the system voltage. An increase in system voltage increases the difference between the initial rotor angle and critical clearing angle allowing the generator rotating through a large angle deviation before reaching the critical clearing angle. Moreover, the deceleration area A_2 is increased. It is obvious that increasing the system voltage is not applicable to a large existing power system as the components of the power system are designed for a specific voltage level and must be replaced before increasing the voltage level. Therefore, increasing the system voltage is only applicable to a very limited extend.

3.1.5 Variable Series Compensation

Thyristor-controlled series capacitor (TCSC) and static synchronous series compensator (SSSC) are capable to act on the power system in a serial manner, contrary to shunt devices. Variable series devices can be used in preventive as well as in emergency control. For emergency control, please refer to section 3.2.6.

The circuit diagram of a TCSC is shown in Fig. 2. It consists of a fixed series capacitor C_2 and a capacitor C_1 in parallel with an inductor L. The thyristor controls the total reactance of the circuit according to (2), where ω_e is the electrical angular frequency and α the firing angle of the thyristor control.

$$X_{TCSC} = \frac{1}{-\omega_e C_1 + \frac{2\pi - 2\alpha + \sin(2\alpha)}{\omega_e L \pi}} \tag{2}$$

Instead of line reinforcement or installation of additional lines, TCSCs offer a strong alternative to improve transient stability by optimizing the transmission impedance [19]. The TCSC reduces the effective series reactance X_{Line} and, thus, reduces the angular separation with the power transfer being constant.

A similar effect can be achieved by use of a SSSC. The circuit diagram and respective vector diagram are shown in Fig. 3. The SSSC injects a voltage, which is variable in magnitude and perpendicular to the line current. The angle of the injected voltage can be ±90° with

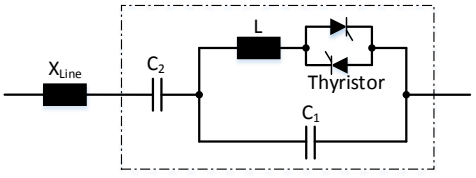

Fig. 2: Circuit diagram of a TCSC

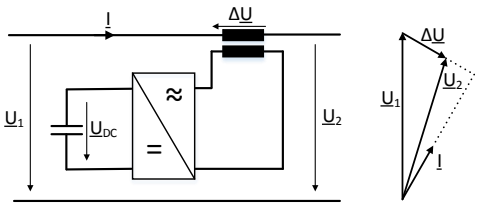

Fig. 3: Circuit and vector diagram of a SSSC

respect to the line current and either emulate an inductive or capacitive reactance [20].

3.2 Emergency Transient Stability Control

3.2.1 Fast Excitation System

A significant improvement of transient stability can be achieved with fast responding excitation systems of SGs by increasing the field current to increase the internal machine voltage and, hence, to evacuate more electrical power during the fault which reduces the acceleration area and leads to an increased CCT.

High speed excitation systems are not very effective for bolted three-phase faults at the generator terminals since the voltage drops to zero. No active power can be evacuated. However, it is very effective for faults occurring further away from the generator, where the voltage at the generator bus is greater than zero [21].

Another technique is a discontinuous excitation control which is referred to as transient stability excitation control where the terminal voltage is kept near the maximum permissible value over the entire positive swing of the rotor angle and returns to normal operation mode after the first swing. The use of fast excitation systems may compromise the damping of local plant oscillations which requires the excitation system to be supplemented with a power system stabilizer (PSS) [13].

In [22–24], the authors introduce non-linear excitation controllers. The controllers are designed robustly, being capable to operate over a wide range of operating conditions. The simulation results show enhanced performance under transient conditions and also improved small signal stability through increased damping of oscillations after the disturbance.

The authors of [22] propose a multi-variable nonlinear controller which takes into account the dynamics of the automatic voltage and speed regulators to achieve simultaneous enhancement of rotor angle stability and post-fault regulation of the terminal voltage. The authors claim that the performance of the control technique is independent from the operation point of the

generator and that it can be applied to generators in any power system.

The authors of [23] propose a linear controller which provides an acceptable performance over a wider operating region as conventional controllers. Information about the nonlinearities of the power system are explicitly included in the design of the controller by using the Cauchy remainder of the Taylor series expansion. However, the design of the controller strongly relies on information of the specific dynamic behaviour of the actual power system.

The authors of [24] propose an partial feedback linearization controller for multi-machine systems by including the speed deviation of SGs as an output function. The proposed technique shows superior behaviour over controllers with exact feedback linearization due to faster settling time after disturbances and reduced oscillations.

3.2.2 Braking Resistor

The concept to use a braking resistor to enhance transient stability can be seen from a similar perspective as fast valving (refer to section 3.2.3) with the difference that it acts on the electrical power instead of the mechanical power. An artificial electrical load is applied during transient disturbance to increase the electrical power and to re-establish the equilibrium, or at least minimize the difference, between mechanical and electrical power.

In [25,26], the authors propose two variants of braking resistor, one with a thyristor rectifier and one with a diode rectifier and chopper. A fuzzy logic controlled braking resistor was proposed in [27]. However, for the practical application of braking resistors careful considerations have to be made regarding installation costs, torsional stress on the shaft and other additional adverse effects which may arise.

3.2.3 Fast Valving

Fast valving of the turbine is an effective technique to improve transient stability by rapidly reducing the mechanical power during the fault [13]. According to [28], the concept of fast valving was introduced for the first time in 1925. During faults, the electrical power drops to a lower value and creates a difference between mechanical and electrical power, leading to an acceleration of the machine. To counteract that imbalance, generators with fast valving capability rapidly lower the mechanical power which is applied to the machine in order to reduce the acceleration power to a minimum. One of the limitations of fast valving is that it can only be applied to thermal units [29].

In [30], fast valving is complemented with a braking resistor and a coordinated control concept of both techniques was introduced. The combined method utilizes the advantages of fast valving and the braking resistor and also overcomes the issues of both techniques when applied separately. For example when faults occur close to the generator terminals, the voltage drops significantly and the breaking resistor cannot be effective until the fault is cleared. However, fast valving can be applied from the very beginning of the fault which allows to effectively control the rotor acceleration during the fault period. Furthermore, the braking resistor only has to share the partial load which reduces duty and heat dissipation.

3.2.4 Generator tripping

Selective tripping of generators for severe contingencies has been used for many years. Various approaches considering very different aspects are found in the literature. Generator tripping based on the energy function, where the kinetic energy of the system is compared to the potential energy, was proposed in [31]. An approach for generator tripping based on rotor angle prediction was proposed by the authors of [32,33]. In [32], the generators to be tripped are determined by a fuzzy-logic controller, whereas a hybrid approach considering look-up tables is used in [33]. The preparation of the look-up tables is done offline by simulation of the power system [34]. The main issues associated to the generator tripping are: Overspeed resulting from tripping of the generator, thermal stress and high torques on the shaft through sudden load change [13].

3.2.5 Variable Shunt Compensation

FACTS with reactive power capability for voltage control at selected points of the power system can contribute to improve the transient stability by increasing the synchronization power flow among the generators [13]. Static var compensator (SVC) and static synchronous compensator (STATCOM) are capable to control the voltage/reactive power at their connection point. Figure 4 shows a typical arrangement of a SVC. It comprises a mechanical reactor and capacitor, a thyristor controlled reactor and capacitor, and a harmonic filter. A standard PI controller for SVCs, which uses the voltage measurement as input to control the reactive power, was introduced in [35].

The circuit diagram of a STATCOM is provided in Fig. 5. The reactive power injection of the STATCOM

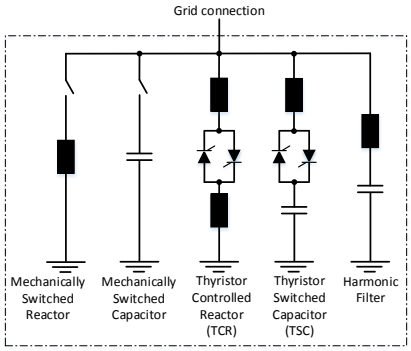

Fig. 4: Circuit diagram of a SVC

is controlled by a pulse-width-modulation (PWM) controller which input is the measured grid voltage at the point of connection.

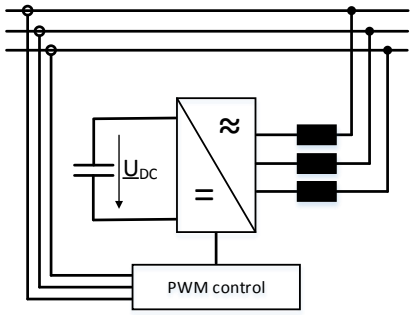

Fig. 5: Circuit diagram of a STATCOM

3.2.6 Variable Series Compensation

A wide variety of control concepts for TCSCs for transient conditions are summarized in [36]. The control concepts for TCSCs under disturbance are ranging from linear, non-linear [37–40] to intelligent [41, 42] concepts.

In [37], the authors propose a concept using non-linear model predictive control including the complete set of differential algebraic equations of the system, whereas the Lyapunov energy function is used in the control proposed in [38]. A control concept using remote signals from phasor measurement units (PMUs) was presented in [39]. The authors of [40] propose an adaptive control strategy by adopting immersion and invariant stabilization and sliding-mode observer in the control design.

The intelligent control concept in [41] utilizes the flexibility of artificial neural networks (ANNs) to circumvent the mathematical modelling of the non-linear power system, instead, the non-linear behavior is approximated by the ANN. In [42], the mathematical modelling of the power system is circumvented by use of a fuzzy logic control which is designed for certain grid conditions using engineering expertise about the power system under consideration.

The control concepts for SSSCs can be also categorized in linear [43], non-linear [44] and intelligent [45–47].

A linear proportional control which is sensitive to deviations of the speed of generators is proposed in [43]. The control signal is derived by multiplying the speed deviation from nominal speed with a constant gain value.

The proposed non-linear controller in [44] tracks the generator's angle trajectory to appropriately change the effective post-fault line reactance in order to bring the generator back to a stable operating point and, moreover, to damp rotor oscillations.

In [45], an ANN-based control concept for SSSCs using speed deviations of generators is presented. The authors of [46] propose to use particle swarm optimization to find the optimal parameters of a controller which consists of a gain, a signal washout and a two-stage phase compensation block. A fuzzy logic control using the active power and voltage at the terminals of the SSSC as input for the control is proposed in [47].

3.2.7 Combined Variable Series and Parallel Compensation

In order to achieve full controllability of the series-injected voltage in magnitude and angle, a unified power flow controller is used. An unified power flow controller (UPFC) combines the capabilities of a STATCOM and a SSSC as it can be seen in Fig. 6. Most commonly, inverter 1 is operated at unity power factor, only supplying the active power demand of inverter 2. Due to the supply of active power to inverter 2, it is capable of exchanging also active power with the grid and, therefore, varying the injected voltage $\underline{\Delta U}$ in the full control range shown in Fig. 6. The limitations of the magnitude of the injected voltage are given by the inverter's capacity.

In [48], an approach using an UPFC to maximize the first swing stability by enlarging the deceleration area through reactive power support was introduced. After the first swing, the controller switches to normal linear operation to damp oscillations. A combined control of active and reactive power control for first swing stability improvement using an UPFC was proposed in [49]. A different approach was introduced in [50], where a Lyapunov energy method based control concept was used. Since the difficulties in constructing an analytical energy function have not been overcome, an energy-

function-based adaptive recurrent neural network controller was designed. Another intelligent control technique using a neural-network based adaptive controller was introduced in [51]. The controller can be treated as an approximation of the Lyapunov control actions and is robust to uncertainties. In [52], the authors propose a method for optimal placement of UPFCs to decrease implementation costs.

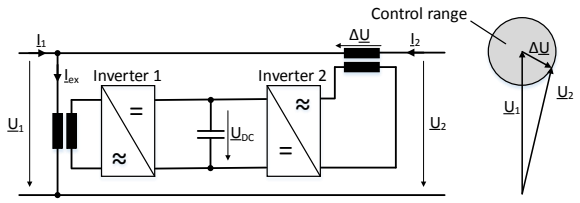

Fig. 6: Circuit diagram of an UPFC

3.2.8 Controlled System Separation

The coordinated separation of the disturbed system into two or more subsystems is a way to prevent a generator or a group of generators from loss of synchronism. The separation concepts use different triggers to initiate the separation process.

In [53], the proposed method is based on on-line voltage waveform measurement and prediction of the phase difference 200 ms ahead. The predicted phase difference is used as a triggering event if a certain limit is exceeded.

A method to determine the optimal point of separation by analyzing the voltage fluctuations in the system was introduced in [54]. The point of separation is determined by the highest voltage magnitude fluctuation and is therefore called out-of-step center. Following this methodology, a separation interface where the system is to be split was derived.

To prevent tripping of out-of-step relays at undesired locations, a blocking scheme by using blinders in the impedance plane for relays was introduced in [55].

The authors of [56] propose an a priori transient stability indicator based on the extended equal area criterion to determine if the islanded power systems remain transiently stable after the network has been split.

The authors of [57] propose an islanding scheme which minimizes the power disruption and power imbalance of the split systems by power flow tracing.

An islanding methodology using constrained spectral clustering is proposed in [58]. The methodology allows to directly determine an islanding solution with minimal power flow disruption for any given number of islands.

3.2.9 High Speed Circuit Breaker, Single-Pole Operation, Auto Re-Closing

Generators are accelerating and picking up kinetic energy during severe faults. The kinetic energy which is picked up by the generator is directly proportional to the fault duration. Therefore, it is desired to clear faults as fast as possible, i.e. the shorter the fault duration the smaller the severity of the disturbance [13,59]. Nowadays, the tripping times of high-speed circuit breakers are around 2 cycles for high voltage and one cycle for low- and medium voltage circuit breakers [60–62]. To achieve this fast clearing times fast overcurrent sensors and dedicated communication equipment are required.

Moreover, it is beneficial to use circuit breakers with independent-pole operation where every phase can be operated separately. That contributes to further transient stability improvement as single-phase to ground faults can be cleared by switching only the pole with the faulty phase instead of switching all three poles, since it allows synchronizing power to flow on the remaining phases. Moreover, the failure of one pole will not affect the operation of the other two poles [21]. However, when using single-pole operation considerations concerning asymmetrical operation of generators have to be made since negative-sequence currents are flowing during the fault. In addition to above techniques, auto re-closing of the breaker can contribute to improve the transient stability by re-establishing the transmission reactance and, thus, increase transmission capacity in post-fault conditions [13,63,64]. The re-closing time has a major impact on the stability and research has been done on determining the optimal time for re-closure of the circuit breaker [65,66]. However, no general rule for the optimal time of re-closure can be defined since many power system properties such as inertia, system configuration and fault location among others are influencing the determination of the optimal re-closure time.

3.2.10 Fault Current Limiter

The application of fault current limiters (FCLs) is very well covered in the literature. Resistive, inductive or combined designs are used to enhance the transient stability during faults. The resistive type is effective in consuming the acceleration energy of generators during faults whereas the inductive type suppresses the voltage drop.

The used FCLs in power systems can roughly be grouped into two categories, namely superconducting

FCLs [67–72] with highly non-linear response to temperature, current and magnetic field variations, and bridge-type FCLs based on solid-state devices [73–76] which are either IGBT or thyristor-controlled.

Superconducting FCLs: The most common configuration of superconducting resistive and inductive FCLs is shown in Fig. 7. FCLs are installed in series of a line. In steady-state, the current I is flowing through the superconductor x_{SC} which has zero resistance. During a fault, when the current exceeds the activation value of the superconductor, the reactance of the superconductor increases instantaneously and causes the current also to flow through the limiting resistor R_{lim} or inductor x_{lim}.

The impact of resistive FCLs on the transient stability behavior is investigated in [68–70, 72]. It was found that the placement of the FCLs and the value of the resistance highly affects the transient stability performance, but generally, a larger resistance showed more robust behavior to changing system parameters.

The authors of [67] investigated the differences between resistive and inductive FCLs. It was found that both types reduce the magnitude of the fault current significantly, but the inductive type showed slightly better performance at damping power oscillations.

A parallel configuration of an inductive FCL with a zinc oxide (ZnO) device and resistor is proposed in [71]. It is shown that the proposed combination of resistive and inductive FCL can significantly improve transient stability by exploiting the voltage drop suppression of the inductive type and the excessive energy consumption of the resistive type.

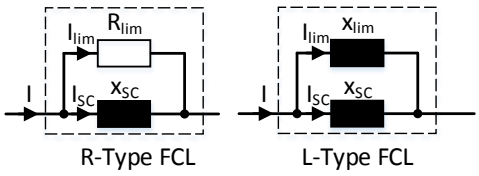

Fig. 7: Most common configuration of superconducting resistive and inductive FCLs

Bridge-type FCLs: bridge-type FCLs utilize actively controlled power electronics to switch the fault current in a limiting branch or opens the circuit to emulate a circuit breaker with the characteristics of the device [77]. Due to the great variety of bridge-type FCL configurations, no figure about standard configurations is shown here.

A method to calculate the optimal resistance of the fault current limiter by finding the resistance value for which the power transfer capability during the fault is equal to the power transfer capability before the fault is proposed in [73]. The authors of [74] propose to use the EAC to calculate the optimal resistance which leads to maximum critical load angle.

In [75], a comparison between a bridge-type and a similar parallel resonance FCL is presented. The results show that the parallel resonance FCL has better performance than the bridge-type FCL for symmetrical and asymmetrical faults.

The authors of [76] propose three non-linear controllers to control a resistive bridge-type FCL. a) a fuzzy logic controller which uses the power and voltage deviation at the point of common coupling (PCC) as input, b) a static non-linear controller which uses the power deviation at the PCC as input, c) an adaptive-network-based fuzzy inference system based controller which uses the voltage deviation at PCC and the speed deviation of the generator as input. The simulation results show only slight differences between the three proposed controllers, therefore, the authors claim that any of the proposed techniques may be chosen to enhance transient stability.

3.2.11 HVDC Transmission Link Control

The number of HVDC links for long-distance transmission of power is continuously increasing. Due to the high controllability of voltage source converters (VSC), using pulse-width-modulation (PWM), in terms of response time and precision, they are very suitable for supporting the AC system by fast and independent control of active and reactive power [78]. The reactive power control usually operates in constant voltage or droop mode. If the converters have LVRT capability, the transient stability can also be enhanced by reactive power provision. When the DC transmission links are operated in constant power mode they do not support the AC system by, e.g. damping oscillations. Hence, it is beneficial to modify the control of the converters in such a way that they support the AC system during disturbances.

A model predictive control (MPC) using on-line measurements collected through a wide-area monitoring system was introduced in [79]. Based on the collected data, a sequence of control actions that maximize a transient stability index over a short time horizon is calculated in every discrete time instant. The used transient stability margin is a combination of an acceleration power, coherency and energy index. The first action of the computed sequence is used as control setting for the HVDC links.

In [80, 81], three control techniques for transient stability improvement by adding supplementary controls to the constant power control of converters are intro-

duced. The DC power flow control signal P_{DC} is the sum of the DC power flow set point P_{DC_0} and the supplementary signal for transient conditions DC_{suppl} as shown in (3).

$$P_{DC} = P_{DC_0} + P_{DC_{suppl}} \tag{3}$$

The three controllers are explained in more detail in the following. Here, the index R and I correspond to rectifier and inverter, respectively. K_P and K_D are the respective proportional and differential gains of the PD controllers.

a) The aim of the first controller is to transfer power from the area where the SGs are accelerating faster to the area where the SGs are slower and, thus, increasing the transient stability by providing synchronization power flow between SGs with different speed. The rotor speeds ω_R and ω_I of the SGs located closest to the inverter and rectifier buses of the HVDC link.

$$\begin{aligned} P_{DC_{suppl}} = K_P(\omega_R - \omega_I) + \\ K_D \cdot \frac{d}{dt}(\omega_R - \omega_I) \end{aligned} \tag{4}$$

b) The second controller's input are the voltage angles φ_{V_R} and φ_{V_I} at both ends of the HVDC link. The voltage angle displacement provides a good image of the mechanical rotor displacement between the generators at either side of the HVDC link. To increase transient stability, the active power flow through the HVDC link is controlled so that the voltage angle is minimized and, hence, the mechanical rotor displacement is decreased.

$$\begin{aligned} P_{DC_{suppl}} = K_P(\varphi_{V_R} - \varphi_{V_I}) + \\ K_D \cdot \frac{d}{dt}(\varphi_{V_R} - \varphi_{V_I}) \end{aligned} \tag{5}$$

c) The third controller receives the inter-area power flow on AC tie-lines which is represented by the sum of all tie-line flows P_{TL_k} with k being the number of tie-lines as input. This control strategy supposes well-defined control areas which are interconnected by HVDC links. The active power flow is modulated according to the power flow between the control areas following (6).

$$\begin{aligned} P_{DC_{suppl}} = K_P \cdot \sum_k P_{TL_k} + \\ K_D \cdot \frac{d}{dt} \sum_k P_{TL_k} \end{aligned} \tag{6}$$

These control concepts are applicable in point-to-point HVDC transmission links, whereas control concepts for multi-terminal HVDC (MT-HVDC) systems are more sophisticated because more factors have to be taken into consideration.

In [82], the authors propose three active power control concepts for MT-HVDC systems based on local and global frequency measurements at the converter buses. Local measurements are used to compare the frequency to the nominal value and control the active power flow according to (4). In order to maintain the required active power balance of the MT-HVDC system, a concept which adds weighting factors to the control signal is proposed. By using global frequency measurements, converters inject a fixed supplementary active power considering the speed of the center of inertia (COI).

A time-optimal control strategy to enhance transient stability by coordinated control of multi-terminal DC grid power injections based on Lyapunov theory is presented in [83].

4 Renewable Energy Source Based techniques

In this section techniques and concepts for transient stability improvement are discussed, which utilize RES-based generators.

4.1 Preventive Transient Stability Control

4.1.1 Increased Voltage Setpoint

RES with capability to control reactive power, such as doubly-fed induction generators (DFIGs), full-scale converter-based wind power plants and PVs could be set to operate at a higher voltage setpoint if necessary. However, the increase of voltage setpoints is only possible to a very limited extend due to the constraints set by grid codes. Depending on the location of the RES in the grid, the increased voltage setpoint improves the flow of synchronizing power. In [84], it is shown that the increase of the voltage setpoint of DFIGs from 1 to 1.05 pu in pre-fault conditions can improve transient stability.

4.2 Emergency Transient Stability Control

4.2.1 Low Voltage Ride-Through

Generally, low voltage ride-through capability of RES has a positive effect on the transient stability of power systems since the disconnection of a large amount of distributed generation would stress the power system even more. Therefore, it is desired that RES remain connected during faults within specified limits. This limits

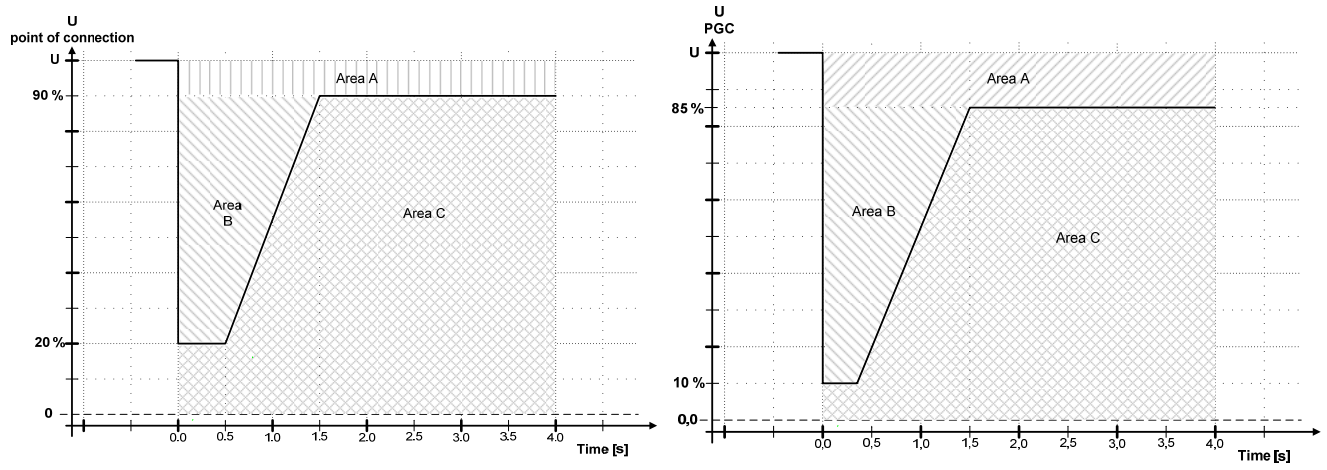

(a) Wind power plants > 1.5 MW

(b) PV power plants > 1.5 MW

Fig. 8: Energinet's requirements for tolerance of voltage drops for (a) wind power plants and (b) PVs with a power output greater than 1.5 MW. **Area A:** The power plant must stay connected to the network and uphold normal production. **Area B:** The power plant must stay connected to the network provide maximum voltage support. **Area C:** Disconnecting the power plant is allowed. [85,86]

are already defined in many network codes where generation units connected to the grid have to comply with certain LVRT capabilities, e.g. reactive power provision during disturbance. The ENTSO-E network code specifies the requirements for generation units connected to the five synchronous areas in Europe [87,88]. The network code is applicable to all generation units. However, national grid codes even specify particular requirements for wind and PV generation.

The Danish network code for wind and PV power plants with power output above 1.5 MW requires units to stay connected for a certain time during disturbances with respect to voltage and frequency excursions [85, 86]. Generation units with a rated current of 16 Ampere per phase or lower do not have any LVRT requirements [89].

As shown in Fig. 8, the requirements for wind and PV power plants in Denmark are slightly different. The requirements for PVs are more demanding than the requirements for wind power plants as they have to be able to withstand voltage drops down to 10 % of the voltage at the point of connection whereas wind power plants only down to 20 %. Similar requirements apply to wind and PV generation units in Germany and other European countries [90,91].

In addition, advanced control strategies to complement and enhance the LVRT capabilities were developed for DFIGs and full-scale converter wind power plants. These techniques aim at improving the transient behavior of the wind power plants and, thereby, supporting the grid during severe disturbances.

DFIGs are equipped with a crowbar in order to protect the rotor-side converter from overcurrents. The crowbar is inserted once the rotor current exceeds the maximum permissible limit and the rotor-side converter is disconnected. When the crowbar is activated, the DFIG operates like a conventional squirrel-cage induction generator and, therefore, will significantly increase the reactive power consumption [92]. To overcome this problem, the authors of [93] proposed a decoupled-DFIG LVRT strategy to control the DFIG during crowbar operation as induction generator and the grid-side converter as STATCOM. The approach aims at harnessing the natural inertia of the generator and provide reactive power support from the grid-side converter.

Wind turbines with fully-rated converter are completely decoupled from the AC grid and, thus, the converter equipped with dedicated controls can provide transient stability enhancing services.

In [94], an approach to enhance LVRT capability of wind power plants with permanent magnet synchronous generators (PMSM) equipped with fully-rated converter was proposed. During faults, the grid-side converter provides voltage support through reactive power provision. The generator-side converter controls the DC-link voltage by adjusting the active power flow. The resulting surplus of mechanical power delivered from the wind turbine rotor is transformed into rotational energy of the generator rotor, i.e. the rotor accelerates. After the grid voltage is recovered, the additional kinetic energy is released to the grid and the rotor decelerates and returns to normal operation.

4.2.2 Wind Power Plants supplemented with FACTS

Many papers about transient stability improvement by complementing wind power plants with FACTS can be found in the literature. The main reason for that is that the majority of wind turbine designs include induction machines (IM). Because of their nature, wind turbines with directly grid-connected IMs (wind power plants of type one and two) are not able to control the reactive power at their terminals, instead reactive power is consumed from the grid. The reactive power consumption even increases during transient conditions. Due to that shortcoming many publications for transient stability improvement of IM based wind generation using FACTS devices [95–103] are found in the literature. The main aim of all papers is to improve transient stability by reactive power support from FACTS. In particular, SVCs and STATCOMs are used to provide reactive power support during transient conditions due to their good controllability and responsiveness.

4.2.3 Virtual Inertia

The provision of virtual inertia has recently gained more importance as the penetration of converter-based RES is increasing. Virtual inertia is usually referred to frequency stability, but it has also a substantial impact on transient stability. Although the installation of virtual inertia devices does not affect the inertia of SGs, but it may reroute some active power flows in the system and therefore changing the CCT in certain situations. It cannot be guaranteed that virtual inertia has an exclusively positive impact on the overall transient stability of the power system, which provides opportunities for further research.

At times of high RES generation, the available rotational inertia is reduced because conventional synchronous machines are shut down. Virtual inertia can be provided by units which have stored additional energy, either in rotational or chemical form. Wind turbines of type three and four, and battery storages equipped with an 'inertia' control algorithm are suitable for virtual inertia provision.

The authors of [104–106] suggest an implementation of virtual inertia control of DFIG wind turbines via a derivative controller which uses the frequency as an input signal to modify the active power setpoint of the machine according to the rate of change of frequency (RoCoF).

In [107, 108], the authors propose virtual inertia provision by adding a supplementary derivative control signal to the grid-side converter of type 4 (type D) wind turbines. The supplementary control signal changes the active power setpoint of the grid-side converter by adding an active power contribution which depends on the deviation of the system frequency.

A general overview about virtual inertia of wind power plants was recently published in [109].

Approaches to provide virtual inertia with PV plants have been introduced in [110–113]. They utilize the DC capacitor as an energy source to provide additional power or even include an energy storage system in the DC circuit to increase the amount of energy to be released during virtual inertia provision.

A novel innovative approach to provide virtual inertia by using electric vehicles (EV) was proposed in [114] and experimentally validated in [115]. The analysis was carried out considering the technical constraints imposed by IEC61851 which states the general requirements for EV charging systems. Virtual inertia provision is achieved by implementation of a droop control which modulates the current of the battery system depending on the RoCoF.

5 Discussion of the Qualitative Comparison

This section presents a qualitative comparison of transient stability improvement techniques to highlight the strengths and weaknesses, and to indicate an expected future trend. A quantitative comparison depends highly on the selected network and specifically analyzed use cases and, therefore, it is not suitable for the purpose of this paper.

Table 1 and 2 present a qualitative comparison of the preventive and emergency control techniques, respectively.The following aspects are evaluated: Installation need of an additional physical device, investment costs and effectiveness in terms of overall system impact. Moreover, the most important considerations of each technique are highlighted and an expected future trend is indicated. For improved visualization, Fig. 9 shows the Kiviat diagrams for preventive and selected emergency improvement techniques that are considered important in the future. The larger the covered area of an improvement technique, the higher is the overall impact of the technique on the power system.

One general observation is that there are more conventional than renewable techniques for transient stability improvement. Due to the transition to renewable-based generation where a growing number of conventional units are being phased-out, new techniques to preserve transient stability including new generation units must be developed for preventive and emergency controls.

Preventive techniques have to be extended by non-disruptive approaches of stability improvement based

Table 1: Qualitative comparison of **preventive** improvement techniques

	Conventional					Renewable
	Re-Dispatch	Load Shedding	Reduction of System Reactances	Upgrade of System Voltage	Variable Series Compensation	Increased Voltage Setpoint
Additional Device	No	No	Yes	No	Yes	No
Investment Costs	Low	Low	High	High	Medium/High	Low
Operational Costs	Medium	High	Low	Low	Low	Low
Effectiveness	High	Medium	Medium	High	Low/Medium	Medium
Notes	Additional costs due to dispatch to more expensive generators.	Last option due to customer interruption.	High investment costs are associated with new lines.	Limited by power system's voltage constraints.	Device design sets limitations for application. Resonance effects to be considered.	Limited by device capability and system's voltage constraints.
Future Trend	Inclusion of renewable generation in re-dispatch procedure.	Other techniques that do not disrupt customers are preferred. Generation located in distribution grids may be shed at the same time.	Distance between generation and load centers is increasing due to far off RES, e.g. off-shore wind parks.	To be considered when designing new grids. Not applicable for existing grids.	Careful cost-benefit evaluation before installation is needed.	Only to be used temporarily in situations with low stability margins.

Table 2: Qualitative comparison of **emergency** improvement techniques

	Conventional											Renewable		
	Fast Excitation System	Braking Resistor	Fast Valving	Generator Tripping	Variable Shunt Compensation	Variable Series Compensation	Combined Series and Parallel Compensation	Controlled System Separation	High Speed Circuit Breaker; Single Pole Operation; Auto Re-Closing	Fault Current Limiter	HVDC Control	LVRT	Converter-based RES	Virtual Inertia
Additional Device	No	Yes	No	No	Yes	Yes	Yes	No	Yes	Yes	No	No	No	Yes
Investment Costs	Low/Medium	Medium/High	Low/Medium	Low	Medium/High	Medium/High	Medium/High	Low	Medium/High	Medium/High	Low	Low	Medium	Medium/High
Operational Costs	Low	Low	Low	Medium	Low	Low	Low	High	Low	Low	Low	Low	Low	Low/Medium
Effectiveness	Medium/High	High	High	High	Medium	Medium	Medium	High	High	Medium	Medium/High	Medium	Medium/High	Medium
Notes	Ineffective for nearby faults. Effective for far faults.	Careful cost-benefit evaluation necessary. Stress on shaft and other adverse effects may arise.	Can be applied to thermal units only. Showed to be effective when combined with braking resistor. Governor upgrade might be needed.	Stress on shaft due to overspeed and sudden load change.	Increases the synchronization power by voltage support at selected nodes.	Control of the effective line reactance during and post fault for improved stability.	Full controllability of series injected voltage in magnitude and angle but expensive equipment.	System separation so that least consumers are disrupted. Difficult dynamic process to determine the location to separate the system.	High speed breakers effectively reduce severity of disturbance. Single-pole operation might be critical due to asymmetrical operation. Difficulties in determining the optimal auto re-closing time.	Superconducting FCLs are sensitive to temperature, current and magnetic field variations whereas bridge-type FCLs include active elements to be controlled.	HVDC links operated in constant power mode do not support AC grid's oscillation damping. Reactive power support at terminals and dedicated active power controls enhance transient stability.	LVRT generally positive as disconnection of large amount of RES stresses power system even more.	Main aim of converter-based RES and STATCOMs is to provide fast responding reactive power support.	Virtual inertia gains more attention with respect to frequency stability, however, virtual inertia also influences the transient stability.
Future Trend	Will stay part of future transient stability improvement, but fewer units may be online because of the substitution due to RES.	Decreased use is foreseen due to transition to RES. Other techniques for RES-based generation to be used and/or developed.	Due to the limited applicability and transition to RES, decreased use is foreseen in the future.	Will still be one of the options for severe grid disturbances to prevent pole-slipping causing even more severe grid disturbances.	Less need for additional shunt devices as newly integrated converter-based RES could provide voltage support.	The foreseen increased number of HVDC connections will allow to control active power flow (and so voltage angle) to certain extend. Less need for serial compensation.	Decreased use of these rather expensive devices due to other emerging possibilities involving converter-based RES units.	Will still be part of grid defense strategy for severe disturbances to save the overall system from large blackouts.	Dedicated communication equipment is foreseen to improve speed and reliability of high speed breakers. Research on effects of asymmetrical single-pole operation and auto re-closing of breakers on RES-based generation is needed.	Fault currents in future power systems might decrease due to current-limited devices, such as converters. Might result also in lower need for fault current limiters.	Higher need for dedicated HVDC control with increasing number of HVDC lines. AC system needs to be supported in terms of voltage support and oscillation damping.	LVRT capabilities will be crucial in future systems with highly decentralized generation to avoid auto-disconnection of large portions of generation.	Trend towards WPP designs with reactive power capability (DFIG & fully-rated converter WPPs) decrease need for supplementary STATCOM.	The relation of transient stability and virtual inertia must be investigated as the implementation of virtual inertia for frequency control will also affect the transient behavior.

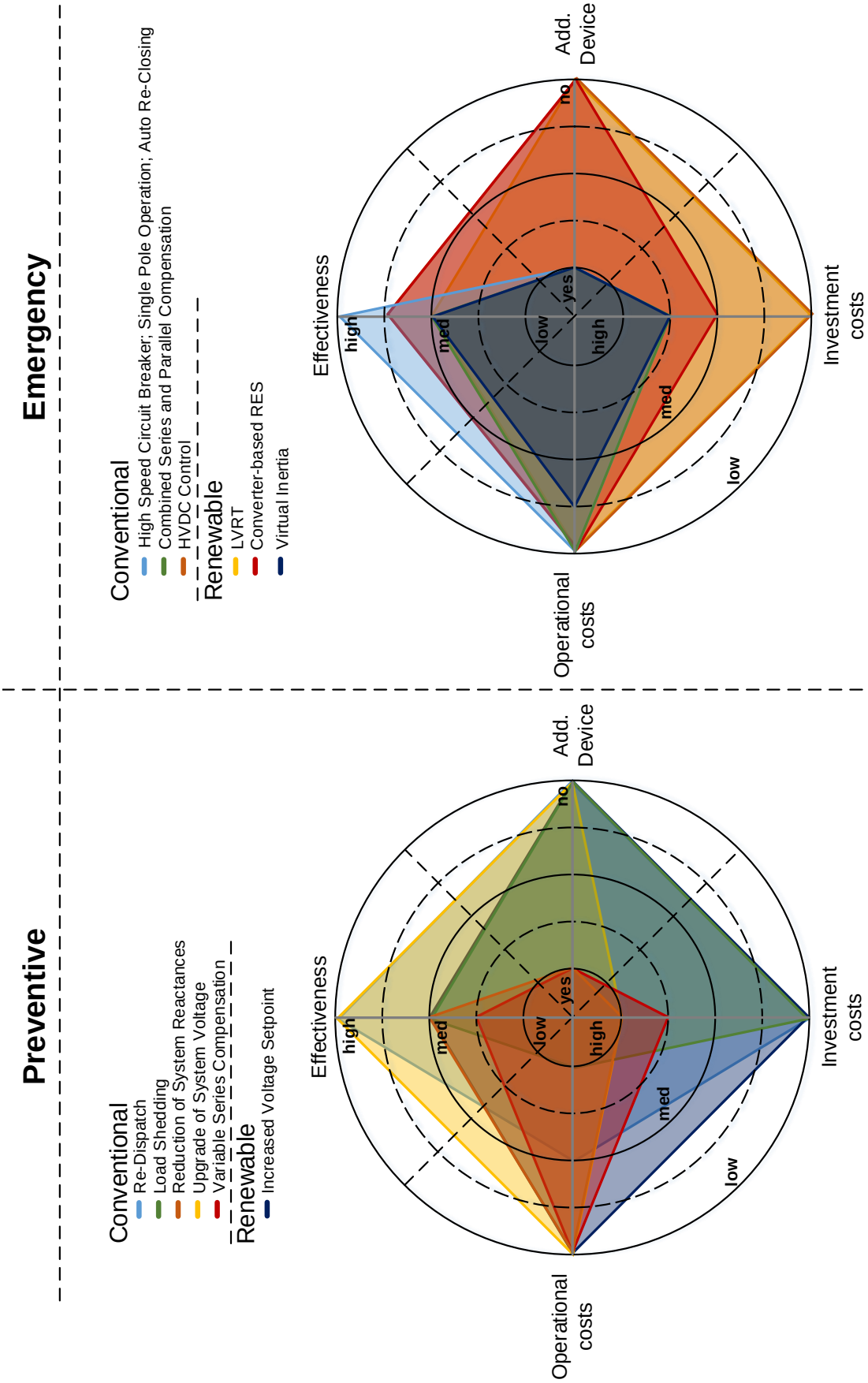

Fig. 9: Kiviat diagrams of preventive and emergency improvement techniques

on RES units. techniques that need low investments are preferred, hence, future research shall focus on inclusion of RES units in existing preventive control strategies. Re-dispatch procedures shall include RES units to relieve SGs if they are operated close to their stability limits. Conventional techniques that are constrained by grid limitations must be carefully considered at the grid planning stage to minimize subsequent investment costs, while preserving stability and a high reliability of electricity supply.

Conventional emergency techniques, such as fast excitation systems, generator tripping, high-speed breakers and controlled system operation will remain an important part of transient stability improvement. The use of braking resistors and fast valving is foreseen to decrease due to their limited application possibilities. The need for shunt and series compensation devices will decrease as the increase of converter-based units pose opportunities for distributed voltage control, and thereby, enhance stability. The importance of dedicated control of HVDC lines to support the AC system will increase with the expansion of HVDC technology. LVRT is already part of most grid codes as it is highly important to preserve stability whereas the (less frequent) opposite case of HVRT is not always thoroughly defined in the grid codes. Temporary high voltages could emerge in situations of sudden load drops and cause a large portion of RES units to disconnect. A discussion about HVRT and an evaluation of the need to include it into grid codes must be started. Virtual inertia is currently heavily discussed with respect to frequency control, but the impact of virtual inertia on the transient stability behavior has not been sufficiently investigated. That aspect is an unexplored area that definitely needs attention to enable the transition to future low inertia systems.

6 Conclusion and Outlook

The paper presented an overview of techniques to improve the transient stability of power systems. The techniques are categorized into two main groups, namely conventional and RES-based. It is distinguished between techniques applying preventive or emergency controls. A qualitative comparison of the techniques including an expected future trend is presented.

There are various conventional preventive techniques, such as re-dispatch of generators or series compensation which are extensively used in practice. Other conventional preventive techniques, such as increase of system voltage and minimization of system reactances are only applicable very limited due to technical and economic constraints.

There is only limited literature on preventive transient stability control using RES. One method was discussed, which temporarily increases the voltage setpoint in order to enhance the maximum power transfer capability. Further research is needed to develop new techniques for preventive transient stability improvement including RES, e.g. RES-based units need to be considered in existing preventive control strategies. A possibility could be to combine RES units with a storage and through coordinated control, e.g. temporary re-dispatch, a certain transient stability margin could be achieved.

A wide variety of conventional emergency techniques were found in the literature. A great share of them aims at voltage support during fault conditions in order to either increase the electrical power which is evacuated from the generator or to increase the synchronizing power flow between the generators. Other techniques are aiming at reducing the fault severity by means of fast fault clearing using high speed breakers with dedicated communication equipment, including single-pole operation and auto re-closing of breakers. Two widely used techniques are selective generator tripping to avoid instability and controlled system separation. Both techniques aim at saving the power system from widespread outage by shedding of critical units, sometimes in combination with load shedding to avoid frequency problems, or splitting the system into functioning subsystems. The control of HVDC links in transmission systems represents a possibility to significantly improve the transient stability of large power systems due to their good controllability. Dedicated HVDC control is seen as an approach with high potential for transient stability improvement of large interconnected systems because HVDC links are usually designed to transmit large powers over long distances and they also have a fast response time.

Regarding transient stability emergency control involving RES, two main categories can be distinguished. A lot of research was carried out aiming to improve LVRT behavior of wind power plants and PVs in order to support the system during disturbances. The research focus on LVRT behavior of RES is owed by the fact that in recent years grid codes also included LVRT capabilities of renewable sources due to their increasing share in the generation portfolio. In addition, research concerning HVRT capabilities need to be carried out to understand if these events would compromise the reliability of the system due to disconnection of large portions of distributed generation. The second area which is seen as promising with respect to transient stability emergency control by RES is the provision of virtual inertia. Virtual inertia is mainly referred to frequency

stability, but there is also a significant potential seen for the improvement of transient stability. However, to the best of our knowledge, there has no research been done about how virtual inertia affects transient stability, e.g. the type and location of the devices used for virtual inertia provision.

The qualitative comparison showed that a mix of conventional and RES-based techniques will be needed in a future power system based on diverse and distributed RES. Conventional techniques need to be further developed and new techniques for RES-based generators need to be investigated.

References

1. KEMA Consulting. Integration of Renewable Energy in Europe. Technical report, Imperial Collaege London, 2014.
2. Nicholas W. Miller, M. Shao, S. Pajic, and R. D'Aquila. Western Wind and Solar Integration Study Phase 3: Frequency Response and Transient Stability. Technical report, National Renewable Energy Laboratory (NREL), Denver, 2014.
3. Prabha Kundur, John Paserba, Venkat Ajjarapu, Göran Anderson, Anjan Bose, Claudio Canizares, Nikos Hatziargyriou, David Hill, Alex Stankovic, Carson Taylor, Thierry Van Vutsem, and Vijay Vittal. Definition and Classification of Power System Stability. *IEEE Transactions on Power Systems*, 21(3):1387–1401, 2004.
4. E. Adzic, V. Porobic, B. Dumnic, N. Celanovic, and V. Katic. PLL Synchronization in Grid-Connected Converters. In *6th PSU-UNS International Conference on Engineering and Technology (ICET)*, pages 1–5, Novi Sad, 2013.
5. M. Bobrowska-Rafal, K. Rafal, M. Jasinski, and M. P. Kazmierkowski. Grid synchronization and symmetrical components extraction with PLL algorithm for grid connected power electronic converters a review. *Bulletin of the Polish Academy of Sciences*, 59(4):485–497, 2011.
6. Xiao-Qiang Guo, Wei-Yang Wu, and He-Rong Gu. Phase locked loop and synchronization methods for grid-interfaced converters: a review. *PRZEGLAD ELEKTROTECHNICZNY (Electrical Review)*, 87(4):182–187, 2011.
7. Arulampalam Atputharajah and Tapan Kumar Saha. Power system blackouts - literature review. In *International Conference on Industrial and Information Systems (ICIIS)*, pages 460–465, Sri Lanka, 2009.
8. Nicholas W. Miller. Transient Stability in a World of Wind and Solar Generation. *IEEE power & energy magazine*, pages 31–39, nov 2015.
9. Prem Kumaar Naik, Niermal-Kumar C. Nair, and Akshya Kumar Swain. Impact of reduced inertia on transient stability of networks with asynchronous generation. *International Transactions on Electrical Energy Stystems*, 26:175–191, 2016.
10. J. Keller and B. Kroposki. Understanding Fault Characteristics of Inverter-Based Distributed Energy Resources. Technical report, National Renewable Energy Laboratory (NREL), Denver, 2010.
11. Shahbaz Ahmed Siddiqui, Kusum Verma, Khaleequr Rehman Niazi, and Manoj Fozdar. A unified control scheme for power system transient stability enhancement through preventive and emergency control. *International Transactions on Electrical Energy Stystems*, 26:365–383, 2016.
12. O. G. C. Dahl. *Electric Circuits: Theory and Applications*. McGraw Hill, Madison, 2 edition, 1938.
13. Prabha Kundur. *Power system stability and control*. McGraw Hill, 1994.
14. A. Alam and E. B. Makram. Transient Stability Constrained Optimal Power Flow. In *IEEE Power & Energy Society General Meeting*, pages 1–6, Montreal, 2006.
15. T.T. Nguyen, V.L. Nguyen, and a. Karimishad. Transient stability-constrained optimal power flow for online dispatch and nodal price evaluation in power systems with flexible AC transmission system devices. *IET Generation, Transmission & Distribution*, 5(3):332, 2011.
16. Edgardo D. Castronuovo, Pablo Ledesma, and Ignacio A. Calle. Advanced application of transient stability constrained-optimal power flow to a transmission system including an HVDC-LCC link. *IET Generation, Transmission & Distribution*, 9(13):1765–1772, 2015.
17. Michael Pertl, J. Tilman G. Weckesser, Michel M. N. Rezkalla, Kai Heussen, and Mattia Marinelli. A Decision Support Tool for Transient Stability Preventive Control. *Electric Power Systems Research*, 147:88–96, 2017.
18. Zhen Wang, Xiaozhe Song, Huanhai Xin, Deqiang Gan, and Kit Po Wong. Risk-Based Coordination of Generation Rescheduling and Load Shedding for Transient Stability Enhancement. *IEEE Transactions on Power Systems*, 28(4):4674–4682, 2013.
19. R. Grünbaum and J. Pernot. Thyristor-Controlled Series Compensation: A State Of The Art Approach For Optimization Of Transmission Over Power Links. Technical report, ABB, 2001.
20. Kalyan K Sen. SSSC - Static Synchronous Series Compensator: Theory, Modeling, and Applications. *IEEE Transactions on Power Delivery*, 13(1):241–246, 1998.
21. Charles J. Mozina. Power System Instability - What Relay Engineers Need to Know. In *64th Annual Conference for Protective Relay Engineers*, pages 103–112, College Station, 2011.
22. J. M. Ramirez, F. V. Arroyave, and R. E. Correa Gutierrez. Transient stability improvement by nonlinear controllers based on tracking. *International Journal of Electrical Power and Energy Systems*, 33(2):315–321, 2011.
23. Jahangir Hossain, Apel Mahmud, Naruttam K. Roy, and Hemanshu R. Pota. Enhancement of Transient Stability Limit and Voltage Regulation with Dynamic Loads Using Robust Excitation Control. *International Journal of Emerging Electric Power Systems*, 14(6):561–570, 2013.
24. M. A. Mahmud, H. R. Pota, M. Aldeen, and M. J. Hossain. Partial Feedback Linearizing Excitation Controller for Multimachine Power Systems to Improve Transient Stability. *IEEE Transactions on Power Systems*, 29(2):561–571, 2014.
25. Riya Saluja and M.H. Ali. Novel Braking Resistor Models for Transient Stability Enhancement in Power Grid System. In *IEEE PES Innovative Smart Grid Technologies Conference (ISGT)*, pages 1–6, Washington, DC, 2013.
26. Riya Saluja, Sagnika Ghosh, and Mohd Hasan Ali. Transient Stability Enhancement of Multi-Machine Power System by Novel Braking Resistor Models. In *IEEE Southeastcon*, pages 1–6, Jacksonville,FL, 2013.
27. Mohd Hasan Ali, Toshiaki Murata, and Junji Tamura. Augmentation of Transient Stability by Fuzzy- Logic

Controlled Braking Resistor in Multi-Machine Power System. In *IEEE Power Tech*, pages 1–7, St. Petersburg, 2005.
28. R.H. Park. Fast Turbine Valving. *IEEE Transactions on Power Apparatus and Systems*, 92(3):1065–1073, 1973.
29. Ramnarayan Patel, T.S. Bhatti, and D.P. Kothari. Improvement of Power System Transient Stability Using Fast Valving: A Review. *Electric Power Components and Systems*, 29(10):927–938, 2001.
30. R. Patel, T. S. Bhatti, and D. P. Kothari. Improvement of power system transient stability by coordinated operation of fast valving and braking resistor. *IEE Proceedings - Generation, Transmission and Distribution*, 150(3):311–316, 2003.
31. Y. Ohura, K. Matsuzawa, H. Ohtsuka, N. Nagai, T. Gouda, H. Oshida, S. Takeda, and S. Nishida. Development of a Generator Tripping System for Transient Stability Augmentation Based on The Energy Function Method. *IEEE Transactions on Power Delivery*, 1(3):68–77, 1986.
32. ME Baydokhty, M Eidiani, H ZEYNAL, H TORKAMANI, and H MORTAZAVI. Efficient Generator Tripping Approach with Minimum Generation Curtailment based on Fuzzy System Rotor Angle Prediction. *PRZEGLĄD ELEKTROTECHNICZNY (Electrical Review)*, 88(9):266–271, 2012.
33. George G. Karady and Jun Gu. A Hybrid Method for Generator Tripping. *IEEE Transactions on Power Systems*, 17(4):1102–1107, 2002.
34. G. G. Karady and Mansour A. Kattamesh. Improving Transient Stability Using Generator Tripping Based on Tracking Rotor-Angle. In *IEEE Power Engineering Society Winter Meeting*, pages 1113–1118, 2002.
35. M. O'Brien and G. Ledwich. Static reactive-power compensator controls for improved system stability. *IEE Proceedings C Generation, Transmission and Distribution*, 134(1):38–42, 1987.
36. X. Zhou and J. Liang. Overview of control schemes for TCSC to enhance the stability of power systems. *IEE Proceedings - Generation, Transmission and Distribution*, 146(2):125–130, 1999.
37. S. Wagh, A. K. Kamath, and N. M. Singh. Non-linear Model Predictive Control for Improving Transient Stability of Power System using TCSC Controller. In *7th Asian Control Conference (ASCC)*, pages 1627–1632, Hong Kong, 2009.
38. S. R. Wagh, A. K. Kamath, and N. M. Singh. A Nonlinear TCSC Controller based on Control Lyapunov Function and Receding Horizon Strategy For Power System Transient Stability Improvement. *2009 Ieee International Conference on Control and Automation, Vols 1-3*, pages 813–818, 2009.
39. Nguyen Tuan Anh, Dirk Van Hertem, and Johan Driesen. Effectiveness of TCSC Controllers Using Remote Input Signals for Transient Stability Enhancement. In *IEEE PowerTech*, pages 1–8, Trondheim, 2011.
40. Lei Zhang, Aimin Zhang, and Junfeng Jing. I&I Stabilization Based Novel Nonlinear Adaptive TCSC Control Algorithm for Improving Transient Stability. In *The 26th Chinese Control and Decision Conference (2014 CCDC)*, pages 1610–1615, Changsha, 2014.
41. X.-Z. Dai, D. He, L. L. Fan, N.-H. Li, and H. Chen. Improved ANN αth-order inverse TCSC controller for enhancing power system transient stability. *IEE Proceedings - Generation, Transmission and Distribution*, 146(6):550–556, 1999.
42. S. Sankara Prasad. Transient Stability Enhancement of Multi-machine Power System using Fuzzy Controlled TCSC. *Journal of Electrical and Electronics Engineering (IOSR-JEEE)*, 1(6):1–7, 2012.
43. Prechanon Kumkratug. Improving Power System Transient Stability with Static Synchronous Series Compensator. *American Journal of Applied Sciences*, 8(1):77–81, 2011.
44. Majid Poshtan, Brij N. Singh, and Parviz Rastgoufard. A Nonlinear Control Method for SSSC to Improve Power System Stability. In *International Conference on Power Electronic, Drives and Energy Systems (PEDES)*, pages 1–7, 2006.
45. V.K. Chandrakar and A.G. Kothari. MFFN based Static Synchronous Series Compensator (SSSC) for Transient Stability Improvement. In *International Conference on Intelligent Systems Applications to Power Systems (ISAP)*, pages 5–8, Niigata, 2007.
46. Sidhartha Panda and N. P. Padhy. A PSO-based SSSC Controller for Improvement of Transient Stability Performance. *International Journal of Electrical, Computer, Energetic, Electronic and Communication Engineering*, 1(9):1295–1302, 2007.
47. V.K. Chandrakar and A.G. Kothari. Fuzzy Logic based Static Synchronous Series Compensator(SSSC) for Transient Stability Improvemen. In *IEEE International Conference on Electric Utility Deregulation, Restructuring and Power Technologies (DRPT)*, pages 240–245, Hong Kong, 2004.
48. M. H. Haque. Application of UPFC to Enhance Transient Stability Limit. In *IEEE Power Engineering Society General Meeting*, pages 1–6, Tampa, 2007.
49. E. Gholipour and S. Saadate. Improving of Transient Stability of Power Systems Using UPFC. *IEEE Transactions on Power Delivery*, 20(2):1677–1682, 2005.
50. Chia Chi Chu and Hung Chi Tsai. Application of Lyapunov-Based Adaptive Neural Network UPFC Damping Controllers For Transient Stability Enhancement. In *IEEE Power and Energy Society General Meeting - Conversion and Delivery of Electrical Energy in the 21st Century*, pages 1–6, Pittsburgh, 2008.
51. Sukumar Mishra. Neural-Network-Based Adaptive UPFC for Improving Transient Stability Performance of Power System. *IEEE Transactions on Neural Networks*, 17(2):461–470, 2006.
52. A Gupta and P.R. Sharma. Static and Transient Stability Enhancement of Power System by Optimally Placing UPFC (Unified Power Flow Controller). In *Third International Conference on Advanced Computing & Communication Technologies*, pages 121–125, 2013.
53. Y. Ohura, M. Suzuki, K. Yanagihashi, M. Yamaura, K. Omata, T. Nakamura, and H. Watanabe. A Predictive Out-Of-Step Protection System Based On Observation Of The Phase Difference Between Substations. *IEEE Transactions on Power Delivery*, 5(4):1695–1704, 1990.
54. Chao Wang, Peng Gao, Taoxi Zhu, and Wei Shao. New method of searching for the out-of-step separation interface based on reactive power. In *IEEE PES Transmission and Distribution Conference and Exposition*, pages 1–5, Chicago, 2008.
55. M. M. Adibi, R. J. Kafka, Sandeep Maram, and Lamine M. Mili. On Power System Controlled Separation. *IEEE Transactions on Power Systems*, 21(4):1894–1902, 2006.
56. Patrick McNabb and Janusz Bialek. A priori transient stability indicator of islanded power systems using Ex-

tended Equal Area Criterion. In *IEEE Power and Energy Society General Meeting*, page 7, San Diego, 2012.
57. Zhenzhi Lin, Seán Noms, Hongbo Shao, and Janusz Bialek. Transient stability assessment of controlled islanding based on power flow tracing. In *Power Systems Computation Conference (PSCC)*, page 7, Wroclaw, 2014.
58. Jairo Quirós-Tortós, Rubén Sánchez-García, Jacek Brodzki, Janusz Bialek, and Vladimir Terzija. Constrained spectral clustering-based methodology for intentional controlled islanding of large-scale power systems. *IET Generation, Transmission & Distribution*, 9(1):31–42, 2015.
59. R. O. Berglund, W. A. Mittelstadt, M. L. Shelton, P. Barkan, C. G. Dewey, and K. M. Skreiner. One-Cycle Fault Interruption at 500 kV: System Benefits and Breaker Design. *IEEE Transactions on Power Apparatus and Systems*, 93(5):1240–1251, 1974.
60. Schneider Electric. Circuit Breaker Characteristic Trip Curves and Coordination. Technical report, Schneider Electric, Cedar Rapids, 2001.
61. Siemens. High-Voltage Circuit Breakers. Technical report, Siemens, 2012.
62. ABB. Power Circuit Breaker 245 kV, up to 63 kA. Technical report, ABB, 2009.
63. Hassan Khorashadi-Zadeh and Zuyi Li. Transmission Line Single Phase Auto Re-Closing Scheme Based on Wavelet Transform and Adatptive Fuzzy Neuro Inference System. In *39th North American Power Symposium (NAPS)*, pages 43–48, Las Cruces, 2007.
64. H. Takani, Y. Sonobe, T. Kagami, F. Kawano, P. Beaumont, G.P. Baber, and G.T. Main. The Application and Advantages of Multi-Phase Autoreclosing. In *10th IET International Conference on Developments in Power System Protection (DPSP)*, pages 1–5, Manchester, 2010.
65. P. Li, B. H. Zhang, Z. G. Hao, Y. F. Rao, Y. T. Wang, Z. Q. Bo, and A. Klimek. Optimizing the Re-closing Time to Improve the Transmission Capacity of Power System. In *43rd International Universities Power Engineering Conference (UPEC)*, pages 1–5, Padova, 2008.
66. P. Li, B. H. Zhang, Z. G. Hao, Z. Q. Bo, A. Klimek, Y. F. Rao, and Y. T. Wang. The study on optimizing re-closing time to improve the transmission capacity. In *IEEE/PES Power Systems Conference and Exposition (PSCE)*, pages 1–6, Seattle, 2009.
67. Y. Goto, K. Yukita, H. Yamada, K. Ichiyanagi, and T. Matsumura. A Study on Power System Transient Stability due to Introduction of Superconducting Fault Current Limiters. In *International Conference on Power System Technology*, pages 275–280, Perth, 2000.
68. G. Y. Yokomizu, K. Yukita, K. Mizuno, K. Ichiyanagi, Y. Yokomizu, and T. Matsumura. Experimental Studies on Power System Transient Stability due to Introduction of Superconducting Fault Current Limiters. In *IEEE Power Engineering Society Winter Meeting*, pages 1129–1134, Singapore, 2000.
69. M. Tsuda, Y. Mitani, K. Tsuji, and K. Kakihana. Application of Resistor Based Superconducting Fault Current Limiter to Enhancement of Power Svstern Transient Stabilitv. *IEEE Transactions on Applied Superconductivity*, 11(1):2122–2125, 2001.
70. M Yagami, S Shibata, T Murata, and J Tamura. Improvement of Power System Transient Stability by Superconducting Fault Current Limiter. In *IEEE/PES Transmission and Distribution Conference and Exhibition*, pages 359–364, Yokohama, 2002.
71. Y. Shirai, K. Furushiba, Y. Shouno, M. Shiotsu, and T. Nitta. Improvement of Power System Stability by Use of Superconducting Fault Current Limiter With ZnO Device and Resistor in Parallel. *IEEE Transactions on Applied Superconductivity*, 18(2):680–683, 2008.
72. Abdulla Emhemed, Ryan M. Tumilty, Nand Singh, Graeme M. Burt, and James R. McDonald. Analysis of Transient Stability Enhancement of LV-Connected Induction Microgenerators by Using Resistive-Type Fault Current Limiters. *IEEE Transactions on Power Systems*, 25(2):885–893, 2010.
73. Mehrdad Tarafdar Hagh, Seyed Behzad Naderi, and Mehdi Jafari. Application of Non-superconducting Fault Current Limiter to Improve Transient Stability. In *International Conference on Power and Energy (PECon)*, pages 646–650, Kuala Lumpur, 2010.
74. M. Tarafdar Hagh, M. Jafari, and S. B. Naderi. Transient Stability Improvement Using Non-superconducting Fault Current Limiter. In *1st Power Electronic & Drive Systems & Technologies Conference (PEDSTC)*, pages 367–370, Tehran, 2010.
75. Mohammad Ashraf, Hossain Sadi, and M. H. Ali. Transient Stability Enhancement of Multi- Machine Power System By Parallel Resonance Type Fault Current Limiter. In *North American Power Symposium (NAPS)*, pages 1–6, Charlotte, 2015.
76. M. Kamal Hossain and M. Hasan Ali. Transient Stability Augmentation of PV/DFIG/SG-Based Hybrid Power System by Nonlinear Control-Based Variable Resistive FCL. *IEEE Transactions on Sustainable Energy*, 6(4):1638–1649, 2015.
77. Technology Watch. Superconducting Fault Current Limiters. Technical report, EPRI, Palo Alto, 2009.
78. Dragan Jovcic and Khaled Ahmed. *High-Voltage Direct-Current Transmission*. John Wiley & Sons, Ltd, Aberdeen, 2015.
79. Y. Phulpin, J. Hazra, and D. Ernst. Model predictive control of HVDC power flow to improve transient stability in power systems. In *IEEE International Conference on Smart Grid Communications (SmartGridComm)*, pages 593–598, Brussels, 2011.
80. J. Hazra, Y. Phulpin, and D. Ernst. HVDC Control Strategies to Improve Transient Stability in Interconnected Power Systems. In *IEEE PowerTech*, pages 1–6, Bucharest, 2009.
81. R. Eriksson, V. Knazkins, and L. Söder. On the assessment of the impact of a conventional HVDC on a test power system. In *iREP Symposium- Bulk Power System Dynamics and Control - VII, Revitalizing Operational Reliability*, pages 1–5, Charleston, 2007.
82. Javier Renedo, Aurelio Garcia-Cerrada, and Luis Rouco. Active Power Control Strategies for Transient Stability Enhancement of AC/DC Grids With VSC-HVDC Multi-Terminal Systems. *IEEE Transactions on Power Systems*, PP(99):1–10, 2016.
83. Robert Eriksson. Coordinated control of multiterminal DC grid power injections for improved rotor-angle stability based on Lyapunov theory. *IEEE Transactions on Power Delivery*, 29(4):1789–1797, 2014.
84. Michael Pertl, Michel Rezkalla, and Mattia Marinelli. A Novel Grid-Wide Transient Stability Assessment and Visualization Method for Increasing Situation Awareness of Control Room Operators. In *IEEE PES Innovative Smart Grid Technologies Conference Asia (ISGT)*, pages 1–6, Melbourne, 2016.

85. Energinet. Technical Regulation 3.2.5 For Wind Power Plants With A Power Ouput Greater Than 11 kW. Technical report, Energinet (TSO Denmark), 2010.
86. Energinet. Technical regulation 3.2.2 for PV power plants with a power output above 11 kW. Technical report, Energinet (TSO Denmark), 2015.
87. ENTSO-E. ENTSO-E Network Code for Requirements for Grid Connection Applicable to all Generators. Technical Report June, ENTSO-E, 2012.
88. ENTSO-E. Draft - Network Code on Requirements for Grid Connection Applicable to all Generators. Technical report, ENTSO-E, Brussels, 2015.
89. Energinet. Technical Regulation 3.2.1. for electricity generation facilities with a rated current of 16 A per phase or lower. Technical report, Energinet (TSO Denmark), 2011.
90. Verband der Netzbetreiber - VDN. TransmissionCode 2007 - Network and System Rules of the German Transmission System Operators. Technical Report August, Verband der Netzbetreiber - VDN e.V. beim VDEW, 2007.
91. Fichtner. Grid Codes for Wind Power Integration in Spain and Germany: Use of Incentive Payments to Encourage Grid-Friendly Wind Power Plants. Technical report, FICHTNER, 2010.
92. Lasantha Meegahapola and Damian Flynn. Impact on Transient and Frequency Stability for a Power System at Very High Wind Penetration. In *IEEE Power and Energy Society General Meeting*, pages 1–8, Minneapolis, 2010.
93. Lasantha Gunaruwan Meegahapola, Tim Littler, and Damian Flynn. Decoupled-DFIG fault ride-through strategy for enhanced stability performance during grid faults. *IEEE Transactions on Sustainable Energy*, 1(3):152–162, 2010.
94. Shuhui Dong, Heming Li, and Yi Wang. Low Voltage Ride Through Capability Enhancement of PMSG-Based Wind Turbine. In *International Conference on Sustainable Power Generation and Supply (SUPERGEN)*, pages 1–5, Hangzhou, 2012.
95. Marta Molinas, S. Vazquez, T. Takaku, J. M. Carrasco, R. Shimada, and T. Undeland. Improvement of Transient Stability Margin in Power Systems with Integrated Wind Generation Using a STATCOM : An Experimental Verification. In *International Conference on Future Power Systems*, pages 1–6, Amsterdam, 2005.
96. A. Arulampalam, M. Barnes, N. Jenkins, and J. B. Ekanayake. Power quality and stability improvement of a wind farm using STATCOM supported with hybrid battery energy storage. *IEE Proceedings - Generation, Transmission and Distribution*, 153(6):701–710, 2006.
97. Marta Molinas, Jon Are Suul, and Tore Undeland. Wind farms with increased transient stability margin provided by a STATCOM. In *Power Electronics and Motion Control Conference (IPEMC)*, pages 1–7, Shanghai, 2006.
98. Guizhen Tian, Shengtie Wang, and G Liu. Power quality and transient stability improvement of wind farm with fixed-speed induction generators using a STATCOM. In *International Conference on Power System Technology (POWERCON)*, pages 1–6, Hangzhou, 2010.
99. Hua Zhou, Hongfen Wei, Xiaoyan Qiu, Jian Xu, Xiwen Wei, and Song Wang. Improvement of Transient Voltage Stability of the Wind Farm using SVC and TCSC. In *Asia-Pacific Power and Energy Engineering Conference (APPEEC)*, pages 1–4, Wuhan, 2011.
100. Hossein Hosseini and Mohsen Kalantar. Transient Stability Enhancement of Power System Including Wind Farms Using Improved ECS. In *3rd IEEE International Symposium on Power Electronics for Distributed Generation Systems (PEDG)*, pages 782–787, 2012.
101. Mohamad Amiri and Mina Sheikholeslami. Transient Stability Improvement of Grid Connected Wind Generator using SVC and STATCOM. In *International conference on Innovative Engineering Technologies (ICIET)*, pages 136–140, Bangkok, 2014.
102. P. Sravanthi, K. Radha Rani, J. Amarnath, and S. Kamakshaiah. Critical Clearing Time and Transient Stability Analysis of SCIG based Wind Farm with STATCOM. In *International Conference on Smart Electric Grid (ISEG)*, pages 1–8, Guntur, 2014.
103. M.G. Hemeida, H. Rezk, and M.M. Hamada. A comprehensive comparison of STATCOM versus SVC-based fuzzy controller for stability improvement of wind farm connected to multi-machine power system. *Electrical Engineering*, 2017.
104. Mattia Marinelli, Stefano Massucco, Andrea Mansoldo, and Mark Norton. Analysis of Inertial Response and Primary Power-Frequency Control Provision by Doubly Fed Induction Generator Wind Turbines in a Small Power System. In *17th Power Systems Computation Conference (PSCC)*, pages 1–7, Stockholm, 2011.
105. Moghammadreza Fakhari Moghaddam Arani and Ehab F. El-Saadany. Implementing virtual inertia in DFIG-based wind power generation. *IEEE Transactions on Power Systems*, 28(2):1373–1384, 2013.
106. Elyas Rakhshani, Daniel Remon, Antoni Mir Cantarellas, and Pedro Rodriguez. Analysis of derivative control based virtual inertia in multi-area high-voltage direct current interconnected power systems. *IET Generation, Transmission & Distribution*, 10(6):1458–1469, 2016.
107. Yi Wang, Jianhui Meng, Xiangyu Zhang, and Lie Xu. Control of PMSG-Based Wind Turbines for System Inertial Response and Power Oscillation Damping. *IEEE Transactions on Sustainable Energy*, 6(2):565–574, 2015.
108. Li Xu, Gang Wang, Lijun Fu, You Wu, and Qiaoming Shi. General average model of D-PMSG and its application with virtual inertia control. In *IEEE International Conference on Mechatronics and Automation (ICMA)*, pages 802–807, Beijing, 2015.
109. X. Wang and W. Du. Virtual Inertia Control of Grid-Connected Wind Farms. In *International Conference on Renewable Power Generation (RPG)*, pages 1–6, Beijing, 2016.
110. Won-sang Im, Cheng Wang, Wenxin Liu, Liming Liu, and Jang-Mok Kim. Distributed Virtual Inertia based Control of Multiple Photovoltaic Systems in Autonomous Microgrid. *IEEE/CAA Journal of Automatica Sinica*, pages 1–9, 2016.
111. Eberhard Waffenschmidt. Virtual inertia grid control with LED lamp driver. In *International Energy and Sustainability Conference (IESC)*, pages 1–6, Cologne, 2016.
112. Eberhard Waffenschmidt and Ron S. Y. Hui. Virtual inertia with PV inverters using DC-link capacitors. In *18th European Conference on Power Electronics and Applications (EPE'16 ECCE Europe)*, pages 1–10, Karlsruhe, 2016.
113. Xiaoyu Wang, Meng Yue, and Eduard Muljadi. PV generation enhancement with a virtual inertia emulator to provide inertial response to the grid. In *IEEE*

Energy Conversion Congress and Exposition (ECCE), pages 17–23, Pittsburgh, 2014.

114. Michel Rezkalla, Antonio Zecchino, Michael Pertl, and Mattia Marinelli. Grid Frequency Support by Single-Phase Electric Vehicles Employing an Innovative Virtual Inertia Controller. In *International Universities Power Engineering Conference (UPEC)*, pages 1–6, Coimbra, 2016.
115. Michel Rezkalla, Antonio Zecchino, Sergejus Martinenas, Alexander M. Prostejovsky, and Mattia Marinelli. Comparison between synthetic inertia and fast frequency containment control based on single phase EVs in a microgrid. *Applied Energy*, in press, 2017.

[Pub. B] A decision support tool for transient stability preventive control

A Decision Support Tool for Transient Stability Preventive Control

Michael Pertl[a], Tilman Weckesser[b],
Michel Rezkalla[a], Kai Heussen[a], Mattia Marinelli[a,*]

[a] *Center for Electric Power and Energy, Department of Electrical Engineering, Technical University of Denmark*
Frederiksborgvej 399, Building 776, 4000 Roskilde, Denmark
[b] *Department of Electrical Engineering and Computer Science at the University of Liège, Belgium*

Abstract

The paper presents a decision support tool for transient stability preventive control contributing to increased situation awareness of control room operators by providing additional information about the state of the power system in terms of transient stability. A time-domain approach is used to assess the transient stability for potentially critical faults. Potential critical fault locations are identified by a critical bus screening through analysis of pre-disturbance steady-state conditions. The identified buses are subject to a fast critical contingency screening determining the actual critical contingencies/buses. These two screenings aim at reducing the computational burden of the assessment, since only contingencies considered as critical are taken into account. The critical clearing times for the critical contingencies are determined. A preventive re-dispatch of generators to ensure a predefined minimum critical clearing time for faults at all buses is proposed, while costs are minimized. The results of the assessment are presented to the control room operator, who decides to accept the suggested dispatch or to repeat the assessment considering additional user-specific constraints. The effectiveness of the proposed method is demonstrated on a standard nine-bus and the New England test system.

Keywords: Control Room Operator, Decision Support, Online Assessment, Preventive Control, Situation Awareness, Transient Stability

*Corresponding author
Email address: matm@elektro.dtu.dk (Mattia Marinelli)

1. Introduction

Observability of power systems has to be increased to improve the situation awareness of control room operators. Situation awareness is a key aspect in maintaining power system security, because it enables anticipation of critical conditions and effectively set preventive actions to mitigate them [1, 2]. Lack of situation awareness was several times identified as one of the major causes for large power system blackouts [3, 4]. Various problems with situation awareness are related to missing information, i.e. the control room operator is not provided with the needed information [5–7]. Therefore, appropriate monitoring, visualization and decision support tools have to be developed to support the decision making process and to prevent or properly respond to electrical incidents in order to maintain power system stability [8, 9]. Dedicated decision support tools are needed to facilitate the incorporation of high shares of renewable energy sources (RES) while keeping the power system operative and stable [10]. However, in this work, RES are not included in the analysis intentionally, as the work is mainly concerned with improving the calculation methods for a required re-dispatch. Since a considerable amount of the RES are converter driven (e.g., photovoltaic and wind turbines), they cannot lose synchronism as they are usually synchronized to the grid by a phase-locked loop. Moreover, due to advanced capabilities, such as voltage support during fault-ride-through situations, RES can contribute positively to maintain transient stability.

Transient stability is an important aspect of power system stability since it describes the ability of a power system to withstand large disturbances and keep synchronism [11]. Maintaining synchronism means that all synchronous generators (SGs) in a system operate at the same rotor speed and none of them falls out-of-step by accelerating or decelerating with respect to the other SGs. Transient instability can lead to widespread outages due to unintended tripping of protection devices which could trigger a cascaded breakdown of the power system [12]. Hence, it is crucial to assess the transient stability of power systems online on a grid-wide basis and set preventive actions if issues are identified [13, 14].

The paper presents a novel online decision support tool for transient stability preventive control, building on experiences of previous tools. The proposed tool takes into account the current grid state and analyzes the grid's capability to withstand three-phase faults for a user-specified duration (desired limit, minimum critical clearing time (CCT), further called CCT_{lim}) at the most severe locations (buses) of the grid. A time-domain (TD) approach is used to assess transient stability on a grid-wide basis. To reduce the computational burden of the TD simulations, a critical bus screening (CBS) and fast critical contingency screening

(FCCS) are carried out prior to the assessment. The CBS identifies potentially critical buses with regard to three-phase faults, by means of pre-disturbance conditions without the need for TD simulations. The FCCS determines the actual critical buses within the set of potentially critical buses by checking whether the system can withstand a three-phase fault for user-specified limit without any SG losing synchronism. This results in a yes/no decision, which eventually determines the critical buses. To achieve the desired minimum CCT for all critical buses, the needed dispatch of SGs is determined. The power is dispatched by means of an optimal power flow (OPF) calculation minimizing the generation costs while respecting technical constraints, such as generators' capacity, maximum line flows and bus voltage limits. Since the method aims at proposing a preventive generation re-dispatch, which ensures that the stability margins in the current operating point are sufficient, the ramp rates of generators are not considered in the OPF. As the preventive control is applied before a contingency occurs, the consideration of costs is an important factor in the assessment. The results of the assessment in terms of needed re-dispatch and associated costs are presented to the control room operator who has to decide whether the proposed re-dispatch is applied or not. The operator may also introduce additional constraints, e.g. the unavailability of generators to take over the dispatched power. The dispatch procedure is re-run, takes into account the additional introduced constraints and delivers a new dispatch proposal. The approach guarantees a minimum CCT for all buses of the power system and, thus, a sufficient transient stability margin.

The main scientific contribution of the paper is twofold. Firstly, a novel fast converging technique to determine the needed dispatch for re-establishing a predefined stability level is presented. Secondly, the paper elaborates on the combination of the transient stability assessment, the dispatch determination and the critical contingency analysis to enable an online application of the approach.

2. Transient Stability Preventive Control - Brief Summary and Relation to the Paper

This section intends to summarize preventive transient stability approaches found in the literature. Moreover, the relation between transient stability assessment and OPF calculation are discussed as both items appear in this work. At this point, only re-dispatch of SGs is discussed as a possible counteraction, whereas many other actions can be applied to enhance transient stability, e.g. load shedding, increase of bus voltage and transmission

impedance reduction.

Numerous approaches to determine the needed dispatch can be found in the literature. They can be classified into two categories: a) determining the dispatch within the multi-machine system and b) converting the multi-machine system in a single-machine equivalent (SIME) and analyzing it as an one-machine against infinite bus (OMIB) system.

Regarding the first category, several approaches have been introduced. An approach which uses the virtually linear relationship between rotor angle and CCT of the SGs is proposed in [15, 16]. Since the relationship is not exactly linear, several TD simulations are necessary to obtain accurate results. Moreover, the estimation of the rotor angles introduces additional uncertainties. In [17], the authors propose to use the almost linear relationship between CCT and active power output of the generator. Several TD simulations are needed to determine the relationship. Specifically, seven CCTs associated with the SG power output were calculated in the paper, which implies a high computational burden.

Transient stability analysis using SIME, where the system is transformed into an OMIB equivalent, is very well covered in the literature [18–24]. The SIME approach transforms a multi-machine system to an OMIB equivalent, based on the fact that a loss of synchronism originates from the separation of one machine against another machine (or groups of machines). Considering that, the machines are separated into two groups: the non-critical and the critical machines which are responsible for the loss of synchronism. After the transformation into an OMIB system, transient stability is assessed by using the equal area criterion (EAC). The SIME parameters have to be updated continuously in every time step in order to achieve accurate results while the source for the parameters is provided by a simultaneously running TD simulation.

Regardless of which approach is used to determine the dispatch, power has to be redistributed between the SGs. In order to do that in a transparent and appropriate way, OPF calculations are used to find a good trade-off between security and economics.

In general, transient stability-constrained OPF can be grouped into two different approaches, called *Global Approach* and *Sequential Approach*. The authors of [18] propose the mentioned grouping and give a comprehensive and up-to-date summary about transient stability in OPF calculations and about real-time stability in power systems in general. In the global approach [22, 25–28], transient stability models are converted into algebraic equations at each time step of the simulation. This non-linear set of equations is then included in the OPF as a stability constraint, which results generally in a large single non-linear pro-

gramming problem. In the sequential approach, transient stability constraints are derived from TD simulations and directly converted into conventional constraints of standard OPF calculations, e.g. maximum active power setpoints of the generators. The advantages of the sequential approach are that the OPF can be solved with a standard OPF solver and the flexibility of choice of the receiving generators for the dispatch. Opposed to these advantages, however, the sequential approach does not guarantee optimality which, therefore, makes the global approach more appealing from a conceptual perspective [18].

Since this paper aims at providing a tool for transient stability preventive control from the operator's perspective, the problem is seen from a different angle. The tool should inform the operator about insufficient transient stability margins and support the operator's decision making by suggesting an appropriate dispatch to achieve the defined stability margin. An interesting transient stability assessment approach for preventive control, that incorporates the critical contingency filtering and ranking method from [29], was proposed in [19, 24]. A sequential approach, based on SIME, has been developed in the mentioned work. Opposed to that, the approach proposed in this manuscript takes into account the full multi-machine system without the need to transform it into an OMIB system. Moreover, in the proposed approach only 2-3 CCTs need to be calculated to determine the dispatch of a generator.

3. Description of the Transient Stability Preventive Control Approach

In emergency control, the incident already occurred and the main aim is to safe the system. Opposed to that, the objective of preventive control is to prepare the power system for future uncertain events which may occur. The system has to be operated and maintained in a state, where it is able to withstand and handle disturbances satisfactorily. Therefore, in preventive control economic aspects have to be taken into account. The system operator would usually refuse to take expensive countermeasures against contingencies that may occur [30] and, thus, a trade-off solution between costs and security has to be found.

The proposed approach for transient stability preventive control utilizes TD simulations, which consider the full dynamics of the power system to calculate the minimal power to be dispatched from the critical machines to non-critical machines in order to re-establish a pre-

defined stability margin in terms of CCT. Since TD simulations require high computational power and the method aims at supporting control room operators in taking their decisions, a CBS is carried out prior to the assessment. As the economic aspect for preventive dispatch is of crucial importance, consecutive OPFs are carried out to minimize generation costs while respecting the technical constraints. That approach enables to derive the best trade-off solution to support the control room operator in its decision making. Moreover, the specified stability limit (minimum CCT) is satisfied and secure operation in terms of transient stability is guaranteed. In this work, the minimum desired CCT (CCT_{lim}) is assumed to be $200\,ms$. That is a reasonable limit, since it can be assumed that the protection equipment will detect and clear the fault by opening the breakers within this time span [31]. The flow chart of the proposed transient stability preventive control approach is shown in Fig. 1. It comprises the elements which are needed to establish a transient stability control and visualizes how they interact. In the following section, all elements are comprehensively described.

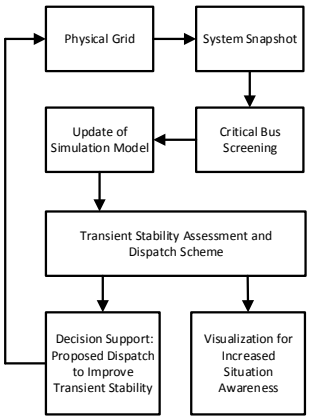

Figure 1: Flow chart of the transient stability preventive control approach

3.1. Physical Grid

This block represents the real physical grid, for which the transient stability control is applied. The feedback from the decision support block represents the interaction of the control room operator with the physical grid. The control room operator has to decide and

approve whether the proposed dispatch is applied to the system or additional constraints are to be considered in the assessment leading to a new dispatch recommendation.

3.2. System Snapshot

A system snapshot is needed to update the TD simulation model with the current system state. Two variants are proposed to obtain a system snapshot. In the first variant, the needed data is extracted from the SCADA system. The needed data includes: breaker status, generation output, activation of capacitor banks, RES generation, line flows and further relevant data. Phasor measurement units (PMUs) are another option to obtain a system snapshot, but that assumes full observability of the power system by PMUs. In case, the needed data is not fully available from either of these sources, a hybrid approach could be used by combining SCADA and PMU data to obtain a full system snapshot [32].

3.3. Critical Bus Screening (CBS)

Based on the current system snapshot, a CBS, which aims at determining the most critical fault locations, is carried out prior to the update of the simulation model. Here, the focus is on assessing bus bar faults. Therefore, in the following the term critical buses is used, instead of the more generic term critical fault location. The CBS analyzes the pre-disturbance conditions and filters out the potentially critical buses with regard to three-phase faults. No TD simulations are needed for the CBS, hence, the needed computational time for further assessment is reduced, as only the set of potentially critical buses is considered. The CBS method is based on the work in [33–35]. A heuristic approach is used to identify the buses which are regarded as most critical. Buses are scanned for three criteria indicating their criticality. Only buses which satisfy all three criteria are regarded as critical and qualify for the analysis in the TD simulation.

Criterion 1 - Bus Properties: Criterion one consists of two sub-criteria. The voltage level of the bus V_{bus} has to be above the specified threshold V_{min}. Only (extra) high voltage buses are considered because faults at higher voltage levels are more severe than at lower voltage levels. Moreover, the number of buses to be considered in the assessment is drastically reduced by excluding low and medium voltage buses.

The bus must be connected to at least one other bus by at least two in-service transmission lines ($ln \geq 2$). If buses would be only connected by one transmission line, the fault clearing by opening the breakers of the line would isolate the generator and it would lose synchronism due to the separation from the main grid. Therefore, these buses are excluded as switching of the breakers following a fault would always cause a loss of synchronism.

Criterion 2 - Bus Injected Active Power vs. Generator Active Power: The active power P_{in}, which is injected in the bus, is compared to the active power P_{SG}, produced by synchronous generators in the vicinity of this bus. The vicinity of the bus is defined as one or two buses away from the generator bus. This means that only buses which are at maximum two buses away from generator buses are considered in the assessment. More distant buses are discarded. The criterion comprises two sub-criteria which define a lower and upper threshold for the injected active power:

a) The injected active power of the bus must be greater than the specified threshold n_{min} of the active power produced by the generators in the vicinity of the bus. The threshold is variable, but it is suggested to set the threshold of the active power, injected in the bus, between $50 - 75\,\%$ of the active power produced by the SGs. This lower threshold ensures that only locally produced active power flows to the bus.

b) The injected active power of the bus must be lower than the specified threshold n_{max} of the active power produced by the generators in the vicinity of the bus. It is suggested to set the upper threshold between $120 - 150\,\%$ of the active power produced by the SGs. This upper threshold ensures that long distance flows are excluded and only local power flows between the upper and lower threshold are considered.

Criterion 3 - Bus Leaving Active Power: The amount of active power P_{out} which is leaving the bus on transmission lines sets the third criterion. Power flows on transformers are not taken into account. This criterion puts into perspective the active power that leaves the bus with the total generated active power of the considered power system. The active power, leaving the bus, must be greater than the specified threshold $P_{out,\,min}$. The threshold is variable, but it is suggested to set it to approximately $1\,\%$ of the total active power output $P_{SG_{tot}}$ of SGs of the considered system.

The criteria of the CBS, including the thresholds, suggested by the authors of [33–35], are summarized in Table 1.

Table 1: Summary of the Critical Bus Screening Criteria

Criterion	**Formulation**	**Suggested Threshold**
1	$V_{bus} \geq V_{min}$ $ln \geq ln_{min}$	highest voltage level $ln_{min} = 2$
2	$n_{min} \leq \frac{P_{in}}{P_{SG}} \leq n_{max}$	$n_{min} = \{0.5 - 0.75\}$ $n_{max} = \{1.2 - 1.5\}$
3	$P_{out} \geq P_{out,min}$	$P_{out,min} \approx 0.01 \cdot P_{SG_{tot}}$

3.4. Update of Simulation Model

The simulation model, which represents the real power system, has to be updated with data from the current system snapshot. The data includes generator schedule, breaker status, dispatch of capacitor banks and RES generation. The updated simulation model is then ready to be used in the TD simulation. Additionally, the results of the CBS are saved in a list which contains the identified critical buses. Only these buses are considered in the assessment.

3.5. Transient Stability Assessment and Dispatch Scheme

The potentially critical buses are analyzed in the transient stability assessment and dispatch scheme, which is based on a hybrid approach using an estimation of dispatch, combined with TD simulations. The flow chart of the dispatch procedure is shown in Fig. 2. The goal of the proposed procedure is to determine the dispatch volume which is needed to achieve the desired CCT and, therefore, return the system in safe state, while respecting technical constraints and minimizing costs.

FCCS: In the first step, a FCCS for the previously identified potentially critical buses is carried out using TD simulations. The goal is to identify the buses which are in fact critical and sort out the non-critical ones. The FCCS delivers a yes/no decision whether the system can withstand a three-phase fault with CCT_{lim} at the potentially critical buses without generators losing synchronism. This indicates whether the CCT of a three-phase fault at a

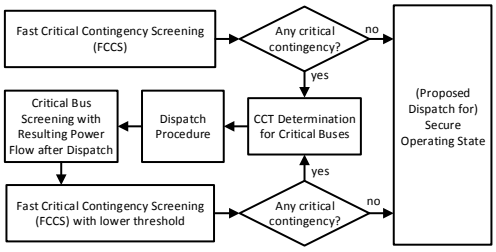

Figure 2: Flow Chart of the Transient Stability Assessment and Dispatch Scheme

bus is above or below the specified limit. However, no margins or CCTs are calculated in this step.

Decision: If the FCCS does not find a critical contingency, i.e. none of the applied three-phase faults caused a loss of synchronism of one or more machines, the assessment ends and a secure operating state, in terms of transient stability, is given. If the screening identifies contingencies where SGs are losing synchronism, the procedure continues with the determined set of critical buses.

CCT Determination: For the set of critical buses, CCTs are determined up to three decimals and the associated SGs which lose synchronism are noted. These SGs are regarded as critical and their active power has to be dispatched. The CCT was numerically determined within DIgSILENT PowerFactory environment using a DPL-script [36]. Consecutive bolted three-phase faults are applied on any line close to the busbar and removed after varying durations by opening the breakers of the line.

Dispatch procedure: The dispatch procedure starts with the SG which is associated with the bus with the lowest CCT and continues consecutively with CCTs in ascending order. On the one hand, this prevents a too large re-dispatch, due to the fact that the CCTs at adjacent buses can be close to each other whereas, generally, the one closer to the SG is lower. On the other hand, it reduces the number of required iterations to reach the optimal dispatch. The dispatch procedure is comprehensively described in Section 4. If the newly calculated set point for the generator is not compatible with the current set point and the time window given for ramping the generator, a new OPF, considering this new constraint, is calculated.

Critical bus screening with resulting power flow after dispatch: After the dispatch of all critical SGs, another CBS is carried out to determine the critical buses of the new load flow condition. That is conducted as preparation for the final FCCS.

FCCS with lower threshold: Another FCCS is carried out in order to verify the success of the dispatch, i.e. if the dispatch has re-established the desired transient stability margins. Since the dispatch procedure introduces an accuracy range of $\pm 5\,ms$ (see *Section 4*, *Step IV*) of the desired CCT, the final FCCS is executed with the lower limit of the accuracy range, i.e. $CCT_{lim} - 5\,ms$. If the FCCS identifies violations of CCTs, the procedure starts again from the CCT determination.

Secure operating state: If no further violations are identified, the procedure is completed and the results are presented to the control room operator.

3.6. Visualization and Decision Support for the Control Room Operator

The results of the transient stability assessment and the proposed dispatch are presented in comprehensive but condensed form to the control room operator as shown in Fig. 7 and 9. The situation awareness of the control room operator is increased as the stability margin is displayed graphically and the buses, at which the CCT is below the limit, are shown in a table format. Additionally, the generators and their respective dispatch to achieve the desired stability margin are shown numerically. Furthermore, the associated costs of the proposed dispatch are stated. If the proposed dispatch does not meet the requirements of the operator for some reason, e.g. one of the selected SGs is not available for the re-dispatch, the operator has the possibility to interact with the decision support system by blocking the power setpoint of the specific SG and restart the dispatch procedure in order to get a new dispatch proposal considering the special requirement.

The amount of information presented to the control room operator is kept low in order not to overload it and to facilitate fast understanding of the condition. Moreover, warning signals could be generated when the CCT is below a specified limit, e.g. 200 ms. Different levels of severity can then be added depending on the size of the critical unit. If there is a need for in-depth information, the control room operator should be given the possibility to

access the underlying data, e.g. reactive power set points.

4. Dispatch Procedure in Detail

Step I

The dispatch procedure starts with the SG that is associated with the contingency with the lowest CCT. The initial power setpoint of the SG and the respective CCT is noted. The two variables of the initial condition are called P_{init} and CCT_{init}, respectively.

Step II

The maximum power setpoint of the SG which satisfies the minimum desired CCT limit has to be determined. Since it cannot be calculated analytically for multi-machine systems, a TD approach using an estimation of the dispatch is proposed. To get the first estimation, it is proposed to use the linear approximation, which is shown in Fig. 3, where η represents the ratio between initial and desired minimum CCT shown in (1), and m the dispatch estimation factor, which is used to calculate the estimated power setpoint P_{est} from the initial setpoint P_{init}, shown in (3). The idea behind the linear approximation of the active power dispatch from the CCT ratio originates from the fact that the relationship is almost linear, but not exactly known unless several Power-CCT pairs are determined. Since the calculation of several Power-CCT pairs poses a computational burden, an alternative approach is presented in this paper. Certainly, the relationship between the active power output of generators and the CCT is not perfectly linear, as various parameters are influencing the CCT. However, the proposed estimation method is only an intermediate step in the dispatch procedure, which showed to be very handy to get a first guess of the required dispatch. The exact dispatch is calculated in the subsequent steps of the procedure. The proposed relationship of m and η shown in Fig. 3 and (2) was determined heuristically, by simulation of numerous scenarios with different grid configurations, and was found suitable for the two presented case studies while it may need to be adjusted for different grids.

$$\eta = \frac{CCT_{init}}{CCT_{lim}} \tag{1}$$

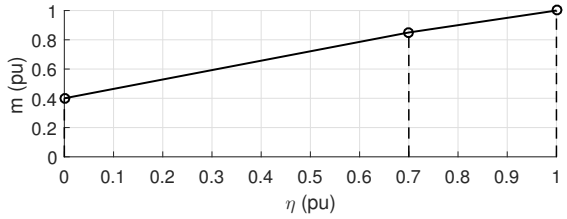

Figure 3: Estimation of the generator's power setpoint

$$m = \begin{cases} 0.5 \cdot \eta + 0.5 \ for \ \eta \geq 0.7 \\ 0.6429 \cdot \eta + 0.4 \ for \ \eta < 0.7 \end{cases} \tag{2}$$

$$P_{est} = m \cdot P_{init} \tag{3}$$

Step III

The estimated power setpoint P_{est} is used as the new power setpoint of the SG. The dispatch, i.e. the difference between the initial and the new setpoint, is distributed to other SGs by employing an OPF calculation minimizing the costs of generation. Technical constraints, such as maximum line flows, voltage levels and maximum/minimum active power of the generators, are considered in the OPF calculation. The active power setpoints of SGs, which were identified as critical within the FCCS, are locked in the OPF calculation as they are not allowed to increase their active power, since they are already critical. Only SGs which are not considered critical are allowed to take over the dispatch. The setpoints obtained by the OPF calculation are the new setpoints for the next step. The OPF calculation was carried out in DIgSILENT PowerFactory environment, which applies an interior-point algorithm based on the Newton-Lagrange method to solve the problem. In general, any other OPF calculation method can be used to solve the OPF problem.

Step IV

After obtaining the new active power setpoints through the OPF calculation, the CCT for the new load flow condition is calculated and the respective CCT is straightforwardly called CCT_{est}. As the power setpoint is only an estimation, the respective CCT will (most likely) not match CCT_{lim}. Therefore, a linearization between the initial and actual setpoint is

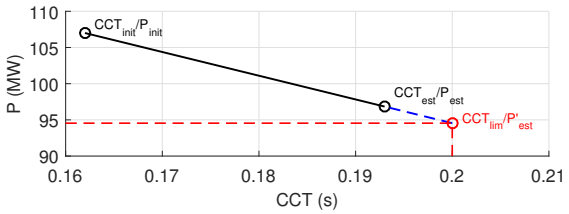

Figure 4: Extrapolation of initial and estimated condition to obtain the next power setpoint P'_{est}, for which CCT'_{est} is determined. (Values of the plot are irrelevant, but they are shown for clarity.)

conducted and the next active power setpoint P'_{est} is obtained from the inter- or extrapolation as shown in Fig. 4. CCT'_{est} for the new setpoint P'_{est} is determined and the procedure is terminated if CCT'_{est} lies between $\pm 5\,ms$ of CCT_{lim}. This $\pm 5\,ms$ accuracy band is suggested in order to avoid too many iterations.

5. Case Study

The capabilities of the approach are demonstrated by using two well-established benchmark grids. Firstly, the approach is applied to the nine-bus system shown in Fig. 6 to highlight the steps of the procedure while keeping the complexity low. Secondly, by using the New England system, shown in Fig. 8, it is shown that the approach is robust when taking into account a larger grid with numerous components and complex dynamic behavior.

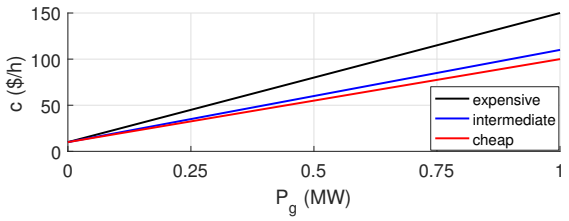

Figure 5: Cost functions of the SGs

In both studies, the initial operating point is determined by an OPF, minimizing the costs of generation using three standard cost functions shown in Fig. 5. Starting from that point, the transient stability preventive control approach is carried out for both benchmark grids. The CBS is only carried out for the New England system since its aim is to reduce the number of considered buses. Loads are modelled as voltage and frequency dependent

(P = const. current, Q = const. impedance, f_p = 1.5, f_q = -1) [37]. The voltage dependence is defined according to the ZIP definition, the frequency dependence is linear and the parameters are set according to the common practice for stability studies [38].

5.1. Case Study 1: Nine-Bus System

The nine-bus system, including the parameters of the elements, was firstly introduced in [39]. Only minor changes were made, such as the frequency which was set to $50\,Hz$ and G_2 and G_3 which are operated in PV mode while G_1 serves as slack generator. The voltage setpoint of all SGs is set to $1\,pu$.

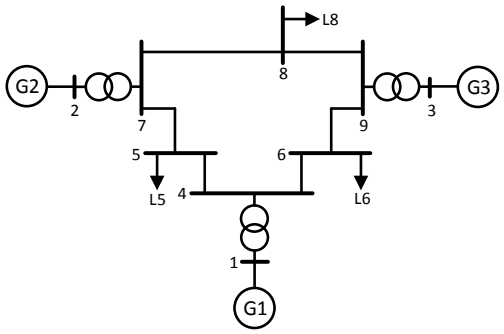

Figure 6: Nine-Bus System

G_1, G_2 and G_3 are associated with the expensive, intermediate and cheap cost functions according to Fig. 5, respectively. Table 2 shows the most important variables, such as active power, loading and costs during the different steps of the dispatch procedure. Initially, G_2 and G_3 are operated at their maximum active power limit, whereas G_1 is less loaded, which is expected due to their cost functions. The starting point of the procedure is the FCCS, as the CBS is not appropriate for this small grid. In the following paragraphs, the procedure is explained stepwise. The labels of the steps correspond to the ones in Section 3 and 4.

FCCS: The FCCS identified the buses six, seven and nine as critical, because SGs are losing synchronism.

CCT Determination: Following the FCCS, the CCTs for the identified buses are determined. The CCTs of all buses are shown in Fig. 7. The CCTs of the buses six, seven and nine are $0.171\,s$, $0.159\,s$ and $0.149\,s$, respectively. All three are below CCT_{lim} and, hence, considered to be critically low.

Dispatch of G_3

Step I: The dispatch starts with the lowest CCT and its associated SG, which is in this case at bus nine ($CCT^{(Bus\ 9)} = 0.149\,s$) and is caused by G_3.

Step II: The power setpoint is estimated according to (1)-(3). The estimation results in $P_{est}^{(G_3)} = 94.93\,MW$.

Step III: The estimated power setpoint for G_3 is fixed in the OPF calculation. Since G_2 is also critical due to low CCT, the maximum active power is constrained to its initial value. It has to be emphasized that it is important to constrain critical SGs to their initial power setpoints since a dispatch to the critical SGs would decrease the CCT even further.

Step IV: Given the newly obtained load flows, the CCT for bus nine is determined and $CCT_{est}^{(Bus\ 9)}$ is equal to $0.191\,s$. The linear extrapolation between the initial and new condition, according to Fig. 4, results in $P'^{(G_3)}_{est} = 91.96\,MW$ and $CCT'^{(Bus\ 9)}_{est} = 0.202\,s$. As $CCT'^{(Bus\ 9)}_{est}$ lies inside the accuracy band of $\pm 5\,ms$, the dispatch of G_3 is finished.

After the dispatch of G_3, the next SG has to be dispatched. $CCT^{(Bus\ 7)}$ is equal to $0.159\,s$ and the associated SG is G_2. Since one SG has already been dispatched, the CCT of bus seven has to be calculated again before starting the procedure.

Dispatch of G_2

Step I: The CCT of bus seven after the dispatch of G_3 is already higher than initially and is equal to $CCT'^{(Bus\ 7)} = 0.175\,s$ while the active power setpoint is still $163.20\,MW$.

Step II: By applying (1)-(3), the estimated power setpoint $P'^{(G_2)}_{est}$ results in $153\,MW$.

Step III: The OPF calculation is carried out with the active power setpoint of G_2 fixed to $153\,MW$ and G_3 to $91.96\,MW$, which was determined by the dispatch procedure of G_3.

Step IV: The CCT for bus seven for the new load flow is $CCT_{est}^{(Bus\ 7)} = 0.209\,s$. The linear interpolation between the initial and the new condition results in $P'^{(G_2)}_{est} = 155.70\,MW$ and $CCT'^{(Bus\ 7)}_{est} = 0.2\,s$. The dispatch procedure for G_2 is finished as $CCT'^{(Bus\ 7)}_{est}$ equals exactly CCT_{lim}.

Discussion of Case Study 1: The results after the dispatch procedure compared to the initial condition are shown in Fig. 7 in graphical and digital form. The critical CCTs are elevated, so that all CCTs in the system meet the specified limit. The CCTs of bus seven

Table 2: Active power setpoints, loading and costs during the dispatch

State		G_1	G_2	G_3
Initial condition	P_g (MW)	163.44	163.20	108.80
	Loading (%)	67	85	85
	costs (\$/h)	22891	16330	9802
	total costs (\$/h)	49023		
After dispatch of G3	P_g (MW)	180.21	163.20	91.96
	Loading (%)	73	85	72
	costs (\$/h)	25240	16330	8286
	total costs (\$/h)	49856 (+833)		
After dispatch of G2	P_g (MW)	187.70	155.70	91.96
	Loading (%)	76	81	72
	costs (\$/h)	26288	15580	8286
	total costs (\$/h)	50154 (+1131)		

and nine are exactly at the limit, i.e. that only the minimal necessary amount of power has been dispatched in order to meet the predefined level of transient stability. An important observation can also be made by comparing the CCTs of the other buses. The CCTs of bus four and five are lower for the new system state, which can be expected due to the fact that G_1 has taken over the dispatched power from G_2 and G_3. Moreover, the CCT of the buses six and eight are also elevated, compared to the initial condition, as they are adjacent to the buses, which were considered in the dispatch. The lower plot visualizes the active power change of the individual generators and the additional costs, which would be caused by the dispatch.

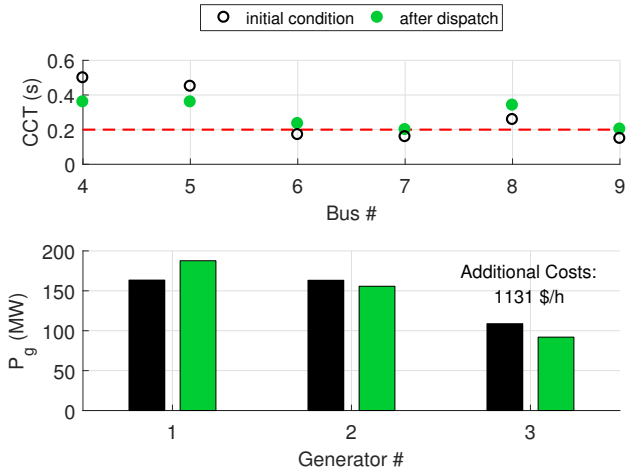

Additional costs of re-dispatch: 1131 \$/h			
	critical CCTs (s)		
Bus	6	7	9
initial	0.171	0.159	0.149
after	0.235	0.2	0.203
	P_g (MW)		
Gen.	1	2	3
initial	163.4	163.2	108.8
after	187.7	155.7	91.96
delta	+24.3	-7.5	-16.84

Figure 7: CCTs and active power setpoints for the initial condition and after the successful re-dispatch

5.2. Case Study 2: New England System

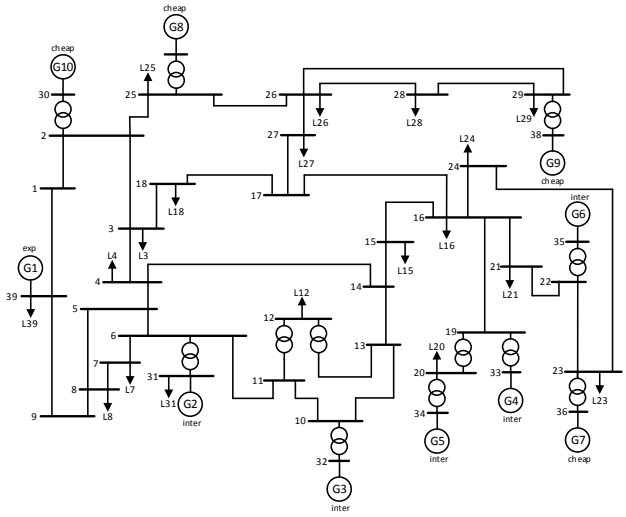

Figure 8: New England System with indication of associated cost functions

The New England system with 39 buses and 10 SGs is a well-established model and has been extensively used for scientific research. Therefore, it is used to show that the newly introduced dispatch approach is robust and can be applied to larger grids. Similar to the nine-bus system, a few minor changes were introduced to the system described in [40]. In this case, nominal frequency was also set to $50\,Hz$ and all generators are operated in PV mode with voltage setpoints of $1.02\,pu$. G_1 serves as slack generator. In this case study, all elements of the transient stability approach, including the CBS, are shown.

CBS: The used thresholds of the CBS and the identified buses, which are considered as potentially critical, are shown in Table 3. Thirteen out of 39 buses are identified to be potentially critical, i.e. only one third of the buses has to be considered in the further assessment, which significantly reduces the computational burden.

FCCS: The FCCS identified the buses 21, 22, 23 and 29 as critical as shown in Table 3.

CCT Determination: The CCTs of the four identified buses are determined. The CCTs are equal to $0.181\,s$, $0.137\,s$, $0.153\,s$ and $0.158\,s$ for bus 21 (G_6), 22 (G_6), 23 (G_7) and 29 (G_9), respectively. All CCTs are below the specified limit (as expected) and considered critically low.

Dispatch of G_6

Table 3: Thresholds and results of CBS and FCCS

Criterion	**Threshold**
1	$V_{min} = 345\,kV$, $ln_{min} = 2$
2	$0.6 \leq \frac{P_{in}}{P_{Gen}} \leq 1.4$
3	$P_{out,\,min} = 62\,MW$
Potentially Critical Buses According to CBS	
2, 5, 10, 11, 13, 16, 21, 22, 23, 25, 26, 29, 39	
Buses, Identified as Critical by FCCS	
21, 22, 23, 29	

Step I: The dispatch starts again with the lowest CCT, which is $0.137\,s$ at bus 22, caused by G_6. Therefore, the initial active power setpoint and the associated CCT are noted.

Step II: The estimated dispatch is calculated by using (1)-(3) and results in $P_{est}^{(G_6)} = 423.47\,MW$.

Step III: The estimated power setpoint for G_6 is fixed in the OPF calculation. Since G_7 and G_9 are also critical, they are not available for re-dispatch and, thus, their active power setpoint is limited to the initial one.

Step IV: Given the newly obtained load flow, the CCT is determined and it is equal to $CCT_{est}^{(Bus\ 22)} = 0.173\,s$. The linear extrapolation between the initial and new conditions, according to Fig. 4, results in $P'\ (Bus\ 22)_{est} = 363.14\,MW$ and $CCT_{est}'^{(Bus\ 22)} = 0.199\,s$. The dispatch of G_6 is done as $CCT_{est}'^{(Bus\ 22)}$ lies between $CCT_{lim} \pm 5\,ms$.

Dispatch of G_7 and G_9

After the dispatch of G_6, the same procedure is carried out for G_7 and G_9, which is shown in Table 4.

Table 4: Variables during the dispatch procedure of each generator

	G_6		G_7		G_9	
	P_g (MW)	CCT (s)	P_g (MW)	CCT (s)	P_g (MW)	CCT (s)
initial	503.90	0.137	594.98	0.155	620	0.158
est	423.47	0.173	528.04	0.2	554.90	0.207
est'	363.14	0.199	-	-	564.19	0.199

Discussion of Case Study 2: Table 4 shows the active power setpoints and its result-

ing CCT throughout the re-dispatch procedure. The procedure for all three SGs converged within one iteration. The estimated setpoint for G_7 was already correctly approximated and the linearization between initial and new condition was not necessary. The CCTs and active power dispatch of the initial condition and after the dispatch procedure are summarized in Fig. 9. It can be seen that all CCTs meet the specified limit after the successful dispatch. The CCTs at bus 23 and 29 are exactly at the limit, whereas bus 22 is even more elevated than it was actually determined. Due to the close proximity of G_7 to G_6, the dispatch of G_7 also affected the CCT at bus 22. Due to the influence of the generators in close proximity, only a near optimal solution is found which illustrates one of the drawbacks of the sequential approach.

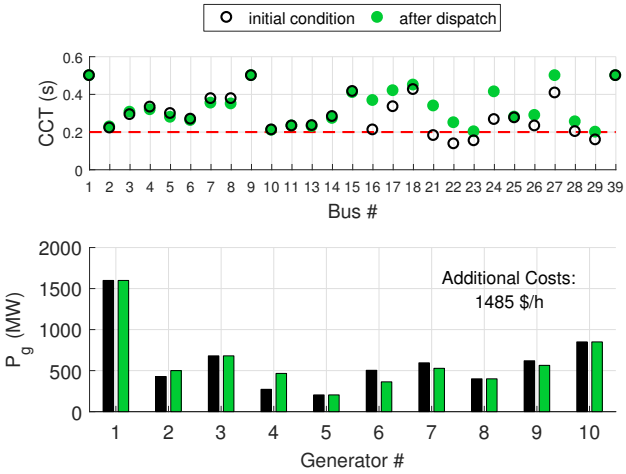

Additional costs of dispatch: 1485 $/h					
	critical CCTs (s)				
Bus	21	22	23	29	
initial	0.181	0.137	0.153	0.158	
after	0.338	0.249	0.201	0.199	
	Pg (MW)				
Gen.	2	4	6	7	9
initial	427.8	272	503.9	595	620
after	500	465.9	363.1	528	564.2
delta	+72.2	+193.9	-140.8	-67	-55.8

Figure 9: CCTs and active power setpoints for initial condition and after successful dispatch

5.3. Evaluation of Execution Time of the Assessment

It is of crucial importance that the decision support tool delivers results within a reasonable time, irrespectively of the size and complexity of the power system. Therefore, the execution time for the nine-bus, New England and for the IEEE 118-bus test system, found in [41], is analyzed. The execution times of the blocks in the flow chart of Fig. 2 including the CBS of the New England system are reported in Table 5.

In order to make the results comparable, the shown execution times are expressed as execution time per critical bus fault location. The total execution time of the different

process steps is divided by the number of assessed buses for which it is carried out. The CBS is only shown for the New England system and is equal to $0.103\,s$. It was not implemented for the two other test systems, but it can be expected to be in the same order of magnitude for larger networks as the calculation complexity of this step is fairly low. The determining factors of the overall execution time are the CCT and FCCS calculations which have the highest execution time per bus. The overall execution time is not shown as it highly depends on the state of the system, i.e. the number of buses, for which the FCCS is carried out and the CCT has to be determined exactly. The execution time of the OPF is also relatively small compared to the other process steps because the optimization only considers the costs. It should be noted, that the execution time of the OPF will increase with increased complexity of the problem, e.g. inclusion of additional objectives. It can be observed that the execution times increase with increased grid size.

Table 5: Results of the execution time evaluation

System	# of SGs	CBS (s)	FCCS/Bus (s)	CCT/Bus (s)	OPF (s)
9-Bus	3	-	0.3	1.13	0.2
39-Bus	10	0.103	0.85	2.59	0.4
118-Bus	54	-	1.08	6.95	0.75

The presented execution times have not been optimized and have been achieved on a standard laptop (quad-core i7 4600, 8 GB RAM) with PowerFactory V 15.2 and Matlab 2016b software. Therefore, one should keep in mind that the execution time will be reasonably lower with more powerful units such as the ones used in control rooms. Moreover, the implementation of the assessment has significant impact on the execution time, e.g. the authors of [42] claim that they can assess the CCT of 39.000 buses within minutes, hence, the authors expect that an efficient implementation of the presented approach, paired with more powerful hardware, will result in acceptable execution times suitable for online application. According to [19], an execution time within $15\,min$ is seen as a reasonable time horizon for online application.

6. Conclusion

The paper presented a decision support tool for control room operators for transient stability preventive control. A novel dispatch procedure for multi-machine systems was introduced. OPF calculations were used to re-distribute the dispatched power while costs are minimized. The sequential approach delivers a near optimal solution in terms of cost minimization. However, the transient stability assessment is carried out transparently and therefore, the control room operator is presented with a traceable dispatch proposal. In order to reduce the computational burden of the approach, the dispatch procedure is complemented with a preceding CBS and a FCCS to reduce the number of buses to be considered in the assessment. Case Study 2 showed that the number of buses can be significantly reduced by applying the CBS and FCCS. The proposed approach shows to be robust when applied to larger power systems. The execution time of the process steps was evaluated for different network sizes. It showed that the FCCS and CCT determination are the two most contribution factors to the overall execution time. However, the execution times have been achieved on a standard laptop (quad-core i7 4600, 8 GB RAM). Considering more powerful hardware used in control rooms and efficient implementation, the authors anticipate acceptable execution times suitable for online application of the tool. In this work, only the minimization of costs, considering technical constraints, was the objective of the OPF calculation. Of course, the OPF calculation can be extended to include multiple objectives, such as grid losses in addition to generation costs. Multi-objective minimization was not considered in this work since the objectives of the minimization depend on the specific power system operator and the OPF calculation can be adapted within the approach in order to meet user-specific needs. Special attention has to be paid to load modeling due to its great impact on the results in terms of CCT. The load behavior of the considered system has to be known in order to achieve realistic results. In fact, incorrect load modeling will result in significant differences in the determined CCT and, therefore, in the calculated dispatch. It was shown, that the dispatch procedure converges usually within one iteration. In worst case, it requires a second iteration to converge. Future work will investigate the sensitivity

of the proposed approach to load modeling. Moreover, an in-depth analysis of the expected execution time for larger and more complex networks will be carried out.

Acknowledgment

Michael Pertl is a PhD student at the Technical University of Denmark (DTU) and is supported by the EU FP7 project ELECTRA (grant: 609687) and the Danish Research Project ELECTRA Top-up (grant: 3594756936313). More information can be found at electrairp.eu.

References

[1] M. Panteli, P. A. Crossley, D. S. Kirschen, D. J. Sobajic, Assessing the Impact of Insufficient Situation Awareness on Power System Operation, IEEE Transactions on Power Systems 28 (3) (2013) 2967–2977. doi:10.1109/TPWRS.2013.2240705.

[2] M. Panteli, D. S. Kirschen, Situation awareness in power systems: Theory, challenges and applications, Electric Power Systems Research 122 (2015) 140–151. doi:10.1016/j.epsr.2015.01.008.

[3] U.S.-Canada Power System Outage Task Force, Final Report on the August 14, 2003 Blackout in the United States and Canada: Causes and Recommendations, Tech. rep., U.S. Department of Energy and Canadian Ministry of Natural Resources (2004).

[4] UCTE Investigation Committee, FINAL REPORT of the Investigation Committee on the 28 September 2003 Blackout in Italy, Tech. rep., Union for the Co-ordination of Transmission of Electricity (UCTE) (2004). arXiv:arXiv:1011.1669v3, doi:10.1017/CBO9781107415324.004.

[5] E. S. Connors, M. Endsley, L. Jones, Situation Awareness in the Power Transmission and Distribution Industry, in: 51st Annual Meeting of the Human Factors and Ergonomics Society, Santa Monica, 2007, pp. 215–219.

[6] M. R. Endsley, E. S. Connors, Situation Awareness: State of the Art, in: Power and Energy Society General Meeting - Conversion and Delivery of Electrical Energy in the 21st Century, Pittsburgh, 2008, pp. 1–4. doi:10.1109/PES.2008.4596937.

[7] M. Endsley, Situation Awareness in the Bulk Power System, in: Human Performance Conference, Atlanta, 2012, p. 45.

[8] M. Panteli, D. S. Kirschen, P. A. Crossley, D. J. Sobajic, Enhancing Situation Awareness in Power System Control Centers, in: IEEE International Multi-Disciplinary Conference on Cognitive Methods in Situation Awareness and Decision Support (CogSIMA), San Diego, 2013, pp. 254–261.

[9] K. Visscher, M. Marinelli, A. Z. Morch, S. H. Jakobsson, Identification of observables for future grids - the framework developed in the ELECTRA project, in: PowerTech, Eindhoven, 2015, pp. 1–6.

[10] L. E. Jones, Strategies and Decision Support Systems for Integrating Variable Energy Resources in Control Centers for Reliable Grid Operations, Tech. rep., Alstom Grid Inc., Washington, DC (2011).

[11] P. Kundur, J. Paserba, V. Ajjarapu, G. Anderson, A. Bose, C. Canizares, N. Hatziargyriou, D. Hill, A. Stankovic, C. Taylor, T. Van Vutsem, V. Vittal, Definition and Classification of Power System Stability, IEEE Transactions on Power Systems 21 (3) (2004) 1387–1401. doi:10.1109/TPWRS.2004.825981.

[12] A. Atputharajah, T. K. Saha, Power system blackouts - literature review, in: International Conference on Industrial and Information Systems (ICIIS), Sri Lanka, 2009, pp. 460–465. doi:10.1109/ICIINFS.2009.5429818.

[13] T. Weckesser, H. Johannsson, S. Sommer, J. Østergaard, Investigation of the Adaptability of Transient Stability Assessment Methods to Real- Time Operation, in: 3rd IEEE PES International Conference and Exhibition on Innovative Smart Grid Technologies (ISGT Europe), Berlin, 2012, pp. 1–9. doi:10.1109/ISGTEurope.2012.6465835.

[14] M. Pertl, M. Rezkalla, M. Marinelli, A Novel Grid-Wide Transient Stability Assessment and Visualization Method for Increasing Situation Awareness of Control Room Operators, in: IEEE PES Innovative Smart Grid Technologies Conference Asia (ISGT), Melbourne, 2016, pp. 1–6.

[15] Y. Kato, S. Iwamoto, Transient stability preventive control for stable operating condition with desired CCT, IEEE Transactions on Power Systems 17 (4) (2002) 1154–1161. doi:10.1109/TPWRS.2002.805019.

[16] K. Yoda, T. Okuda, T. Ohtaka, S. Iwamoto, K. Nagaura, H. Ito, Y. Onoue, Transient Stability Preventive Control with Optimal Power Flow, in: International Conference on Power System Technology (POWERCON), Chengdu, 2004, pp. 102–107.

[17] H. Takada, Y. Kato, S. Iwamoto, Transient Stability Preventive Control Using CCT and Generation Margin, in: Power Engineering Society Summer Meeting, Vancouver, 2001, pp. 881–886.

[18] S. Savulescu, Real-Time Stability in Power Systems, 2nd Edition, Springer, 2014. doi:10.1007/978-1-4614-0134-6.

[19] A. Bihain, D. Cirio, M. Fiorina, R. Lopez, D. Lucarella, S. Massucco, D. Ruiz-Vega, C. Vournas, T. Van Cutsem, L. Wehenkel, Omases : A Dynamic Security Assessment Tool for the New Market Environment, in: IEEE PowerTech, Bologna, 2003, pp. 1–8.

[20] D. Ruiz-Vega, M. Pavella, A Comprehensive Approach to Transient Stability Control: Part INear Optimal Preventive Control, IEEE Transactions on Power Systems 18 (4) (2003) 1446–1453. doi:10.1109/TPWRS.2003.818708.

[21] R. Zárate-Miñano, T. V. Cutsem, F. Milano, A. J. Conejo, Securing Transient Stability Using Time-Domain SimulationsWithin an Optimal Power Flow, IEEE Transactions on Power Systems 25 (1) (2010) 243–253.

[22] A. Pizano-Martinez, C. R. Fuerte-Esquivel, D. Ruiz-Vega, A New Practical Approach to Transient Stability-Constrained Optimal Power Flow, IEEE Transactions on Power Systems 26 (3) (2011) 1686–1696. doi:10.1109/TPWRS.2010.2095045.

[23] C. Machado Ferreira, F. P. Maciel Barbosa, C. I. Faustino Agreira, Transient Stability Preventive Control of an Electric Power System Using a Hybrid Method, in: 11th International Middle-East Power System Conference (MEPCON), Aswan, 2008, pp. 141–145.

[24] D. Cirio, D. Lucarella, G. Vimercati, S. Massucco, A. Morini, F. Silvestro, D. Ernst, M. Pavella, L. Wehenkel, Application of an Advanced Transient Stability Assessment and Control Method To a Realistic Power System, in: Power Systems Computation Conference (PSCC), Liege, 2005, pp. 1–8.

[25] D. Gan, R. Thomas, R. Zimmerman, Stability-Constrained Optimal Power Flow, IEEE Transactions on Power Systems 15 (2) (2000) 535–540. doi:10.1109/59.867137.

[26] M. La Scala, M. Trovato, C. Antonelli, On-line dynamic preventive control:An algorithm for transient security dispatch, IEEE Transactions on Power Systems 13 (2) (1998) 601–610. doi:10.1109/59.667388.

[27] A. Pizano-Martinez, C. R. Fuerte-Esquivel, D. Ruiz-Vega, Global transient stability-constrained optimal power flow using an OMIB reference trajectory, IEEE Transactions on Power Systems 25 (1) (2010) 392–403. doi:10.1109/TPWRS.2009.2036494.

[28] A. Pizano-Martinez, C. R. Fuerte-Esquivel, E. Zamora-Cardenas, D. Ruiz-Vega, Selective transient stability-constrained optimal power flow using a SIME and trajectory sensitivity unified analysis, Electric Power Systems Research 109 (2014) 32–44. doi:10.1016/j.epsr.2013.12.003.

[29] D. Ernst, D. Ruiz-Vega, M. Pavella, P. M. Hirsch, D. Sobajic, A Unified Approach to Transient Stability Contingency Filtering, Ranking and Assessment, IEEE Transactions on Power Systems 16 (3) (2001) 435–443. doi:10.1109/59.932279.

[30] D. Ruiz-Vega, M. Pavella, A Comprehensive Approach to Transient Stability Control: Part IIOpen Loop Emergency Control, IEEE Transactions on Power Systems 18 (4) (2003) 1454–1460. doi:10.1109/TPWRS.2003.818707.

[31] J. L. Pardo, J. C. Elmore, V. G. Duong, 500 kV IPT Breaker Failure Protection: An Application of Dual Timer Scheme for Short Critical Clearing Time, in: 65th Annual Conference for Protective Relay Engineers, College Station, 2012, pp. 120–128. doi:10.1109/CPRE.2012.6201226.

[32] M. Glavic, T. Van Cutsem, Reconstructing and tracking network state from a limited number of synchrophasor measurements, IEEE Transactions on Power Systems 28 (2) (2013) 1921–1929. doi:10.1109/TPWRS.2012.2231439.

[33] V. Kolluri, S. Mandal, M. Y. Vaiman, M. M. Vaiman, S. Lee, P. Hirsch, Fast Fault Screening Approach to Assessing Transient Stability in Entergy's Power System, in: IEEE Power Engineering Society General Meeting, Tampa, 2007, pp. 1–6.

[34] S. Lee, L. Min, M. Vaiman, Fast Fault Screening for Real-Time Transient Stability Assessment, Tech. rep., Electric Power Research Institute (EPRI) and V&R Energy System Research Inc. (2010).

[35] M. Y. Vaiman, M. M. Vaiman, A. Gaikwad, Fast Fault Screening Methodology for Transient Stability Analysis of Bulk Power Systems, in: IEEE Power and Energy Society General Meeting, Vancouver, 2013, pp. 1–5.

[36] DIgSILENT PowerFactory, Use of DPL to determine the critical clearing time of a fault (2016). URL http://goo.gl/JOdtnk

[37] M. Marinelli, M. Pertl, M. Rezkalla, M. Kosmecki, S. Canavese, A. Obushevs, A. Morch, The Pan-European Reference Grid Developed in the ELECTRA Project for Deriving Innovative Observability Concepts in the Web-of-Cells Framework, in: 51th International UniversitiesPower Engineering Conference (UPEC), Coimbra, 2016, pp. 1–6.

[38] K. Sun, Power System Operations & Planning Load Modeling (2015).

[39] P. M. Anderson, A. A. Fouad, Power System Control and Stability, 1st Edition, Iowa State University Press, Ames, 1977.

[40] DIgSILENT PowerFactory, Description of the 39 Bus New England System, Tech. rep., DIgSILENT GmbH, Gomaringen (2015).

[41] P. Demetriou, M. Asprou, J. Quiros-Tortos, E. Kyriakides, IEEE 118-bus modified test system (2016). URL http://www.kios.ucy.ac.cy/testsystems/index.php/dynamic-ieee-test-systems/ieee-118-bus-modified-test-system

[42] S. Kolluri, M. Li, A. Lazo, P. Yu, M. Vaiman, M. Vaiman, Automated Critical Clearing Time Calculation for Analyzing Faults at Entergy, in: IEEE/PES Transmission and Distribution Conference and Exposition (T&D), Dallas, 2016, pp. 1–5. doi:10.1109/TDC.2016.7520001.

[Pub. C] Voltage estimation in active distribution grids using neural networks

Voltage Estimation in Active Distribution Grids Using Neural Networks

Michael Pertl, Kai Heussen, Oliver Gehrke, Michel Rezkalla
Department of Electrical Engineering (Center for Electric Power and Energy)
DTU – Technical University of Denmark
Contact: mpertl@elektro.dtu.dk

***Abstract*- The power flow in distribution grids is becoming more complicated as reverse power flows and undesired voltage rises might occur under particular circumstances due to integration of renewable energy sources, increasing the occurrence of critical bus voltages. To identify these critical feeders the observability of distribution systems has to be improved. To increase the situational awareness of the power system operator data driven methods can be employed. These methods benefit from newly available data sources such as smart meters. This paper presents a voltage estimation method based on neural networks which is robust under complex load and in-feeder generation situations. A major advantage of the proposed method is that the power system does not have to be explicitly modeled.**

***Index Terms*—Voltage Estimation, Active Distribution Grid, Neural Network, Distributed Generation**

I. INTRODUCTION

The integration of renewable energy sources (RES) into the electric power system represents a key pillar of the energy policy within the European Union and their respective countries to improve the security of supply and diversify the energy supply. A large amount of RES is being connected to distribution grids, e.g. photovoltaic generators on residential rooftops [1]. As a result, distribution grid operation is becoming more challenging with increased penetration of decentralised generation units with fluctuating output like photovoltaics (PV). The power flow in distribution grids is becoming more complicated as reverse power flows and undesired voltage rises might occur under particular circumstances, e.g. when low demand and high PV generation coincide [2], [3]. To avoid voltage variations beyond the acceptable limits, different control techniques are used today to regulate the voltage in power systems (e.g. control of tap-changing transformers). However, in order to actively control the voltage, the system state must be known, i.e. data from a sufficient number of measurement points in the system must be available in real time, possibly augmented by estimation tools.

Large parts of today's distribution grids, in particular at the lower voltage levels, are not equipped with a sufficient amount of remote readable measurement points. This creates a need for advanced methods for the estimation of distribution system state from sparse and low quality measurements [4]–[7].

Prior research has focused on the application and adaptation of the (well understood) methods for conventional state estimation in transmission grids to distribution grids which aim to make state estimation applicable in distribution grids, either by adapting the used algorithm or with regards to optimal placement of measurement sensors [5], [6], [8]–[10]. Some other publications about state estimation for distribution grids introduce the usage of neural networks (NNs), also called artificial neural networks (ANNs) to generate pseudo measurements for the state estimator to improve the accuracy of the calculation [11]–[13].

A novel data-driven bottom-up monitoring approach for distribution grids, based on NNs, was introduced in [14]. It was shown that a monitoring approach with NNs can be implemented cost efficiently and with low computational effort. NNs have been widely applied to power system monitoring and control where conventional methods had reached their limitations [15].

This paper presents a method for voltage estimation in distribution grids with a high penetration of RES using available measurements, e.g. smart meter data. The proposed method establishes a NN model for estimating the voltage at particular low voltage (LV) buses without the need to establish additional measurement points. The method is shown to be robust in the presence of complex load and generation patterns within the feeders. The established model can be implemented as a real-time estimator with low cost and computational effort as shown in [14].

The advantages of the method compared to conventional state estimation are: a) use of available measurements which gives high flexibility to the model, b) no need to establish additional measurement points, c) parts of the model can be pre-calculated offline, reducing computational effort, d) non iterative calculation of the estimated voltages, e) suitable for real-time monitoring since the method is computationally light, f) admittance matrix not needed, g) active and reactive power injection data within the network is not needed

The method does not yield the voltage angle as a part of the solution. Voltage angles can be assumed to be small in distribution grids while the voltage magnitude is of much greater interest to the distribution system operator.

II. METHOD

A. A Neural Network Approach for Voltage Estimation

NNs belong to the family of statistical learning methods which are capable of approximating or estimating the

relationship between any number of given inputs and outputs (targets). The NN has to be trained with datasets from the input and desired output parameters in order to learn the relationship between them, i.e. determine the weights and biases of the model. This opens the opportunity to use them for a wide variety of applications where non-trivial or non-analytical relationships between a number of parameters exist and a solution with conventional methods becomes too complex and unhandy.

For the voltage estimation model a two layer cascade-forward neural network was used as shown in Figure 1. The model consists of an input and an output layer. The size of each element is determined by the number of inputs, outputs and used neurons. The number of neurons was determined empirically, trials with networks of between 6 and 18 neurons yielded an optimal number of 14 as the best trade-off between accuracy and overfitting. The grey bar represents the input vector with R rows where R is determined by the number of input variables. The weight matrices are given as capital **W** with the respective indices IL and OL for *input layer* and *output layer*. The size of the weight matrices is determined by the number of used neurons (S^1=14) and input variables (R=10) for the input layer and by the number of output variables (S^2=6) for the output layer. The bias vectors are given with the parameter **b** indexed in the same way as the weights. The number of rows for the two bias vectors is determined by the number of neurons and output variables, respectively. The transfer functions of the input and output layer is given underneath the green and blue rectangle in Figure 1.

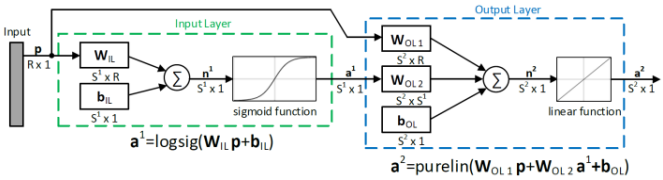

Figure 1. Two layer cascade-forward NN for the voltage estimation model. Bold capital letters in the figure represent matrices while bold lower case letters represent vectors. The size of each element is given underneath.

The method for establishing a NN model is shown in Figure 2. It can be seen that input parameters, desired output parameters and a training algorithm is needed to create a NN model. To establish the NN, the Matlab *Neural Net Fitting* toolbox was used. Some modifications of the code were made: a) type of the NN was set to cascade-forward network, b) training goal (sum squared error) was set to 10^{-5}. A step-by-step procedure for modelling of a NN is given below:

1. Collect necessary data – input and desired output data (targets)
2. Create network – selection of NN-type
3. Configure the network – define properties of the network: Neurons, training algorithm, training goal
4. Initialise the weights and biases – is done automatically by the algorithm
5. Train the network – training of NN based on the input and output data provided considering the settings defined in step 3
6. Validate the network – during the training of the NN the algorithm validates the network in order to prevent overfitting
7. Use of the network – after training of the network it can be used or retrained. The results of different trainings can vary due to different initial values for weights and biases

As shown in Figure 2, desired input and output variables have to be defined before starting to model the NN. The choice of input is of crucial importance for the accuracy of the model, otherwise randomly chosen input parameters with no/weak relation to the output parameters would negatively affect the functionality of the NN model. In this case, ten input and six output parameters were defined for the model. The input parameters are measured at the main LV bus marked in red while the output parameters are measured at the LV buses marked in blue (see Figure 3).

The input parameters are the phase-ground voltages of all three phases, the negative-sequence voltage and the active and reactive power exchange of the three feeders.

The output parameters are the phase-ground voltages from all three phases for each of the two buses.

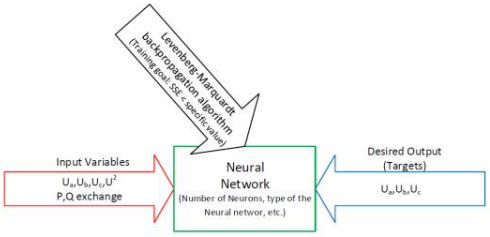

Figure 2. Method for neural network approach

A training algorithm has to be used to train the NN. Therefore, the Levenberg-Marquardt backpropagation algorithm was put in place since it is a commonly used algorithm for NN training which is suitable for most of the fitting problems while keeping the computation time within reasonable limits.

B. Simulation model of a distribution grid in PowerFactory

As mentioned before, historical data has to be collected before starting to model a NN. The data for the analysis has been generated by simulation of a distribution grid in the PowerFactory simulation software. The distribution grid is based on a LV benchmark microgrid proposed in [16]. The benchmark grid is comprised of three radial feeders connected to a common LV bus which in turn is connected to an external grid via a MV/LV transformer.

The proposed grid was modified with respect to the amount of distributed generation (DG) in order to produce a particularly challenging distribution grid as a base case for the analysis. The

units highlighted in green represent distributed PV generation, of single- and three-phase systems. The load profiles are different on every feeder and represent different consumption patterns and different weighting of residential, commercial and industrial loads according to [16]. The LV bus highlighted in red is defined as the reference bus where the input parameters for the voltage estimation model are taken from. The two LV buses highlighted in blue define the buses for which the voltage is estimated.

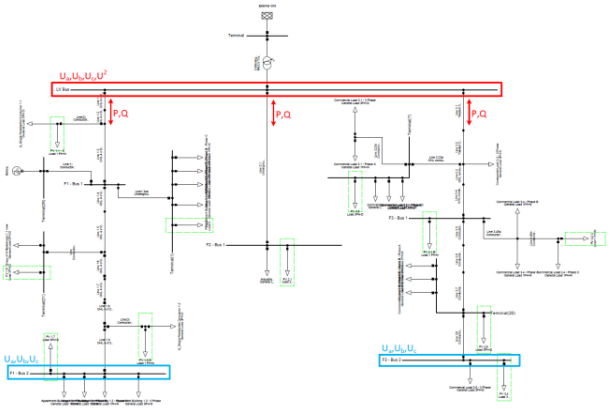

Figure 3. Distribution grid simulation model in PowerFactory

C. Simulation scenarios

Five different scenarios were simulated using the distribution grid shown in Figure 3. The scenarios, listed in Table 1, differ in terms of load and PV injection level. All simulations were carried out as time domain simulations over a period of 24 h, i.e. every scenario corresponds to one day of different load and PV injection. The scenarios are derived from a single base case which defines a certain load and PV injection and which is referred to as the 100 % case. The feeders are enumerated from left to right.

TABLE 1 SIMULATION SCENARIOS FOR DATA COLLECTION

Scenario	Feeder I		Feeder II		Feeder III	
	Load (%)	PV (%)	Load (%)	PV (%)	Load (%)	PV (%)
1	0	100	100	100	0	100
2	0	100	100	100	200	100
3	200	100	100	100	0	100
4	200	100	100	100	200	100
5	100	0	100	0	100	0

Between the scenarios, load and PV injection level vary from 0 to 200 % of the base case. The first four scenarios describe four different load/PV scenarios while scenario five is a pure load scenario without embedded PV generation. On the basis of these five scenarios a NN was built to estimate the voltage of the two LV buses marked in blue (see Figure 3).

III. RESULTS

A. Validation case 1

Feeder I represents a generation feeder and Feeder III a heavily loaded feeder. The load on Feeder I is 10% of the base case load while it is 190 % on Feeder III. The PV generation on Feeder I is 190 % of base case generation and only 10 % on Feeder III. Load and PV generation on Feeder II remains identical to the base case. The load/generation setup is presented in Table 2.

TABLE 2 LOAD AND PV GENERATION FOR VALIDATION CASE 1

Validation case	Feeder I		Feeder II		Feeder III	
	Load (%)	PV (%)	Load (%)	PV (%)	Load (%)	PV (%)
1	10	190	100	100	190	10

Figure 4 shows the input parameters supplied to the NN. The input parameters are the three phase-ground voltages, the negative-sequence voltage and active and reactive power exchange from all three feeders.

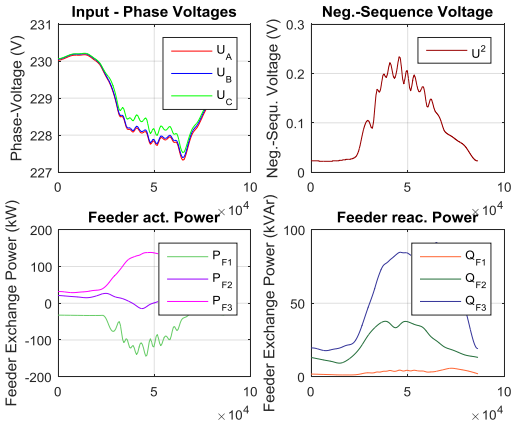

Figure 4. Input parameters for validation case 1

The active power of feeder I has a negative sign which means that active power is delivered from this feeder. In contrast, the active power from feeder III has a positive sign which means that the feeder is consuming active power.

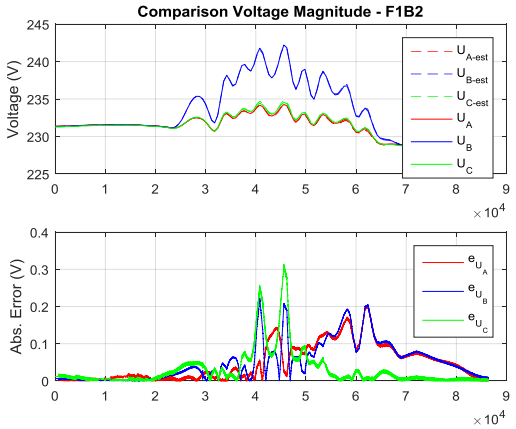

Figure 5. Estimated and real values for LV bus on Feeder I

The comparison between the estimated and real values for the phase-ground voltages at the two LV buses on Feeder I and

III is shown in Figure 5 and Figure 6. The upper subplot shows the estimated (dashed) and real (solid) values for each bus while the lower plot shows the absolute error between the estimated and real values. The error between the real and estimated voltages is below 0.6 V for both buses and therefore the difference between the dashed and the solid line is hardly noticeable in the plot.

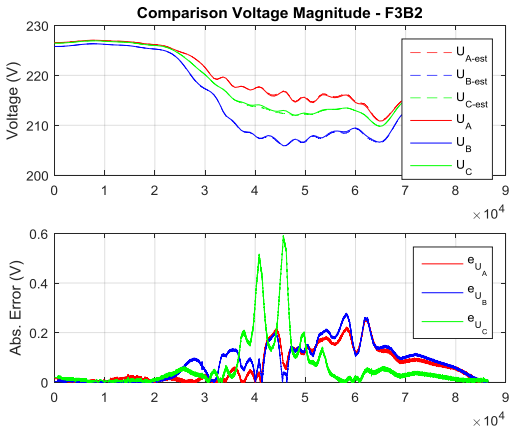

Figure 6. Estimated and real values for LV bus on Feeder III

However, it can be seen that the absolute error reaches its maximum at around midday, coinciding with the PV generation peak. Before and after this period the error is smaller. Because the voltage estimation model has been established with five scenarios which differ primarily in terms of load distribution, this is expected behaviour: The voltage estimator had not been trained with a high PV penetration scenario, therefore its ability to respond to large swings in PV production is limited. Furthermore, it can be seen that the voltages on both buses differ significantly over the course of the day while the voltage estimation model had no problem to capture the different trends with high accuracy.

B. Validation case 2

The load on all feeders is set to the base case (100 %). and the PV generation on all feeders is increased to 130 – 170 % with regard to the base case. The compact setup for the simulation case is depicted in Table 3.

TABLE 3 LOAD AND PV GENERATION FOR VALIDATION CASE 2

Validation case	Feeder I		Feeder II		Feeder III	
	Load (%)	PV (%)	Load (%)	PV (%)	Load (%)	PV (%)
2	100	130	100	150	100	170

The variation of the input parameters over time is depicted in Figure 7, differs significantly in terms of active and reactive power and voltage trend compared to validation case 1. The high penetration of distributed PV generation changes the load flow condition within all feeders significantly. This means that the voltage estimation model for the two buses has to estimate the voltages under completely different conditions.

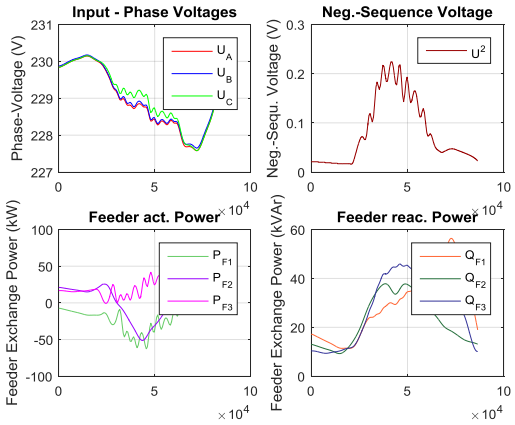

Figure 7. Input parameters for validation case 2

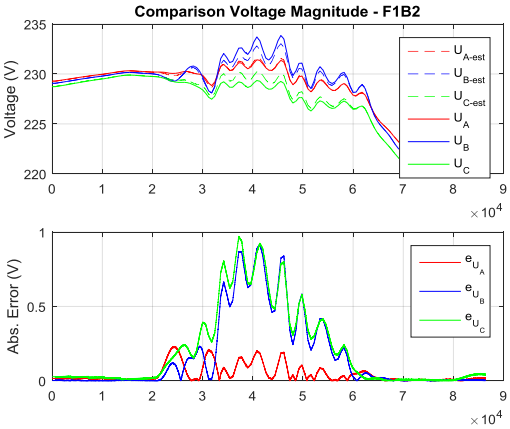

Figure 8. Estimated and real values for LV bus on Feeder I

When analyzing the results in Figure 8 and Figure 9, it can be seen that the absolute error has increased significantly compared to validation case 1 due to higher PV penetration. The error increases again when the PV injection reaches the highest values at around noon. It is clearly visible that the estimated voltages (dashed lines) differ from the real values (solid lines).

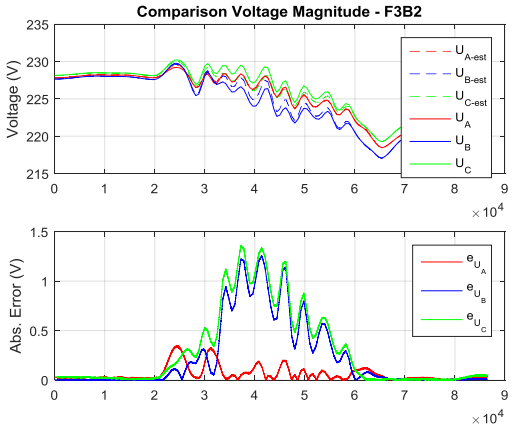

Figure 9. Estimated and real values for LV bus on Feeder III

However, as in validation case 1, the error is smaller when PV injection is small or zero as is the case in the morning, evening and during night. As discussed for validation case 1, the largest errors appear when the PV injection reaches its maximum since no case with high PV injection was considered when establishing the voltage estimation model.

IV. CONCLUSION

It has been shown that NNs can be applied for voltage estimation in active distribution grids with high penetration of DG. However, when establishing a NN for voltage estimation, the selection of meaningful input parameters is of crucial importance since the accuracy of the estimation is highly dependent on the correlation between input and output parameters. As demonstrated, the error of the estimation increases when the PV penetration reaches the highest level due to the fact that no such scenario was considered when training the NN. This can be improved when such scenarios are included in the training. One of the main advantages of the method is that no admittance matrix is needed since the relation between the input and desired output parameters is approximated by the NN. Furthermore, unlike conventional state estimation methods the method does not require iterative calculations. Additionally, there is no need for power injection data from distributed generation units and the method is robust under complex load and in-feeder generation situations.

V. FUTURE WORK

For the purpose of this paper the NN was trained exclusively on simulated data. In order to make the method applicable in practice, further investigation with real data from a distribution grid is needed. In this context improved filtering of input data has to be investigated. Additionally, heuristics are needed for determining the optimal frequency of NN retraining as the grid evolves.

ACKNOWLEDGEMENTS

Michael Pertl is a PhD student at the Technical University of Denmark (DTU) and is supported by the EU FP7 project ELECTRA (grant: 609687) and the Danish Research Project "ELECTRA Top-up" (grant: 3594756936313). More information can be found at electrairp.eu.

REFERENCES

[1] European Commission, "Integration of Renewable Energy in Europe," 2014.

[2] E. Caamaño-Martín, H. Laukamp, M. Jantsch, T. Erge, J. Thornycroft, H. De Moor, S. Cobben, D. Suna, and B. Gaiddon, "Interaction between photovoltaic distributed generation and electricity networks," Prog. Photovoltaics Res. Appl., vol. 16, no. 7, pp. 629–643, 2008.

[3] E. Caamano, J. Thornycroft, H. De Moor, and S. Cobben, "State-of-the-Art on Dispersed PV Power Generation: Publications review on the impacts of PV Distributed Generation and Electricity networks (Technical Report)," 2007.

[4] A. Al-Wakeel, J. Wu, M. Verga, and N. Jenkins, "State estimation of low voltage microgrid using an iteratively reweighted least squares method," in CIRED Workshop, 2014, no. 0383, pp. 1–5.

[5] I. Cobelo, A. Shafiu, N. Jenkins, and G. Strbac, "State estimation of networks with distributed generation," Eur. Trans. Electr. Power, vol. 17, no. 1, pp. 21–36, 2007.

[6] A. Shafiu, N. Jenkins, and G. Strbac, "Measurement location for state estimation of distribution networks with generation," IEE Proc. Gener. Transm. Distrib., vol. 152, no. 2, p. 240, 2005.

[7] X. Han, S. You, F. Thordarson, D. V. Tackie, S. M. Østberg, O. M. Pedersen, H. W. Bindner, and N. C. Nordentoft, "Real-time Measurements and their Effects on State Estimation of Distribution Power System," in Innovative Smart Grid Technologies Europe (ISGT Europe), 2013, pp. 1–5.

[8] M. Pignati, M. Popovic, S. Barreto, R. Cherkaoui, G. D. Flores, J. Le Boudec, M. Paolone, P. Romano, S. Sarri, T. Tesfay, D. Tomozei, and L. Zanni, "Real-Time State Estimation of the EPFL-Campus Medium-Voltage Grid by Using PMUs," in 6th IEEE PES International Conference and Exhibition on Innovative Smart Grid Technologies, 2015.

[9] J. Wu, Y. He, and N. Jenkins, "A robust state estimator for medium voltage distribution networks," IEEE Trans. Power Syst., vol. 28, no. 2, pp. 1008–1016, 2013.

[10] A. Abdel-Majeed, S. Tenbohlen, D. Schöllhorn, and M. Braun, "Meter placement for low voltage system state estimation with distributed generation," in 22nd International Conference and Exhibition onElectricity Distribution (CIRED), 2013, no. 0640, pp. 1–4.

[11] A. Bernieri, G. Betta, C. Liguori, and A. Losi, "Neural networks and pseudo-measurements for real-time monitoring of distribution systems," IEEE Trans. Instrum. Meas., vol. 45, no. 2, pp. 645–650, 1996.

[12] T. Nakagawa, Y. Hayashi, and S. Iwamoto, "Neural network application to state estimation computation," in Proceedings of the First International Forum on Applications, 1991, pp. 188–192.

[13] A. Abdel-Majeed, C. Kattmann, S. Tenbohlen, and R. Saur, "Usage of Artificial Neural Networks for pseudo measurement modeling in low voltage distribution systems," 2014 IEEE PES Gen. Meet. | Conf. Expo., pp. 1–5, 2014.

[14] M. Ferdowsi and A. Lowen, "New monitoring approach for distribution systems," in IEEE International Conference on Instrumentation and Measurement Technology, 2014, pp. 1506–1511.

[15] L. H. Hassan, M. Moghavvemi, H. a. F. Almurib, and O. Steinmayer, "Current state of neural networks applications in power system monitoring and control," Int. J. Electr. Power Energy Syst., vol. 51, pp. 134–144, 2013.

[16] S. Papathanassiou, N. Hatziargyriou, and K. Strunz, "A benchmark low voltage microgrid network," in CIGRE Symposium"Power systems with dispersed generation: technologies, impacts on developement, operation and performances," 2005.

[Pub. D] Validation of a robust neural real-time voltage estimator for active distribution grids on field data

Validation of a Robust Neural Real-Time Voltage Estimator for Active Distribution Grids on Field Data

Michael Pertl[a], Philip J. Douglass[b], Kai Heussen[a], Koen Kok[a,c,*]

[a] *Center for Electric Power and Energy, Technical University of Denmark, Frederiksborgvej 399, Building 776, 4000 Roskilde, Denmark*
[b] *Danish Energy Association, Vodroffsvej 59, 1900 Frederiksberg C, Denmark*
[c] *Netherlands Organization for Applied Research, TNO, Anna van Buerenplein 1, 2595DA The Hague, The Netherlands*

Abstract

The installation of measurements in distribution grids enables the development of data driven methods for the power system. However, these methods have to be validated in order to understand the limitations and capabilities for their use. This paper presents a systematic validation of a neural network approach for voltage estimation in active distribution grids by means of measured data from two feeders of a real low voltage distribution grid. The approach enables a real-time voltage estimation at locations in the distribution grid, where otherwise only non-real-time measurements are available. The method shows robust behavior in all analyzed aspects, which is vital for real world applications. A methodology to select the most relevant input variables and find the best achievable performance for a particular number of inputs is presented. Moreover, the paper shows that the performance is not sensitive to the number of neurons in the hidden layer of the neural network as long as the model is not underdetermined. The paper examines the quantity of historical data needed to establish an adequately functioning model. To accommodate grid evolution and seasonal effects, the impact of different retraining intervals is investigated. Furthermore, the performance of the model during periods of high PV generation is evaluated. The validation shows that accurate voltage estimation models for distribution grids with high share of dispersed generation can be established with approximately one month of historical data. The model has to be retrained every 10 to 20 days to retain estimation mean squared errors below 0.35 V^2. It was also found that the performance does not decline during times of high PV generation.

Keywords: Active Distribution Grids, Data Driven Methods, Distributed Generation, Neural Networks, Real-Time Voltage Estimation, Renewable Energy Sources

*Corresponding author
Email address: koen.kok@tno.nl (Koen Kok)

1. Introduction

Renewable energy sources (RES) are continuously being installed at all voltage levels in today's electric power systems [1]. A large share is being installed in the distribution grid, even at the lowest voltage level. Distribution feeders are transitioning to host both, energy users and producers and, thus, the power flow of distribution grids changes significantly in the presence of dispersed generation units [2]. Moreover, voltage becomes more volatile with the fluctuating power output of photovoltaics (PV) and increasing number of single-phase charging electric vehicles [3, 4]. The operation of distribution grids becomes more challenging as distribution grids transform from traditionally passive behavior to more active behavior with a considerable share of generation. To operate an active distribution system, operators need to increase the observability of distribution grids. Today, observability of distribution systems is generally low due to their large size. Observability usually translates into a need for additional measurement sensors, such as smart meters. Obviously, costs prohibit achieving full observability of distribution grids and, hence, complementary methods must be used. Data driven methods benefit from the availability of offline measurements from different sources and offer a cost-efficient alternative to the installation of additional real-time measurements.

Conventional state estimation approaches, such as [5–7] assume that the network topology and accurate line parameters are given. The state estimation accuracy depends highly on accurate line parameters and topology knowledge and seriously degrades in presence of inaccurate parameters [8, 9].

Unlike conventional state estimation approaches, in the approach described in this paper there is no need to model the network as admittance matrix and no iterative process is needed for the estimation after the model has been established. A major difference in the application point of view, is also that only variables for which prior measurements are available can be estimated. For this work, it is assumed that the network topology remains constant between training and observation. Similar to conventional state estimation, topology changes have to be detected in parallel and accounted for. This high flexibility paired with higher speed, accuracy and efficiency compared to their conventional counterparts makes data driven approaches interesting for complex problems and development of online applications [10].

A hierarchical bottom-up distribution system monitoring approach using neural networks (NNs) was proposed in [11]. This hierarchical approach in [11] splits up the monitoring problem to each voltage level. Local estimators are trained to estimate the voltage at certain nodes at the lowest voltage level by using voltage and current measurements at the

medium-voltage/low-voltage transformer. The estimation results are communicated to the upper-level estimator and, thereby, generating an overall picture of the distribution system.

The authors of [12, 13] study how data from phasor measurement units (PMUs) impact the accuracy of NN-based estimation of voltage magnitude and angle. They conclude that the NN-based estimator including input data from PMUs achieves similar results as a classic state estimation algorithm. The current work is based on less expensive non-synchronized measurements.

A NN with two hidden layers and entropy-based selection of input variables is proposed in [14], and it was found that the selection of appropriate input variables is of crucial importance.

The authors of [15] employ a NN voltage estimator to calculate the voltage profile along a feeder. Remote terminal units (RTUs) send the resulting voltage profile to a master controller aiming at enhancing the operation of an on-load tap-changer (OLTC) transformer for voltage regulation.

In the above works and throughout the literature, NN-based voltage estimation approaches are tested and validated by means of simulation models alone. Generally, a large number of different load flow scenarios are simulated and the results of the simulations are divided into training and test set. In contrast, this work focuses on necessary steps towards implementation in real environment by setting the framework for a neural real-time voltage estimator and validation based on actual distribution grid measurements.

This paper builds on the approach proposed in [16] where the conceptual framework and a numerical implementation for a distribution grid model with three feeders including PV generation was implemented and analyzed. It is proposed to estimate the voltage at specific low voltage (LV) buses by use of NNs trained on voltage and power measurements from substation level only. Various generation and consumption scenarios including reverse power flow scenarios are analyzed in terms of estimation accuracy. The results showed the method to be promising for all analyzed scenarios concluding in the need for a validation in real world environment. This manuscript specifically focuses on the validation of the NN-based voltage estimation approach on field data from a real distribution grid, in particular, estimating the phase-neutral voltage magnitudes (U_a, U_b, U_c) at a downstream bus of a distribution feeder based on available measurements from the substation. A general sketch of an active LV distribution grid which includes distributed generation (DG) among loads is shown in Fig. 1. The substation and the downstream measurement are highlighted in red and blue, respectively. In the training phase, historical measurements from the substation and from the downstream bus are used to train the estimator. In the estimation phase, substation measurements are fed into the estimator and the voltages of the downstream bus

are calculated in real-time (order of milliseconds on a standard laptop). Voltage angles are not considered because they are typically small in LV grids while the voltage magnitude is from paramount interest [17]. This paper presents the intermediate step towards implementation of a neural real-time voltage estimator (NRTVE) in an operating environment, such as integration into an existing SCADA system. A considered application of the proposed approach is real-time voltage estimation at buses where measurements, such as smart meters, are installed, but data is not available in real-time. For these buses, a real-time estimator could be established to increase the observability of the distribution grid. The provided assessment of accuracy and sensitivity will serve online monitoring well. However, reactive applications such as voltage control would impose further engineering requirements and development steps to be considered.

The key contributions of the manuscript are twofold:

I The framework to establish a highly accurate neural real-time voltage estimator is described.

II The capabilities and limitations of the approach under practical considerations are analyzed, in particular:

- i Methodology to select the most relevant input variables and find the best achievable performance for a particular number of inputs.
- ii It is shown that the performance is not sensitive to the number of neurons as long as the model is not underdetermined.
- iii The quantity of historical data needed to train an adequately functioning model is analyzed.
- iv The impact of the retraining interval on the performance of the model is determined.
- v It is shown that the performance of the model is not sensitive to the level of PV generation.

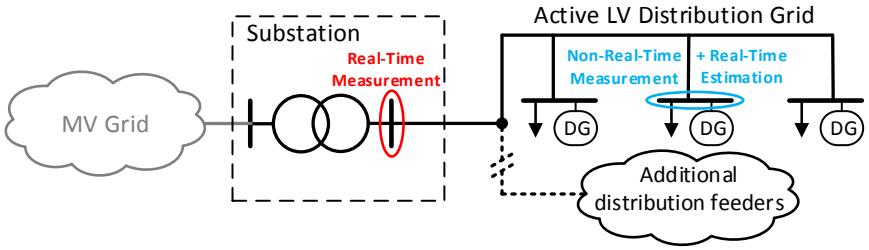

Figure 1: Sketch of an active low voltage distribution grid indicating the substation and downstream measurements

2. Architecture and Training of the Neural Real-time Voltage Estimator

Two different phases of the NRTVE are distinguished: training and real-time estimation, as shown in Fig. 2. The NRTVE is established in the training process by use of an suitable training algorithm. Prior to the training, the architecture and number of neurons in the hidden layer have to be defined. After the training process, the NRTVE can be used for real-time voltage estimation at the specific bus. Distribution network operation is characterized by faults, topology changes and outages. The proposed model is exclusively established for normal operating conditions found in the available data. For estimation under abnormal conditions, a separate model would need to be trained and a change detection would have to be implemented as the characteristics of the disturbed grid are different than in normal operation. Moreover, for changing topologies separate models need to be trained. Here, no topology change occurred.

The calculation of a bus voltage with a trained NN is in the order of milliseconds as it can be directly calculated and no further iterations are needed after the training. That computation time is deterministic is crucial for real-time applications, since it has to be accounted for the worst case. All available input and the three output variables are indicated in Fig. 2. The colors used for the input and output arrows are aligned with the colors in Fig. 1 and 3.

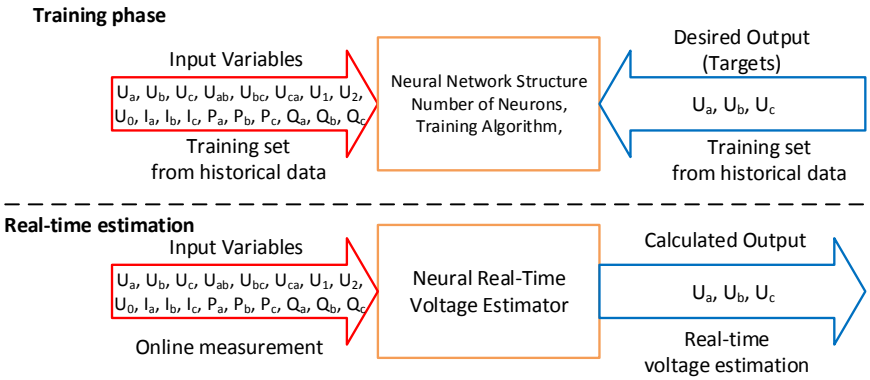

Figure 2: Training phase and real-time estimation phase

2.1. Architecture

A great number of NN architectures can be imagined [18–22]. As this is a fitting problem, a feed-forward NN with one hidden layer is used as that is sufficient for most fitting problems [23]. A multilayer perceptron with hyperbolic tangent-sigmoid neurons in the hidden layer and linear neurons in the output layer is chosen. Additional hidden layers can be added if

the performance is not satisfactory. The term performance refers to the mean squared error (MSE) between the model output and the real measured values. Inputs and outputs are scaled to values between ± 1 since the hyperbolic tangent-sigmoid function in the hidden layer operates between ± 1. Large inputs would mainly generate values in the saturated area of the sigmoid function and in order to exploit the full flexibility of the transfer function it is advised to scale the inputs to values in the linear region.

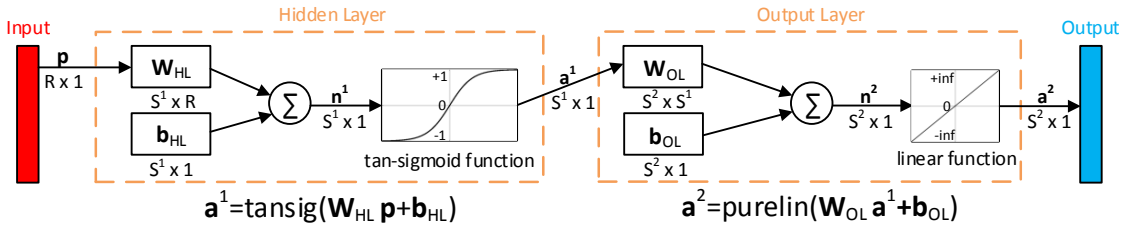

Figure 3: Architecture of the feed-forward neural network. Bold capital letters represent matrices and bold lower case letters vectors. The size of each element is given underneath.
$\mathbf{W_{HL}}/\mathbf{W_{OL}}$ = weight matrices, $\mathbf{b_{HL}}/\mathbf{b_{OL}}$ = bias vectors,
$S^1 = \#$ *neurons*, $R = \#$ *input variables*, $S^2 = \#$ *output variables*.

2.2. Training Algorithm

The choice of training algorithm depends on the problem type and complexity of the NN. The well known Levenberg-Marquardt algorithm, first introduced in [24], is used to train the NNs because it is usually the fastest training method for function approximation up to a few hundred weights and biases. It is very accurate and it shows superior convergence behavior over other algorithms [23, 25]. The weights and biases are updated according to (1) with $\mathbf{J}$ being the Jacobian matrix, $\mathbf{I}$ the identity matrix, $\mathbf{e}$ the network errors and μ the parameter determining the algorithm behavior during the training.

$$\mathbf{w}_{n+1} = \mathbf{w}_n - [\mathbf{J}^T\mathbf{J} + \mu\mathbf{I}]^{-1}\mathbf{J}^T\mathbf{e} \tag{1}$$

If μ is zero it is Gauss-Newton method and when μ is large it becomes gradient decent. The algorithm starts with a small value μ_{init}. If one step does not yield a smaller error (MSE), μ is increased by multiplication with μ_{inc}. If the the next step produces a smaller error, μ is multiplied by μ_{dec} to approach Gauss-Newton method which converges faster. The work was carried out in the Matlab environment. The training parameters and its corresponding values are shown in Table 1.

The training parameters are set up such that the algorithm stops when either the maximum number of consecutive failed validations is reached, the performance gradient falls below the minimum threshold or the maximum number of training epochs is reached. The

maximum number of epochs and failed validations has been increased above the default values in Matlab's NN implementation, while the other parameters are suggested default values.

The number of training epochs must be reasonably high in order not to stop training prematurely. The number of maximum failed validations is usually the stopping condition met first which highly speeds up the training and, moreover, prevents overfitting. Validation checks are carried out on the validation data set after every epoch during the training process. However, the validation data set is only used to check the performance; it is not used for the training, i.e. only the training set is used for training.

The weights and biases are initialized using the technique from Nguyen-Widrow [26] because it highly improves the speed of training and the optimality of the achieved solution [23, 25]. As there is a random factor in the initialization, different results are obtained by different trainings. Therefore, every training is rerun five times and the best solution is selected to get a solution which approaches the global minimum, as suggested in [27].

3. Available data for the analysis

This section describes the data that was available to conduct the analysis. All measurements were taken in a LV distribution grid. Seven power quality meters, which comply with measurement class A defined in IEC 61000-4-30 [28], are placed in two different feeders. Both feeders include loads and rooftop PV generation. Two meters are placed at the substation and five downstream the feeder. Considering Fig. 1, two meters are located at the red measurement point and five at the blue one, respectively. The distribution feeders are located in a residential area of Copenhagen region. For reasons of confidentiality, exact specifications cannot be disclosed.

Table 1: Training parameters of the Levenberg-Marquardt algorithm

Parameter abbreviation	Value	Explanation
$epochs$	2500	max. epochs to train
$goal$	0	performance goal (MSE)
min_grad	10^{-7}	minimum improvement from one epoch to the next
val_fail	10	maximum consecutive validation fails
μ_{init}	10^{-3}	initial mu
μ_{dec}	0.1	mu decrease factor
μ_{inc}	10	mu increase factor
μ_{max}	10^{10}	maximum mu

The measurements were taken over a period of approximately 1.5 years starting from 01.10.2014 until 14.05.2016. The resolution is a mixture of 1-min and 10-min measurements, i.e. in some periods a measurement is averaged over 10 minutes and in other periods averaged over one minute. As synchronized data from exactly two different meters is needed, the measurement data has to be filtered to extract the measurements with the same time stamp of the considered meters. The five possible combinations of substation and downstream meters including their set size, measurement period and PV generation are shown in Table 2. All datasets include the available measurements shown in Table 3.

Table 2: Available meter combinations including set size, measurement period and indication of PV generation on the feeder. $S = substation\ meter$, $D = downstream\ meter$

Meter combination	$S_1 - D_1$	$S_1 - D_2$	$S_1 - D_3$	$S_2 - D_4$	$S_2 - D_5$
Data points	274,739	274,515	213,660	83,985	84,693
Period	01.10.2014-14.05.2016	01.10.2014-14.05.2016	30.11.2015-14.05.2016	01.10.2014-14.05.2016	01.10.2014-14.05.2016
PV on feeder	yes	yes	yes	yes	yes

Table 3: Measured variables

Variable	Explanation
U_a, U_b, U_c	phase-to-neutral voltages (V)
U_{ab}, U_{bc}, U_{ca}	phase-to-phase voltages (V)
U_1, U_2, U_0	positive-, negative- and zero-sequence voltage (V)
I_a, I_b, I_c	currents (A)
P_a, P_b, P_c	active powers (W)
Q_a, Q_b, Q_c	reactive powers (VAr)

4. Selection of input variables

The performance of the trained NN depends on the selected input variables. A trade-off between the number of selected inputs and the model performance must be found. Input variables with negligible or low impact on the output variables should be excluded to reduce the model complexity. As input variables are excluded, the performance of the NN will get worse because even low impact input variables contain a certain amount of useful information which is lost when the variable is not used. To identify the most relevant input variables, relationships between the input and output variables, which can be linear but also non-linear, must be discovered. There is no general algorithm to optimally select the input variables, but the most commonly used relevance measure found in the literature is the

Pearson correlation [29]. Accordingly, the input variables are ranked by the order of their correlation with the output variables according to (2), where X and Y are the two variables and k is the number of data points of each variable.

$$R_{(X,Y)} = \frac{\sum_{i=1}^{k}(x_i - \overline{x})(y_i - \overline{y})}{\sqrt{\sum_{i=1}^{k}(x_i - \overline{x})^2 \sum_{i=1}^{k}(y_i - \overline{y})^2}} \tag{2}$$

However, if the input variables are correlated themselves, the correlation ranking approach does not consider this redundancy. Hence, it is not suitable to find a trade-off between selected input variables and performance. In the following, the ranking approach is elaborated by use of a dataset which contains measurements of the meter combination $S1 - D_1$ from $01.10 - 01.11.2014$, corresponding to 3124 data points for training and 670 for validation and testing each. In order to produce comparable results, the same data sets are used for training, validation and testing throughout the whole input selection process. The number of neurons in the hidden layer is set to 10 and is not changed during the input selection process. The exact number of neurons is not of great importance during the selection process because validation checks are carried out during the training process. However, the number of chosen neurons must be high enough so that the model is not underdetermined.

4.1. Ranking approach

The correlation between the input and output variables and among the inputs are shown in Fig. 4 and 5, respectively. Note, here the estimated output is used to calculate the correlation, i.e. a NN is trained, then the correlation is calculated with the inputs and estimated outputs of the test set. Some of the input variables are highly correlated with the output variables and, as expected, some of the inputs are highly correlated with each other. The results of the correlation assessment can be viewed from an electrotechnical perspective.

Input/Output correlation: The phase-neutral, phase-to-phase and positive-sequence voltages are highly positively correlated with the outputs, e.g. if the voltage at the substation is low, the voltage at buses at buses downstream the feeder will also be low and vice versa. On the other hand, the currents and powers have a negative correlation to the outputs, e.g. if the current (power) flow at the substation increases, the voltage drop over the line will increase and the voltage at buses downstream the feeder will be lower. The mentioned relationships start to deviate as soon as DG is installed at the feeder, e.g. higher bus voltages when close to producing PV units.

Input/Input correlation: Some of the input variables are highly correlated with each other. The correlation among the phase-neutral and phase-to-phase voltages is very high despite the unbalanced conditions at the feeder. Naturally, the positive-sequence voltage

is highly correlated with the phase-neutral and phase-to-phase voltages. The currents and active powers are also highly correlated due to their electrical interrelation. However, slight negative correlations between currents (active powers) and the voltages are present. Moreover, slight positive correlations between reactive and active powers are present.

The correlation among inputs suggests that the input variables contain redundant information which has to be considered in the input selection process. Hence, a ranking approach, which considers the correlation between inputs and outputs and among the inputs, is proposed to find an optimal trade-off between number of selected inputs and performance of the model. Two important preceding considerations for the ranking approach are made:

- As the correlation between any input variable and the three output variables is virtually the same, the average value is used, i.e. when referring to the correlation of an input variable to the output, the average to all three output variables is meant.

- The input variables are grouped into six categories. The categories (indicated in curly brackets) are chosen from an electrotechnical perspective because an established NN should either include all or none of the associated group variables. Otherwise the input selection will consist of a mix of node and branch parameters. Hence, it was found suitable to categorize the variables accordingly: 1) phase-neutral voltages $\{U_{ph}\}$, 2) phase-to-phase voltages $\{U_{pp}\}$, 3) voltage's sequence-components $\{U_{0,1,2}\}$, 4) currents $\{I\}$,
  5) active powers $\{P\}$, 6) reactive powers $\{Q\}$.

Note: Here, the variables are grouped into categories during the input selection process from an electrotechnical perspective, but if these considerations do not apply, the method can also be applied to individual variables.

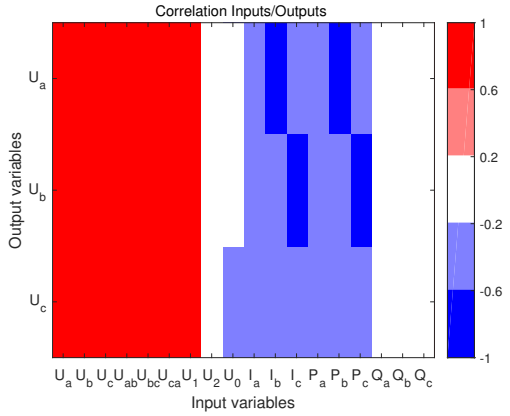

Figure 4: Correlation between input and output variables

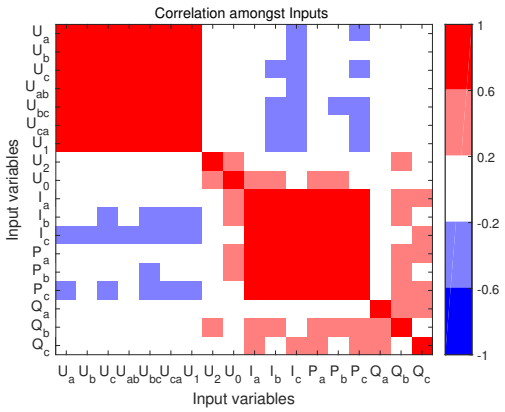

Figure 5: Correlation among input variables

The variable importance VI_C for a particular input category C is introduced as a ranking index. The calculation of VI is shown in (3) and it consists of two terms. The first term $R_{I,O}$ describes the average correlation of the particular input category C (which includes several variables X) with the output Y whereas Ind_C denotes the indices of the variables within a category. Note that it is the absolute value of the correlation which is averaged, with values close to 1 indicating the strongest correlation. The second term $R_{I,I}$ describes the average correlation between the particular input category and the other input variables. This value does not necessarily need to be close to zero, but it has to be optimized if the model complexity is to be reduced while maintaining acceptable performance. In order to express the impact of redundancy, an additional parameter $\beta \geq 0$ is introduced. If $\beta = 0$, the variable importance equals the correlation between inputs and outputs, ignoring the correlations between input categories. The greater the value of β, the more importance is given to reducing the redundancy of input variables. The choice of β depends on the purpose of the developed NN, e.g. β can be chosen to be zero if the model complexity does not matter, but if the aim is to sort out as many input variables as possible while keeping satisfying performance, β must be increased. To find an optimal trade-off between model complexity and performance β must be varied.

$$VI_C = R_{I,O} - \beta \cdot R_{I,I} \tag{3}$$

with

$$R_{I,O} = \frac{1}{n_C} \sum_{\substack{i=1 \\ i \in Ind_C}}^{n_C} |R_{(X_i,Y)}| \quad and \quad R_{I,I} = \frac{1}{n_C} \sum_{\substack{i=1 \\ i \in Ind_C}}^{n_C} \frac{1}{m - n_C} \sum_{\substack{j=1 \\ j \notin Ind_C}}^{m} |R_{(X_i,X_j)}| \tag{4}$$

where n_C is the number of variables in the category and m the total number of variables.

A backward elimination approach is used to sort out the least important variable categories step-by-step, i.e. all variables are selected initially and one after another category with the lowest ranking gets eliminated. The approach is computationally heavier than other approaches because a NN has to be trained for all available input variables and and with varying β-values, however, this computation only needs to be done once, offline. The advantage of the backward elimination approach is that it shows the maximum achievable performance when all input variables are used and how it declines when some of them are sorted out. However, it is a 'greedy' algorithm because it eliminates the least relevant variables one by one while the global optimum might be found only by trying all possible combinations. As this is computationally infeasible, a greedy approach is used instead. After the training of a NN with all input variables, the variable to be eliminated has to be determined according to (3). In order to achieve the different input variable combinations, the elimination process needs to be repeated with different β-values. Beta is varied between 0 and 3 in 0.2 increments. The range of the variation originates from the fact that the largest correlation among input categories is about one third of the input-output correlation.

The results of the VI calculation for three selected β-values is shown in Fig. 6. The category with the lowest VI index is eliminated. It is clearly visible from Fig. 6 that the results for different β-values deviate significantly from each other. When β equals 0 and 1, the reactive powers have the lowest VI index. When β equals 3, the currents are eliminated first. This elimination procedure is carried out until one only variable category is left.

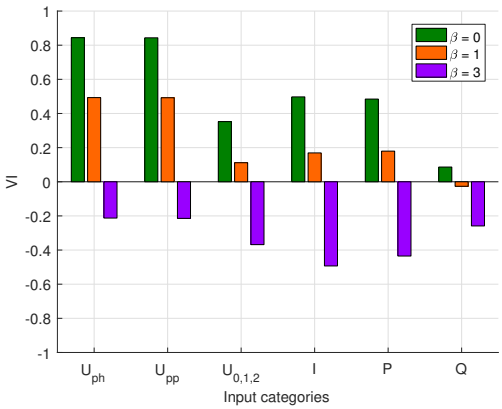

Figure 6: Variable importance for different values of β when all input categories are selected.

The results of the elimination process are shown in Fig. 7. The left plot shows the results for all beta variations and the right plot for three selected beta values. NNs with varying input variable combinations achieve different performances. The black line shows the best

achievable performance for a given number of input variables. The performance declines slightly when the first two categories are sorted out, i.e. 12 input variables are selected. It starts to decline more between 12 and six variables when the next two categories are eliminated and it highly drops when one category is left only. Considering the blue lines, it can be seen that the variation of beta is necessary in order to find a trade-off solution because the results change significantly with variation of beta and no one value of beta gave the smallest error for all number of input variables.

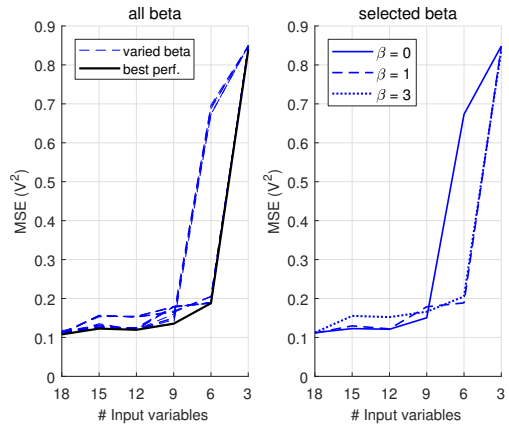

Figure 7: The blue lines represent the performance throughout the input elimination process with β varied between $0 - 3$.

In order to discuss the elimination process more in detail, three 'interesting' β-values are shown separately in the right plot of Fig. 7. The stepwise eliminated categories for these three cases are shown in Table 4. Comparing the performance of the first two cases ($\beta = \{0, 1\}$), it can be seen that the performance between 18 and 12 inputs is the same in both cases because the same categories were sorted out, namely Q and $U_{0,1,2}$. In the next step two different categories are sorted out. In one case it is the active powers and in the other the currents. Recalling from Fig. 5, the active powers and currents are highly correlated and, thus, the performance with nine inputs shows only slight differences. However, the next step shows the most interesting difference between the two cases. When β equals zero, the currents are sorted out next, which means that no branch variables are included in the inputs anymore, but node variables only, i.e. phase-neutral and phase-to-phase voltages. In the other case, the phase-to-phase voltages are sorted out and the input variables are composed of node and branch variables, i.e. phase-neutral voltages and active powers. In the third case ($\beta = 3$), the variable selection differs completely from the prior cases. It can be seen that the error increases more at the beginning when the first two categories are sorted out due to the fact that the correlation among input variables is given a high weight in the selection process.

That highlights the importance of considering the correlation among inputs and between inputs and outputs to find the optimal combination of parameters, which lies somewhere in between and is found by varying the parameter beta.

Table 4: Eliminated input variables for the three selected β-values

# inputs		18	15	12	9	6	3 (final)
eliminated category	$\beta = 0$	Q	$U_{0,1,2}$	P	I	U_{pp}	U_{ph}
	$\beta = 1$	Q	$U_{0,1,2}$	I	U_{pp}	P	U_{ph}
	$\beta = 3$	I	$U_{0,1,2}$	U_{ph}	Q	P	U_{pp}

The assessment was also carried out for the other meter combinations using datasets from different periods of the year. The results showed the same behavior, but with different input parameter combinations. Therefore, the input selection assessment must be carried out for each feeder separately because every feeder has its particular electrical characteristics.

Concerning the sensitivity of results to the number of neurons in the NN, Fig. 8 shows the test performance of the NN with the best performance input selection for different number of neurons in the hidden layer. It can be seen that the test performance stabilizes in all cases before 10 neurons are reached and, thus, the choice to use 10 neurons during the selection process is reasonable. Twelve input variables are used for the further studies. The four categories U_{ph}, U_{pp}, P and I are chosen. The results showed that the reactive powers and sequence components are sorted out when achieving best performance with 12 input variables. Moreover, the input selection process showed clearly that satisfying performance is maintained when these two categories are eliminated.

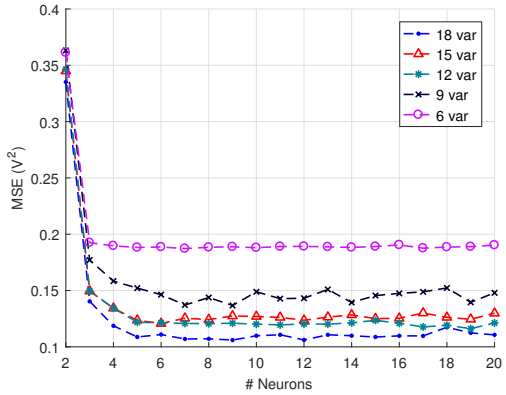

Figure 8: Performance of NNs with the determined input selections for different number of neurons

5. Data quantity and retraining analysis

This section analyses the relationship between the performance of NN models and the historical data quantity that is used to establish them and how often they have to be retrained to be suitable for real-time application. The section aims at answering two questions:

i How much historical data is needed to create a model with a satisfying performance for real-time application?

ii When does the model have to be retrained in order to maintain satisfying performance for real-time application?

Note: Satisfying performance is achieved when the accuracy of the estimation is comparable to the measurement uncertainties of meters, such as meters of class A and B, defined in IEC 61000-4-30, which shall not exceed ± 0.1 *and* $\pm 0.5\,\%$ *of the declared input voltage, respectively.*

5.1. How much historical training data is needed?

The analysis is carried out for four meter combinations in order to derive meaningful information about the needed data quantity. In order to consider seasonal effects, one full year of measurements was used from each meter combination. Generally speaking, a point in time is chosen to represent the present which is denoted by $t_{0,n}$ with $n \in [1, 73]$, i.e. the analysis is carried out for 73 different t_0 from 01.01.2015 to 27.12.2015 in 5 day steps. Time before and after t_0 represents the past and future, respectively. Fig. 9 shows a graphical representation of the approach. The initial condition is depicted in black letters, whereas $t_{0,1}$ denotes the starting point of the analysis. The second out of the 73 iterations is shown in green color. The final iteration at the end of the year is shown in purple. The different steps of the calculation procedure are explained in the following and are referred to Fig. 9:

I Set starting point t_0, i.e. $t_{0,1}$ which is in this case 01.01.2015 00:00.

II Train a NN with data from the past 3 days. The training and validation dataset is denoted by $TVS_{1,1}$. The historical data is randomly split into 85 % for training and 15 % for validation.

III Evaluate the performance of the established model on the test set denoted by TS_1 which consists of the 7 days following $t_{0,1}$.

IV Repeat step 2 and 3, increasing the amount of data that is used for training and validation by 3 days in each step until the maximum considered amount of 90 days is reached, i.e. $[TVS_{1,1} \rightarrow TVS_{2,1}$ ... $TVS_{30,1}]$.

V Once step 4 is completed, i.e. the performance of the NN with training set size from 3 to 90 days is evaluated, t_0 is shifted forward in time by 5 days (e.g. $t_{0,1} \rightarrow t_{0,2}$ ... $t_{0,73}$) and steps 2-4 are repeated.

VI The procedure finishes when the end of the year (27.12.2015) is reached.

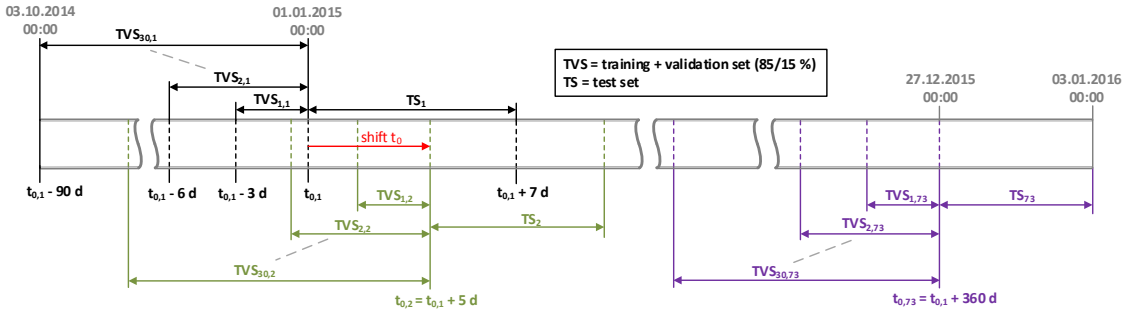

Figure 9: Visualization of the approach for the data quantity analysis. Initial condition = black, second iteration = green and last iteration = purple.

In order to clearly visualize the results, they are averaged per month as shown in Fig. 10. The results of the four different meter combinations show similar behavior. It must be pointed out that the general statement for machine learning that more data will provide better performance is not valid in this case. It can be seen clearly that the performance stabilizes at about 30 days of data and there is even a slight tendency that performance starts to decline afterwards. The analysis is carried out as close as possible to real world conditions by taking the test set data from the "future", which would be the same when applied in practice. A possible explanation for the stabilization of performance could be that the data which is too far in the past does not reflect the current grid situation and, therefore, the more recent data is sufficient to establish a suitable model. It can be seen that the performance of the approach differs for the different meter combinations. The best performance is achieved for the meter combination $S_2 - D_5$, whereas the worst for $S_2 - D_4$. At the combinations $S_1 - D_1$ and $S_1 - D_2$ there is a tendency that the performance is slightly worse during summer months than during the rest of the year which may be inferred from the larger amount of installed PV generation compared to the other feeder.

5.2. How often does the model have to be retrained?

According to the outcome of the data quantity analysis, the performance of the voltage estimation model stabilizes at around 30 days of historical data. Hence, 30 days of historical data are considered in the training process of the further analysis. Fig. 11 shows the visualization of the retrain assessment procedure. Similar as in the data quantity analysis, one

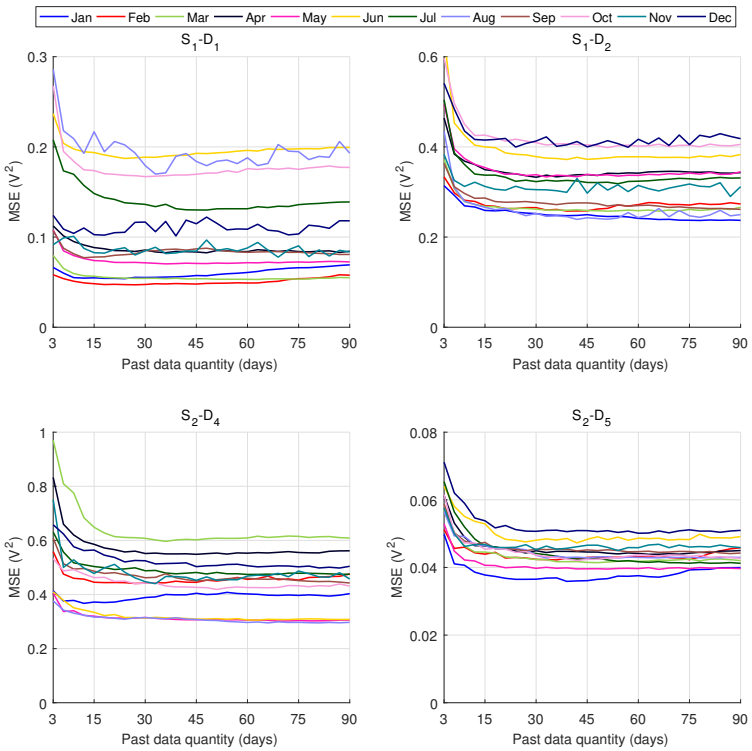

Figure 10: Results of the data quantity analysis for four different meter combinations

full year of data from 01.01.2015 until the 27.12.2015 is taken into account. For consistency, the same notation is used in Fig. 11 as in Fig. 9. The steps of the procedure are explained in the following:

I Set starting point t_0, i.e. $t_{0,1}$ which is again 01.01.2015 00:00.

II Train a NN with data from the past 30 days. The training and validation dataset is denoted by $TVS_{10,1}$. The indices 10 originates from the fact that a granularity of 3 days was used before, i.e. $3\,days \cdot 10 = 30\,days$. The data is randomly split into 85 % for training and 15 % for validation.

III The error of the estimation from the model is calculated for the test set denoted by TS_1 which set size depends on the retrain interval RI, e.g. it is 7 days when the model is retrained every 7 days.

IV Shift t_0 forward in time by the amount of days which are defined by the retrain interval RI (e.g. $t_{0,1} \rightarrow t_{0,2}$) and repeat steps 2 and 3 with respective TVS and TS.

V Once the errors are calculated for the whole year, the performance of the model is evaluated over the whole period, i.e. MSE is calculated.

VI Repeat step 1 to 5 with different RIs.

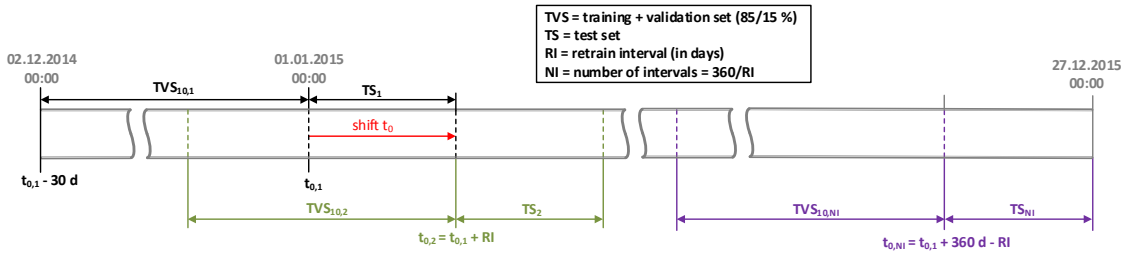

Figure 11: Visualization of the approach for the retrain analysis. Initial condition = black, second iteration = green and last iteration = purple.

The results of the retraining analysis for the same four meter combinations as in the previous section with varying retraining intervals are shown in Fig. 12. The plot shows the results on the y-axis only up to $MSE = 0.8\,V^2$ and the retrain interval on an logarithmic x-axis. There is a clear trend that the performance declines with an increased retrain interval. The performance of all meter combinations declines only slightly up to an RI of 10 days. The performance of $S_1 - D_1$ and $S_1 - D_2$ drops significantly when the RI is greater than 40 days. However, the performance for $S_2 - D_4$ and $S_2 - D_5$ is much more stable and does not decline so much. It can be concluded that the RI highly depends on the properties of the feeder, e.g. amount of PV generation. Certainly, the modelling errors can be kept at an reasonably low level with adequate choice of the RI. Since the training procedure only takes a few seconds (on a standard computer with Intel i7 processor with 8 GB RAM) with a training/validation set of 30 days with a resolution of about 1 minute averaged measurements.

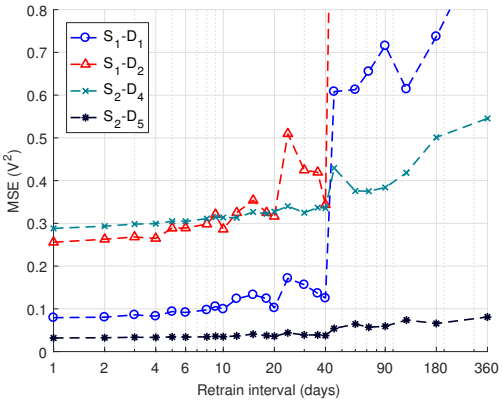

Figure 12: Model performance versus retraining interval

In order to quantify the quality of the estimation, the confidence interval of the expected error of the estimation is calculated. Fig. 13 shows the error distribution of the meter combination $S_1 - D_1$ for a retrain interval of 1 day over the evaluation period of one full year. It can be clearly seen that the errors are normally distributed. Hence, considerations of

the normal distribution can be applied. Therefore, the mean μ and the standard deviation σ can be calculated and they are equal to $7.8\,mV$ and $333.7\,mV$, respectively. Fig. 13 shows the mean and 3σ - confidence interval of the estimation. According to the normal distribution theory, $99.73\,\%$ of the estimations lie between an interval of $\mu \pm 3\sigma$ which is equal to $7.8 \pm 3 \cdot 333.7\,mV = \underline{[-0.9934\,V\ \ 1.0090\,V]}$.

To evaluate how the retraining interval affects the quality of the estimation, the mean and respective 3σ - confidence interval for the four considered meter combinations versus the retrain interval is shown in Fig. 14. A general trend can be observed for all meter combinations, namely that the mean value remains for all of them close to zero. However, the standard deviation and, therefore, the confidence interval increases with longer retrain intervals. The results also show different confidence intervals which, however, correspond to the results of the performance of the estimation shown in Fig. 12, i.e. the width of the confidence interval reflects the performance of the model. As shown in Fig. 12, the best performance is achieved at the meter combination $S_2 - D_5$ and, indeed, the same meter combination shows the narrowest confidence interval. The same applies for the other meter combinations in descending order.

In order to assess the model performance during high PV in-feed, a scatter plot of the active power flow at the substation meter S_1 versus the estimation error of the meter combinations $S_1 - D_1$ and $S_1 - D_2$ for June 2015 with a retrain interval of 1 day is shown in Fig. 15. These meter combinations are chosen because this feeder contains more PV generation. The active power is presented on the x-axis and the error on the y-axis. Positive active power means 'normal' power flow direction into the feeder and negative means reverse power flow due to excess of PV generation over consumption. The maximum occurring power flow into the feeder is approximately $14\,kW$ and the largest reverse power flow peaks at about $-11\ kW$, i.e. a broad range of power flow conditions is covered during the evaluation

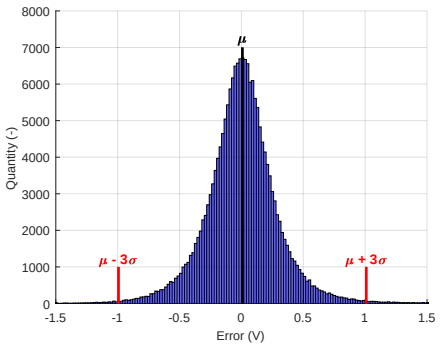

Figure 13: Error distribution of $S_1 - D_1$ for a RI of 1 day with $\mu = 7.8\,mV$, $\sigma = 333.7\,mV$.

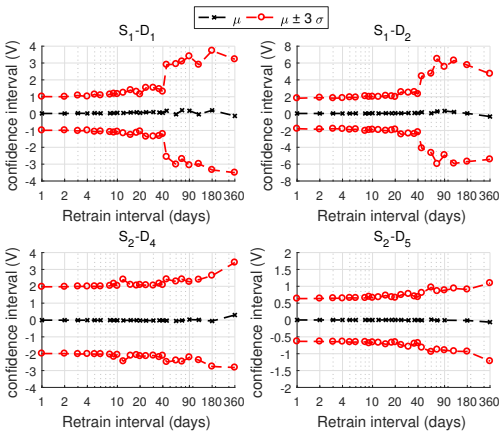

Figure 14: Mean error μ with 3-σ confidence interval of the voltage estimations for all meter combinations

period. However, no significant differences in the model performance over varying load flow conditions can be identified, i.e. the model performance does not perform worse during high PV in-feed compared to 'normal' conditions without any distributed generation. That means, that the NN estimation model is suitable for high accuracy voltage estimation under presence of distributed generation.

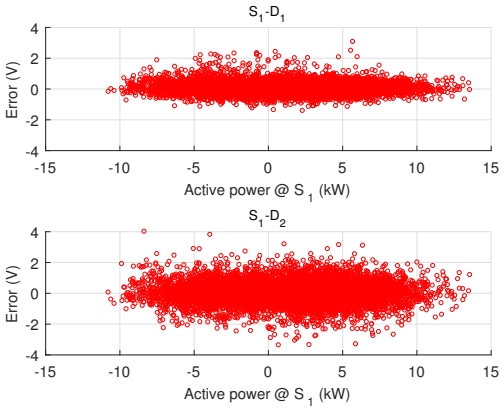

Figure 15: Active power flow at substation versus estimation error of the meter combinations $S_1 - D_1$ and $S_1 - D_2$ for June 2015.

6. Conclusion

This paper presented the validation of a neural real-time voltage estimator for active distribution grids. In particular, the phase-neutral voltages at a bus, downstream from the feeder, are estimated using measurements from the substation of the feeder. The model can be used for real-time voltage estimation as the output of the model can be deterministically

calculated from the input after the model has been established. A possible application of the approach is real-time estimation at buses where measurements, such as smart meters, are installed, but data is not available in real-time. Historical measurement data can be used to establish and retrain the model in appropriate time intervals. Based on data gathered from an operating public LV power system, the method is shown to be robust and, therefore, applicable in real world. The accuracy achieved by the method is in the same order of magnitude as the measurement uncertainty of a physical measurement device.

A novel approach to select the appropriate inputs of the model has been introduced. The correlation between inputs and outputs and among inputs is used to eliminate input variables with low impact on the output error. Reducing redundancy of inputs keeps model complexity, and thus computation time, within reasonable limits. It was shown that the presented input selection approach is capable of sorting out input variables to determine the best achievable performance with a certain amount of input variables. Analysis of the performance as a function of the quantity of historical data has clearly showed that the general statement that better models are produced with more data is not valid in this case. Instead, the assessment showed that the performance of the model stabilizes when about one month of historical data is used in the training process and does not improve further if more data is used. There is even a slight trend that the model performance declines when more data is used.

The analysis of the impact of the retraining interval on the model performance showed that, generally, the performance is better with shorter retraining intervals. It was observed that the performance declines only slightly up to an retrain interval of 10 days. However, the performance for some meter combinations drops significantly for larger retrain intervals while it only declines slightly for others. Therefore, it is concluded that the retrain interval should be kept below 20 days.

It was shown that the error of the estimation is normally distributed and, thus, the confidence interval of the estimation error was calculated over different retrain intervals. Corresponding to the results of the performance analysis over different retrain intervals, the standard deviation of the estimation error increases with increasing retrain intervals. The width of the 3σ - confidence interval which includes 99.73 % of the calculated estimations is different for every meter combination, but at maximum $3\sigma \approx \pm$ 2 V. That means, that the produced error, for retrain intervals under 20 days, is approximately 0.87 % of the nominal phase-neutral voltage (230 V), which is still acceptable considering the measurement uncertainty of 0.5 % for class B meters defined in IEC 61000-4-30. Besides, the method is also found to be accurate during periods of high PV generation, as the errors during periods of high load, and periods of high PV production do not show noticeable differences.

Further research on the robustness of the estimation to wrong or missing data has to be conducted, as corrupted data certainly affects the performance of the model. Moreover, the approach could be extended to include additional input variables, e.g. solar irradiation, aiming at improving the performance of the estimation.

Acknowledgment

Michael Pertl is a PhD student at the Technical University of Denmark (DTU) and is supported by the EU FP7 project ELECTRA (grant: 609687) and the Danish Research Project ELECTRA Top-up (grant: 3594756936313). More information can be found at electrairp.eu. Koen Kok's contribution was financed by the TNO Early Research Program on Energy Storage & Conversion (ERP EC&S) through the SOSENS project.

References

[1] KEMA Consulting, Integration of Renewable Energy in Europe, Tech. rep., Imperial Collaege London (2014).

[2] T. J. Hammons, Integrating renewable energy sources into European grids, International Journal of Electrical Power and Energy Systems 30 (8) (2008) 462–475. doi:10.1016/j.ijepes.2008.04.010.

[3] K. Knezovic, M. Marinelli, R. J. Moller, P. B. Andersen, C. Træholt, F. Sossan, Analysis of voltage support by electric vehicles and photovoltaic in a real Danish low voltage network, in: Universities Power Engineering Conference (UPEC), Cluj-Napoca, 2014, p. 6. doi:10.1109/UPEC.2014.6934759.

[4] K. Knezović, M. Marinelli, Phase-wise enhanced voltage support from electric vehicles in a Danish low-voltage distribution grid, Electric Power Systems Research 140 (2016) 274–283. doi:10.1016/j.epsr.2016.06.015.

[5] S. Sarri, M. Paolone, R. Cherkaoui, A. Borghetti, F. Napolitano, C. A. Nucci, State estimation of Active Distribution Networks: Comparison between WLS and iterated kalman-filter algorithm integrating PMUs, in: IEEE PES Innovative Smart Grid Technologies Conference Europe, Berlin, 2012, pp. 1–8. doi:10.1109/ISGTEurope.2012.6465871.

[6] J. Wu, Y. He, N. Jenkins, A robust state estimator for medium voltage distribution networks, IEEE Transactions on Power Systems 28 (2) (2013) 1008–1016. doi:10.1109/TPWRS.2012.2215927.
URL http://ieeexplore.ieee.org/lpdocs/epic03/wrapper.htm?arnumber=6313963

[7] A. Ranković, B. M. Maksimović, A. T. Sarić, A three-phase state estimation in active distribution networks, International Journal of Electrical Power & Energy Systems 54 (2014) 154–162. doi:10.1016/j.ijepes.2013.07.001.

[8] F. F. Wu, Power system state estimation: a survey, International Journal of Electrical Power & Energy Systems 12 (2) (1990) 80–87. doi:10.1016/0142-0615(90)90003-T.

[9] A. Monticelli, Electric power system state estimation, Proceedings of the IEEE 88 (2) (2000) 262–282. doi:10.1109/5.824004.

[10] L. H. Hassan, M. Moghavvemi, H. a.F. Almurib, O. Steinmayer, Current state of neural networks applications in power system monitoring and control, International Journal of Electrical Power & Energy Systems 51 (2013) 134–144. doi:10.1016/j.ijepes.2013.03.007.
URL http://www.sciencedirect.com/science/article/pii/S014206151300104X

[11] M. Ferdowsi, A. Lowen, New monitoring approach for distribution systems, in: IEEE International Conference on Instrumentation and Measurement Technology, Montevideo, 2014, pp. 1506–1511.
URL http://ieeexplore.ieee.org/xpls/abs{_}all.jsp?arnumber=6860997

[12] O. Ivanov, M. Gavrilas, State Estimation with Neural Networks and PMU Voltage Measurements, in: International Conference and Exposition on Electrical and Power Engineering (EPE), Iasi, 2014, pp. 983–988.

[13] O. Ivanov, M. Gavrilas, B. Neagu, Intelligent monitoring and control in transmission and distribution networks, in: International Conference on Optimization of Electrical and Electronic Equipment (OPTIM), Bran, 2014, pp. 185–191. doi:10.1109/OPTIM.2014.6850918.

[14] Y.-Y. Hsu, C.-C. Yang, Fast voltage estimation using an artificial neural network, Electric Power Systems Research 27 (1993) 1–9.

[15] R. Kamali, R. Sharifi, H. Radmanesh, S. Fathi, Online voltage estimation for distribution networks in presence of distributed generation, Indian Journal of Science and Technology 9 (18) (2016) 1–5. doi:10.17485/ijst/2016/v9i18/71484.

[16] M. Pertl, K. Heussen, O. Gehrke, M. Rezkalla, Voltage Estimation in Active Distribution Grids Using Neural Networks, in: IEEE Power and Energy Society General Meeting, Boston, 2016, p. 5.

[17] M. Paolone, A. Borghetti, C. A. Nucci, A synchrophasor estimation algorithm for the monitoring of active distribution networks in steady state and transient conditions, in: 17th Power Systems Computation Conference (PSCC), Stockholm, 2011, pp. 1–8.

[18] S. Haykin, Neural networks - a comprehensive foundation, 2nd Edition, Pearson Education, 1999. arXiv:arXiv:1312.6199v4, doi:10.1017/S0269888998214044.

[19] M. Y. Rafiq, G. Bugmann, D. J. Easterbrook, Neural network design for engineering applications, Computers and Structures 79 (2001) 1541–1552. doi:10.1016/S0045-7949(01)00039-6.

[20] B. M. Wilamowski, Neural Network Architectures and Learning, in: International Conference on Industrial Technology (ICIT), Maribor, 2003, pp. 1–12.

[21] B. M. Wilamowski, Neural network architectures and learning algorithms, IEEE Industrial Electronics Magazine (2009) 56–63doi:10.1109/ICIT.2011.5754336.

[22] B. Wilamowski, Neural Network Architectures, in: Intelligent Systems, 2nd Edition, Taylor & Francis, 2011, Ch. 6, pp. 1–17. doi:doi:10.1201/b10604-9.
URL http://dx.doi.org/10.1201/b10604-9

[23] M. T. Hagan, H. B. Demuth, M. H. Beale, O. De Jesús, Neural Network Design, 2nd Edition, PWS Publishing Co. Boston, MA, 1996.

[24] D. W. Marquardt, An Algorithm for Least-Squares Estimation of Nonlinear Parameters, Journal of the Society for Industrial and Applied Mathematics 11 (2) (1963) 431–441. arXiv:arXiv:1011.1669v3, doi:10.1137/0111030.

[25] M. T. Hagan, M. B. Menhaj, Training Feedforward Networks with the Marquardt Algorithm, IEEE Transactions on Neural Networks 5 (6) (1994) 989–993. doi:10.1109/72.329697.

[26] D. Nguyen, B. Widrow, Improving the learning speed of 2-layer neural networks by choosing initial values of the adaptive weights, in: International Joint Conference on Neural Networks (IJCNN), San Diego, 1990, pp. 21–26.

[27] L. Hamm, B. W. Brorsen, M. T. Hagan, Comparison of Stochastic Global Optimization Methods to Estimate Neural Network Weights, Neural Processing Letters 26 (3) (2007) 145–158. doi:10.1007/s11063-007-9048-7.

[28] IEC, IEC Standard 61000-4-30: Testing and measurement techniques -power quality measurement methods (2016).

[29] R. May, G. Dandy, H. Maier, Review of Input Variable Selection Methods for Artificial Neural Networks, in: Methodological Advances and Biomedical Applications, InTech, 2011, pp. 19–44.

[Pub. E] An equivalent time-variant storage model to harness EV flexibility: forecast and aggregation

An Equivalent Time-Variant Storage Model to Harness EV Flexibility: Forecast and Aggregation

Michael Pertl, *Graduate Student Member, IEEE,* Francesco Carducci, Michaelangelo Tabone, *Member, IEEE,* Mattia Marinelli, *Senior Member, IEEE,* Sila Kiliccote, *Member, IEEE,* and Emre C. Kara*, *Member, IEEE*

***Abstract*—This paper address the problem of forecasting the aggregate flexible demand from tens to thousands of electric vehicle supply equipment (EVSEs). First, it presents an equivalent time-variant storage model for flexible demand at an aggregation of EVSEs. The proposed model is generalizable to different markets, and also to different flexible loads. Model parameters representing multiple EVSEs can be easily aggregated by summation, and forecasted using autoregressive models. The forecastability of uncontrolled demand and storage parameters is evaluated using data from 1341 non-residential EVSEs located in Northern California. The benefits of aggregation and forecastability are demonstrated using an energy arbitrage scenario. Purchasing energy day ahead is less expensive than in the real-time market, but relies on a uncertain forecast of charging availability. The results show that the forecastability significantly improves for larger aggregations. This helps the aggregator make a better forecast, and decreases the cost of charging in comparison to an uncontrolled case by 60% with respect to an oracle scenario.**

***Keywords*—Aggregation, Data Analysis, Demand Response, Electric Vehicles, Power System Flexibility.**

I. Introduction

By the end of 2015, 1.26 million electric cars were on the road worldwide. The global Clean Energy Ministerial's Electric Vehicles Initiative (EVI) 20 by 20 target calls for 20 million electric vehicles (EVs) by 2020 globally. The Paris declaration on Electro-Mobility and Climate Change and Call to Action sets a global goal of 100 million electric cars and 400 million electric 2- and 3-wheelers by 2030 [1]. Substantial market growth is needed to increase the current EV population of 1.26 million towards these ambitious targets.

From an infrastructural point of view, this rapid growth of EVs introduces several challenges to today's electric power systems. For example, in distribution systems, uncontrolled EV charging will dramatically increase demand at some nodes, potentially exceeding the capacity of existing infrastructure, impeding voltage control, and offsetting the balance between phases [2]. On the other hand, EV charging is often flexible in time, and presents an opportunity to control the timing of demand to benefit distribution, transmission, and/or generation systems [3], [4]. These control strategies are usually referred to as smart charging or vehicle-to-grid (V2G) where the former restricts power flow into the battery only, and the latter allows power flow into and from the battery. [5] further identifies two control strategies that fit either of these paradigms. A) Direct centralized control where an aggregator clusters and controls a large number of EVs [6], [7]—aggregators can be a third party organization or the owners of the EVSEs—and, B) Indirect and fully decentralized control where the control authority stays with the EV owner [8]. This work addresses the challenges of aggregating large populations of EVs to facilitate centralized control approaches. The particular control strategies for individual EVs is beyond the scope of this paper.

The aggregation of multiple EVs connected to EVSEs is necessary for several reasons. In order to participate in a market, a minimum resource capacity is generally required. The European EPEX spot market [9], the Nordic Nord Pool spot market [10] and the demand response (DR) programs of the California Independent System Operator (CAISO) [11] require a minimum capacity of 100 kW. Moreover, studies show that the economical benefit increases by aggregating EVs [12], [13]. Naturally, a population of EVSEs offer more flexibility in terms of deferrable load than a single EVSE [14], [15].

Aggregations of multiple EVSEs are typically modeled as equivalent time-varying battery storage. The storage model can be controlled to fulfill specific objectives and serve as a demand side flexibility asset, e.g. it could be used by an aggregator to directly participate in the wholesale market and minimize operational costs [5], [16]. Third party aggregators or distribution system operators (DSOs) could provide ancillary services to the transmission system operators (TSOs) using the aggregate EVSEs [17]–[19]. The aggregators and DSO could also use the equivalent storage model for short-term planning purposes in order to avoid abnormal conditions when grid is operated close to its technical limits [20], e.g. day-ahead scheduling of demand to avoid congestion.

Many studies focus on modelling equivalent storage systems based on several strong assumptions on the predictability of EV charging. For instance, in [21] the aggregation model needs input from the EV owner about the preferred state-of-charge (SOC) for the next day or the next hours. Then the aggregator uses this information to forecast the demand and flexibility to participate in the day-ahead market. In [22], the arrival and departure times of individual EVs are assumed to be known

M. Pertl and M. Marinelli are with the Department of Electrical Engineering, Technical University of Denmark, Frederiksborgvej 399, 4000 Roskilde, Denmark, e-mail: {mpertl,matm}@elektro.dtu.dk

F. Carducci is with DIISM, Universita Politecnica delle Marche, Ancona, 60121, Italia, e-mail: francesco.carducci@pm.univpm.it

M. Tabone is with Stanford University, Stanford, CA, 94305, USA, e-mail: mtabone@stanford.edu

S. Kiliccote and E.C. Kara (* corresponding author) are with the SLAC National Accelerator Laboratory, Menlo Park, CA, 94025, USA, e-mail: {silak,emrecan}@slac.stanford.edu

beforehand. This requirement introduces great uncertainties if the actual and foreseen arrival/departure times deviate from each other. The authors of [23] assume that arrival times are uniformly distributed and all loads (EVs to be charged) are identical with respect to energy demand, charging session duration and maximum power consumption. Thus, in order to use EV charging for ancillary services or energy arbitrage, it is important to understand how well EV charging patterns are able to be forecasted. More specifically, it is important to understand the effects of any uncertainty in these forecasts on the operation of an equivalent time-varying storage model.

A modelling approach that overcomes these drawbacks is proposed in this paper. The proposed general storage model allows the aggregation of multiple EVSEs. The proposed model represents many vehicles and can be used to participate in different markets, e.g. high frequency regulation markets and long time-scale energy markets. Fig. 3 presents the proposed equivalent time-variant storage model, which is inspired by a model for thermostatically controlled loads (TCL) proposed in [24]. The model is defined by a limited number of parameters: the storage capacity C, the maximum/minimum charging power P_{max}/P_{min}, the actual charging/discharging rate P_{act}, the current energy content of the equivalent storage C_{act} and the energy capacity arriving/leaving the system α_E and β_E. The advantages of the proposed model are: a) it is applicable in different markets b) many EVSEs can be aggregated in the model by summing parameters, c) storage parameters can be forecast by using conventional time series methods such as autoregressive models without the need for more advanced algorithms, d) there is no need for information about the exact arrival and departure times in the future, e) it supports aggregating EVSEs of different charging levels.

The impact of aggregation on forecasting uncertainty is analyzed, as this is of key importance for practical applicability. The forecastability of the uncontrolled demand is analyzed as it is valuable information for short-term planning in power system operation. The impact of aggregation on forecast uncertainty of the storage parameters is analyzed because it is of crucial importance to enable the equivalent storage model to be used as a flexibility asset. One envisioned application of the proposed storage model is presented, showing how the day-ahead charging schedule can be optimized from an aggregator perspective by minimizing the costs of charging.

The contributions of this paper are threefold: 1) an equivalent time-variant storage model for EVSEs aggregation is proposed, 2) the effect of aggregation on the forecastability is analyzed and 3) an envisioned application of the equivalent storage model is presented to show the benefit of aggregation.

The analysis is carried out using data collected from over 1341 non-residential EVSEs, located throughout 75 zip code regions in Northern California, spanning one year. A more detailed description of the data is given in section II. The equivalent storage model is described in section III. The aggregation metric, forecasting method and forecasting results are discussed in section IV. One envisioned application of the storage model—which highlights the benefits of aggregation—is shown in section V.

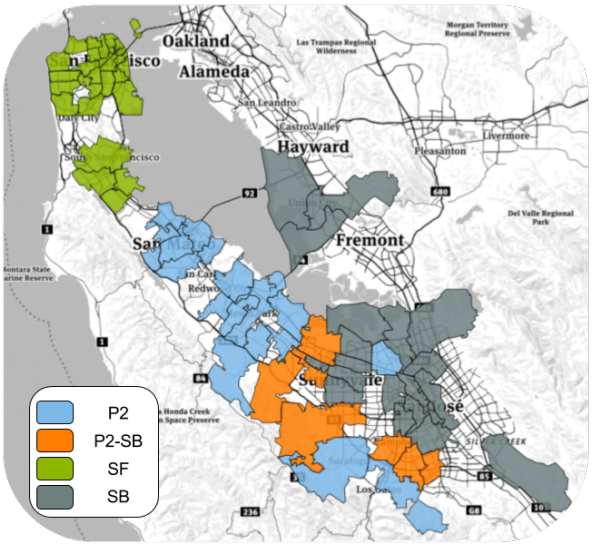

Fig. 1. Zip code regions forming the VAPs [25].

II. Dataset

A. EVSE characteristics

The data set for this study was provided by ChargePoint. It includes data from 1341 EVSEs throughout 75 zip code regions in Northern California with 451,999 charging sessions covering the full year of 2013. For each charging session, i.e. from plug-in to departure of an EV, following data is reported:

1) Plug-in and departure time stamps
2) Average and peak power every 15 min
3) Charged energy every 15 min
4) Charging port type
5) Zip code
6) Non-residential building category

In order to join data from the EVSEs with local information that is identified by zip code, virtual aggregation points (VAPs) are created by aggregating EVSEs within a contiguous set of zip codes. The VAPs mostly coincide with the Pacific Gas and Electric Company's (PG&E) sub-load aggregation points (sub-LAPs). A more detailed description of the VAPs is given in [25].

The spatial distribution of the four VAPs with the most charging sessions is shown in Figure 1. All four VAPs are adjacent and located in San Francisco Bay Area. The number of zip code regions that form each of the VAPs, number of charging sessions and number of charging session per day are summarized in Table I. More than 99 % of the charging sessions in the dataset are from Level 2 EVSEs with a capacity between 4 - 7 kW unidirectional. About two third of the EVSEs are located at workplaces, the rest is distributed over hospitals, parking areas, universities and airports.

B. Data Preprocessing

The dataset is preprocessed before the analysis. Charging sessions with an energy less than 0.1 kWh are removed.

TABLE I. SUMMARY OF VAPS USED IN THIS STUDY.

VAP	Region	# of zip code regions	# of charging sessions	# of charging sessions/day
P2-SB	Peninsula and South Bay	7	207501	568.50
SB	South Bay	21	112250	307.53
SF	San Francisco	30	72996	199.99
P2	Peninsula	17	59252	162.33

Time stamps of charging sessions are checked to sort out simultaneous charging sessions of the same EVSE due to time stamp errors. The energy of every interval is crosschecked with the corresponding charging power of the interval, when mismatching, the session is sorted out. The EV arrival times are rounded down and the EV departure times are rounded up to the nearest 15 min interval to harmonize the data.

C. Qualitative Effect of Aggregation

To highlight the effect of aggregation on the consumption pattern of EVs, Fig. 2 shows a time-domain plot of different EV aggregation sizes for a weekly period. As expected, the higher the number of aggregated EVSEs, the less volatile the pattern becomes. This suggests that the charging demand becomes more forecastable as the size of the EVSE aggregation increases, an observation that is studied in detail in section IV-D. Weekdays show a significantly higher demand than weekends, which may be due to the fact that most of the EVSEs are located at workplaces.

III. EQUIVALENT TIME-VARIANT STORAGE MODEL

A. Equivalent Storage Parameters

A storage model can be described by a number of parameters that are related to physical quantities. The main advantage of the storage model is that all parameters can be evaluated

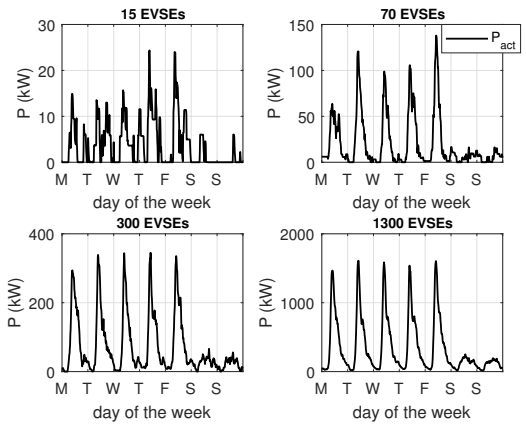

Fig. 2. Weekly demand at different aggregations.

per EVSE and easily aggregated by summation over an arbitrary number of EVSEs. The model consists of seven time-dependent parameters described as follows:

$\alpha_{\mathbf{E}}(\mathbf{t})$ in (kWh): The capacity boosting rate α_E represents the amount of capacity added to the equivalent storage at time t. It is proportional to the amount of capacity connecting to the system at time t. Equation (1) shows how α_E is aggregated for an arbitrary number of EVSEs, n_{EVSEs}. E_i represents the amount of energy to be charged during charging session of EV i. Equation (2) defines $\delta_{a,i}$, which is a Kronecker impulse function centered at the arrival time of the i-th EV; it assumes the value 1 during the interval that the EV arrives and 0 elsewhere.

The capacity added at each time is equal to the amount of energy that will be charged in initializing sessions, not the actual total capacity of EV batteries that are connecting. The latter would include any residual energy left in batteries when they plug in as well as any uncharged capacity that remains when they depart.

$$\alpha_E(t) = \sum_{i=1}^{n_{EVSEs}} E_i \cdot \delta_{a,i}(t) \tag{1}$$

$$\delta_{a,i}(t) = \begin{cases} 1 \text{ at arrival time of EV i} \\ 0 \text{ otherwise} \end{cases} \tag{2}$$

$\beta_{\mathbf{E}}(\mathbf{t})$ in (kWh): The energy dissipation rate, β_E, represents the amount of energy and capacity leaving from the system when a car is unplugged. Now, E_i represents the amount of energy that has been charged during the session, while $\delta_{d,i}$ is a Kronecker impulse function centered at the EV departure time. Note that the energy removed from the system is of equal magnitude as the added capacity when plugging in, but with opposite sign.

$$\beta_E(t) = \sum_{i=1}^{n_{EVSEs}} -E_i \cdot \delta_{d,i}(t) \tag{3}$$

$$\delta_{d,i}(t) = \begin{cases} 1 \text{ at departure time of EV i} \\ 0 \text{ otherwise} \end{cases} \tag{4}$$

$\mathbf{C}(\mathbf{t})$ in (kWh): The total capacity of the system at time t equals the sum of capacity at the previous time step and the added and removed capacity from plugging or unplugging EVs, respectively.

$$C(t) = C(t-1) + \alpha_E(t) + \beta_E(t) \tag{5}$$

$\mathbf{C_{act}}(\mathbf{t})$ in (kWh): The state variable C_{act} describes the actual energy content of the equivalent storage.Δt is the granularity of time, which is 15 minutes throughout this work.

$$C_{act}(t) = C_{act}(t-1) + P_{act}(t) \cdot \Delta t + \beta_E(t) \tag{6}$$

$\mathbf{P_{act}}(\mathbf{t})$ in (kW): Charging/discharging rate of the EVs plugged into the system at time t. A positive sign represents charging while a negative sign represents discharging.

$\mathbf{P_{min}}(\mathbf{t})$ and $\mathbf{P_{max}}(\mathbf{t})$ in (kW): The minimum/ maximum charging rate of all EVs connected at time t. P_i^+ and P_i^- are the physical limitations of the minimum/maximum charging

rate of individual EVSEs. P_i^- can be negative if the EVSEs have vehicle-to-grid (V2G) capability.

$$P_{min}(t) = P_{min}(t-1) + \sum_{i=1}^{n_{EVSEs}} P_i^- \cdot \delta_{a,i}(t) + \sum_{i=1}^{n_{EVSEs}} -P_i^- \cdot \delta_{d,i}(t) \quad (7)$$

$$P_{max}(t) = P_{max}(t-1) + \sum_{i=1}^{n_{EVSEs}} P_i^+ \cdot \delta_{a,i}(t) + \sum_{i=1}^{n_{EVSEs}} -P_i^+ \cdot \delta_{d,i}(t) \quad (8)$$

SOC(t) in (%): The state-of-charge (SOC) of the storage is derived from the other parameters and the state variable. It is defined according to the general convention as the actual energy content of the equivalent storage $C_{act}(t)$ divided by the total capacity $C(t)$. In the case that the total capacity is zero, we define the SOC to be zero.

$$SOC(t) = \begin{cases} \frac{C_{act}(t)}{C(t)} \cdot 100\ \% \text{ for } C(t) \neq 0 \\ 0 \text{ else} \end{cases} \quad (9)$$

The minimum charging/discharging power of the EVSEs can be set to a negative number corresponding to the V2G capability of the EVSE. However, if V2G is available, additional considerations around the assumption that there is no residual energy left in the battery when the EV is connected, shall be made.

In a V2G scenario with unknown residual energy storage capacity, only the energy that has been charged into the battery can be used for V2G operation. A constraint for the minimum SOC at the end of charging session needs to be defined. The resulting costs may be lower than in a pure charging scenario. From a theoretical standpoint, the optimum may be found only if the residual energy storage capacity is known when an EV connects. While the proposed storage model does allow for V2G capability, we consider assessments of the value of V2G as beyond the scope of this paper.

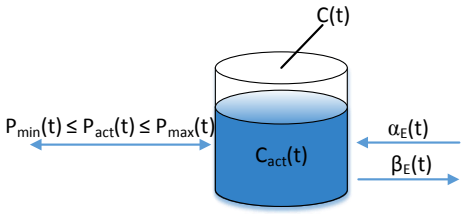

Fig. 3. Proposed equivalent time-variant storage model.

B. Example Storage Parameter Evolution over Time

For better understanding of the storage parameters, Fig. 4 shows an example of the storage parameter evolution over a 24 hour period for two EVSEs. The example is taken from original measurement data and presents current practice of uncontrolled charging. The top subplot shows the evolution of the total/actual storage capacity and the added or removed capacity of the system during arrivals and departures of EVs. At $t = 5.45$ the first EV arrives and adds about 20 kWh to the system, i.e. the total storage capacity at that time is equal to α_E as the capacity is a function of the previous capacity plus α_E and β_E as shown in (5). At the same time the maximum charging rate of the storage increases from zero to 6.6 kW (level 2 EVSE) as seen in the middle subplot. The EVSEs do not to have vehicle-to-grid (V2G) capability, hence, the minimum charging power is zero as no discharging is possible. The EV immediately starts to charge with about 5 kW after plugged to the EVSE. At 06.45 a second EV arrives and plugs to another EVSE. The second EV's added capacity α_E is larger than the one of the first EV. The total capacity increases and is now the sum of the two connected EVs. The maximum power increases to 13.2 kW as the other EVSE is also of level 2 type. Also the second car starts immediately to charge and P_{act} increases to about 10 kW. The SOC drops as the second EV connects as the total capacity suddenly increases while the actual energy continuously increases as the cars are being charged at a finite rate. After connection of the second EV, both EVs charge until full, sometime between 12.00 and 13.00. At 13.30 the first EVSE leaves and the storage capacity is reduced by the same amount that was added at 05.45, hence, the total capacity is equal to the added capacity of the second EV. However, no charging happens anymore as the EV has already been fully charged. The second EV leaves at 17.30 and all parameters drop to zero as no EV is connected anymore.

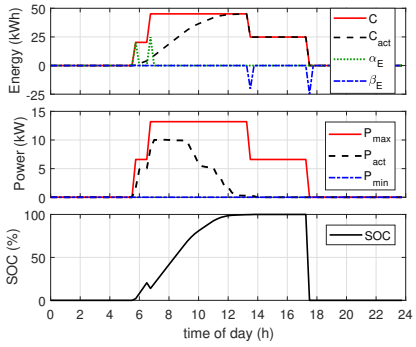

Fig. 4. Storage parameter evolution for two EVSEs over 24 h period.

IV. Influence of Aggregation on Short-Term Forecastability

A. Aggregation Metric

A metric that allows comparison of different aggregation levels has to be established before forecasting the parameters of the proposed storage model. Aggregating over the number of EVSEs is not a suitable metric for comparison because the energy demand of different EVSEs could be different. Comparing EVSEs with different energy demand levels would not deliver insightful results. Therefore, it is proposed to aggregate EVSEs by the average daily energy demand over the past two weeks before the forecasting period as shown in (10). For example, an aggregation level of 100 kWh can be achieved by combination of different numbers of EVSEs

depending on how frequently the EVSEs have been used. The aggregation can be achieved by a small number of EVSEs with many charging sessions or by a larger number of EVSEs with a lower charging frequency.

$$E_{agg} = \sum_{i=1}^{n_{EVSEs}} \overline{E}_i^{14\,d} \tag{10}$$

B. Autoregressive Forecast Models

Autoregressive integrated moving average (ARIMA) models are used for short-term forecasting of the parameters. An ARIMA model is fit for each parameter using the Box-Jenkins methodology for analyzing the autocorrelation function (ACF) and partial autocorrelation function (PACF) of the input series [26]. The analysis is carried out for four parameters: P_{act}, P_{max}, C and α_E. The motivation behind selection of these parameters is given in sections IV-D and IV-E.

The Box-Jenkins procedure suggested to use seasonal autoregressive (AR) models without moving average (MA) terms for all parameters. However, the models for the four parameters have different numbers of autoregressive lags and differencing.

The general AR model, including seasonality, is shown in (11). It consists of a constant k, model order p, coefficient ϕ_i of the i-th order, and seasonality s. The seasonality s is equal to 672 data points, which corresponds to one week (96 data points/day $\cdot$ 7 days = 672/week). The parameter D is the order of differencing of the time series. The parameters of all autoregressive models are summarized in Table II.

The evolution of α_E represents a point process which is not suitable for AR models, instead, the cumulative sum of α_E is forecasted. Forecasting the cumulative sum of α_E is actually more convenient for the application presented in Section V.

$$y_{(t)} = k + y_{(t-s)} + \sum_{i=1}^{p} \phi_i (y_{(t-i)} - y_{(t-i-s)}) \tag{11}$$

The coefficients of the AR models are derived for each aggregation level. In order to obtain the coefficients, 20 random combinations of EVSEs are produced for each aggregation level and day to be forecasted. The average of the coefficients of the 20 models yields the model parameters for the specific aggregation level and day to be forecasted. The data used to generate the 20 random EVSE combinations only include 'past' data from before the forecasting period.

To justify this approach the variation of the coefficients for 1000 different combinations of EVSEs for one aggregation level is shown in Fig. 5. The four subplots show the results for the four considered parameters P_{act}, P_{max}, C and α_E. The variation of the coefficients is relatively small and therefore only the averaged model with fixed coefficients is used instead of refitting AR coefficients for every combination of EVSEs.

TABLE II. SUMMARY OF THE AR MODEL PARAMETERS

Parameter / Model	p	s	D
P_{act}	2	672	0
C, P_{max}	4	672	0
α_E	3	672	1

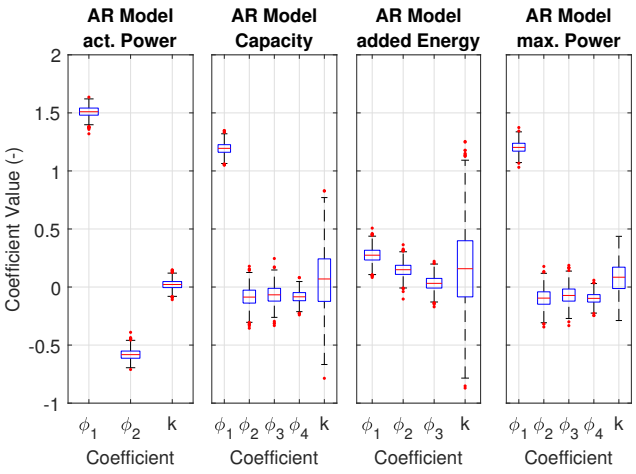

Fig. 5. Variation of AR model coefficients for 1000 EVSE combinations.

This approach reduces the computational effort of producing the forecast significantly.

C. Metric for Forecast Performance

Several performance metrics such as Mean Average Error (MAE), Root Mean Squared Error (RMSE), Mean Average Percentage Error (MAPE) and Coefficient of Variation (CV) are used in the forecasting literature. The two most commonly used metrics are CV and MAPE [27]. In this work the CV is used to quantify the performance of the forecasts because it is suitable to compare time series at different scales [27], i.e. different aggregation levels. The CV is the ratio of the RMSE to the mean of the signal as shown in (12) where y denotes the signal and $\hat{y}$ its forecast.

$$CV(y,\hat{y}) = \frac{\sqrt{\frac{1}{T}\sum_{t=1}^{T}(\hat{y}(t)-y(t))^2}}{\frac{1}{T}\sum_{t=1}^{T} y(t)} \tag{12}$$

D. Forecastability of Uncontrolled Demand

Even if no EV charging is able to be controlled, grid operators are interested in forecasting of charging in order to plan generation to match demand. Uncertainty in this forecasts causes grid operators to procure more expensive reserve generation to manage unexpected changes in demand.

The three upper subplots in Fig. 6 show a day-ahead forecast of the demand for a low, medium and high aggregation level. Clearly, a higher aggregation level improves the accuracy of the forecast significantly. The CV decreases from 70 % to 46 % and 21 % for the medium and high aggregation, respectively.

To further demonstrate this trend, 1000 random combinations of EVSEs for each aggregation level for seven consecutive days are forecast. Forecasting for an entire week captures effects that may occur on weekdays or on weekends only. The performance of each forecast is evaluated by means of the CV.

The results of the performance assessment are shown in the lower subplot in Fig. 6. The forecast uncertainty considerably

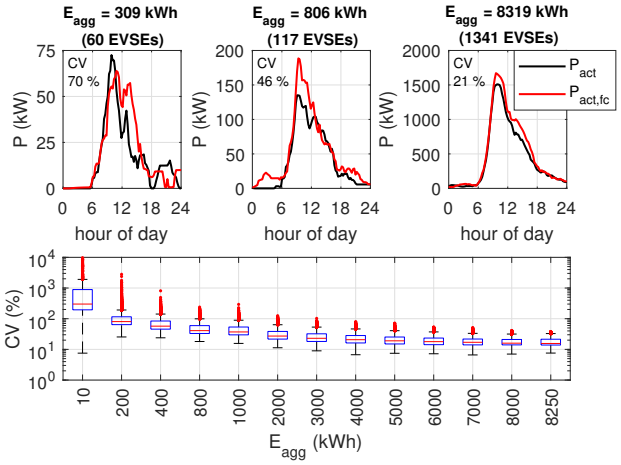

Fig. 6. Time-domain plot of forecast for three different aggregation levels and variation of forecast errors versus aggregation level.

decreases with higher aggregation levels. The median of the forecast performance approaches about 16 % whereas the 25$^{\text{th}}$ and 75$^{\text{th}}$ percentiles lie at 14 % and 21 %, respectively. The results confirm the hypothesis drawn from the qualitative assessment of Fig. 2 that the demand at higher aggregation levels is forecastable with lower uncertainty. It is expected that the use of more advanced forecasting algorithms will further improve the performance but one should note that the basic AR models used in this analysis performed well.

E. Forecastability of Storage Parameters

The storage model, described in Section III, consists of seven parameters. Depending on the application of the model, different parameters need to be forecasted. If the storage model wants to be used as an flexibility asset for short-term planning, e.g. scheduling next day's charging pattern, the storage forming parameters C, P_{min}, P_{max}, α_E and β_E need to be forecasted.

In this paper, the forecasting performance of the parameters C, P_{max} and cumulative sum of α_E are analyzed. Only these three parameters are needed to run the optimization of the energy arbitrage scenario shown in Section V. The parameters P_{min} and β_E are not included in the analysis, but they have similar properties as their counter equivalents P_{max} and α_E, respectively, i.e. the forecast performance is assumed to be in the same order of magnitude.

To determine the relationship between uncertainty of forecast and aggregation level, the storage parameters for 1000 random combinations of EVSEs for each aggregation level are forecasted for the next day. The performance of each forecast is evaluated by means of the CV. This procedure is carried out for seven consecutive days from Monday to Sunday to capture effects that may occur on weekdays or on weekends only.

Performance assessments of the forecasts are shown in Fig. 7. The uncertainty for all storage parameters significantly decreases for higher aggregations. The achieved performance for day-ahead forecasts for all storage parameters lies at around 10 % for the highest aggregation in this paper. The plot includes results for 7 days from Monday till Sunday and no significant differences in the forecast performance of weekdays and weekends are observed.

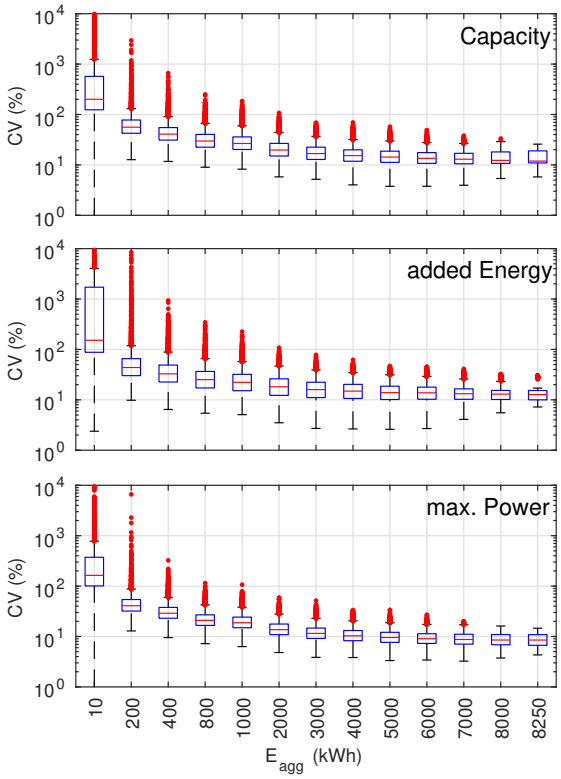

Fig. 7. Variation of forecast accuracy versus aggregation level.

V. Application of the Storage Model

This section presents an example application of the storage model for participation in a day-ahead market from an aggregator's perspective. The benefit of aggregation by reducing the forecast uncertainty on the costs is analyzed, i.e. how much additional costs are caused due to imperfect forecasting of the storage parameters. The storage parameters C, P_{max} and α_E are forecasted for the next day. The EVs do not have V2G capability and therefore P_{min} is equal to zero. The parameter β_E is not forecasted as it is not needed for this analysis.

In order to put the application in context with the current practice, three scenarios are considered given a day-ahead price p_{DA} from the CAISO day-ahead market from June 01, 2017 and a real-time price p_{RT} that is arbitrarily chosen to be 1.5 times the day-ahead price.

1) **uncontrolled charging $\mathbf{P}_{uc}$** (current practice): the costs are determined by multiplying the uncontrolled demand with the real-time price as shown in (13),

2) **controlled charging with forecasted storage parameters**

$\mathbf{P}_{fc}$ (application of storage model): the power schedule is arranged, such that costs are minimized over the day-ahead price. An additional cost evaluated on the real-time price is added for deviating from the optimum due to imperfect forecast of storage parameters as shown in (14),
3) **controlled charging with perfect forecast** $\mathbf{P}_{opt}$ (benchmark case): the optimal case describes the minimal costs for the given market context due to a perfect forecast of all involved parameters and is calculated according to (15).

$$cost_{uc} = \sum_{t=1}^{96} P_{uc}(t) \cdot p_{RT}(t) \tag{13}$$

$$cost_{fc} = \sum_{t=1}^{96} P_{fc}(t) \cdot p_{DA} + |P_{fc}(t) - P_{opt}(t)| \cdot p_{RT}(t) \tag{14}$$

$$cost_{opt} = \sum_{t=1}^{96} P_{opt}(t) \cdot p_{DA}(t) \tag{15}$$

The optimized charging schedules for 15 min intervals (96 intervals/day) for scenario 2) and 3) is derived by use of the linear optimization problem described in (16). The total costs are minimized by optimally scheduling the demand given the day-ahead price and the forecasted and original storage parameters, respectively. The day-ahead price is the locational marginal cost from one node of the CAISO day-ahead market from June 01, 2017 and the real-time price is equal to 1.5 times the day-ahead price. The first constraint describes the physical power limits within charging is possible. The second constraint describes the initial energy state of the storage. It is set to 50 % of the total capacity, this value is arbitrary and can be chosen as preferred. The third constraint tracks the energy state and ensures that the energy content of the storage is between zero and the total capacity for every 15 min interval Δt. C_0 is the initial energy, $\sum_{i=1}^{t} -P_{act}(i) \cdot \Delta t$ is the cumulative sum of the charged energy and $\sum_{i=1}^{t} \alpha_E(i)$ is the cumulative sum of the added energy. The fourth constraint ensures that the SOC at t_{96} of the storage model is again 50 % as defined also for the beginning of the day and, thus, the storage model is in the same state at the beginning and at the end of the day.
The forecasted parameters are checked for certain conditions to guarantee a feasible solution in the optimization: a) P_{max} must be greater than zero at all times, b) cumulative sum of α_E must be greater or equal than the cumulative sum of the positive changes of C. Moreover, boundary conditions are defined, such that the storage capacity, the maximum power and the SOC at t_1 and t_{96} are equal, respectively.

$$\begin{aligned} &\min_{P} \sum_{t=1}^{96} P(t) \cdot p_{DA}(t) \\ &\text{subject to} \\ &0 \leq P(t) \leq P_{max}(t) \\ &C_0 = \tfrac{C(t_1)}{2} \\ &0 \leq C_0 + \sum_{i=1}^{t} (-P(i) \cdot \Delta t + \alpha_E(i)) \leq C(t) \\ &C_0 + \sum_{t=1}^{96} -P(t) \cdot \Delta t + \alpha_E(t) = \tfrac{C(t_{96})}{2} \end{aligned} \tag{16}$$

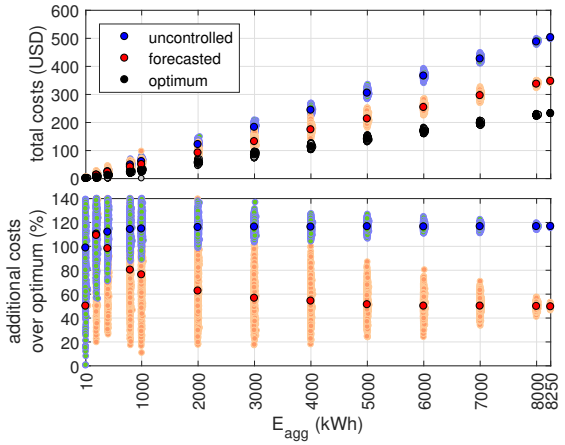

Fig. 8. Total costs and additional costs of the uncontrolled and forecasted scenario over the optimal scenario for different aggregation levels.

Similar to the forecastability assessment in sections IV-D and IV-E, 1000 random EVSE combinations for each aggregation level are generated. For each combination, the storage parameters are forecasted, an optimization is run, and the total costs for each scenario are evaluated.

The upper plot in Fig. 8 shows the total costs for each scenario for all random EVSE combinations in light and the median cost in dark colors. Obviously, the total costs are increasing with increasing aggregation level. To quantify the additional costs that are added on top of the optimal case due to imperfect forecasts, the difference between the costs of the uncontrolled/forecasted scenario to the optimum are normalized over the optimum, i.e. $(cost_{\{uc,fc\}} - cost_{opt})/cost_{opt}$. The lower plot shows the additional costs added to the optimum in percent of the total optimal costs. The additional costs due to imperfect forecasts decrease with higher aggregation level. The median cost of uncontrolled charging stabilizes at an aggregation of about 1000 kWh, but is more than double of the minimal costs whereas the costs of the forecasted scenario add around 50 % on top of the optimal costs.

VI. Conclusion

The paper presented a novel equivalent time-variant storage model for aggregation of EVSEs with plugged EVs. The advantages of the proposed storage model are: a) the storage model is kept general to be applicable in different market contexts, b) the storage parameters can be easily aggregated by summation and applied to any aggregation level, c) storage parameters can be forecasted by use of conventional methods such as autoregressive models without the need for complicated forecasting algorithms, d) no need of information about the exact arrival and departure times in the future, e) EVSEs of different charging levels can be included in the storage model.

The forecasting performance can be significantly enhanced by aggregating EVSEs. Median CVs as low as 16 % were achieved for the forecast of uncontrolled demand for the highest aggregation level. The forecast uncertainty of the storage parameters was even lower with an CV of about 10 %.

The benefit of aggregation was shown by means of a practical application of the storage model for minimizing the costs by optimizing the day-ahead schedule. The total costs when using the storage model in the given market context are only about 50 % higher than the benchmark with perfect forecast whereas uncontrolled charging costs more than double.

Future work will focus on a control strategy to break down the aggregated signals to modulate the individual EV's charging profile. Moreover, a flexibility assessment of different charging locations is needed to determine whether there exists an optimal combination of categories.

ACKNOWLEDGMENT

We would like to thank ChargePoint for providing the data used in this study. This project is supported by the US Department of Energy SunShot initiative (SUNLAMP 0000-1756) and the TomKat Center for Sustainable Energy. SLAC National Accelerator Laboratory is operated for the US Department of Energy by Stanford University under Contract DE-AC02-76SF00515. Michael Pertl and Mattia Marinelli acknowledge the support of the EU FP7 project ELECTRA (grant: 609687; website: electrairp.eu).

REFERENCES

[1] International Energy Agency, "Global EV Outlook 2016 - Beyond one million electric cars," tech. rep., International Energy Agency, Paris, 2016.

[2] S. Martinenas, K. Knezovic, and M. Marinelli, "Management of Power Quality Issues in Low Voltage Networks using Electric Vehicles: Experimental Validation," *IEEE Transactions on Power Delivery*, vol. 32, no. 2, pp. 971–979, 2017.

[3] K. Knezović, M. Marinelli, P. Codani, and Y. Perez, "Distribution grid services and flexibility provision by electric vehicles: A review of options," in *Universities Power Engineering Conference (UPEC)*, (Stoke-on-Trent), p. 6, 2015.

[4] M. M. N. Rezkalla, A. Zecchino, M. Pertl, and M. Marinelli, "Grid Frequency Support by Single-Phase Electric Vehicles Employing an Innovative Virtual Inertia Controller," in *International Universities Power Engineering Conference (UPEC)*, (Coimbra), p. 6, 2016.

[5] M. D. Galus, M. Gonzalez Vaya, T. Krause, and G. Andersson, "The role of electric vehicles in smart grids," *Wiley Interdisciplinary Reviews: Energy and Environment*, vol. 2, pp. 384–400, 2013.

[6] C. Guille and G. Gross, "A conceptual framework for the vehicle-to-grid (V2G) implementation," *Energy Policy*, vol. 37, no. 11, pp. 4379–4390, 2009.

[7] C. Quinn, D. Zimmerle, and T. H. Bradley, "The effect of communication architecture on the availability, reliability, and economics of plug-in hybrid electric vehicle-to-grid ancillary services," *Journal of Power Sources*, vol. 195, no. 5, pp. 1500–1509, 2010.

[8] D. S. Callaway and I. A. Hiskens, "Achieving Controllability of Electric Loads," *Proceedings of the IEEE*, vol. 99, no. 1, pp. 184–199, 2011.

[9] EPEX SPOT SE, "Trading on EPEX Spot," 2016.

[10] Nord Pool Spot AS, "Trading Appendix 3: Product Specifications - Physical Markets," 2011.

[11] J. Powers, "Implementation Overview for PDR," 2014.

[12] A. Brooks and T. Gage, "Integration of Electric Drive Vehicles with the Electric Power Grid - a New Value Stream," in *18th International Electric Vehicle Symposium and Exhibition*, (Berlin), pp. 20–24, 2001.

[13] W. Su and M.-y. Chow, "Performance Evaluation of an EDA-Based Large-Scale Plug-In Hybrid Electric Vehicle," *IEEE Transactions on Smart Grids*, vol. 3, no. 1, pp. 308–315, 2012.

[14] Z. Ma, D. Callaway, and I. Hiskens, "Decentralized Charging Control for Large Populations of Plug-in Electric Vehicles: Application of the Nash Certainty Equivalence Principle," in *IEEE Conference on Control Applications (CCA)*, (Yokohama), pp. 191–195, 2010.

[15] F. Parise, M. Colombino, S. Grammatico, and J. Lygeros, "Mean field constrained charging policy for large populations of Plug-in Electric Vehicles," in *IEEE Conference on Decision and Control*, (Los Angeles), pp. 5101–5106, 2014.

[16] A. Y. Saber and G. K. Venayagamoorthy, "Plug-in vehicles and renewable energy sources for cost and emission reductions," *IEEE Transactions on Industrial Electronics*, vol. 58, no. 4, pp. 1229–1238, 2011.

[17] W. Su, H. Rahimi-Eichi, W. Zeng, and M.-y. Chow, "A Survey on the Electrification of Transportation in a Smart Grid Environment," *Ieee Transactions on Industrial Informatics*, vol. 8, no. 1, pp. 1–10, 2012.

[18] ENTSO-E, CEDEC, GEODE, EURELECTRIC, and E. f. S. Grids, "TSO-DSO Data Management Report," tech. rep., TSO DSO data management Project Team, Brussels, 2015.

[19] M. G. Vayá, L. Baringo, T. Krause, G. Andersson, P. Almeida, F. Geth, and S. Rapoport, "EV Aggregation Models for Different Charging Scenarios," in *23rd International Conference on Electricity Distribution (CIRED)*, (Lyon), p. 5, 2015.

[20] J. A. Pecas Lopes, F. J. Soares, and P. M. Rocha Almeida, "Integration of electric vehicles in the electric power system: A conceptual framework for integrating electric vehicles into electric power systems is given; impacts and benefits arising from their use are discussed," *Proceedings of the IEEE*, vol. 99, no. 1, pp. 168–183, 2011.

[21] R. J. Bessa, F. J. Soares, J. A. Peças Lopes, and M. A. Matos, "Models for the EV aggregation agent business," in *IEEE PES PowerTech*, (Trondheim), p. 8, 2011.

[22] P. Sánchez-Martín, G. Sánchez, and G. Morales-España, "Direct load control decision model for aggregated EV charging points," *IEEE Transactions on Power Systems*, vol. 27, no. 3, pp. 1577–1584, 2012.

[23] D. Madjidian, M. Roozbehani, and M. A. Dahleh, "Emulating Batteries with Deferrable Energy Demand: Fundamental Trade-offs and Scheduling Policies," 2016.

[24] H. Hao, B. M. Sanandaji, K. Poolla, and T. L. Vincent, "Aggregate flexibility of thermostatically controlled loads," *IEEE Transactions on Power Systems*, vol. 30, no. 1, pp. 189–198, 2015.

[25] E. C. Kara, J. S. Macdonald, D. Black, M. Bérges, G. Hug, and S. Kiliccote, "Estimating the benefits of electric vehicle smart charging at non-residential locations: A data-driven approach," *Applied Energy*, vol. 155, pp. 515–525, 2015.

[26] G. E. P. Box, G. M. Jenkins, and G. C. Reinsel, *Time Series Analysis - Forecasting and Control*. New Jersey: John Wiley & Sons, Inc., 4 ed., 2008.

[27] R. J. Hyndman, "Measuring forecast accuracy," 2014.

Michael Pertl (GSM' 14) was born in Klagenfurt, Austria, in 1988. He has received his BSc and Dipl.-Ing. (MSc equivalent) in Electrical Engineering from the Technical University of Graz, Austria, in 2013 and 2014, respectively. He is currently pursuing the PhD degree in Electrical Engineering at the Technical University of Denmark. His research interests include power system modelling, integration of renewable energy sources and data-driven approaches applied to power systems.

Francesco Carducci was born in Tolentino, Italy, in 1989. He received the B.S. and M.S. degree in mechanical engineering from Universita Politecnica delle Marche, Ancona, in 2012 and 2014 respectively. He is currently a Ph.D. candidate in Industrial Engineering at the Universita Politecnica delle Marche. His research interests include Smart Grid, Demand Response, Energy Storage Systems and Machine Learning.

Michaelangelo Tabone (M' 14) is a Postdoctoral Fellow funded by the TomKat Center for Renewable Energy at Stanford University. He received his M.S. (12) and Ph.D. (16) from the Energy and Resources Group at the University of California, Berkeley, and received a B.S. in Chemical Engineering and a B.A. in Political Science from the University of Pittsburgh in 2010. Tabones research focuses on leveraging rapidly evolving data collection and processing techniques to promote sustainable energy systems.

Mattia Marinelli (M'10-SM'17) was born in Genoa, Italy, in 1983. He received the B.Sc. and M.Sc. degrees in electrical engineering from the University of Genoa, in 2005 and 2007, respectively, and the European Ph.D. degree in power systems, from the same university in 2011. Since 2012, he has been with the Technical University of Denmark. His research interests include power system integration studies, wind and solar data analysis, electric vehicles, and distributed energy resources modeling.

Sila Kiliccote (M'11) is the leader of Grid Integration Systems, and Mobility (GISMo) group at SLAC National Accelerator Laboratory and Managing Director of Grid innovation at Stanford University. Her research interests include load flexibility, energy and resource management, and data science application in power systems planning and operations.

Emre C. Kara (M'14) is an Associate Staff Scientist at the Grid Integration Systems, and Mobility (GISMo) group at SLAC National Accelerator Laboratory. Prior to that, he was a Postdoctoral Researcher at Lawrence Berkeley National Laboratory (LBNL), Berkeley, CA, USA. He received his Ph.D. degree from Carnegie Mellon University, Pittsburgh, PA, USA in 2014. His research interests include data-driven modeling and control of distributed energy resources, and electrification of transportation.

Department of Electrical Engineering
Center for Electric Power and Energy (CEE)
Technical University of Denmark
Elektrovej, Building 325
DK-2800 Kgs. Lyngby
Denmark

www.elektro.dtu.dk/cee
Tel: (+45) 45 25 35 00
Fax: (+45) 45 88 61 11
E-mail: cee@elektro.dtu.dk